The Handbook of Environmental Chemistry 33
Series Editors: Damià Barceló · Andrey G. Kostianoy

Tamim Younos
Tammy E. Parece *Editors*

Advances in Watershed Science and Assessment

Springer

The Handbook of Environmental Chemistry

Founded by Otto Hutzinger

Volume 33

More information about this series at
http://www.springer.com/series/698

Advances in Watershed Science and Assessment

Volume Editors: Tamim Younos · Tammy E. Parece

With contributions by

S.N. Ahmed · B. Badgley · M.E. Bauer · K.R. Bencala · V.E. Brando · M. Bresciani · P.L. Brezonik · J.B. Campbell · D.H. Doctor · H. Duan · J. Ducnuigeen · S.D. Eagle · A.L. Garey · J.D. Gerst · C. Giardino · C. Hagedorn · C.J. Heyer · V. Klemas · S.A. Loiselle · E. Matta · H.L.N. Moltz · A. Nagel · L.G. Olmanson · W. Orndorff · T.E. Parece · A. Pieterse · M.E. Schreiber · C.L. Schultz · B.F. Schwartz · L.A. Smock · P. Villa · T. Younos

Springer

Editors
Tamim Younos
The Cabel Brand Center for Global Poverty and Resources Sustainability Studies
Blacksburg, VA
USA

Tammy E. Parece
Department of Geography
Virginia Polytechnic Institute and State University
Blacksburg, VA
USA

The Handbook of Environmental Chemistry
ISSN 1867-979X ISSN 1616-864X (electronic)
ISBN 978-3-319-14211-1 ISBN 978-3-319-14212-8 (eBook)
DOI 10.1007/978-3-319-14212-8
Springer Cham Heidelberg New York Dordrecht London

Library of Congress Control Number: 2015931643

Printed on acid-free paper

Springer is part of Springer Science+Business Media (www.springer.com)

In memory of
Dr. Vernon O. Shanholtz and
Dr. G.V. Loganathan

Editors-in-Chief

Prof. Dr. Damià Barceló

Department of Environmental Chemistry
IDAEA-CSIC
C/Jordi Girona 18–26
08034 Barcelona, Spain
and
Catalan Institute for Water Research (ICRA)
H20 Building
Scientific and Technological Park of the
University of Girona
Emili Grahit, 101
17003 Girona, Spain
dbcqam@cid.csic.es

Prof. Dr. Andrey G. Kostianoy

P.P. Shirshov Institute of Oceanology
Russian Academy of Sciences
36, Nakhimovsky Pr.
117997 Moscow, Russia
kostianoy@gmail.com

Advisory Board

The Handbook of Environmental Chemistry Also Available Electronically

The Handbook of Environmental Chemistry is included in Springer's eBook package *Earth and Environmental Science*. If a library does not opt for the whole package, the book series may be bought on a subscription basis.

For all customers who have a standing order to the print version of *The Handbook of Environmental Chemistry,* we offer free access to the electronic volumes of the Series published in the current year via SpringerLink. If you do not have access, you can still view the table of contents of each volume and the abstract of each article on SpringerLink (www.springerlink.com/content/110354/).

You will find information about the

– Editorial Board
– Aims and Scope
– Instructions for Authors
– Sample Contribution

at springer.com (www.springer.com/series/698).

All figures submitted in color are published in full color in the electronic version on SpringerLink.

Aims and Scope

Since 1980, *The Handbook of Environmental Chemistry* has provided sound and solid knowledge about environmental topics from a chemical perspective. Presenting a wide spectrum of viewpoints and approaches, the series now covers topics such as local and global changes of natural environment and climate; anthropogenic impact on the environment; water, air and soil pollution; remediation and waste characterization; environmental contaminants; biogeochemistry; geoecology; chemical reactions and processes; chemical and biological transformations as well as physical transport of chemicals in the environment; or environmental modeling. A particular focus of the series lies on methodological advances in environmental analytical chemistry.

Series Preface

With remarkable vision, Prof. Otto Hutzinger initiated *The Handbook of Environmental Chemistry* in 1980 and became the founding Editor-in-Chief. At that time, environmental chemistry was an emerging field, aiming at a complete description of the Earth's environment, encompassing the physical, chemical, biological, and geological transformations of chemical substances occurring on a local as well as a global scale. Environmental chemistry was intended to provide an account of the impact of man's activities on the natural environment by describing observed changes.

While a considerable amount of knowledge has been accumulated over the last three decades, as reflected in the more than 70 volumes of *The Handbook of Environmental Chemistry,* there are still many scientific and policy challenges ahead due to the complexity and interdisciplinary nature of the field. The series will therefore continue to provide compilations of current knowledge. Contributions are written by leading experts with practical experience in their fields. *The Handbook of Environmental Chemistry* grows with the increases in our scientific understanding, and provides a valuable source not only for scientists but also for environmental managers and decision-makers. Today, the series covers a broad range of environmental topics from a chemical perspective, including methodological advances in environmental analytical chemistry.

In recent years, there has been a growing tendency to include subject matter of societal relevance in the broad view of environmental chemistry. Topics include life cycle analysis, environmental management, sustainable development, and socio-economic, legal and even political problems, among others. While these topics are of great importance for the development and acceptance of *The Handbook of Environmental Chemistry,* the publisher and Editors-in-Chief have decided to keep the handbook essentially a source of information on "hard sciences" with a particular emphasis on chemistry, but also covering biology, geology, hydrology and engineering as applied to environmental sciences.

The volumes of the series are written at an advanced level, addressing the needs of both researchers and graduate students, as well as of people outside the field of

"pure" chemistry, including those in industry, business, government, research establishments, and public interest groups. It would be very satisfying to see these volumes used as a basis for graduate courses in environmental chemistry. With its high standards of scientific quality and clarity, *The Handbook of Environmental Chemistry* provides a solid basis from which scientists can share their knowledge on the different aspects of environmental problems, presenting a wide spectrum of viewpoints and approaches.

The Handbook of Environmental Chemistry is available both in print and online via www.springerlink.com/content/110354/. Articles are published online as soon as they have been approved for publication. Authors, Volume Editors and Editors-in-Chief are rewarded by the broad acceptance of *The Handbook of Environmental Chemistry* by the scientific community, from whom suggestions for new topics to the Editors-in-Chief are always very welcome.

Damià Barceló
Andrey G. Kostianoy
Editors-in-Chief

Volume Preface

A watershed depicts a geographic boundary where the precipitation falling within the bounded land area flows to streams, rivers, and lakes or seeps into the subsurface water system situated within the watershed. Thus, in a watershed, a strong dynamic interaction exists between land and natural water systems, which can significantly impact water availability and water quality for various human uses and ecosystem health. Water resource managers and researchers have deployed the watershed concept in water assessment studies since the 1960s. However, recent advances in geospatial analysis, satellite imagery, electronics, computer software, and wireless and Internet technologies have facilitated a revolutionary change from limited (spatially and temporally) manual and discrete methods of assessment to real-time and broad-spatial-coverage-capable methods of assessment. Research and development in these new technologies provide tremendous and exciting opportunities for watershed assessment, sustainable management of land and water resources, and ecosystem preservation around the world.

This volume presents a discussion of concepts, methods, and case studies of innovative and evolving technologies in the arena of watershed assessment. Themes discussed in this volume include (1) development and applications of geospatial, satellite imagery, and remote sensing technologies for land monitoring, (2) development and applications of satellite imagery for monitoring inland water quality, (3) development and applications of water sensor technologies for real-time monitoring of water quantity and water quality, and (4) advances in biological monitoring and microbial source tracking (MST) technologies.

This volume contains ten chapters. The chapter "Land Use/Land Cover Monitoring and Geospatial Technologies: An Overview" discusses remote sensing, its technological evolution, and remote sensing applications in land use and land cover mapping and monitoring. The chapter "Using Remote Sensing to Map and Monitor Water Resources in Arid and Semiarid Regions" provides an overview of satellite and airborne remote sensing technologies and applications to management of water resources and drought monitoring in arid and semiarid regions. The chapter "Imaging Spectrometry of Inland Water Quality in Italy Using MIVIS: An Overview"

presents examples of applications of using Multispectral Infrared and Visible Imaging Spectrometer (MIVIS) imagery for monitoring inland water quality parameters and detecting submerged vegetation, cyanobacteria blooms, and floating materials of terrestrial origin (e.g., oil). The chapter "Using Remote Sensing to Assess the Impact of Human Activities on Water Quality: Case Study of Lake Taihu, China" demonstrates the potential of remote sensing for detecting harmful algal blooms and using the technology for integrated assessment of watershed dynamics. The chapter "Remote Sensing for Regional Lake Water Quality Assessment: Capabilities and Limitations of Current and Upcoming Satellite Systems" discusses satellite imagery advances and limitations for regional scale measurements of lake water characteristics.

The chapter "Interactive Geospatial Analysis Tool for Estimating Watershed-Scale Consumptive Use: Potomac River Basin Case Study," presents a basin-wide analysis and mapping tool that incorporates water use data from multiple political jurisdictions and estimates consumptive water use for effective management of water resources. The chapter "Advances in Water Sensor Technologies and Real-Time Water Monitoring" is an overview of state-of-the-art technologies in water sensor technologies for water quantity and water quality measurements, data collection, and transport platforms. The chapter "Instrumenting Caves to Collect Hydrologic and Geochemical Data: Case Study from James Cave, Virginia" presents information about the instrumentation, data collection, processing, and management and makes recommendations for hydrologic and geochemical monitoring of cave systems in karst environments. The chapter "Principles for the Development of Contemporary Bioassessment Indices for Freshwater Ecosystems" discusses bioassessment, the use of ecological assemblages, primarily fish, macroinvertebrates, and algae, as indicators of anthropogenic impairment in aquatic systems, and focuses on analytical approaches for improving the effectiveness of bioassessment indices for detecting anthropogenic impairment in freshwater ecosystems. The chapter "Microbial Source Tracking—Advances in Research and a Guide to Application" discusses the main drivers of MST and the evolving MST research development and technology and presents a guideline for decision-making on where, when, and how to deploy MST.

In "Land Use/Land Cover Monitoring and Geospatial Technologies: An Overview," Parece and Campbell state that the availability of multispectral satellite data beginning in 1972 has significantly advanced the ability of researchers to systematically monitor and evaluate land use/land cover changes and their impacts on water quality and quantity. In that context, practitioners have developed classification schemes specifically tailored for use with remotely sensed imagery and for systematic assessment of land use change. Land observation technologies in the twenty-first century include the use of lasers for 3D analyses and unmanned aerial systems. Such technologies have enabled land use assessment to contribute not only to its original focus in urban and regional planning but to a broad range of environmental and social issues.

In "Using Remote Sensing to Map and Monitor Water Resources in Arid and Semiarid Regions," Klemas and Pieterse state that in arid environments, the exploration and monitoring of water resources is a prerequisite for water

accessibility and rational use and management. Authors argue that conventional land-based techniques must be complemented by using satellite and airborne remote sensors. Authors describe using various technology applications: multispectral and radar sensors for mapping surface water systems, microwave radiometers for sensing soil moisture in the unsaturated zone, multispectral cameras for mapping freshwater wetlands, thermal infrared radiometers for detecting freshwater springs, and satellite remote sensors and satellite gravitational surveys with ancillary data analysis to infer groundwater behavior from surface expressions and to estimate groundwater aquifer storage.

In "Imaging Spectrometry of Inland Water Quality in Italy Using MIVIS: An Overview," Giardino, Bresciani, Matta, and Brando state that airborne imaging spectrometry is a powerful tool to investigate key biophysical parameters in inland waters. Authors present examples of applications using airborne MIVIS imagery of Italian inland waters acquired at a spatial resolution varying from 3 to 5 m. Examples include the retrieval of water quality parameters (i.e., chlorophyll-*a*, suspended particulate matter, and colored dissolved organic matter), the detection and monitoring of submerged vegetation, the observation of cyanobacteria bloom in productive lakes, and the signal reflected by floating materials of terrestrial origin (i.e., pollens and oil).

In "Using Remote Sensing to Assess the Impact of Human Activities on Water Quality: Case Study of Lake Taihu, China," Villa, Duan, and Loiselle state that the capacity of remote sensing to deliver spatial and temporal information about fundamental environmental dynamics makes it an ideal tool for performing an integrated assessment of water quality stressors and the causes of water quality deterioration at watershed scale. Authors focus on harmful algal blooms in Lake Taihu, as a case study. The temporal and spatial variabilities of the conditions in Lake Taihu and its watershed were derived from satellite data to produce a monthly time series of algal bloom coverage, aquatic vegetation extent, and land cover. Environmental features related to nutrient loading, climate conditions, and agricultural practices were also used to analyze the driving forces of algal blooms.

In "Remote Sensing for Regional Lake Water Quality Assessment: Capabilities and Limitations of Current and Upcoming Satellite Systems," Olmanson, Brezonik, and Bauer state that remote, satellite-based, sensing is a cost-effective way to gather information needed for regional water quality assessments in lake-rich areas. For example, in the Midwest United States, historic and recent Landsat water clarity assessments have been conducted on >20,000 lakes to investigate spatial and temporal patterns and explore factors that affect lake water quality. Advances over the past decade have enabled the use of satellite imagery for regional scale measurement of lake characteristics, such as clarity and chlorophyll. The spatial characteristics of Landsat imagery allow for the assessment of all lakes greater than ~4 ha, but the broad nature and placement of its spectral bands have assessments limited largely to water clarity. Improvements of the recently launched Landsat-8 and the upcoming ESA Sentinel-2 and Sentinel-3 satellites will expand capabilities further and enable assessment of other optically related water quality characteristics, such as colored dissolved organic matter and mineral-suspended solids.

In "Interactive Geospatial Analysis Tool for Estimating Watershed-Scale Consumptive Use: Potomac River Basin Case Study," Ducnuigeen, Ahmed, Bencala, Moltz, Nagel, and Schultz state that temporal and spatial watershed-scale information is needed on both the total amount of water withdrawal and the portion of withdrawn water which is not returned to the source for effective water resource management decisions. Authors present a case study of consumptive water use model developed for the Potomac River Basin in the United States. The model and associated tools consist of a basin-wide analysis and mapping tool that incorporates monthly water use data from multiple political jurisdictions, estimates consumptive water use, displays raw and summary information in an interactive geospatial format, and shares information with stakeholders via an interactive web-based mapping tool.

In "Advances in Water Sensor Technologies and Real-Time Water Monitoring," Younos and Heyer state that traditional discrete water quantity measurements and water quality sampling do not provide sufficient data to capture temporal and spatial changes that occur during episodic events. In recent decades, significant advances in water-monitoring technologies have occurred; sensors, remote monitoring, and data-transfer technologies allow real-time and continuous water monitoring and can capture temporal changes and provide broader spatial coverage of water quantity and quality in a watershed. Authors present and discuss various types of sensors for water quantity and water quality measurements, examples of commercially available water quantity and water quality monitoring devices, data collection and transport platforms, and data management and quality assurance/quality control for water monitoring. Authors conclude that water sensor technologies and associated computer hardware/software and telemetry technologies are evolving fields of research and technology development and discuss some of the limitations of existing technologies.

In "Instrumenting Caves to Collect Hydrologic and Geochemical Data: Case Study from James Cave, Virginia," Schreiber, Schwartz, Orndorff, Doctor, Eagle, and Gerst state that karst aquifers are productive groundwater systems, supplying approximately 25 % of the world's drinking water. Sustainable use of this critical water supply requires information about rates of recharge and quality in karst aquifers. Caves are an important feature in karst environments. Authors provide detailed information about the instrumentation, data processing, and data management and show examples of collected hydrologic and geochemical datasets for an instrumented cave study site in Virginia, United States. The cave has been instrumented for continuous measurement of the temperature and rate of precipitation; water temperature, specific conductance, and rate of epikarst dripwater; temperature of the cave air; and temperature, conductivity, and discharge of the cave stream. The chapter provides recommendations on instrumentation and methods of measurement for cave water.

In "Principles for the Development of Contemporary Bioassessment Indices for Freshwater Ecosystems," Garey and Smock define "bioassessment" as the use of biota to assess the nature and magnitude of anthropogenic impacts to natural water systems. Authors particularly focus on an important and specific type of

bioassessment: the use of ecological assemblages, primarily fish, macroinvertebrates, and algae, as indicators of anthropogenic impairment in aquatic systems. Authors provide an introduction to the process of developing assemblage-level indices that provide quantitative estimates of the ecological integrity of freshwater ecosystems and discuss recent developments that have improved the effectiveness of bioassessment strategies. Authors conclude that developments, such as advanced predictive modeling techniques, coupled with emerging technologies and the development of large-scale bioassessment programs will continue to improve our understanding of how aquatic assemblages are affected by anthropogenic impairment.

In "Microbial Source Tracking—Advances in Research and a Guide to Application," Badgley and Hagedorn state that MST is a still-new and developing discipline that allows users to discriminate among the many potential sources of fecal pollution in environmental waters. Authors further explain that the main area of research in MST focuses on the identification of source-specific genetic markers that can be used to detect contributions from different hosts such as humans, livestock, and wildlife. Authors discuss the main drivers of MST and how these have shaped the development of past and present methodological approaches, plus current research initiatives such as community analysis that could usher in yet another new and improved methodological basis for the entire field of MST. Finally, a tiered system is presented as a recommended means to navigate the multiple options for MST analyses that will assist the reader in how best to use MST within the context of more traditional approaches. This chapter can serve as a guide for decision-making on where, when, and how to deploy MST.

Chapters presented in this volume primarily focus on advanced methods of land and water monitoring in aquatic ecosystems. Except for limited application in "Interactive Geospatial Analysis Tool for Estimating Watershed-Scale Consumptive Use: Potomac River Basin Case Study," this volume does not include watershed models, another avenue of important research relevant to watershed assessment and management. However, spatial and temporal land- and water-monitoring technologies and analysis discussed in this volume will significantly contribute to developing improved watershed models, model verification, and applications.

We hope this volume serves as a textbook and reference material for graduate students and researchers involved in watershed science and environmental studies. Equally, we hope this volume serves as a valuable guide to experts in governmental agencies who are concerned with water availability and water quality issues and engineers and other professionals involved with the design of land- and water-monitoring systems.

Blacksburg, VA Tamim Younos
Blacksburg, VA Tammy E. Parece

Contents

Land Use/Land Cover Monitoring and Geospatial Technologies: An Overview

Tammy E. Parece and James B. Campbell

Contents

Abstract Accurate and detailed land use and land cover information forms an important resource for hydrologic analysis; remote sensing forms a critical resource for acquiring and analyzing broad-scale land use information. Although aerial photography is an important resource for land use information, it was the availability of multispectral satellite data beginning in 1972 that significantly advanced the

T.E. Parece (✉) • J.B. Campbell
Department of Geography, Virginia Polytechnic Institute and State University, Blacksburg, VA, USA
e-mail: tammyep@vt.edu

T. Younos, T.E. Parece (eds.), *Advances in Watershed Science and Assessment*, The Handbook of Environmental Chemistry 33,
DOI 10.1007/978-3-319-14212-8_1

ability of remote sensing researchers to systematically monitor and evaluate land use/land cover changes and their impacts on water quality and quantity. In that context, practitioners developed classification schemes specifically tailored for use with remotely sensed imagery and for systematic assessment of land use change. Since then, land observation technologies have evolved to allow extensive and intricate land use monitoring techniques, and now, in the twenty-first century, include the use of lasers for 3-D analyses and unmanned aerial systems. Such technologies have enabled land use assessment to contribute not only to its original focus in urban and regional planning but to a broad range of environmental and social issues. This chapter provides an overview of remote sensing, its technological evolution, and remote sensing applications in land use and land cover mapping and monitoring, with a focus upon implications for watershed assessment and management.

Keywords Electromagnetic spectrum • Land cover • Land use • Remote sensing • Water resources

1 Introduction

Land use and land cover mapping date back to Egyptian and Babylonian civilizations thousands of years BC [1] and have long formed essential components to understanding Earth's resources including water, its most vital resource. Approximately, 70 % of Earth's surface is covered with water versus 30 % land cover. And, it's estimated that, over time, humans have modified over 50 % of the natural land cover [2], thereby creating conditions that affect natural water resources and its quality.

Key land use changes that adversely impact water resources include deforestation, desertification, and urbanization. Deforestation outcomes typically change to either agricultural or urban land uses. Although land conversion from forests to agriculture impacts water quality, the level of impact is highly dependent on agricultural practices (i.e., tillage technique, chemical use versus organic practices, or size and type of conservation easements). Current agricultural practices have a greater impact on water quantity because of over-withdrawal from groundwater supplies (estimated up to 35 %) or diversion of water into water-poor areas for irrigation purposes [3, 4].

Urbanization is the most extreme form of land cover and land use changes as it results in losses of agricultural and forested lands coupled with notable expansion of impervious surface cover [5, 6]. These effects, combined with associated decreases in vegetative cover, result in significant local hydrologic modifications [7–9] and habitat destruction [10]. Hydrologic modifications represent the most significant water quality and quantity issues present today [7, 9, 11]. Stormwater runoff from impervious surfaces in urban areas degrades water quality through

higher water temperatures, increased runoff volume and rate, and elevated levels of contaminants in surface waters [8, 9, 12, 13]—effects which extend well beyond specific urban regions, vitiating downstream waterbodies [14].

Remote sensing techniques can be used to map and monitor changes in land use and land cover locally and over large expanses and to evaluate impacts of these changes. Remote sensing techniques involve collecting data from a distance, then analyzing and interpreting collected data for specific purposes. In this chapter, remote sensing refers to collection and analysis of information using aerial photography and/or satellite imagery for the purpose of monitoring the Earth's surface. With the capacity to remotely sense the Earth's surface, the science of land use/land cover mapping has gained the ability to evaluate large areas at economical costs.

In this chapter, we present methods for classifying land use and land cover and sources of land use and land cover data; discuss remote sensing principles and use of the electromagnetic spectrum in classification and analyses of land use and land cover; provide a brief history of remote sensing and introduce two types of imagery—aerial photos and satellite imagery; present how remotely sensed land use and land cover is used in hydrological analyses; and finally introduce the newest remote sensing technologies and their applications for land use and land cover monitoring.

2 Land Use/Land Cover Classification

2.1 Definition of Land Use and Land Cover

Land use and *land cover* are terms frequently used interchangeably. However, these terms have significantly different meanings and applications. Land cover refers to physical features on the surface of the Earth—vegetation, water, the built-up land. Whereas, land use specifically refers to the human (economic) utility of what is on the Earth's surface. In some instances, terms used to describe land cover can also describe land use, for example, forest describes the type of vegetated cover but also describes a use for industries such as forest products. Although remote sensing can be used to identify both, often we can think of broad-scale imagery (e.g., satellite imagery) as primarily portraying land cover, whereas the fine detail of aerial photography or similar imagery might be required for identification of land use.

Land use mapping is accomplished by partitioning an image into units, usually polygons, and then assigning each unit to a specific category. Land use/land cover classifications are strictly naming systems such that each classification contains a description defining uses falling within a system of mutually exclusive categories. As an example—a definition for a water classification is *Open Water—all areas of open water, generally with less than 25 % cover of vegetation/land cover* [15].

2.2 Land Use and Land Cover Classification Systems

The precision in a land use classification (known as *taxonomic detail*) should match to the intended use of the analysis and is usually defined by the map user. For example, in Fig. 1, the left-hand image shows fine detail subdividing forest cover to represent forested wetlands (light green) and deciduous forest (dark green), as might be required to support ecological or hydrological analyses. The right-hand image, representing a coarser classification, symbolizes forest cover as a single class, as might support an analysis of regional land use.

Thus, the value of land use and land cover information resides in application of a systematic classification system with a structure organized to support the user's application of the information for its intended purpose. An important modern milestone marks the beginnings of systematic uses of geospatial data for land use information, when in the 1960s, the State of New York (USA) recognized the importance of mapping land use and its natural resources. In conjunction with researchers at Cornell University, the Land Use and Natural Resources Inventory (LUNR) mapping project was completed with one hundred different land use classes [16]. Significant detail was required for this mapping project as it was subsequently used for urban planning, economic development, and environmental planning. In the early 1970s, the State of Minnesota (USA) also completed a state-wide land use map but only for nine different land use categories (Orning and Maki 1972, as referenced in [17]). Such projects introduced important advances in systematizing the classification of land use data for large areas, but retained a local, often ad hoc, character that inhibited application to multi-temporal analysis or to applications that encompass broad-scale land areas.

In 1976, Anderson et al. [17] introduced a framework for standardization of land use and land cover tailored for remote sensing classification. The Anderson classification system, the most widely used classification scheme today, consists of multiple levels of classification designed to be compatible with remotely sensed imagery acquired at varied scales and levels of detail. It is comprised of a hierarchal

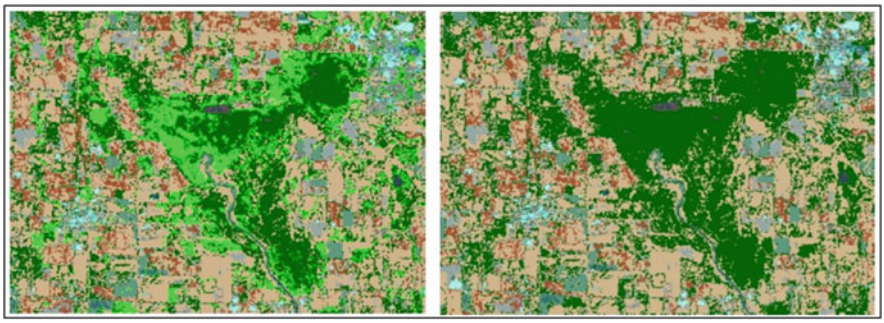

Fig. 1 Effects of taxonomic detail in land use classification—fine detail (*left*) and coarse detail (*right*). *Source*: Landsat 5 imagery from the United States Geological Survey, processed by the second author for specific land cover/land use classes

Table 1 Samples of classification Levels 1, 2, and 3 from [17]

Level 1	Level 2	Level 3
1 Urban or built-up land	11 Residential	111 Single-family units
		113 Group quarters
		116 Transient lodging
	13 Industrial	
	17 Other urban	
2 Agricultural land	21 Cropland and pasture	211 Cropland
		212 Pasture
	23 Confined feeding operations	
4 Forestland	41 Deciduous forestland	
	43 Mixed forestland	
5 Water	51 Streams and canals	511 Intracoastal waterway
		512 Canals associated with residential development
		513 Canals associated with utility, commercial, or industrial development
	52 Lakes	521 Freshwater ponds
	54 Bays and estuaries	541 Tidal marshes
		542 Open water

grouping of three levels, allowing for applicability at multiple resolutions. Level 1 can be used when finer details are not needed, such as for national or regional scales, and is more appropriate for land cover identification. Yet, Level 3 is available when finer detail is needed at a local scale and can be more readily described as land uses (Table 1).

Without a standard classification framework, it is difficult to identify changes occurring over time, compare between places, and to avoid duplication of efforts. As such, the Anderson system has been used as the basis for many other classification systems in the United States. For instance, classifications used by the Multi-Resolution Land Characteristics Consortium (MRLC) for the National Land Cover Database (NLCD) for the coterminous United States is a modified Anderson system [18]. One difference between the Anderson system and the NLCD scheme is that water is defined in three categories under Anderson (Table 1), but the NLCD limits it to one—open water [15].

Caution should be exercised when comparing datasets from the same source as classification methods may have changed over time. NLCD data have been prepared from analysis of satellite data (specifically Landsat Thematic Mapper, discussed later in this chapter) for 1992, 2001, 2006, and 2011. The history of the NLCD forms an example of the hazards of changing classification methods, as improvements implemented to prepare the 2001 data prevent systematic comparison of results between the 2001 and the 1992 datasets. Therefore, changes made for the 2001 classification mean that the 1992 and 2001 classes are not compatible for

compiling land cover change [19–21]. More generally, land use change studies, or regional mosaics, require compatibility with respect to the classification system, level of detail, spatial scale, date, and projection. Analysts, therefore, should devote special attention to consistency in land use classification in such situations.

2.3 Sources of Land Use/Land Cover Data

For any specific region, there are likely to be several sources for acquiring land use or land cover data derived from remotely sensed imagery, with alternative dates, coverage, and classification systems. For the United States, the NLCD (mentioned above) provides land cover data with broad-scale coverage (e.g., national, regional, or state levels). For finer scales, such as cities or comparable local areas, more detailed data completed from sensors with finer spatial resolution is readily available in most jurisdictions. However, the data, likely organized by political or administrative boundaries, will not match to drainage basin (watershed) boundaries.

Data for other countries each follow procedures and classification strategies specific to local needs and traditions. In considering national land cover mapping systems, the analyst will encounter wide variations in costs, dates, availability, classification, and completeness of coverage. Some examples:

The Canada Land Inventory, available for rural Canada, provides data covering land use and cover categories for agriculture, forestry, wildlife, and recreation. The maps were generated in the 1960s, 1970s, and early 1980s and many Canadian jurisdictions still use them for land use planning [22].

The European Environment Agency provides downloadable land use and land cover data for Pan-European urban areas with populations greater than 100,000 people. The Urban Atlas was completed using multispectral data, and the categories are based on the European Coordination of Information on the Environment (CORINE) classification system [23].

The Centre for Ecology and Hydrology provides land cover mapping data for the United Kingdom (for 1990, 2000, and 2007 [24]), but each of these three maps has been produced as a number of different products with varying data formats and spatial resolutions. The United Kingdom also has generalized land use data available through their generalized land use website [25].

Land cover maps for Africa have been generated by both the US Geological Survey [26] and the European Space Agency [27].

3 Electromagnetic Radiation Use in Remote Sensing

Sensors that measure the sun's electromagnetic radiation provide the foundation for obtaining and analyzing aerial photographs and other imagery used to monitor the Earth's surface. Electromagnetic energy from the sun that is reflected off the Earth's

surfaces and that portion which is absorbed and reradiated as thermal energy are both used in remote sensing analyses. The reflective portion of the spectrum (0.38–3.0 μm[1] wavelengths) has direct application in remote sensing analyses, and different wavelength ranges have different applications. Sensors record this data as images for scientific analysis. Remote sensing methods that measure the sun's electromagnetic radiation form the basis for *passive remote sensing*. In *optical remote sensing*, sensors record reflected solar energy as brightness values, thereby detecting features (both natural and man-made) on the Earth's surface.

In *active remote sensing*, instruments transmit man-made radiation to illuminate the Earth's surface. The man-made energy reflects off features (both natural and man-made) and is received and analyzed to form an image. Sonar, radar, and Lidar are examples of such remote sensing systems. The main focus of this chapter is on passive remote sensing, i.e., optical remote sensing.

A major consideration for optical remote sensing is atmospheric interference with incoming radiation—scattering. Scattering specifically refers to radiation reflected by particles in the atmosphere before it reaches the surface of the Earth. The level of interference depends on many factors, including:

- The altitude of the aircraft or satellite, i.e., sensors on low-flying aircraft have less atmosphere to penetrate.
- The wavelength of the radiation—the shorter, blue wavelengths are scattered about four times as much as the longer, red wavelengths (specifically designated Rayleigh scattering, caused by larger atmospheric molecules).
- The presence of dust, pollen, water droplets, and smoke (designated Mie scattering).
- The presence of larger airborne particles (designated non-selective scattering).

All factors noted above cause scattering but the form and magnitude of the scattering vary.

Another key consideration is the amount of reflected radiation from the features (both natural and man-made) on the surface of the Earth. When energy reaches the Earth's surface, it is either reflected, retransmitted, or absorbed. Different objects and features reflect or re-emit radiation in various ways. Observing or measuring these properties establishes spectral properties of individual objects (their spectral signatures). A particular object's spectral properties vary either over the course of a day, from night to day, over the course of a year, or over the course of several years. Variation in spectral properties allows remote sensing analysis to distinguish objects/features from one another and compare changes between the same object/feature over time.

Figure 2 shows the spectral properties of two features—healthy vegetation and clear, calm water. The *y*-axis represents percent of reflected energy. The *x*-axis

[1] All wavelength ranges discussed within this chapter are approximations. Different disciplines define the specific divisions of the electromagnetic spectrum in various wavelengths. Most definitions are extremely close in value.

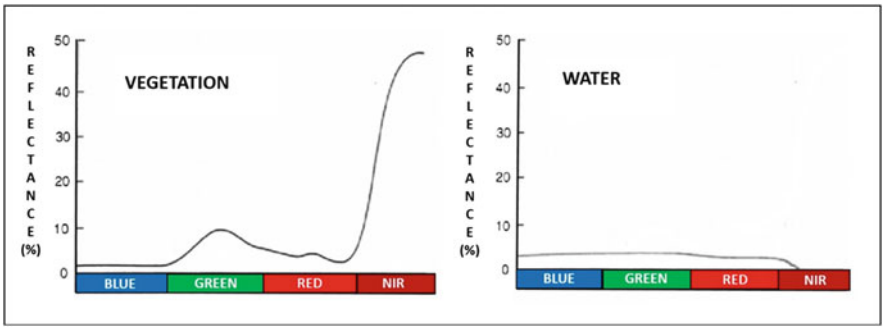

Fig. 2 Spectral signatures of vegetation and water [28] (Permissions, Campbell_Guilford_4_June_2014)

represents four segments of the electromagnetic spectrum—blue visible, green visible, red visible, and the near infrared (NIR). As this figure demonstrates, the percent of radiation that is reflected from water is very low across all portions of the visible spectrum. Whereas for vegetation, reflectance has a slight peak in the green, drops off in the red, but substantially increases in the near infrared (NIR).

As stated earlier, optical sensors measure returned energy and record it as a brightness value for the object. In the case of absorption, the energy recorded is greatly reduced. The brightness of the object also depends on many other factors. For instance, the surface of the object (rough or smooth) as is related to the wavelength of the energy will redirect the energy in different ways. If the surface is rough, the energy will be redirected in multiple directions; if smooth, the energy is redirected mostly in the same direction. This redirected energy may or may not be in the direction of the sensor and thus affects the amount of returned energy recorded by the sensor.

Figure 3 is an example of how a passive or optical sensor records the brightness values of different objects/features. This is a portion of a satellite image, Landsat 5 (natural color image, Path 17, Row 34), acquired over the Commonwealth of Virginia (USA) on April 4, 2010. The dark object in the lower right is Smith Mountain Lake. Since water absorbs and re-emits only a very small percent of energy that reaches it, the lake shows as an object darker than the surrounding vegetation. Urban areas (the City of Roanoke is in the upper left) are very bright because they reflect strongly across the entire visible spectrum and because the smooth surfaces of roads and some roofs are reflecting more energy directly back to the sensor.

The first remotely sensed images acquired were aerial photos. Early aerial photos were produced as black and white images, formed from brightness across the three visible portions of the electromagnetic spectrum. Prevailing technology allowed display only as a single black and white image (a one-band image).

Fig. 3 Natural color scene, Smith Mountain Lake (*lower right*) is much darker than the surrounding vegetation. The City of Roanoke, Virginia (USA) (*upper left*), and smaller urban areas appear very bright. *Source*: Landsat 5 imagery acquired on April 4, 2010, from the United States Geological Survey and processed by first author as a natural color image

As technology improved, sensors were not only able to collect the data in multiple bands[2] (initially just across the visible spectrum—blue, green, and red) but also able to display images as natural color. These multispectral images advanced remote sensing analyses by using spectral signatures of different features, as defined by individual spectral bands.

Additional advances in technology permitted sensors to collect radiation outside the visible spectrum, first in the near infrared (NIR) and later the longer wavelengths, mid (MIR) and far infrared (FIR). Human eyes cannot see these portions of the spectrum, but cameras and other image sensors can measure this radiation and record it as brightness values. These brightness values can then be represented using the colors of the visible spectrum. Thus, we can use visible radiation to display the nonvisible. Specialized software is used for this display and the user chooses which bands are displayed in the software's view screen. Specific images will be discussed in later sections of this chapter.

Software used to display remotely sensed images is also used for analyzing the images for specific applications. Each pixel of an individual band of an image has a set of brightness values, representing a feature's spectral signature within that pixel. These values can be enhanced in various ways, which forms the basis of remote sensing analyses. The features can be analyzed within an individual band but multiband analyses are more robust. Some of the most frequently used techniques in spectral enhancement are spectral ratios and indices. For example, when using

[2] The number of bands of an image refers to how many divisions of the electromagnetic spectrum were used to create that image. For the exact electromagnetic spectral divisions for each band, you must refer to the metadata that accompanies the image.

Landsat imagery, dividing band 4 (NIR) by band 3 (red) enhances the presence and vigor of vegetation.

Aerial cameras typically collect up to four bands (blue, green, red, and NIR). Sensors for other multispectral images can be located on satellites or placed on an aircraft for a specific collection campaign. Further advances in the design of imaging systems permit separation of finer subdivisions of the spectrum to form hyperspectral imagery by using more than 200 very specifically defined segments of the electromagnetic spectrum. Hyperspectral applications are discussed later in this chapter (Sect. 6.2).

4 History of Mapping and Remote Sensing

4.1 Background

Land use and land cover mapping in our current understanding dates at least to the late 1600s when estate managers in Western Europe began to map landowners' forests, fish ponds, croplands, and pastures [29]. Such maps were prepared through direct ground surveys and manual drawings. Many significant mapping projects were accomplished with these methods. The mapping of the Americas during the European Age of Exploration (1400s–1800s) and the mapping of the western United States by Lewis and Clark in the early 1800s form two major examples. These missions were undertaken to explore, identify, and map land areas, but ultimately these maps were used to determine the land's potential uses for settlements, transportation hubs, agriculture, and natural resource extraction.

Systematic mapping, specifically for land use inventory, began in the early twentieth century. L. Dudley Stamp produced the Land Utilization Survey for Britain in the 1930s [30]. This broad-scale inventory was generated from information provided by volunteers who reported land use information for their home regions. With technological advances, i.e., the development of cameras, computers, and space exploration, by mid-century remote sensing potential and applicability became the primary avenue of land use/land cover mapping and monitoring.

Initially, availability of suitable aerial photography focused applications of remote sensing mainly to urban settings, most often, to support planning and economic development programs. However, over time, improved access to higher-quality imagery, and especially the routine availability of satellite imagery, expanded applications to include rural regions and wildland landscapes, enabling acquisition of broad-scale land use data to support hydrologic analysis.

4.2 Mapping Using Aerial Photography

Aerial photography has been in existence for over 100 years using kites, balloons, airplanes, and most recently unmanned aerial vehicles (commonly called drones).

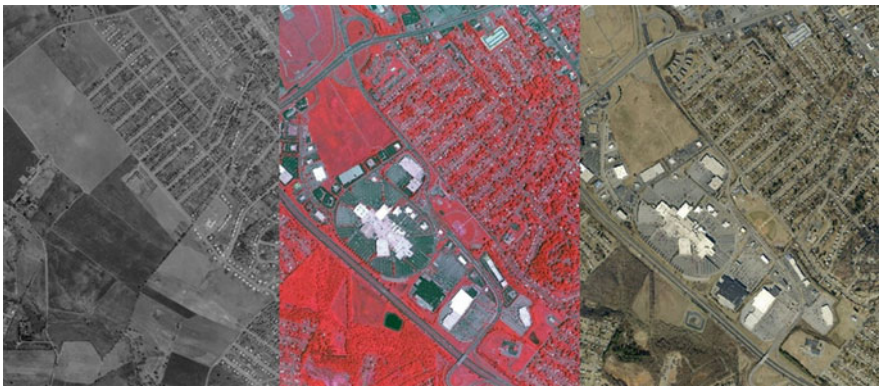

Fig. 4 1960 panchromatic image (*left*), 2008 color infrared image, bands 4-3-2 (*middle*), and 2011 natural color image (*right*) of northwest Roanoke, Virginia, USA. Sources identified in text

During the 1930s, scientists at the Tennessee Valley Authority (TVA) in the United States developed methods for systematic interpretation of aerial photography to extract land use and agricultural information, as well as rural settlement patterns [31, 32]. Those methods are no longer used but form the foundation for extracting land use information from aerial photographs.

Aerial photos can be taken in three different forms. Panchromatic is a one-band image; the visible portion of the electromagnetic spectrum is combined to produce a black and white image. A natural color image is taken using the three visible portions (**r**ed, **g**reen, and **b**lue—abbreviated RGB) of the spectrum, each in a separate band, and then overlaid to produce a color photo. A color infrared (CIR) photo is taken with the green and red visible bands and also the near infrared section of the spectrum; such photos are displayed as color infrared photos. Applications for these three different types of aerial photos vary but all are useful for mapping land use.

Figure 4 provides a side-by-side comparison of the three types of aerial photos for the northwest region of the City of Roanoke, Virginia (USA). On the far left is a panchromatic image from 1960 acquired by the United States Geological Survey (USGS). The CIR image (middle) was obtained by the United States Department of Agriculture (USDA) as part of its National Agricultural Imagery Program (NAIP) in 2008. For this image, NIR is being displayed in red, the red portion of the spectrum as green, and the green portion as blue. Since NIR is being displayed as the red band (as stated in Sect. 3, vegetation has the highest reflection in NIR), vegetation shows as red in the image. CIR imagery is extremely useful for evaluating and analyzing vegetation land cover. The 2011 natural color image (on right) was taken as part of the Virginia Base Mapping Program, which acquires annual aerial photos of the Commonwealth of Virginia (USA).

Developing a land use map from an aerial photo is accomplished in different ways. In the 1930s TVA project, it was accomplished with hand-drawn annotations on the aerial photos. As technology changed, this process also changed. A combination of photo-overlay technique and a computer database was used in the LUNR

Fig. 5 An example of the photo-overlay technique in GIS, delineating man-made surface cover (cyan polygons) to help identify a transportation land use within an urban area. Completed within GIS using high-resolution (15 cm by 15 cm pixel size) 2008 aerial photos from the Virginia Base Mapping Program. Area location is northwest Roanoke, Virginia, USA; the airport dominates the photo. *Source*: Image provided by the first author

project (mentioned earlier in Sect. 2.2); most specifically, mapping of land use and identification of natural resources for New York State (USA) were accomplished by using Mylar transparencies overlaid on aerial photographs [33], for 1 km^2 cells [28], and hand-drafted [17]. The land use identified from the aerial photos was then combined with reference data from other sources (public records, direct observation, etc.); a computerized map was produced from the results [1, 17].

With the increase in computing power, hand delineation of land use from aerial photos is no longer necessary, and it can be accomplished in either of two ways. One technique employs computer software that uses specialized algorithms to evaluate the spectral properties of the image, looking for similarities. Simply put, once these similarities are identified, the program will assign all pixels with these spectral values to specific classes. The algorithms will also assign unidentified pixel values to a specific class, depending on the algorithm's parameters. Specifics of these algorithms' methodologies are beyond the scope of this chapter (see [28] for some specifics).

Another technique employs computer software to apply the photo-overlay method. Aerial photos, georeferenced[3], are added to the program, and each land use polygon is delineated by the user within a geographic information system (GIS) using the aerial photo as a guide. Figure 5 is such an example; man-made objects (impervious surface land cover) are represented as cyan polygons to assist in

[3] Georeferencing means to define a specific location on the surface of the Earth for an image, usually with a specific geographic coordinate system.

identification of a specific land use class (transportation) within an urban region (City of Roanoke, Virginia, USA).

In addition to identifying specific land use classes, aerial photos enable time series mapping of land use changes, an important analysis to identify how land use has impacted water quality and quantity. Figure 3 (noted earlier) shows a comparison of the northwestern part of the City of Roanoke from 1960 to 2011. The 1960 photo shows some urban development for residential areas but also large expanses of agricultural lands.

The two later images in Fig. 3 (2008 and 2011) show that urban land has replaced former agricultural lands and includes additional residential areas throughout the region, an airport, a large shopping mall, and other commercial areas. This time series shows that permeable land surfaces have been extensively replaced by impervious surfaces, greatly altering the hydrologic characteristics of the land. These changes, agriculture to urban, have greatly degraded the water quality of streams within the Roanoke River watershed. The City of Roanoke has substantial drainage problems and experiences frequent flooding due to increased stormwater runoff from impervious surfaces. The Virginia Department of Environmental Quality has listed several segments of the Roanoke River system within the city as impaired, i.e., they do not meet established water quality standards due to the presence of contaminants such as *Escherichia coli*, heavy metals, and high water temperature [34].

4.3 Mapping Using Satellite Imagery

The 1950s was the beginning of a race into space as governments across the world established satellite systems for telecommunications, defense initiatives, and weather monitoring. During the 1960s, astronauts from the US' Gemini and Apollo missions created a large archive of photos of the Earth from space. In the late 1960s, one of the first broad-scale land cover maps was created from these photos [35]. This map, of the southwestern United States, demonstrated the capability of remotely sensing land cover employing imagery acquired from outside the Earth's atmosphere.

Weather satellites can be used to monitor the Earth's surface, but their major purpose is monitoring weather patterns using data at coarse spatial resolutions, relative to the needs for land surface analysis. The first land observation satellite was launched in 1972 (Landsat 1), a joint project of the USGS, the USDA, and the US National Aeronautics and Aerospace Administration (NASA). With the advent of land observation satellites, land use/land cover mapping and monitoring changed dramatically. This system established the utility of satellites to acquire imagery over large areas, to provide a continuous stream of images, and to record multitemporal images over the same area.

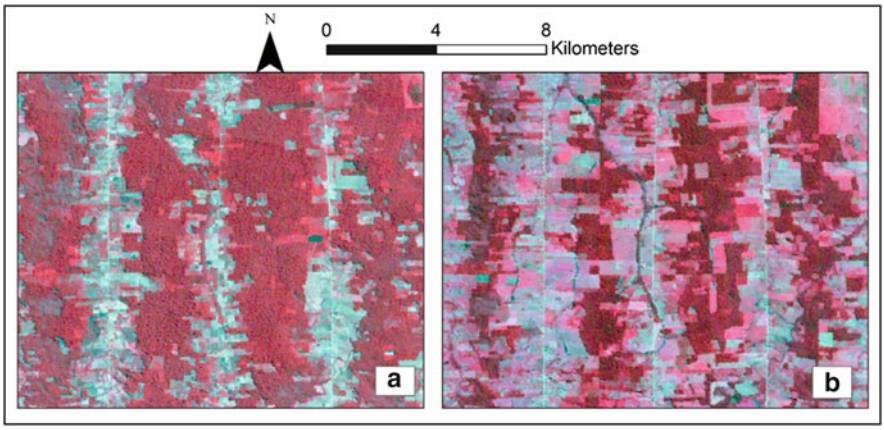

Fig. 6 Portions of two Landsat 5 TM scenes acquired over the same region of the Amazon rainforest in 1992 (**a**) and 2002 (**b**). *Dark red* is the forested area and the images show substantial deforestation from 1992 to 2002. *Source*: United States Geological Survey, processed by the first author and displayed as CIR (bands 4-3-2)

Figure 6 shows portions of two Landsat 5 Thematic Mapper (TM) scenes (Path 231, Row 68) acquired over the same region of the Amazon rainforest in 1992 (a) and 2002 (b). The images are displayed as CIR (bands 4-3-2) to enhance the presence of vegetation. The darkest areas of red are dense forest, the white areas are settlements including roads, and the light red or pink areas are agriculture. A stream is visible in the middle of the image. Comparing 2002 to 1992, a substantial reduction in forest area has occurred. The stream is more prominent in the 2002 image as much of the forest canopy, which would have reflected the radiation, is now gone and the radiation is being absorbed by the water.

Landsat is the longest continuous program of land observation satellites in the world. The most recent Landsat satellite (Landsat 8) was launched in February of 2013. Sensors aboard each satellite have been improved as technology has advanced and new uses for the imagery established. Landsat images (and images from other land observation satellites) are acquired, again, using the electromagnetic spectrum and most are equipped with passive remote sensors. The Landsat satellites have acquired more than 3.5 million images of the Earth's land surfaces since 1972. The USGS manages the Landsat imagery archives and all Landsat images are freely available to the public since 2009 [36].

France, in collaboration with European partners, launched its first land observation satellite (SPOT) in 1986. SPOT is a series of satellites with the most recent launch in 2012. Many other countries today have land observation satellites in orbit, each with specific characteristics and capabilities; Table 2 provides an outline of characteristics for a selection of these satellites. The nature of the images varies with respect to sensors, numbers of bands and bandwidths, spatial resolutions (pixel size), and land area covered in a single scene (image swath).

Table 2 A select listing of land observation satellites

Satellite (launch year)	Sponsoring entity (website)	Resolution (pixel size) (m)	Image swath (km)
Landsat system (1972–present)	United States [37]	15–120	170
IKONOS (1999)	Satellite Imaging Corporation [38]	1 and 4	11.3–13.8
SPOT system (1986–2012)	France [39]	10 and 20	3,600
CBERS (1 and 2) (1999)	China/Brazil [40]	260	890
DEIMOS 1 (2009)	Elecnor [41]	22	600
MODIS (1999)	United States [42]	250, 500, and 1,000	2,330

These satellites can carry one or more sensors, and sensors from satellite to satellite can vary in design and capabilities. Satellite sensors can be either active or passive (see Sect. 3). Passive sensors can be multispectral (acquiring images across several different segments of the electromagnetic spectrum) or hyperspectral (acquiring images across hundreds of segments of the electromagnetic spectrum—see Sect. 6.2). Passive sensors collect reflective shortwave radiation or emitted longwave (thermal) radiation. Active sensors can include sonar or radar (both beyond the scope of this chapter) or Lidar (see Sect. 6.1). The characteristics of a specific sensor depend on the purposes of the satellite system for which it is being designed. Multispectral sensors can be designed to acquire reflected radiation in a very limited range of the electromagnetic spectrum (e.g., blue, green, and red visible) or a much wider range (the blue visible through the far infrared).

Different models of passive sensors acquire images, basically, in the same way. The sensor records the energy from either the reflected or re-emitted radiation over a specific area of the Earth's surface. Such an area is defined by two parameters—the image swath, which represents the area of land covered in one orbital pass of the satellite, and the pixel size, which represents the smallest area that forms an individual brightness value on the image. This returned energy is directed by a mirror onto instruments that focus and transmit the energy to detectors. The detectors record the energy as brightness values in the form of digital numbers. Sensors vary in their capability to record a range of brightness values; brightness values are in binary format. For example, Landsats 4–7 use 8 bits, and Landsat 8 uses 12 bits. (An 8-bit sensor can record up to 256 different brightness values for each pixel, whereas a 12-bit sensor can record up to 4,096.)

The data is transmitted to ground stations positioned in different areas of the world, depending on the satellite system. The images are rectangular arrays of pixels. Most images are available for a fee. Processing of Landsat or any other satellite image requires specialized imaging software. Governments, corporations, and educational institutions each use a variety of software packages to display and analyze satellite images. Two private corporations—Google and ESRI—have each

processed a complete set of all Landsat images for land use/land cover changes, which are readily available for time series viewing over the Internet.

Table 2 provides only a selection of existing systems; many other land observation satellites are in orbit. The specifics listed in Table 2 are important when choosing imagery for a specific application. Larger pixel sizes facilitate faster processing, especially with analyses over large areas. However, a larger pixel size means that the land use spatial detail within that pixel is more likely coarser, and it represents a mixture of land uses or land covers, especially in urban areas.

5 Significance of Land Use/Land Cover Mapping for Hydrologic Studies

Land use impacts hydrology largely through its influence upon the natural hydrologic cycle. Vegetated surfaces, especially during the growing season, will redirect rainfall through the ability of leaves, branches, and trunks to intercept raindrops and to delay water movement to the soil surface. Forest soils act like sponges, retaining water so that it is slowly released to groundwater or to flow to streams and rivers over days, weeks, and months. Open, grassy surfaces likewise capture and slow the movement of water and retain soil moisture. In contrast, pavement and compacted or indurated soils impede infiltration and increase surface runoff. Runoff from impervious surfaces consequently flow to streams, rivers, and storm sewers and contribute to flooding and contamination of surface waters.

5.1 Land Use and Curve Numbers

Land use impact is significant for hydrologic analysis because it is a key variable in hydrologic models that predict surface runoff from precipitation events. In traditional hydrologic analysis developed by the USDA Natural Resources Conservation Service (NRCS), this relationship is described by the runoff *curve number* (CN), an empirical approximation of the runoff from a precipitation event in a specific drainage basin.

Curve numbers have been derived for a variety of surfaces and categorized by climate and by land use (both broadly and specifically defined) (Table 3) [43]. For each drainage area examined, analysts examine aerial imagery (often aerial photography, although uses of other forms of imagery may soon increase as their availability increases) to characterize surface conditions and hydraulic properties of local land cover, on a parcel-by-parcel basis. Analysts select curve numbers for each parcel of interest using methods outlined by NRCS, including:

- Land use (from designated classes)
- Hydrologic soil group, defined to identify hydrologic behavior of local soils (as selected from tables that represent soil units)

Table 3 Selected land use classes and NRCS curve number designations [43]

	Runoff curve numbers by hydrologic soil groups			
Land use	A	B	C	D
Rural				
Fallow	76	85	90	93
Row crop (contoured)	65	75	82	86
Small grain	63	75	83	87
Pasture	49	69	79	84
Close-seeded legumes or rotation meadow	64	75	83	85
Meadow	30	58	71	78
Woods	43	65	76	82
Impervious surfaces (paved)	98	98	98	98
Urban				
Residential housing	46	65	77	82
Commercial and business	89	92	94	95
Industrial	81	88	91	93
Streets and roads	98	98	98	98
Open areas	49	69	79	84
Connected impervious areas	98	98	98	98
Arid/semiarid				
Herbaceous	–	71	81	89
Oak-Aspen	–	48	57	63
Pinyon-juniper	–	58	73	80

Curve numbers were selected from a much larger set of options for local conditions and usually represent median conditions/designations when possible. Curve number values are for specified land use classes and hydrologic soil groups (larger values for CNs indicate faster runoff [44])

- Additional specifics of each site (such as soil parcel size, characteristics of impervious surfaces, climate, local condition of the surface, or hydrologic condition)

From such analyses, hydrologists can model the hydrologic behavior of landscapes to form the basis for maintaining water quality and management of runoff.

Two examples of using remotely sensed imagery to identify land use in hydrologic analyses are provided below.

Carlson [45] used Landsat 5 TM images to extract land use for the Spring Creek Watershed in central Pennsylvania (USA) for two separate years—1986 and 1996. He used these classified images in an urban growth model to project land use for 2025. Then, using CNs for each land use classification, he calculated actual runoff coefficients, urban flood ratios, and peak flow rates (using a 25-year storm) for each year—1986, 1996, and 2025.

In a second example, Melesse and Wang [46] used Landsat imagery to extract land use to document changes over time in comparing two different hydrologic models. For one study site—the Red River, North Dakota (USA)—Landsat images (1974–2001) were used to classify land cover to determine that urban extent had

increased by 54 %. Monthly precipitation data was then used to determine river discharge for two time frames, 1974–1992 and 1993–2002. The results showed a higher runoff to precipitation ratio for the later period. For their second study site, Simms Creek watershed in Florida (USA), they used Landsat imagery (2000 and 1984) to identify urban land use. This time, they used Manning's roughness coefficient, SCS-CNs, and simulated rainfall. They found more areas of 100 % impervious surfaces in 2000 than in 1984 and also found an increase in peak discharge and reduced time to peak in 2000 as compared to 1984.

5.2 Urban Land Use and Hydrology

Hydrology of urban areas is extremely complex [47]. Urban hydrology includes stormwater runoff from impervious surfaces, less evapotranspiration, less groundwater infiltration, treatment and distribution of potable water, and wastewater treatment and discharge. The initial focus of urban hydrology planning was identification of the most efficient ways to redirect stormwater flow in the shortest amount of time [48]. This strategy increased impervious surface area designations beyond those designed for roadways and buildings, and which channelized streams above and below the ground surface (Figs. 7 and 8).

Urbanization, therefore, often creates unfavorable hydrologic regimes characterized by rapid runoff, urban flooding, and reduced water quality. Urban planners, hydraulic engineers, and environmentalists agree that the spatial distribution of impervious surfaces has significant effects on water quality [49]. Thus, managing and reducing urbanization's impacts, identifying runoff volumes and rates, identifying the extent of contaminant sources, and tracking temporal changes in urban hydrology are first addressed by evaluating the extent of impervious surfaces [48].

One of the most extensive remote sensing analyses of impervious surfaces was completed by the Multi-Resolution Land Characteristics Consortium (MLRC) as

Fig. 7 Reedy Creek, Richmond, Virginia (USA). Impervious surfaces have replaced the natural stream channel and habitat. The channel was designed to remove stormwater from residential, commercial, and industrial land uses (Photo by the first author)

Fig. 8 Stroubles Creek, Blacksburg, Virginia (USA). The stream channel is redirected underground beneath the town's central business district and the university (Virginia Tech) campus (Photo by the first author)

part of the NLCD (mentioned in Sect. 2). This dataset is the most widely utilized in the United States for impervious surfaces and was developed to identify "percent developed imperviousness" [50]. The 2006 dataset was developed using regression tree software from both leaf-on and leaf-off Landsat images and images from National Oceanic and Atmospheric Administration's (NOAA) Defense Meteorological Satellite Program [50]. The National Land Cover Database Impervious Surfaces (NLCD IS) dataset is a continuous layer with a gradient of imperviousness from 0 to 100 %, whereby the value of each 30 m^2 pixel is the percent of impervious surfaces present within that pixel [21]. A new NLCD IS was released in April 2014 after a 2011 update and subsequent validation (for specifics on the update—see [19]). Figure 9 shows the extent of impervious surfaces for northwest Roanoke, Virginia (USA), in 2006 (a) and 2011 (b), and the areas of change between the two datasets (c).

Individual researchers have developed different methods for extracting impervious surfaces from remotely sensed imagery. As previously mentioned, pixel size varies from sensor to sensor, and within an urban environment, land use/land cover is extremely variable and creates a fine-scale heterogeneity in spectral values due to mixed pixels.[4] In most case studies, researchers are evaluating the extent or change in impervious surfaces and the resultant impact on water quantity and quality.

For example, one study evaluated changes in impervious surface cover in three sub-watersheds in Atlanta, Georgia (USA)—the Line, Flat, and Whitewater Creek sub-watersheds—to determine if increasing urbanization was impacting the freshwater mussel population [51]. Investigators used three Landsat images (1979, 1987, and 1997) to calculate changes in impervious surfaces. They also conducted four mussel inventories in the 1990s and used pre-1992 historical records to determine if any change occurred in mussel populations over time. They then used changes in

[4] A mixed pixel means that more than one land use/land cover type is present within the spatial extent of the pixel; as such the spectral value cannot be matched to one specific feature.

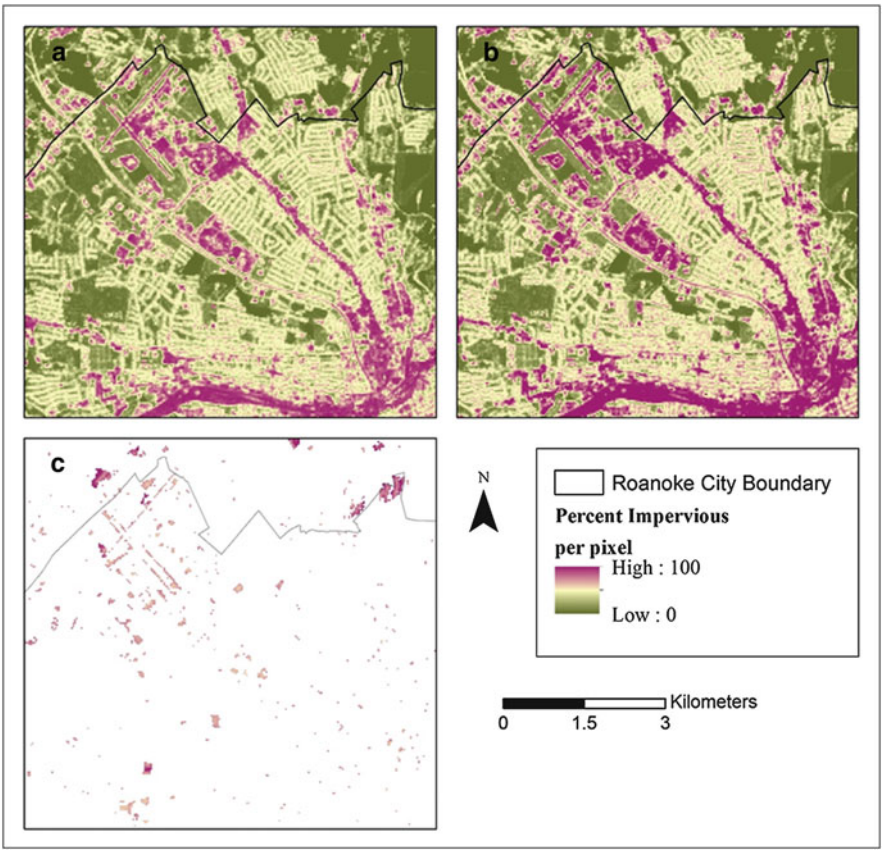

Fig. 9 The NLCD IS for Roanoke, Virginia (USA), and the per pixel impervious percent, from 0 to 100. (**a**) Impervious surfaces in 2006, (**b**) impervious surfaces in 2011, (**c**) the locations of change in per pixel percent imperviousness from 2006 to 2011. Source identified in text

impervious surfaces as an ecological indicator to assess the impacts on water quality and mussel populations. Their study of fourteen different sites determined that the sub-watershed with the highest rate of change in impervious surfaces also had the highest decline in mussel species diversity.

For the second example, researchers using Landsat 5 TM images from 1987, 1999, 2000, and 2007 analyzed impervious surface changes as an environmental health indicator for Lake Kasumigaura Basin, Japan (Lake Kasumigaura is the second largest lake in Japan) [52]. Their results showed that, by 1987, the watershed had already been impacted by land use change (all sub-basins had at least 10 % impervious surfaces). They also found that, by 2007, nine of the 22 sub-basins had greater than 25 % imperviousness and qualified as a degraded watershed. They concluded that if the trend continues, by 2017 more than 50 % of the Lake Kasumigaura Basin will fall into the degraded category.

6 Future Applications

Accurate and timely land use data, and land use change data, form important components of addressing land use planning and land use policy for the twenty-first century. Remote sensing provides one of the most important tools for acquiring and analyzing such data. In this context, we can expect changes to current strategies. Changes may promote integration of information and target acquisition of imagery to acquire land use data of smaller regions at greater spectral and spatial detail. For example, investigations of the urban heat island can benefit from integration of land use data with detailed thermal data to better define the role of land use in urban temperatures (e.g., see [53, 54]). Likewise, hyperspectral data, not normally employed for land use survey, can play a role in detecting regions where there is a legacy of contaminated soils, environmental hazards, and related risks to public health.

This section will explore three nascent technologies for remote sensing of land cover—Lidar, hyperspectral images, and unmanned aerial systems. The technologies, themselves, are not new, but researchers are exploring new applications in the context of land use/land cover assessment.

6.1 Lidar

Lidar (light detecting and ranging) is a form of active remote sensing. Lidar technology is based on applications of lasers (Fig. 10). Light is generated by the laser (1) which travels through fiber optic cables to a rotating mirror (2). The light is directed through bundled optical cables (3), which are twisted to provide a directed beam through lenses to the feature(s)/object(s) of interest. Reflected light is returned to the sensor (4), through a separate set of bundled fiber optic cables, to a second rotating mirror, and then transmitted (5) via fiber optic cables to the receiver (6). The transmission of the laser beam and the registration of the returns are controlled by the electronics.

The Lidar sensor records the time it takes for the returned (reflected) light to reach the sensor and translates the time delay as distance to the object. After processing of the returns, in aerial systems this distance then determines the height of that particular feature above ground. In ground-based (terrestrial) systems, the measurement is the distance from the sensor. Analysis of these distances, using appropriate software, results in surface elevation models, forest modeling, and other applications. The Lidar sensors are also equipped with geographic referencing equipment so the returns can be spatially located on the Earth's surface. Lidar sensors can be placed on aircraft, satellites, in ground-based vehicles, or on a stationary tripod on the ground (Fig. 11).

Because Lidar transmits light energy, as photons, the pulses penetrate even the smallest openings. The number of pulses per second and time delays between pulses

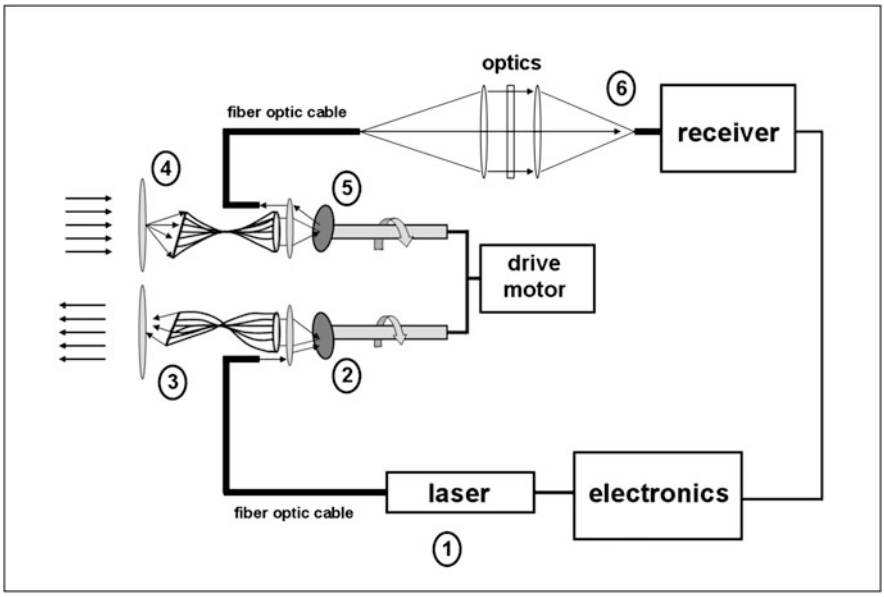

Fig. 10 A schematic of a Lidar scanner [28] (Permissions, Campbell_Guilford_11_August_2014)

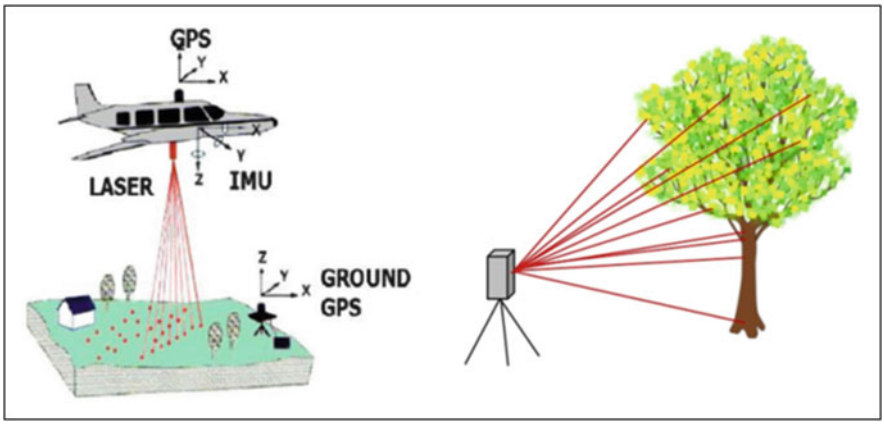

Fig. 11 Airborne Lidar system on the *left*. Terrestrial Lidar system on the *right*. *Sources*: left, USGS; right, second author

depend upon the design of each individual sensor. Sensors can be designed to either transmit light as waveform or as discrete returns. For discrete returns, sensors record the time and intensity of individual returns (from 1 to 5) of each pulse. The number of returns depends also on the complexity of the terrain, i.e., in an open area, only one return may be recorded after the pulse hits the ground, whereas a

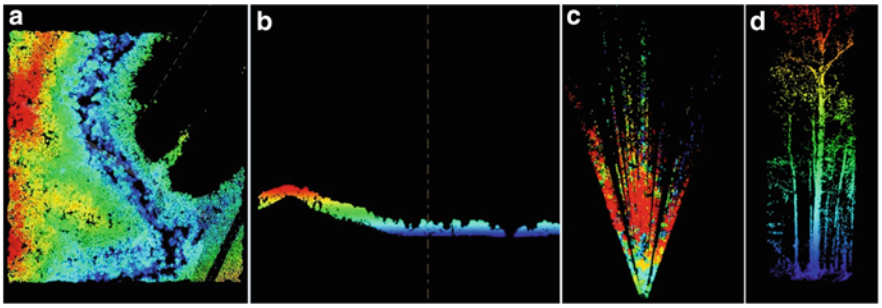

Fig. 12 Lidar point clouds over a Canadian region of the boreal forest. Images (**a**) and (**b**) are airborne Lidar, (**a**) point cloud from above and (**b**) point cloud as seen from the side. Images (**c**) and (**d**) are ground-based acquisition, (**c**) point cloud from above, and (**d**) point cloud as seen from the sensor's origin (*Credit*: First author using V. Thomas data)

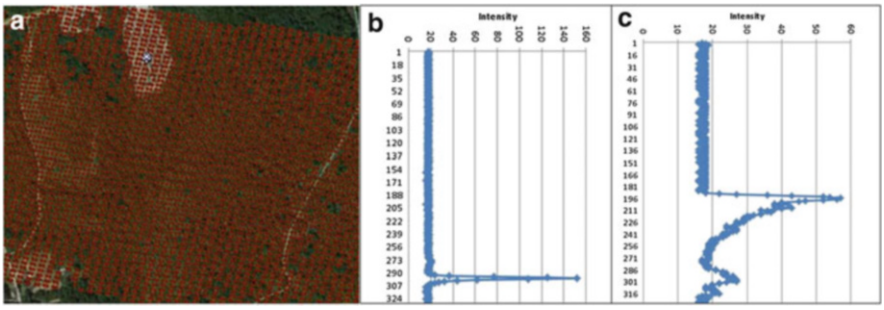

Fig. 13 LVIS waveform Lidar acquired over the Patuxent Watershed, Maryland, USA, (**a**) overhead view displays as a point cloud, (**b**) represents a pulse that hit a road, and (**c**) represents a pulse for a forested area (*Credit*: First author using data downloaded from LVIS website [55])

forest could have multiple returns after hitting leaves and branches of trees, underlying shrubs, and then the ground.

Figure 12 shows examples of discrete-return Lidar of a Canadian segment in the boreal forest. Images (a) and (b) are airborne Lidar, (a) point cloud from above and (b) point cloud as seen from the side. Gaps in the point cloud are areas where pulses were absorbed by water. Images (c) and (d) are ground-based Lidar acquisitions, (c) point cloud viewed from above, the energy originates from sensor (bottom of the image) and spreads out the farther it gets from the sensor. Gaps in this image are areas where the pulse hit an impenetrable object—tree trunks. Image (d) is the point cloud as seen from the ground-based Lidar sensor. The colors within each image represent differing elevations, as assigned by the software user.

For waveform Lidar, the sensor records the entire returned pulse; the image of the waveform is dependent on the terrain. The return's pulses appear as a point cloud when displayed with software (Fig. 13a), but when examining an individual pulse, the terrain is displayed as a wave with varying intensities, as portions of the

pulse returns to the sensor after hitting features on the surface of the Earth. Figure 13 shows the display of Laser Vegetation Imaging Sensor (LVIS) [55] waveform Lidar which was acquired over the Patuxent Watershed, Maryland (USA), in 2003 and 2004. Overhead view displayed as a point cloud (a). When viewing the data for a specific point, it displays as one wavelength—(b) represents a pulse that hit a road (a low, flat surface), and (c) represents a pulse for a forested area (several vegetation layers at different elevations).

Because of Lidar's ability to show differing heights, it is useful for three-dimensional modeling, for distinguishing between different tree species, to see into areas shadowed from nearby taller features/objects, and for providing fine-scale delineation between features (the latter is dependent upon the density of the point cloud). Some examples of applications of Lidar for land use or land cover identification include:

In coastal mapping for Camp Lejeune, North Carolina (USA), researchers fused elevations extracted from Lidar with IKONOS imagery to classify roads, water, marshes, roofs, trees, and sand [56]. Investigators opined that fine-scale classification was needed to distinguish features with similar spectral characteristics. They found that using Lidar surface elevations along with the multispectral imagery increased their accuracy for these classifications.

In applications to distinguish features within shadowed areas, researchers have used Lidar data with aerial images to extract land use for rural Spain [57]. These researchers found that the combination of these two types of data allowed extraction of land uses within shadowed areas. In a second study, researchers successfully used aerial photos and Lidar to identify land use in shadows within an urban area—the City of Alcalá, Madrid, Spain [58].

For another urban study, researchers used the combination of Lidar and aerial photos to enhance urban land use analysis for Austin, Texas (USA) [59]. Most specifically, they used a building detection algorithm to identify buildings from Lidar data and then used seven spatial characteristics of these buildings to help classify varying residential land uses.

In a watershed study, for the Garonne and Allier River watersheds in France, researchers used airborne Lidar and SPOT images for land cover classification [60]. Nine separate land cover types were classified—five different types of riparian forests, along with gravel, low vegetation, water, and bare earth.

6.2 Hyperspectral Imagery

Hyperspectral remote sensing is the collection of spectral data forming images with hundreds of bands, each band no more than a few nanometers wide. Hyperspectral data does not necessarily cover a broad region of the electromagnetic spectrum, but divides the spectrum into smaller segments. As an example, Fig. 14 shows differences in bandwidths and total wavelength coverage between images acquired with Landsats 7 and 8—multispectral sensors and Airborne Visible/Infrared Imaging

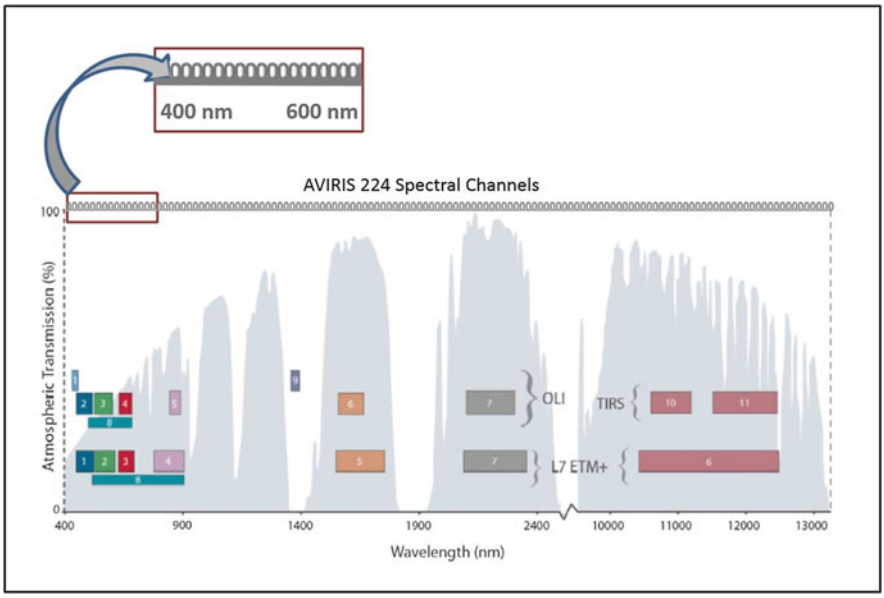

Fig. 14 Comparison of spectral channels for Landsat (multispectral, depicted by colored shapes, *bottom*) and AVIRIS (a hyperspectral sensor with 224 narrow channels, *top*). *Shaded patterns* represent wavelengths where the atmosphere will transmit electromagnetic radiation. Inset represents detail of hyperspectral channels (Landsat diagram credit: USGS; AVIRIS annotations by second author)

Spectrometer (AVIRIS) [61]—a hyperspectral sensor. Landsat acquires images using only 11 noncontiguous bands: nine bands between 0.43 and 2.29 μm and two bands from 10.6 to 12.51 μm. In contrast, AVIRIS acquires images in 224 contiguous bands from 380 to 2,500 nm (or 0.38–2.5 μm), each band only 10 nm wide.

Dividing the electromagnetic spectrum into smaller divisions allows for comparison of spectral properties gathered for specific features to match to spectra gathered in the field (many such spectra are already recorded in spectral libraries). Such comparisons permit detailed analyses of specific biophysical properties, which characterize land use or land cover to permit more precise identification. Hyperspectral evaluations have long been used by energy companies to identify landforms characteristic of mineral-rich regions. Some examples of using hyperspectral imagery in very detailed land use analyses are described below.

One study, of two different regions in Italy, analyzed Multispectral Visible and Infrared Imaging Spectrometer (MIVIS) imagery [62]. For the Tessera region near Venice, researchers differentiated several types of cultivated vegetation—soybeans, corn, sugar beets, alfalfa, wheat stubble, along with mixed woods, water, and urban. For the second location, the Pollino Mountain of Basilicata, they differentiated between several uncultivated vegetative areas—mixed beech forest, fir wood, pine wood, holm oak wood, along with high mountain prairies, xerophilous prairies, and barren and urban lands.

Two different studies in Greece used Hyperion imagery [63]. For an area north of Athens, Greece, researchers differentiated several forest types—conifers and broad-leaved—and identified transitional woodland/scrubland, heterogeneous agricultural areas, scrubland to herbaceous vegetation, sparsely vegetated areas, bare rocks, urban, burnt areas, and sea [64]. For the island of Crete, researchers differentiated between sparsely vegetated areas, permanent crops, heterogeneous agricultural areas, sclerophyllous vegetation, natural grasslands, bare land, and sea [65].

And, for a specific hydrologic analysis, a study for the Woluwe catchment in Belgium [66] analyzed CHRIS-Probe imagery [67]. Researchers differentiated eight land cover classes—forest, agriculture and grassland, water, bare soil, construction site, white buildings, city buildup, and dark buildings. In this study, the color of man-made objects can affect the accuracy of the land cover classification schemes and, as such, the resultant hydrologic model. These researchers used the land cover results as inputs into the WetSpass model to evaluate groundwater recharge.

6.3 Unmanned Aerial Systems

Unmanned aerial systems (UAS) are lightweight aerial vehicles (both fixed and rotary winged, commonly called drones) that carry cameras or other imaging sensors (either passive or active). The vehicles are piloted from a remote location and, typically, the ground-based pilot uses a wireless link to visually monitor the imaged area in real time. UAS origins are found from military uses (dating back to World War I) and from radio-controlled model airplanes used by hobbyists. Images acquired by UAS are saved on a storage device contained within the airborne vehicle and then downloaded after landing or streamed live to the remote operator. Figure 15 is an example of UAS using a fixed-wing aircraft, sensors are located on the wings of the aircraft.

Fig. 15 Fixed-wing UAV (Photo by the second author)

In some situations, UAS offer many advantages over other aerial (aircraft and satellite)-borne sensors:

- Rapid deployment [68], e.g., fine-scale inspection of hydrologic behavior of varied land use classes, associated storm drains, and drainage systems during and immediately after rainfall/snowmelt events.
- More economical mapping [69, 70], especially over small areas [71–73], e.g., spot updates of areas within broader surveys (such as the NLCD) believed to have changed since original compilation.
- Flown at very low altitudes (as low as a several hundred millimeters) and thus obtain extremely fine detail of a specific area [74].
- Used as a substitute for manual field data collection, such as animal surveys [48], situations harmful to human life [75], or validation of information derived from the coarser detail acquired from higher altitudes.
- Used to investigate problematic areas not clearly identifiable on conventional imagery, e.g., flown under cloud cover [70, 76] or in areas masked by shadows or large buildings.

Some specific examples of existing UAS remote sensing applications include:

- Slope and small stream mapping within Universiti Teknologi Malaysia precinct [71].
- Elephant population survey in Burkina Faso, Africa. Researchers found that UAVs were extremely useful in monitoring elephant populations, and of special importance, the elephants seemed to ignore the UAS as they were flying overhead [77].
- Marine mammal survey in Shark Bay, Western Australia. Researchers were able to identify several species of mammals, fly the UAS repeatedly within the same flight time over multiple altitudes, and repeat the flight pattern over the course of several consecutive days [69].
- Test flights over Mt. Etna, Italy. Researchers analyzed gas composition of volcanic plumes (where gaseous plumes are fatal to humans) [75].
- Orthoimages and digital surface model development at an 11 cm spatial resolution for an agricultural region in Córdoba, Spain. Researchers used the resultant images to classify two types of agricultural land uses—terraces and non-terraces [78].
- Rangeland vegetation species classification in southern New Mexico (USA) [79].

We anticipate that future applications of UAS technology in environmental and land use observations will be especially useful in urban areas, where the use of manned vehicles is restricted due to space and safety concerns, for imaging large-scale agricultural fields (where locating a small area of insect infestation may be difficult at higher altitudes), and in forest evaluations (where a tree canopy may prevent observation by sensors from above).

7 Conclusions

Monitoring the health of water—Earth's most precious resource—relies upon an astute understanding of the land surfaces which supply, transport, filter and store water, and regulate water temperatures as it flows to lakes, rivers, and aquifers. Remote sensing's use of airborne and satellite sensors forms the foundation of our ability to monitor large expanses of the Earth's surface and, in fine detail, to record variations in water resources.

These capabilities provide a better understanding of the impacts of human alterations to the Earth's surface upon water quality and water supply. The spatial perspective of remotely sensed imagery provides insight into interactions between varied land covers and land uses. It allows anticipating threats of hazardous materials for water quality, forecasting variations in water supply, and assessing diversions for agriculture, industry, recreation, and other confining impacts of hazardous spills along with mitigating such threats. Remote sensing technologies have significant potential for understanding climate change impacts.

The land use and land cover analyses outlined in this chapter provide some of the most important tools for sustaining, and improving, our ability to monitor the extent and quality of water resources. Employed in coordination with other capabilities described in this chapter, remote sensing can form a framework for understanding interrelationships between the many dimensions of water resources and for illuminating their spatial and temporal variations.

With continued launching of land observation satellites, our ability to map and monitor the Earth's changing surface will become more robust. As sensor technologies continue to change and additional analyses of existing imagery are identified, the ability to classify land cover and land use will be accomplished in even finer detail across broader regions, with greater flexibility in timing, and in acquiring sequential coverage. Greater computing power will allow us to store greater volumes of data over time, acquire larger volumes of data in the future, and fuse various data sources with imagery to perform superior evaluations of water quantity and quality. Looking forward with these advances, as outlined in Sect. 6, Lidar will enhance our ability to visualize and analyze in three dimensions, hyperspectral imagery will allow us to identify spectral signatures of features/objects at finer details, and unmanned aerial systems will be able to map land cover and identify land uses in areas previously not accessible to humans.

Acknowledgement We thank Dr. Valerie Thomas, Virginia Tech, Department of Forest Resources and Environmental Conservation, Blacksburg, Virginia, for providing the Lidar data mentioned in Sect. 6.1 Lidar.

References

1. Campbell JB (1997) Land use and cover inventory. In: Philipson WR (ed) Manual of photographic interpretation, 2nd edn. American Society of Photogrammetry and Remote Sensing, Bethesda, pp 335–364
2. Hooke RL, Martin-Duque JF (2012) Land transformation by humans: a review. GSA Today 22(12):4–10
3. United Nations (2005) Millennium ecosystem assessment. Island Press, Washington, DC, p 917
4. Younos T, Parece TE (2012) Water use and conservation. In: Stoltman J (ed) 21st century geography: a reference handbook. Sage, Los Angeles, pp 447–456
5. Deelstra T, Girardet H (2000) Urban agriculture and sustainable cities. In: Bakker N, Dubbeling M, Gündel S, Sabel-Koschella U, deZeeuw H (eds) Growing cities, growing food: urban agriculture on the policy agenda, a reader on urban agriculture, Deutsche Stiftung für Internationale Entwicklung, Zentralstelle für Ernährung und Landwirtschaft. Feldafing, Germany, pp 43–66
6. Pickett STA, Cadenasso ML, Grove JM, Nilon CH, Pouyat RV et al (2001) Urban ecological systems: linking terrestrial ecological, physical, and socioeconomic components of metropolitan areas. Annu Rev Ecol Syst 32:127–157
7. DeBusk K, Hunt WF, Hatch U, Sydorovych O (2010) Watershed retrofit and management evaluation for urban stormwater management systems in North Carolina. J Contemp Water Res Educ 146:64–74
8. Welker AL, Wadzuk BM, Traver RG (2010) Integration of education, scholarship, and service through stormwater management. J Contemp Water Res Educ 146:83–91
9. Slonecker ET, Jennings DB, Garofalo D (2001) Remote sensing of impervious surfaces: a review. Remote Sens Rev 20(3):227–255
10. Burton GA Jr, Pitt RE (2002) Stormwater effects handbook: a toolbox for watershed managers, scientists and engineers. Lewis, Washington, DC, p 929
11. Civco DJ, Hurd JD, Wilson EH, Arnold CL, Prisloe MP Jr (2002) Quantifying and describing urbanizing landscapes in the Northeast United States. Photogramm Eng Remote Sens 68(10): 1083–1090
12. Davis AP, Traver RG, Hunt WF (2010) Improving urban stormwater quality: applying fundamental principles. J Contemp Water Res Educ 146:3–10
13. Center for Watershed Protection (2003) Impacts of impervious cover on aquatic systems: watershed protection research monograph. Ellicott City, p 158
14. Bhaduri B, Minner M (2001) Long-term hydrologic impact of urbanization: a tale of two models. J Water Resour Plann Manage 127(1):13–19
15. United States Geological Survey (2012) The USGS. Land Cover Institute. NLCD 92 land cover class definitions. http://landcover.usgs.gov/classes.php. Accessed 5 Apr 2014
16. Hardy EE, Shelton RL (1970) Inventorying New York's land use and natural resources. NY Food Life Sci 3(4):4–7
17. Anderson JR, Hardy EE, Roach JT, Witmer RE (1976) A land use and land cover classification system for use with remote sensor data. Department of the Interior No. 964, Washington, DC
18. Multi-Resolution Land Characteristics Consortium (2006) National land cover database. http://www.mrlc.gov/finddata.php. Accessed 19 Dec 2012
19. Jin S, Yang L, Danielson P, Homer C, Fry J et al (2013) A comprehensive change detection method for updating the national land cover database to circa 2011. Remote Sens Environ 132: 159–175
20. Xian G, Homer C, Fry J (2009) Updating the 2001 National land cover database land cover classification to 2006 by using Landsat imagery change detection methods. Remote Sens Environ 113:1133–1147

21. Fry J, Xian G, Jin S, Dewitz J, Homer C et al (2011) Completion of the 2006 national land cover database for the conterminous United States. Photogramm Eng Remote Sens 77: 858–864
22. Government of Canada, Agriculture and Agri-Food Canada (2013) Canada land inventory. http://sis.agr.gc.ca/cansis/nsdb/cli/index.html. Accessed 19 May 2014
23. European Environment Agency (2013) Urban Atlas classification system (CORINE). http://www.eea.europa.eu/data-and-maps/data/urban-atlas. Accessed 19 May 2014
24. The Centre for Ecology and Hydrology (2007) United Kingdom land cover mapping. http://www.ceh.ac.uk/accessinglcmdata.html. Accessed 19 May 2014
25. United Kingdom Government (2005) Generalized land use data. http://data.gov.uk/dataset/land_use_statistics_generalised_land_use_database. Accessed 19 May 2014
26. United States Geological Survey (2012) Land cover institute. http://landcover.usgs.gov/landcoverdata.php. Accessed 19 May 2014
27. United Nations Global Land Cover Network (2013) Globcover-derived national land cover databases for Africa. http://www.glcn.org/databases/lc_gc-africa_en.jsp. Accessed 19 May 2014
28. Campbell JB, Wynne RH (2011) Introduction to remote sensing, 5th edn. Guilford, New York, 647
29. Kain RJP (2007) Maps and rural land management, early modern Europe. In: Woodward D (ed) The history of renaissance cartography: interpretive essays history of cartography 3 (Part 1). University of Chicago Press, Chicago, pp 705–718
30. Stamp LD (1948) The land of Britain: its use and misuse. Longmans, London, 507
31. Hudson GD (1936) The unit area method of land classification. Ann Assoc Am Geogr 26 (2):99–112
32. Boyce RR (2004) Geographers and the Tennessee valley authority. Geogr Rev 94(1):23–42
33. Garrett J, Waters D (1996) Preserving digital information. Report of the task force on archiving of digital information commissioned by The Commission on Preservation and Access and The Research Libraries Group. http://www.clir.org/pubs/reports/pub63watersgarrett.pdf
34. Virginia, Department of Environmental Quality (2010) GIS data sets. http://www.deqvirginiagovConnectWithDEQVEGISVEGISDatasetsaspx. Accessed 13 June 2012
35. Thrower NJ (1970) Land use in the Southwestern United States from Gemini and Apollo Imagery. Ann Assoc Am Geogr 60(1):208–209
36. United States Geological Survey (2014) Landsat missions. http://landsat.usgs.gov/. Accessed 1 Apr 2014
37. United States Geological Survey (2014) Landsat missions timeline. http://landsat.usgs.gov/about_mission_history.php. Accessed 7 May 2014
38. Satellite Imaging Corporation (2014) IKONOS satellite. http://www.satimagingcorp.com/gallery-ikonos.html. Accessed 10 May 2014
39. Airbus Defense and Space (2014) Spot satellite imagery. http://www.astrium-geo.com/en/143-spot-satellite-imagery/. Accessed 15 May 2014
40. China-Brazil Earth Resources Satellite (2011). CBERS satellite. http://www.cbers.inpe.br/ingles/satellites/history.php. Accessed 15 May 2014
41. Elecnor (2014) Deimos imaging. http://www.deimos-imaging.com/. Accessed 15 May 2014
42. United States National Aeronautics and Space Administration (2014) MODIS Web. http://modis.gsfc.nasa.gov/. Accessed 15 May 2014
43. United States Department of Agriculture (1986) Urban hydrology for small watersheds. Technical Release 55 (TR-55) 2nd edn, Natural Resources Conservation Service, Conservation Engineering Division, Washington, DC, p 164
44. United States Department of Agriculture (2007) Hydrologic soil groups. Chapter 7, National Engineering Handbook. (Part 630, Hydrology). Natural Resources Conservation Service, Conservation Engineering Division, Washington, DC, p 14
45. Carlson TN (2004) Analysis and prediction of surface runoff in an urbanizing watershed using satellite imagery. J Amer Water Resour Assoc 40(4):1087–1098

46. Melesse A, Wang X (2007) Impervious surface area dynamics and storm runoff response. In: Weng Q (ed) Remote sensing of impervious surfaces. CRC, Boca Raton, pp 369–386
47. McPherson MB, Schneider WJ (1974) Problems in modeling urban watersheds. Water Resour Res 10(3):434–440
48. Carlson TN (2007) Impervious surface area and its effect on water abundance and water quality. In: Weng Q (ed) Remote sensing of impervious surfaces. CRC, Boca Raton, pp 353–367
49. Brabec E, Schulte S, Richards PL (2002) Impervious surfaces and water quality: a review of current literature and its implications for watershed planning. J Plan Lit 16(4):499–514
50. Multi-Resolution Land Characteristics Consortium (2006) National land cover database percent developed imperviousness. http://www.mrlc.gov/nlcd06_data.php. Accessed 19 Dec 2012
51. Gillies RR, Brim Box J, Symanzik J, Rodemaker EJ (2003) Effects of urbanization on the aquatic fauna of the Line Creek watershed, Atlanta—a satellite perspective. Remote Sens Environ 86(3):411–422
52. Yang F, Matsushita B, Fukushima T (2010) A pre-screened and normalized multiple end-member spectral mixture analysis for mapping impervious surface area in Lake Kasumigaura Basin, Japan. ISPRS J Photogramm Remote Sens 65(5):479–490
53. Ruddell BL, Chow WTL (2014) Microclimate analysis of observations in a master-planned residential community in Arizona. In: 94th American meteorological society annual meeting, Atlanta, 2–6 Feb 2014
54. Parece TE, Campbell JB, Carroll D (2014) Assessing variations in urban heat island effects within Roanoke, Virginia. In: American society of photogrammetry and remote sensing annual conference. Louisville, 23–28 Mar 2014
55. United States National Aeronautics and Space Administration (2014) About LVIS. http://lvis.gsfc.nasa.gov. Accessed 24 May 2014
56. Lee DS, Shan J (2003) Combining Lidar elevation data and IKONOS multispectral imagery for coastal classification mapping. Mar Geod 26(1/2):117–127
57. Buján S, González-Ferreiro E, Reyes-Bueno F, Barreiro-Fernández L, Crecente R et al (2012) Land use classification from Lidar data and ortho-images in a rural area. Photogramm Rec 27(140):401–422
58. de Agirre AM, Malpica JA (2012) Detecting shadows in a segmented land use land cover image with LIDAR data. IGARSS 33rd Canadian symposium on remote sensing, Munich, 22–27 July 2012, pp 5458–5461
59. Meng X, Currit N, Wang L, Yang X (2010) Object-oriented residential building land-use mapping using lidar and aerial photographs. American society of photogrammetry and remote sensing 2010 annual conference, San Diego, 26–30 Apr 2010
60. Antonarakis A, Richards K, Brasington J (2008) Object-based land cover classification using airborne LiDAR. Remote Sens Environ 112(6):2988–2998
61. NASA Jet Propulsion Laboratory (2014) Airborne visible/infrared imaging spectrometer. http://aviris.jpl.nasa.gov/. Accessed 5 June 2014
62. Amato U, Antoniadis A, Carfora MF, Colandrea P, Cuomo V et al (2013) Statistical classification for assessing PRISMA hyperspectral potential for agricultural land use. IEEE J Sel Topics Appl Earth Observ Remote Sens 6(2):615–625
63. United States Geological Survey (2011) Earth observing, sensors—hyperion. http://eo1.usgs.gov/sensors/hyperion. Accessed 6 June 2014
64. Petropoulos GP, Arvanitis K, Sigrimis N (2012) Hyperion hyperspectral imagery analysis combined with machine learning classifiers for land use/cover mapping. Exp Syst Appl 39(3):3800–3809
65. Petropoulos GP, Kalaitzidis C, Prasad Vadrevu K (2012) Support vector machines and object-based classification for obtaining land-use/cover cartography from Hyperion hyperspectral imagery. Comput Geosci 41:99–107
66. Ampe EM, Vanhamel I, Salvadore E, Jef D, Bashir I et al (2012) Impact of urban land-cover classification on groundwater recharge uncertainty. IEEE J Sel Topics Appl Earth Observ Remote Sens 5(6):1859–1867

67. European Space Agency (2014) Earth online. https://earth.esa.int/web/guest/-/proba-chris-level-1a-1488. Accessed 18 June 2014
68. Berni J, Zarco-Tejada PJ, Suarez L, Fereres E (2009) Thermal and narrowband multispectral remote sensing for vegetation monitoring from an unmanned aerial vehicle. IEEE Trans Geosci Remote Sens 47(3):722–738
69. Hodgson A, Kelly N, Peel D (2013) Unmanned aerial vehicles (UAVs) for surveying Marine Fauna: a Dugong case study. PLoS One 8:1–15
70. Herwitz SR, Johnson LF, Dunagan SE, Higgins RG, Sullivan DV et al (2004) Imaging from an unmanned aerial vehicle: agricultural surveillance and decision support. Comput Electron Agric 44(1):49–61
71. Ahmad A, Tahar KN, Udin WS, Hashim KA, Darwin N, et al (2013) Digital aerial imagery of unmanned aerial vehicle for various applications, Penang, 29 Nov–1 Dec 2013, pp 535–540
72. Primicerio J, Di Gennaro S, Fiorillo E, Genesio L, Lugato E et al (2012) A flexible unmanned aerial vehicle for precision agriculture. Precis Agric 13:517–523
73. Shim DH, Han J, Yeo H-T (2009) A development of unmanned helicopters for industrial applications. In: Oh P, Piegl L, Valavanis K (eds) Unmanned aircraft systems. Springer, The Netherlands, pp 407–421
74. Anderson K, Gaston KJ (2013) Lightweight unmanned aerial vehicles will revolutionize spatial ecology. Front Ecol Environ 11(3):138–146
75. Astuti G, Giudice G, Longo D, Melita CD, Muscato G et al (2009) An overview of the "Volcan Project": an UAS for exploration of volcanic environments. In: Oh P, Piegl L, Valavanis K (eds) Unmanned aircraft systems. Springer, The Netherlands, pp 471–494
76. Lu H, Li Y-S, Lin X-C (2011) Classification of high resolution imagery by unmanned aerial vehicle. Sci Surv Mapp 36(6):106–108
77. Vermeulen C, Lejeune P, Lisein J, Sawadogo P, Bouché P (2013) Unmanned aerial survey of elephants. PLoS One 8:1–7
78. Diaz-Varela RA, Zarco-Tejada PJ, Angileri V, Loudjani P (2014) Automatic identification of agricultural terraces through object-oriented analysis of very high resolution DSMs and multispectral imagery obtained from an unmanned aerial vehicle. J Environ Manage 134: 117–126
79. Laliberte AS, Goforth MA, Steele CM, Rango A (2011) Multispectral remote sensing from unmanned aircraft: image processing workflows and applications for rangeland environments. Remote Sens 3:2529–2551

Using Remote Sensing to Map and Monitor Water Resources in Arid and Semiarid Regions

Victor Klemas and Aline Pieterse

Contents

Abstract Life on Earth depends on water. Yet water resources are severely stressed by the rapid growth of the human population and activities. In arid environments the exploration and monitoring of water resources is a prerequisite for water accessibility and rational use and management. To survey large arid areas for water, conventional land-based techniques must be complemented by using satellite and airborne remote sensors. Surface water systems can be mapped using multispectral and radar sensors; soil moisture in the unsaturated zone can be remotely sensed with microwave radiometers using indirect indicators, such as

V. Klemas (✉)
School of Marine Science and Policy, University of Delaware, Newark, DE, USA
e-mail: klemas@udel.edu

A. Pieterse
Department of Geological Sciences, University of Delaware, Newark, DE, USA

T. Younos, T.E. Parece (eds.), *Advances in Watershed Science and Assessment*, The Handbook of Environmental Chemistry 33,
DOI 10.1007/978-3-319-14212-8_2

microwave emissivity; freshwater wetlands can be mapped using multispectral cameras; and freshwater springs can be detected using thermal infrared radiometers. Satellite remote sensors and satellite gravitational surveys can be used in combination with ancillary data analysis to infer groundwater behavior from surface expressions and to estimate groundwater aquifer storage. This chapter provides an overview of satellite and airborne remote sensing techniques for managing water resources and monitoring drought in arid and semiarid regions.

Keywords Groundwater exploration • Remote sensing springs • Soil moisture sensing • Water remote sensing • Wetland mapping

1 Introduction

Only a small fraction of the Earth's water is available as freshwater, a key resource in many economic activities ranging from agriculture to industrial production. At present, water resources are severely stressed and particularly scarce in arid regions of the world. In many arid and semiarid regions, water shortage is a major obstacle to sustainable development and poverty alleviation and the cause of serious conflicts between some countries. Water shortage in arid regions can be further aggravated by the global climate change that is predicted to severely impact these regions. Thus, exploration, mapping, and monitoring of water resources are a prerequisite for the availability, accessibility, fair utilization, and rational management of water resources in arid and semiarid regions [1–3].

Since water availability in arid regions is both sporadic and variable in intensity, traditional water resources assessment relying on ground-based techniques and data can often lead to poor estimates of key drivers of hydrologic processes [4]. For example, most ground-based rain gauge networks are inadequate to capture spatial and temporal heterogeneity of precipitation [5]. Therefore, conventional hydrological measurements combined with satellite and airborne remote sensors can be useful and cost-effective and for mapping and monitoring water resources. Furthermore, remotely sensed data can be used in large-scale geologic/hydrologic models to simulate hydrologic processes, quantify the spatial and temporal water distribution, and prepare maps of groundwater potential zones [3, 6–8].

A key to remote sensing of groundwater is the realization that shallow groundwater flow is often driven by surface forcing parameterized by geologic properties inferred from surface data [9]. Thus, satellite data is especially effective if it is used with ancillary data analysis to infer groundwater behavior from surface expressions. Groundwater and surface water are closely connected in both arid and humid environments [10]. In arid environments, streams and lakes can be separated from the water table by a large vadose zone. During wet seasons, groundwater may become perched below surface water and then dissipate during dry seasons. Because water typically controls the growth of vegetation in arid areas, an

outcropping of groundwater can usually be identified in remotely sensed images by its vegetative spectral signature. The problem in arid environments is that much of the groundwater flow emerging at the surface is intermittent. Therefore, time series of ground data and multiple remotely sensed images are required to distinguish steady groundwater flow from storm-driven or seasonal behavior [9].

Topographically driven groundwater flow implies that groundwater will be recharged over broad upland areas and discharged at relatively focused lowlands as surface water. In arid areas, evapotranspiration may also play a role. From a remote sensing point of view, water can thus be present in many forms, where each requires a different remote sensing approach in order to be detected and mapped.

Exposed surface water can be mapped using visible, near-infrared and radar imagers. Soil moisture is best measured with microwave radiometers or radar. Vegetation indicating the presence of springs can be mapped with multispectral imagers, while freshwater springs entering water bodies can be detected with thermal infrared (TIR) sensors. Gravitational surveys from satellites have been used to estimate groundwater aquifer storage.

The objective of this chapter is to review the most effective remote sensing techniques for detecting and mapping water resources in arid and semiarid environments. This chapter has been divided into sections addressing application of remote sensing technologies to detecting exposed surface waters, groundwater, soil moisture, freshwater springs, wetlands, and monitoring drought and potential drought conditions in arid and semiarid regions.

2 Identification and Mapping of Arid and Semiarid Regions

Identification and mapping of arid and semiarid regions is a prerequisite for water availability, accessibility, fair utilization, and rational management. Gamo et al. [11] developed a method for classifying arid lands. The objective of that project was to prepare internally consistent maps of arid regions on a global scale in an effort to understand the conditions of existing arid regions, especially deserts and soil degradation areas. They delimited arid regions on a global scale by combining climate data, i.e., aridity index (AI), and vegetation data, i.e., vegetation index (VI). The AI shows the degree of climatic dryness and the VI denotes the abundance of vegetation. The annual AI was estimated by the ratio of mean annual precipitation to mean annual potential evapotranspiration, using the Thornthwaite method. The VI was derived on a global scale in real time from satellite remote sensing images produced by the NASA/NOAA Advanced Very High Resolution Radiometer (AVHRR) visible and near-infrared bands. The long-term mean of yearly maximum normalized difference vegetation index (NDVI) (ymx) was used as an indicator of vegetation condition.

Arid regions of the world were classified by Gamo et al. [11] into four categories:

- Category A, severe deserts, where both aridity and vegetation indices are very small
- Category G, semiarid regions, where the VI is proportionally related to the AI
- Category I, irrigated areas and oases, where the vegetation is relatively abundant despite severe dryness
- Category S, soil degradation areas, where the vegetation is poor despite relatively humid conditions

The standard deviation of NDVI (ymx) is very small for severe deserts and much larger in semiarid areas. Thus, the Sahara desert (Category A) was clearly distinguished from the Sahel; the latter belongs to Category G and drought occurs frequently there between rainy seasons. Desert areas were further classified into severe deserts (Category A), grassland deserts (Category G), and soil degradation deserts (Category S). As a result, a map was produced showing the global distribution of arid regions using these unified criteria with both physical and biological meaning [11].

3 Detecting and Mapping Inland Surface Waters

Surface waters include streams, rivers, ponds, lakes, and other exposed inland water bodies. Remote sensing provides an effective means for mapping the location, extent, and changes of surface water bodies over time [12, 13]. For example, remotely sensed seasonal changes of lake water extent can be combined with available topographic data to estimate water volumetric storage changes and thus more accurately manage water resources [14–16].

A variety of passive and active remote sensors with visible and microwave bands can be used to estimate inundation area and delineate water boundaries [17]. The land–water boundary can be easily defined using the near-infrared radiation (NIR) region of the electromagnetic spectrum. Land appears much brighter than water because water strongly absorbs the NIR. Most multispectral and hyperspectral sensors include suitable NIR bands. Moderate resolution satellites, such as Landsat Thematic Mapper (TM) and SPOT (Satellite Pour l'Observation de la Terre), have been used to study surface water bodies and determine their extent in arid and semiarid regions. For example, Sharma et al. [2] used the Landsat TM to map small surface water bodies in arid areas of India and compared them to Survey of India topographical maps. They found major reductions in areal extent of the water bodies over 28 years, mainly due to cultivation and urbanization in these desert regions. Data from high-resolution commercial satellites, such as IKONOS and QuickBird, have been used to produce more detailed maps of small freshwater areas. Figure 1 shows a high-resolution NIR IKONOS satellite image, containing bogs, lakes, and wetlands in northern Wisconsin, USA.

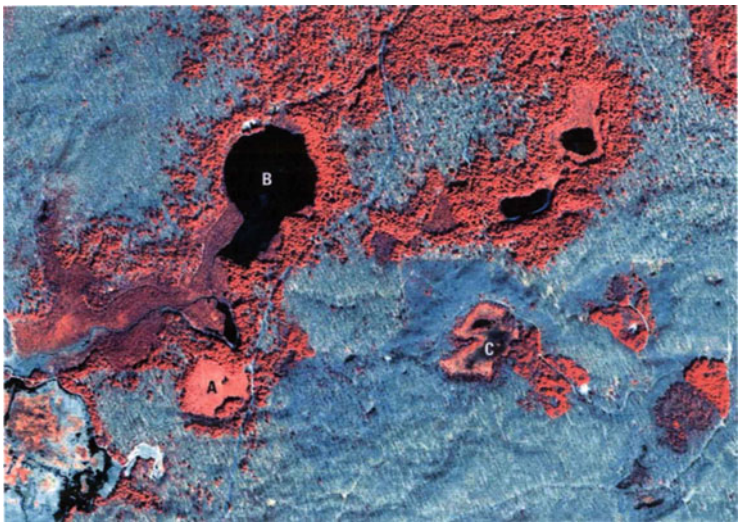

Fig. 1 High-resolution near-infrared IKONOS satellite image of bogs (**a**), lakes (**b**), and wetlands (**c**) of northern Wisconsin, USA, spring 2005. Image courtesy of Space Imaging Corp

In African arid and semiarid regions, rainfall amounts vary drastically within a season and between seasons; as such, surface water availability can radically change. Detecting the change when surface water sites are filled by rainfalls and when they are drained out is key information for the assessment of water availability and environmental conditions, providing alerts on vector-/insect-borne diseases or managing human activities. Combal et al. [18] used the VEGETATION instrument onboard SPOT satellites to detect surface water, using the NIR at a resolution of 1 km over Africa. The surface water was detected every 10 days and broadcast to users by means of the EUMETCast broadcasting system operated by EUMETSAT. EUMETCast is a multiservice dissemination system that uses geostationary satellites to multi-cast data to a wide user community. The detection of surface water coupled with the broadcasting system provided the capacity for operational monitoring of surface water at continental to regional scales. The continuity of surface observations allowed for seasonal assessment of water availability [18].

Where clouds, trees, and other vegetation obscure the water surface, synthetic aperture radar (SAR) can be used to detect surface water. SAR can penetrate clouds to detect standing water through emergent aquatic plants and forest canopies [19]. Water bodies scatter the pulses emitted by radars. Since most SAR sensors use a side-looking antenna, open waters appear dark as the radar pulses are not returned (backscattered) to the radar antenna. If a wet surface is covered by vegetation, the radar pulse bounces between the vegetation and wet surface, and the backscattered return signal will be stronger than if the surface would have been dry [20]. Table 1 shows the characteristics of some typical SAR satellites. Note the good ground resolution and different polarization features. Some newer satellites are also operating in the L-band (15–30 cm) and X-band (2.4–3.75 cm).

Table 1 Overview of synthetic aperture radar (SAR) satellites

Satellite	ERS-1 and ERS-2	RADARSAT	Envisat
Sensor	SAR	SAR	ASAR
Launch dates (s)	July 17, 1991	Nov 4, 1995	Mar 1, 2002
	Apr 20, 1995		
Frequency	5.3 GHz	5.3 GHz	5.3 GHz
Wavelength	5.6 cm	5.6 cm	5.6 cm
Polarization	VV	HH	VV, HH, VH, HV
Incidence angle	20–26°	10–59°	15–45°
Swath width	100 km	50–500 km	100–405 km
Ground resolution	25 × 25 m	8 × 100 m	25 × 25 m

Radar altimetry has been used to obtain point measurements of water surface elevation in order to determine volumetric water storage [16, 21]. For example, Cazenave et al. [22] and Kostianoy et al. [23] report using satellite altimetry data to investigate seasonal, interannual, and space-time variability of the level of water bodies in arid areas of Turkmenistan, including the Caspian Sea water level. They were able to monitor the water level (filling) of the Altyn Asyr Lake since its construction began in July 2009. The synergistic application of combined radar and optical remote sensing was shown to be particularly effective for the analysis of the morphometric characteristics and sea (lake) level of these water bodies.

Airborne bathymetric Lidar has also been used to map water surfaces and to estimate the water volume of lakes by producing elevation models for the water surface and the lake bottom [24, 25]. Some airborne Lidar systems combine near-infrared wavelengths for topography and green wavelengths for bathymetry, allowing water depths to be determined with accuracies of about 10 cm. Bathymetric Lidars can penetrate down to about the equivalent of three Secchi depths and provide bathymetric data down to 6 m depths in lakes of low turbidity.

4 Detecting Subsurface Waters

Subsurface water consists of soil moisture (unsaturated or vadose zone) and groundwater aquifer (saturated zone).

4.1 Determining Soil Moisture

Soil moisture is an indicator of subsurface water that is found in the unsaturated zone above the water table. Soil moisture has an important role in the calculation of water and energy budgets needed for climate studies. Soil moisture improves meteorological and climate predictions and is important for assessing agricultural

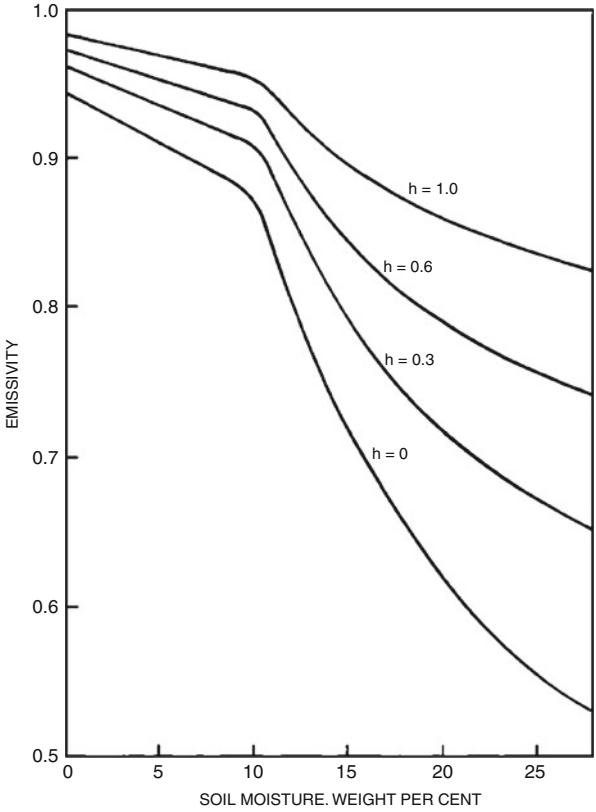

Fig. 2 Calculated emissivity for a soil using several values of the roughness parameter k. Reprinted from Choudhury et al. [28] with permission from John Wiley and Sons

conditions, irrigation management, and studies of desertification, all of which are especially important in arid and semiarid regions.

Soil moisture also plays a significant role in forecasting arid region droughts. In dry regions of the world, like the Sahel, cloud formation and the rate and distribution of precipitation are partly controlled by the wetness of the soil [26]. The wetness of the terrain influences how much energy it absorbs from the Sun, which in turn affects atmospheric convection, cloud formation, and precipitation. This relationship creates a feedback loop, where rainfall affects the chances of additional precipitation in the days that follow. Thus, a positive feedback would promote floods and drought.

Because microwave radiation is sensitive to soil moisture, microwave remote sensors provide a unique capability for mapping soil moisture over large areas of the Earth's land surface [27]. Both active radars and passive microwave systems can sense soil moisture. Microwave radiometers detect the brightness temperature, which equals the product of the emissivity and the surface temperature of the soil. At frequencies below 5 GHz the emissivity of soils varies over a wide range from about 0.6 for wet, saturated soils to greater than 0.9 for dry soils. Figure 2 shows the strong relationship between soil moisture and emissivity in the 21 cm microwave

band for different values of soil roughness. The microwave radiometer measurement of soil moisture is also affected by the density of any vegetative cover, including grass, shrubs, and trees.

Radars measure the backscattering coefficient, which is a measure of reflectivity. Passive and active methods are related through Kirchhoff's law, $e = 1-r$, where e is the emissivity and r is the reflectance. Since an increase in soil moisture decreases its emissivity, it simultaneously increases the radar reflectivity or backscatter. Radar is more sensitive to surface roughness and dense vegetation structure than optical sensors but is less affected by surface temperature and provides good spatial resolution.

Early remote sensing of soil moisture was performed from aircraft [29–31]. More recently satellite sensors are numerous and able to provide information on surface soil moisture. Remotely sensed surface soil moisture data sets have been acquired with scatterometer observations of the Active Microwave Instrument (AMI) on the European Remote Sensing satellites (ERS-AMI) and the Advanced Scatterometer (ASCAT) on MetOp. Multifrequency radiometers have also been used, including the Advanced Scanning Microwave Radiometer (AMSR-E), the Scanning Multichannel Microwave Radiometer (SMMR), and the Microwave Imager (TMI) on the Tropical Rainfall Measuring Mission (TRMM). Yet despite the importance of soil moisture information, until recently there have been no projects specifically dedicated to measuring soil moisture globally with adequate temporal or spatial sampling [32–34].

With the launch of microwave radiometers on the Soil Moisture and Ocean Salinity (SMOS) and AQUA satellites, soil moisture (along with other parameters such as sea surface salinity) can now be obtained nearly continuously over a large fraction of the Earth's surface [35, 36]. AQUA is a sister satellite to Terra, the first of the large Earth observation satellites (EOS), launched in 1999 to monitor the "health of the planet," with Terra emphasizing land and AQUA emphasizing water. AQUA and SMOS data are providing information on the moisture content of the soil, vegetation conditions (heavily dependent on water), and on many other aspects of the Earth's climate system.

The L-band 2-D interferometric radiometer on SMOS receives the radiation emitted from the Earth's surface, which then can be related to the moisture content in the first few centimeters of soil over land [36–39]. Microwave measurements are largely unaffected by solar illumination and cloud cover, yet accurate soil moisture estimates are still limited to regions that have either bare soils or low amounts of vegetation cover. In the absence of significant vegetation cover, soil moisture dominates the signal received by a microwave radiometer [40, 41]. The low-frequency microwave range of 1–3 GHz (10–30 cm wavelength) is considered best for soil moisture sensing due to its sensitivity to soil moisture, reduced atmospheric attenuation, and greater vegetation penetration at these longer wavelengths. Since mid-July 2010, SMOS has been delivering images of "brightness temperature" to the science community, which are used to produce global maps of soil moisture every 3 days (along with maps of ocean salinity) averaged over 30 days.

The combined use of satellite data from multispectral and TIR radiometers has also shown promise for the retrieval of latent and sensible heat, as well as surface soil moisture variations. These data are important for monitoring plant growth and productivity, irrigation management, modeling atmospheric and hydrological cycles, and improving the accuracy of weather forecast models.

Blending optical data, passive microwave emissivity, and radar backscatter, the Global Inundation Extent from Multi-Satellite (GIEMS) data set is one of the most comprehensive data sets of surface wetness [12, 13]. GIEMS is a coarse scale data set with about 25 km spatial resolution and monthly time-steps available for almost two decades. Recently both high-resolution SAR data [42] and optical images from the MODIS imagery [43] have been used for downscaling GIEMS.

Detecting water in arid regions by means of soil moisture remote sensing still faces many challenges. The spatial resolution over land needs to be improved. As stated earlier, accurate soil moisture estimates are limited to regions that have either bare soils or low amounts of vegetation cover. Better corrections for surface roughness, vegetation cover, soil temperature, and topography must be devised. Until recently, the moisture in only the top few centimeters of the soil could be detected. The Soil Moisture Active Passive (SMAP) satellite mission, planned for the 2015–2020 time frame, is designed to use advanced modeling and data assimilation to provide data on deeper root-zone soil moisture and net ecosystem exchange of carbon [44, 45].

4.2 Detecting Groundwater

Groundwater accounts for about 98 % of the total freshwater budget on Earth. The remaining 2 % is divided between rivers, lakes, freshwater wetlands, and moisture in the atmosphere. Groundwater supplies about 40 % of the drinking water in the USA and 70 % in China and is the main source of domestic water supply in most European countries [46]. Groundwater exists within the matrix of sedimentary rocks, occupying pore spaces between sediment grains, housed within rock fractures, or held within large underground caverns [10, 47].

Shallow-layer groundwater within a few centimeters of the surface may be detected by SAR microwave radiometry or TIR imagery in certain geologic settings [48]. However, groundwater aquifers located deep below the land surface cannot be detected directly by electromagnetic remote sensors and are usually surveyed with gravitational techniques. Groundwater discharges to the surface via springs that feed rivers, lakes, and wetlands and can be mapped by many different remote sensing systems, as described in later sections of this chapter. In arid environments, the surface discharge of groundwater may also be indirectly detected by remote sensing, if the discharge produces areas of unusually dense vegetation [49].

High-resolution gravitational surveys have been used to estimate groundwater storage [50, 51]. However, gravitational instruments have no vertical resolving power, so that measurement of subsurface water pools requires removing the

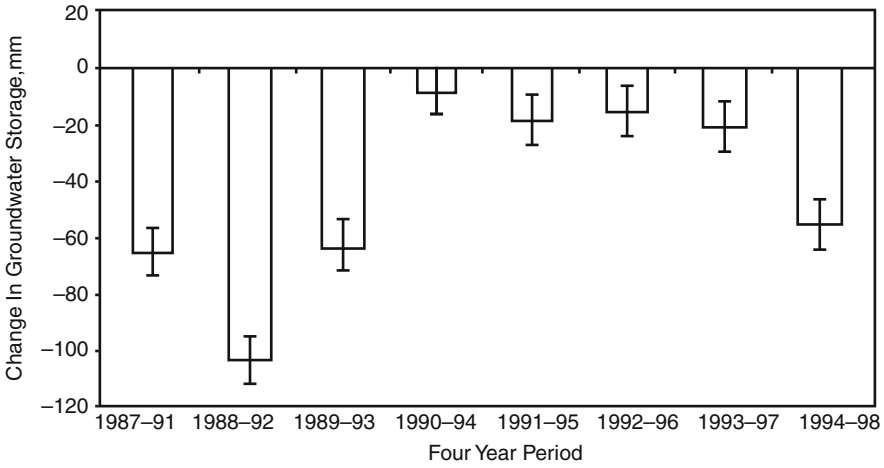

Fig. 3 Four-year changes in the central USA. High Plains aquifer water storage with error bars that represent the total uncertainty in GRACE-derived estimates. Reprinted from Rodell and Famiglietti [54] with permission from Elsevier

influence of water stored in the unsaturated soil zone. For aerial surveys, corrections must also be made for water stored in vegetation. For satellite gravity surveys, one must correct the water effects of the atmosphere in addition to the vegetation.

At present, there is only one satellite mission that can directly estimate the quantity of groundwater stored deep beneath the Earth's surface. It accomplishes this by measuring the Earth's gravity field which is influenced by the quantity of groundwater below the surface. As groundwater is consumed or recharged, water-induced gravity anomalies change through time. The Gravity Recovery and Climate Experiment (GRACE) mission, launched in 2002, consists of two identical satellites orbiting in unison at the same altitude but with a separation of 220 km. The two satellites monitor the relative position of each other using microwave-ranging instruments. As they pass over a gravity anomaly, the leading spacecraft approaches and speeds up due to higher angular momentum. This causes the two satellites to increase separation. After the first spacecraft passes the anomaly, it slows down again; meanwhile the following satellite accelerates, then decelerates over the same point. By recording satellite separation, gravity is mapped; cycles of growing/shrinking separation indicate the size and strength of the gravity anomalies, from which the quantity of groundwater can be estimated [49].

Due to atmospheric variability and observational errors, accurate estimates of water mass can only be obtained for regions that are several hundreds of kilometers or more in scale [52]. Thus, estimating water storage changes in large aquifer systems is currently feasible [53]. Rodell and Famiglietti [54] used computer simulations and GRACE performance parameters to show that groundwater storage changes as small as 9 mm could be measured in the US High Plains aquifer system. As shown in Fig. 3, in the High Plains the magnitude of annual groundwater storage changes averaged 19.8 mm between 1987 and 1998. They expected that the

uncertainty in deriving estimates of aquifer storage changes from GRACE observations would arise mainly from the removal, via land surface modeling, of the effects of soil moisture changes from the gravity signal. Rodell and Famiglietti [54] were predicting the total uncertainty to be about 8.7 mm. Comparing the 4-year groundwater storage change bars with the estimated GRACE uncertainty bars in Fig. 3, one can see that such estimates would have been useful for tracking groundwater changes in the High Plains aquifer during most 4-year periods.

Yirdaw et al. [55] investigated the Canadian Prairie drought by employing total water storage anomalies obtained from the GRACE remote sensing satellite mission. The obtained GRACE-based total water storages were validated using storages estimated from the atmospheric-based water balance P-E (precipitation-evaporation) computation in conjunction with measured streamflow records. The results from their study corroborated the potential of the GRACE-based technique as a useful tool for the characterization of the 2002/2003 Canadian Prairie droughts.

Li et al. [56] assimilated anomalies of terrestrial water storage (TWS) observed by the GRACE satellite mission into the NASA Catchment land surface model in western and central Europe for a 7-year period. GRACE data assimilation led to improved runoff estimates (in temporal correlation and root mean square error) even in basins smaller than the effective resolution of GRACE. Signals of drought in GRACE TWS correlated well with the MODIS NDVI in most areas. Although they detected the same droughts during warm seasons, drought signatures in GRACE-derived TWS exhibited greater persistence than those in NDVI throughout all seasons, in part due to limitations associated with the seasonality of vegetation [56].

To derive estimates of aquifer storage changes from GRACE observations, one faces the challenge of removing the effects of soil moisture changes from the gravity signal by means of land surface modeling. Plans for a follow-on mission to GRACE may result in groundwater storage estimates that are more accurate and of greater relevance to typical large aquifer systems [57]. The GRACE follow-on mission is scheduled for 2017 and would refly the identical GRACE spacecraft and instruments but supplement the micrometer-level accuracy microwave measurement with a laser interferometer with nanometer-level accuracy.

Models are being developed to identify groundwater potential zones [6–8]. For example, Asadi et al. [1] have performed a model study for sites in the Hyderabad and other districts of India, which identifies groundwater potential zones using IRS-ID PAN and LISS-III satellite geocoded data on a 1:50,000 scale. The information from base maps, drainage maps, watershed maps, geomorphology maps, groundwater table maps, and groundwater infiltration maps were used as data layers in a GIS to prepare a database. Then the relationships between the GIS data layers were analyzed and integrated to prepare the groundwater potential zones map.

Machiwal et al. [58] used ten thematic layers in a GIS, including data obtained by remote sensing, and multi-criteria decision-making techniques (MCDM) to delineate groundwater potential zones in the Udaipur district of Rajasthan, India. The GIS layers included topographic elevation, land slope, geomorphology, geology, soil type, pre- and post-monsoon groundwater water depths, annual net

recharge, annual rainfall, and proximity to surface water bodies. These thematic layers were studied by principal component analysis techniques to select the most influential layers for groundwater prospecting. Seven thematic layers were selected, and their features were assigned suitable weights according to their relative importance with regard to groundwater occurrence. The selected thematic maps were integrated by weighted linear combination methods in a GIS environment to generate the groundwater potential maps [58].

A recent example of successfully combining traditional geology and cutting-edge digital tools to reveal underground aquifers in drought-stricken areas is described by Gramling [59]. Accordingly, a scientific team led by geologist Alain Gachet, head of Radar Technologies International (RTI), found large water aquifers in northwestern Kenya where a drought was devastating the land, causing crops to collapse, livestock to die, and prompting a food crisis that affected millions of inhabitants in Kenya, Somalia, South Sudan, and Ethiopia. The team is part of the UNESCO Groundwater Resources Investigation for Drought Mitigation in Africa Program.

The area explored by Gachet's team, Turkana County, Kenya, is bordered in the east by Lake Turkana, a water-filled depression that is part of the East African Rift, a region having a stretched and fractured crust. Between the fractures, sunken blocks of land called grabens form sediment-filled troughs that are several kilometers deep. The troughs were a primary target, because they are potential traps for groundwater. To identify them, RTI used powerful computer programs to merge refined geological knowledge with large samples of data from ground sensors and space-based remote sensors. The data used included traditional geologic maps, hydrologic data, satellite images, and gravity and seismic survey data. Gachet's team also used commercial satellite radar images to detect soil moisture. RTI developed image-processing technology, WATEX, which "erases" obstacles, such as rocks and villages that can obscure the images, to reveal traces of moisture that can suggest the presence of an aquifer. WATEX helped identify five likely aquifers under the desert, each more than 100 m below the surface, containing water resources totaling at least 250 billion cubic meters. So far, drilling has confirmed existence of two of the aquifers. The RTI team expects to find many more deeply buried groundwater aquifers in arid regions, such as South Sudan and Sudan's Darfur state [59].

5 Detecting Freshwater Springs and Biomass

Freshwater springs can occur on dry land, in wetlands, and along the coast. Springs occur when groundwater is confined by a low-permeability geologic formation, which constrains water to a focused discharge point. Fractures in hard rock and confining clay units are typical conduits for spring flow [60]. Springs may discharge at the land surface or below the open water surface. In arid areas, freshwater springs and irrigated areas induce the growth of a dense vegetation cover, including trees,

shrubs, or grasses. Detecting biomass production is a common approach used to identify the presence of freshwater springs.

5.1 Detecting Freshwater Plumes

Where groundwater enters a lake or coastal waters, it may display a thermal, chemical, or vegetation signature that can be sensed remotely. To detect and map freshwater plumes, remote sensors exploit differences in temperature, salinity, turbidity, or color from ambient background water [61, 62]. Groundwater discharges in submarine springs have been detected using airborne and satellite TIR sensors [63, 64]. Thermal anomalies on beaches or in coastal waters are often associated with freshwater springs.

In the United Arab Emirates, a critical shortage of water is the limiting factor in municipal, industrial, and agricultural development. Most of the precipitation of up to 400 mm falls in some of the higher mountainous areas and much of it infiltrates into the ground. Thomson and Nielsen [65] did a study to determine to what extent this water was infiltrating into the sea and was therefore lost to human use and where such losses were occurring. The period of February to March was considered the best time of the year to conduct an airborne TIR study for locating springs, since the sea surface temperatures were at a minimum during this time of the year. Two flights were conducted in the early morning to minimize effects of surface heating by the sun and to take advantage of low tide conditions [66]. The sea state was moderate and winds were light during both flights. Coincident with the airborne data, surface temperatures of several different materials were measured at a number of locations along the coast, including asphalt roads, sand, etc. Aerial photos at a scale of 1:60,000 were also analyzed to aid in the identification of possible groundwater discharge sites. At the time of the airborne data collection, groundwater temperatures were about 13 °C higher than the sea surface temperature, and any groundwater discharges would appear warmer than the surrounding sea water. Colder discharges would indicate surface runoff from recent storms. Analysis of the thermal imagery indicated eight possible areas of groundwater discharge which were pinpointed on a topographic map and each identified with the name of the nearest village [65]. All groundwater discharges occurred at the shoreline-seawater interface, and no offshore springs were detected.

Groundwater discharges are usually not uniformly distributed but are strongest near the shoreline and decrease exponentially away from the shoreline. The spatial distribution of spring discharges into streams, bays, and lakes has been studied using TIR and multispectral sensors on aircraft and satellites [9]. Multi-beam sonar has also been used to characterize submarine freshwater springs down to depths of tens of meters [67].

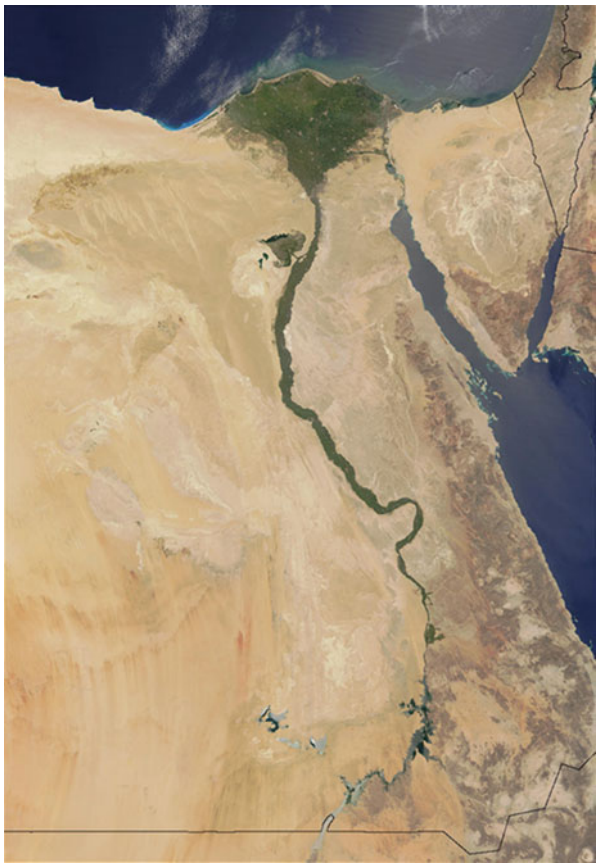

Fig. 4 True color Terra MODIS image from August 23, 2003 of the Nile River Valley with snakes in a vegetated green line from Lake Nasser in southern Egypt to the edge of the Mediterranean Sea, where it widens out into a highly productive, vast delta. *Credits*: NASA

5.2 Determining Biomass Production

Figure 4 shows a Terra MODIS image of the Nile River, which brings much-needed water and silt to the Nile Valley, turning it into an oasis of agriculture and life. The reason that the Nile River and some of the oases in Egypt are highly visible in this image is because the river and springwater irrigate the soil and produce dense vegetation that contrasts strongly with the surrounding arid land. At the apex of the delta is Cairo, which appears as a gray-brown spot. The leaf-shaped patch of green branching off the western side of the Nile is a depression that has been used as irrigated agricultural area since 1800 BC.

Arid areas generally have sparse vegetation showing little biomass production. However, where a freshwater spring emerges, biomass production is usually much higher than normal. Aboveground biomass is usually evaluated by using one of several vegetation indices [68, 69]. The most common index used is the NDVI, which is expressed as the difference between the red and NIR reflectances divided

by their sum [70, 71]. These two spectral bands represent the most detectable spectral characteristics of green plants. This is because the red radiation is absorbed by the chlorophyll in the surface layers of the plant (*palisade parenchyma*) and the NIR is reflected from the inner leaf cell structure (*spongy mesophyll*) as it penetrates several leaf layers in a canopy. Since the NIR reflectance depends on the abundance of plant tissue and the red reflectance indicates the leaf surface health condition of the plant, the NDVI can be related to plant biomass or stress. It has been shown by researchers that time series of remote sensing data can be used effectively to identify long-term trends and subtle changes of NDVI by means of principal component analysis [68, 72, 73]. However, the NDVI must be used with caution in areas with less than 20 % vegetation cover because the vegetation spectra will be distorted by the soil reflectance. Care must also be used in areas where the vegetation fraction is higher than 50 % and the signal is pushed into the saturated region of the nonlinear transfer curve.

Visible, infrared, and microwave sensors have varying sensitivities to aboveground vegetation biomass. Optical and radar remote sensing methods and empirical and statistical regression models, some using NDVI, have been applied to estimate the amount and variability of aboveground biomass [74–78]. Remote sensing has been used to collect large amounts of biomass data on a global scale for forested areas, such as upland forests, forested wetlands, and mangroves [79]. Extensive work is under way with L-band SAR to develop operational biomass programs across a range of countries, using an approach that is effective over a biomass range of 0–200 tons/ha [80].

5.3 Biomass as a Drought Indicator

Drought is a gradual phenomenon, slowly taking hold of an area and stressing its vegetation. In severe cases, drought can last for many years with devastating effects on agriculture and water supplies. The underlying cause of most droughts, deficiency in precipitation, can be related to variations in large-scale atmospheric circulation patterns and the locations of anticyclones, or high pressure systems. Sometimes, whirling masses of air separate from the main westerly airflow and effectively prevent the usual west to east progression of weather systems. When these "blocking systems" persist for extended periods of time, weather extremes such as drought, floods, heat waves, and cold snaps can occur [81].

One of the worst droughts of the twentieth century occurred in the Horn of Africa in 1984 and 1985. Figure 5 shows the NDVI anomaly for August 1984. Within this figure, dark red/brown indicates the most severe drought, light yellow areas are normal, and green areas have denser than normal vegetation. This figure demonstrates the widespread areas of severe drought that can be mapped using remote sensing techniques.

The NDVI anomaly indicates the vigor of vegetation relative to the long-term average. Using NOAA's AVHRR, scientists have been collecting images of the

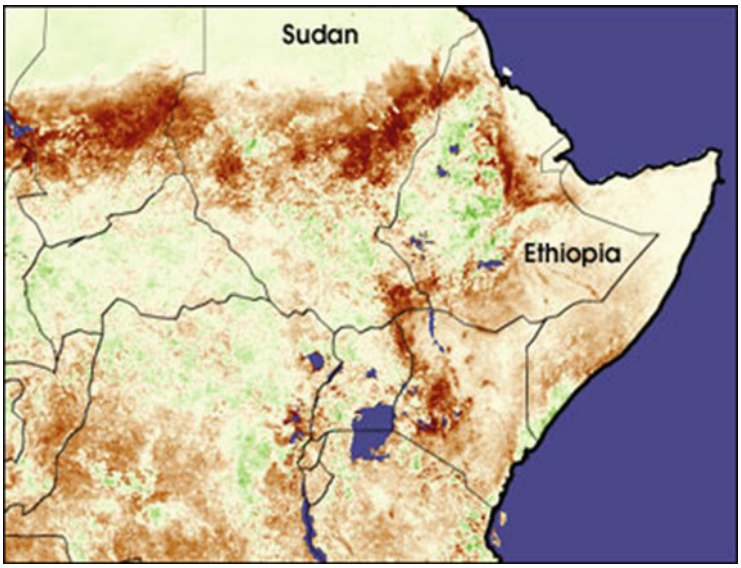

Fig. 5 This image shows the Normalized Difference Vegetation Index (NDVI) anomaly of the Horn of Africa for August 1984. The NDVI anomaly indicates the vigor of vegetation relative to the long-term average. *Dark red/brown* indicates the most severe drought, *light yellow* areas are normal, and *green* areas have denser than normal vegetation. *Courtesy*: NOAA National Weather Service

Earth's surface. By carefully measuring the wavelengths and intensity of visible and near-infrared light reflected by the land surface back up into space, scientists use the "Vegetation Index" (NDVI) to quantify the concentrations of green leaf vegetation around the globe [82]. Then by combining the daily Vegetation Indices into 8-, 16-, or 30-day composites, scientists create detailed maps of the Earth's green vegetation density that identify where plants are thriving and where they are under stress (i.e., due to lack of water). To obtain the NDVI values for vegetation biomass or stress studies in smaller areas, higher resolution satellite systems, such as Landsat TM or SPOT, are being used [69].

6 Detecting and Mapping Wetlands

Freshwater wetlands include bottomland hardwoods, riparian forests, bogs, vernal pools, and emergent marshes.

Freshwater wetlands greatly influence water quality, increase detention times of floodwaters, provide habitat for wildlife, serve as spawning and nursery grounds for fish, and contribute to the aquatic food chain [85, 86]. Wetlands also provide flood protection, protection from storm and wave damage, water quality improvement through filtering of agricultural and industrial waste, and recharge of aquifers

[4]. Freshwater wetlands can be an important source of groundwater recharge and water in arid and semiarid areas [87]. However, wetlands have been exposed to a wide range of stress-inducing alterations, including dredge and fill operations, hydrologic modifications, pollutant runoff, eutrophication, impoundments, and fragmentation by roads and ditches.

For more than three decades, remote sensing techniques have been used effectively to detect, map, and monitor tidal wetlands [88–92]. For instance, the US Fish and Wildlife Service (FWS) through its National Wetlands Inventory has provided federal and state agencies and the private sector with scientific data on wetlands location, extent, status, and trends. To accomplish this important task, FWS has used multiple sources of aircraft and satellite imagery and on-the-ground observations [92]. Most states have also created a wide range of tidal wetland inventories, using both aircraft and satellite imagery. The aircraft imagery frequently included natural color and color infrared images. The satellite data consisted of both high-resolution (1–4 m) and medium-resolution (10–30 m) multispectral imagery.

The Landsat TM has been a reliable source for land cover data [93]. Its 30 m resolution and spectral bands have proven adequate for observing land cover changes over large areas (e.g., the Horn of Africa). Freshwater wetlands have been mapped using Landsat TM and other medium-resolution data [94–97]. The availability of high spatial resolution (0.4–4.0 m) satellite data has significantly improved the capacity for mapping isolated and upstream freshwater wetlands [89, 98, 99]. However, the cost per sq. km. of imagery and its analysis increases very rapidly from using medium-resolution to high-resolution imagery. Therefore, large wetland areas or entire watersheds should be mapped using medium-resolution sensors, such as Landsat TM at 30 m, and only small, critical areas should be examined with high-resolution sensors, such as IKONOS at 1–4 m resolution [98].

Airborne geo-referenced digital cameras providing color and color infrared digital imagery are particularly suitable for accurate mapping of small freshwater wetland sites or interpreting satellite data. For example, in Fig. 6, the wetlands map shown on the left was derived from an airborne ADS-40 digital camera image shown on the right. At a spatial resolution of 0.5 m, the ADS-40 digital imagery was able to identify three key species of marsh vegetation (i.e., *Phragmites, Typha*, and *Spartina*). Digital cameras are often used on small aircraft flown at low altitudes (e.g., 200–500 m) and can be used to guide and supplement field data collection [98, 100]. Most digital cameras are capable of recording reflected visible to near-infrared light. In some cases digital camera spectral bands can be matched with specific satellite imaging band, e.g., blue, green, red, and near-infrared bands matching the bands of the IKONOS satellite multispectral imager [101]. Digital camera imagery can be integrated with GPS information and used with geographic information system software for a wide range of modeling applications [102].

Groundwater discharges in wetlands can also be identified by the unique vegetation species they may support. For example, in *Spartina alterniflora* tidal marshes groundwater discharges have been identified because they decrease the local salinity and thus attract other species to grow, such as invasive *Phragmites australis*

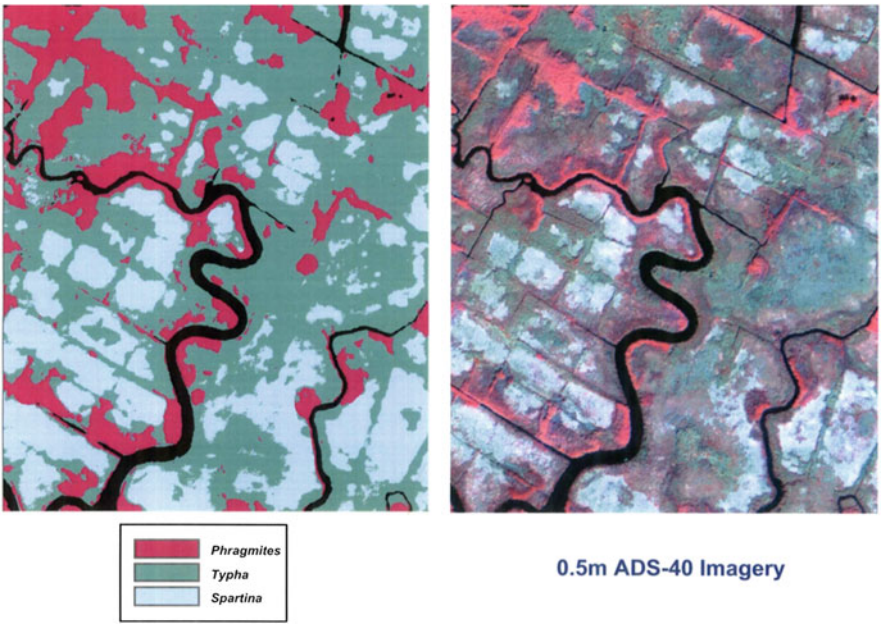

Fig. 6 The wetlands map shown on the *left* was derived from an airborne ADS-40 digital camera image on the right. Note that three different marsh vegetation species were identified. *Credits*: NOAA National Ocean Service, Charleston, SC, USA

[103]. Since most freshwater discharges in wetlands and in shallow waters are small, high spatial resolution remote sensors must be used to detect them.

New advanced techniques have been developed for mapping wetlands and even identifying wetland types and plant species indicating the presence of water [91, 98, 104–107]. The integration of hyperspectral imagery and Lidar-derived elevation has also significantly improved the accuracy of mapping wetland vegetation. Hyperspectral images help distinguish wetland species, and the Lidar data help separate species by their height [108]. Major plant species within a complex, heterogeneous wetland have been classified using multi-temporal high-resolution QuickBird satellite images, field reflectance spectra, and Lidar height information [109]. Using Lidar, hyperspectral and radar imagery, and narrow-band vegetation indices, researchers can discriminate between some wetland species and also estimate biochemical and biophysical parameters of wetland vegetation, such as water content, biomass, and leaf area index [69, 109–112].

SAR sensors on satellites provide the increased spatial resolution that is necessary in regional wetland mapping. SAR data have been used extensively for this purpose [113–118].

The sensitivity of microwaves to water and their ability to penetrate vegetative canopies make SAR also ideal for the detection of hydrologic features below the vegetation [119–125]. The presence of standing water interacts with the radar signal

differently depending on the dominant vegetation type/structure [20] as well as the biomass and condition of vegetation [126, 127]. In areas of open water without vegetation, specular reflection occurs and a dark signal (weak or no return) is observed [128]. Specular reflectance also occurs in wetlands dominated by lower biomass herbaceous vegetation when a layer of water is present [129]. Conversely, the radar signal is often increased in forested wetlands when standing water, such as flooding, is present due to the double-bounce effect, i.e., the radar pulse is reflected strongly by the water surface away from the sensor (specular reflectance) but is then redirected back towards the sensor by a second reflection from a nearby tree trunk [128, 130].

Wetland InSAR is a unique application of the interferometric synthetic aperture radar (InSAR) technique that detects elevation changes of aquatic surfaces. Most other InSAR applications detect displacements of solid surfaces [131]. The technique works because the radar pulse is backscattered twice (double bounce) from the water surface and vegetation. Wetland InSAR provides high spatial resolution hydrologic observations of wetlands and floodplains that cannot be obtained by any terrestrial-based methods. InSAR observations of wetlands have been acquired over various wetland environments using L-, C-, and X-bands and different polarizations [132, 133]. L-band data are most suitable for the wetland InSAR applications. However, the X- and C-band radar signals, which primarily interact only with the upper sections of the vegetation, were also found to be useful. In general, promising applications of InSAR for wetland observations include high spatial resolution water level monitoring, detection of flow patterns and flow discontinuities, and constraining high-resolution flow models [131].

7 Drought Monitoring and Prediction

Accurate mapping and monitoring of drought severity is important for water management and drought mitigation efforts. A system for drought monitoring and prediction can be a vital tool to facilitate drought response while saving money, time, and lives [134]. Drought indicators can be based on one variable or a combination of variables. Different indicators describe various aspects of droughts; however, holistic, comprehensive drought assessment requires multiple indicators. Drought indices integrate large amounts of data, such as precipitation, vegetation condition, snowpack, streamflow, and other water presence/supply indicators, to monitor drought severity in a comprehensive framework and to measure how much the climate in a given period has deviated from historically established normal conditions [135, 136]. These indicators can be obtained from different sources, including satellite observations, model simulations, and reanalysis of past data.

One example of a system for monitoring and predicting drought is the Global Integrated Drought Monitoring and Prediction System (GIDMaPS) developed in 2012 by researchers at the University of California, Irvine [83]. The system gathers and synthesizes land-atmosphere model simulations and remote sensing

observations to generate 1- to 4-month drought predictions. The system helps farmers, commodity investors, local governments, and global relief organizations plan for and react to droughts [84].

GIDMaPS is designed as a cyber-infrastructure system to facilitate drought analysis based on multiple indicators and input data sets. The system can support advanced data management, acquisition, storage, and visualization. The system integrates data from multiple institutions and provides historical and near-real-time drought conditions as well as probabilistic future forecasts [83]. Currently the monitoring and prediction information are based on three indicators: standardized precipitation index (SPI) as a measure of meteorological drought, standardized soil moisture index (SSI) as indicator of agricultural drought, and the multivariate standardized drought index as a composite agro-meteorological drought index. From the main interface, users can select the input data, drought indicator, year, and month to visualize or download drought information [84]. Other investigators have been able to predict agricultural drought through the prediction of agricultural yield using models based on the SPI and the NDVI [137].

Recent advances in remote sensing from satellites and radar, as well as the use of thousands of daily in situ precipitation measurements, have significantly improved drought monitoring capabilities [138]. Significant advances in mitigating drought impacts have also been made by forecasting the conditions that result in drought. Meteorologists at the NOAA Climate Prediction Center (CPC) are using medium-range forecast models to predict soil moisture 2 weeks into the future. For the longer term, meteorologists are using statistical techniques and historical drought information to construct analogues to current conditions. They then create forecasts up to several seasons ahead of time based on past events. CPC is also using sophisticated computer models that link ground and ocean conditions to the overlying atmosphere to create forecasts of temperature, precipitation, and soil moisture months in advance [138].

8 Conclusions

In arid and semiarid environments, the exploration, detection, mapping, and monitoring of water resources are a prerequisite for freshwater availability, accessibility, fair utilization, and rational management. Arid lands, including soil degradation and irrigated areas, have been classified based on vegetation and aridity indices using remotely sensed data. The arid regions have been delimited on a global scale by combining climate data, i.e., aridity index (AI), and vegetation data, i.e., vegetation index. Maps of the global distribution of arid regions have been produced using these unified criteria that have both physical and biological meaning. To monitor and predict droughts, systems exist that use multiple drought indicators to allow users to visualize and download drought information. Significant advances in mitigating drought impacts have also been made by forecasting the conditions that result in drought.

Satellite and airborne remote sensing has proven to be a relatively cost-effective and useful approach for detecting, mapping, and monitoring surface and subsurface water as compared to conventional hydrological methods. Moderate resolution satellites, such as Landsat TM and SPOT, and high-resolution satellites, such as IKONOS and QuickBird, have been used to study surface water bodies and determine their extent in arid and semiarid regions. Remotely sensed seasonal changes of lake water area/extent can be combined with available topographic data to estimate water volumetric storage changes. Where clouds, trees, and other vegetation obscure the water surface, SAR is being used, since it can penetrate clouds and vegetation to detect standing water. Radar altimetry has been applied to obtain point measurements of water surface elevation in order to determine volumetric water storage.

Soil moisture is an indicator of subsurface water that is found in the unsaturated zone above the water table. Soil moisture information is required to improve meteorological and climate predictions and for assessing agricultural conditions, irrigation management, hydrologic problems, and studies of desertification. Both active radars and passive microwave systems can sense soil moisture. However, soil moisture remote sensing still faces many challenges: the spatial resolution over land needs improvement, accurate soil moisture estimates are limited to regions with either bare soils or low amounts of vegetation cover, and better corrections for surface roughness, vegetation cover, soil temperature, and topography must be devised. Until recently, the moisture in only the top few centimeters of the soil could be detected. The SMAP satellite mission, planned for the 2015–2020 time frame, is designed to use advanced modeling and data assimilation to provide information on deeper root-zone soil moisture.

To identify groundwater potential zones, powerful computer programs are being developed to merge refined geological knowledge with large samples of data from ground sensors and space-based remote sensors. The data used include traditional geologic maps, hydrologic data, satellite images, and gravity and seismic survey data. Thematic layers in a GIS, including remote sensing data, and multi-criteria decision-making (MCDM) techniques are being used to delineate groundwater potential zones. The selected thematic maps can then be integrated by weighted linear combination methods in a GIS environment to generate the groundwater potential maps.

Only one satellite mission can directly estimate/measure the quantity of groundwater stored deep beneath the Earth's surface. The GRACE mission accomplishes this by measuring the Earth's gravity field which is influenced by the quantity of groundwater below the surface.

Freshwater springs can occur on dry land, in wetlands, and along the coast. Springs may discharge at the land surface or below the water surface. In arid areas, freshwater springs and irrigated areas induce the growth of a dense vegetation cover, including trees, shrubs, or grasses. Vegetated areas can be detected by remote sensors on aircraft and satellites and thus help find locations of freshwater springs.

Freshwater wetlands can be an important source of groundwater recharge and water in arid and semiarid areas. High spatial resolution (0.6–4.0 m) satellite and airborne hyperspectral sensors have significantly improved the capacity for mapping freshwater wetlands. However, the cost per sq. km. of imagery and the accompanying analysis rises very rapidly as one goes from medium-resolution (e.g., 30 m) to high-resolution imagery. Airborne geo-referenced digital cameras are particularly suitable for mapping small freshwater wetland sites. To detect changes of water level in wetlands, InSAR is being used. InSAR provides high spatial resolution hydrologic observations of wetlands and floodplains that cannot be obtained by any terrestrial-based methods.

Airborne and satellite remote sensors are showing considerable promise for detecting, mapping, and monitoring surface water, soil moisture, freshwater springs, and associated vegetation in arid and semiarid regions of the Earth. Satellite-based remote sensing of groundwater is still an unresolved problem. At present, the best that can be achieved with satellite sensors is to determine the spatial distribution of groundwater discharge and recharge areas, storage changes over large areas, or measurement of surface water heads in large water bodies. Combining satellite measurements with physically based models seems to offer renewed hope for detecting groundwater aquifers.

References

1. Asadi SS, Rani N, Vasantha Rao BVT, Raju MV (2012) Estimation of groundwater potential zones using remote sensing and GIS: a model study. Int J Adv Sci Res Tech 2:265–275
2. Sharma KD, Singh S, Singh N, Kalla AK (1989) Role of satellite remote sensing for monitoring of surface water resources in an arid environment. Hydrol Sci J 34:531–537
3. Yan E, Milewski A, Sultan M, Abdeldayem A, Soliman F, Abdel Gelil K (2010) Remote sensing based approach to improve regional estimation of renewable water resources for sustainable development. In: Proceedings of US-Egypt workshop on space technology and geo-information for sustainable development, Cairo, Egypt, 14–17 June 2010
4. Odum EP (1993) Ecology and our endangered life-support systems, 2nd edn. Sinauer, Sunderland, p 320
5. Krajewski WF, Smith JA (2002) Radar hydrology: rainfall estimation. Adv Water Resour 25:1387–1394
6. Jha MK, Chowdhury A, Chowdary VM, Peiffer S (2007) Groundwater management and development by integrated remote sensing and geographic information systems: prospects and constraints. Water Resour Manag 21:427–467
7. Sener E, Davraz A, Ozcelik M (2005) An integration of GIS and remote sensing in groundwater investigations: a case study in Burdur, Turkey. Hydrogeol J 13:826–834
8. Solomon S, Quiel F (2006) Groundwater study using remote sensing and geographic information systems (GIS) in the central highlands of Eritrea. Hydrogeol J 14:1029–1041
9. Becker MW (2006) Potential for satellite remote sensing of ground water. Ground Water 44:306–318
10. Brutsaert W (2005) Hydrology: an introduction. Cambridge University Press, Cambridge, p 605
11. Gamo M, Shinoda M, Maeda T (2013) Classification of arid lands, including soil degradation and irrigated areas, based on vegetation and aridity indices. Int J Remote Sens 34:6701–6722

12. Papa F, Prigent C, Aires F, Jimenez C, Rossow WB, Matthews E (2010) Interannual variability of surface water extent at the global scale, 1993–2004. J Geophys Res 115 (D12):D12111
13. Prigent C, Papa F, Aires F, Rossow WB, Matthews E (2007) Global inundation dynamics inferred from multiple satellite observations, 1993–2000. J Geophys Res 112(D12):D12107
14. Frappart F, Papa F, Famiglietti JS, Prigent C, Rossow WB, Seyler F (2008) Interannual variations of river water storage from a multiple satellite approach: a case study for the Rio Negro River Basin. J Geophys Res 113:D21104. doi:10.1029/2007JD009438
15. Frappart F, Papa F, Güntner A, Werth S, Ramilien G, Prigent C, Rossow WB, Bonnet MP (2010) Interannual variations of the terrestrial water storage in the Lower Ob' Basin from a multisatellite approach. Hydrol Earth Syst Sci 14(12):2443–2453
16. Smith LC, Pavelsky TM (2009) Remote sensing of volumetric storage changes in lakes. Earth Surf Proc Land 34:1353–1358
17. Alsdorf DE, Rodríguez E, Lettenmaier DP (2007) Measuring surface water from space. Rev Geophys 45:RG2002. doi:10.1029/2006RG000197
18. Combal B, Haas E, Andigue J, Nonguierma A, Bartholome E (2009) Operational monitoring of water bodies in arid and semi-arid regions with SPOT-VEGETATION satellite: contribution of Eumetcast and recent research projects. Secheresse 20:48–56
19. Smith LC (1997) Satellite remote sensing of river inundation area, stage, and discharge: a review. Hydrol Process 11:1427–1439
20. Hess L, Melack J, Simonett D (1990) Radar detection of flooding beneath the forest canopy: a review. Int J Remote Sens 11:1313–1325
21. Calmant S, Seyler F, Cretaux JF (2008) Monitoring continental surface waters by satellite altimetry. Surv Geophys 29(4–5):247–269. doi:10.1007/s10712-008-9051-1
22. Cazenave A, Bonnefond P, Dominh K, Schaeffer P (1997) Caspian sea level from TOPEX-POSEIDON altimetry: level now falling. Geophys Res Lett 24:881–884
23. Kostianoy AG, Lebedev SA, Solovyov AM (2011) Satellite monitoring of water resources in Turkmenistan. In: Fifteenth international water technology conference, IWTC-15, Alexandria, Egypt, 31 March–02 April 2011
24. Hofle B, Vetter M, Pfeiffer N, Mandlburger G, Stotter J (2009) Water surface mapping from airborne laser scanning using signal intensity and elevation data. Earth Surf Proc Land 34:1635–1649
25. Paine JG, Andrews JR, Saylam K, Tremblay TA, Averett AR, Caudle TL, Meyer T, Young MH (2013) Airborne lidar on the Alaskan North Slope: wetlands mapping, lake volumes, and permafrost features. Lead Edge 32:798–805
26. Schultz C (2014) Spatial resolution key to properly forecasting arid-region drought. Eos 95 (13):116
27. Calvet JC, Wigneron JP, Walker JP, Karbou F, Chanzy A, Albergel C (2011) Sensitivity of passive microwave observations to soil moisture and vegetation water content: L-band to W-band. IEEE Trans Geosci Remote Sens 49:1190–1199
28. Choudhury BJ, Schmugge TJ, Chang A, Newton RW (1979) Effect of surface roughness on the microwave emission from soils. J Geophys Res 81:3660–3666
29. Chanzy A, Schmugge TJ, Calvet JC, Kerr Y, van Oevelen P, Grosjean O, Wang JR (1997) Airborne microwave radiometry on a semi-arid area during HAPEX-Sahel. J Hydrol 188–189:285–309
30. Jackson TJ, LeVine DM, Hsu AY, Oldak A, Starks PJ, Isham JD, Haken M (1999) Soil moisture mapping at regional scales using microwave radiometry: the Southern Great Plains Hydrology Experiment. IEEE Trans Geosci Remote Sens 37:2136–2150
31. John B (1992) Soil moisture detection with airborne passive and active microwave sensors. Int J Remote Sens 13:481–491
32. Barre HMJ, Duesmann B, Kerr YH (2008) SMOS: the mission and the system. IEEE Trans Geosci Remote Sens 46:587–593

33. Kerr YH, Waldteufel P, Wigneron JP, Martinuzzi JM, Font J, Berger M (2001) Soil moisture retrieval from space: the Soil Moisture and Ocean Salinity (SMOS) mission. IEEE Trans Geosci Remote Sens 39:1729–1735
34. Prigent C, Aires F, Rossow WB (2006) Land surface microwave emissivities over the globe for a decade. Bull Am Meteorol Soc 87:1573–1584
35. Kerr YH (2007) Soil moisture from space: where are we? Hydrogeol J 15:117–120
36. Kerr YH, Waldteufel P, Wigneron JP, Delwart S, Cabot F, Boutin J, Escorihuela MJ, Font J, Reul N, Gruhier C, Juglea SE, Drinkwater MR, Hahne A, Martin-Neira M, Mecklenburg S (2010) The SMOS mission: new tool for monitoring key elements of the global water cycle. Proc IEEE 98:666–687
37. Font J, Camps AJ, Borges A, Martin-Neira M, Boutin J, Reul N, Kerr YH, Hahne A (2010) SMOS: the challenging sea surface salinity measurement from space. Proc IEEE 98:649–665
38. McMullan KD, Brown MA, Martin-Neira M, Rits W, Ekholm S, Marti J, Lemanczyk J (2008) SMOS: the payload. IEEE Trans Geosci Remote Sens 46:594–605
39. Merlin O, Walker JP, Chehbouni A, Kerr Y (2008) Towards deterministic downscaling of SMOS soil moisture using MODIS derived soil evaporation efficiency. Remote Sens Environ 112:3935–3946
40. Jackson TJ, Schmugge TJ (1991) Vegetation effects on the microwave emission of soils. Remote Sens Environ 36:203–212
41. Njoku EG, Entekhabi D (1996) Passive microwave remote sensing of soil moisture. J Hydrol 184:101–129
42. Aires F, Papa F, Prigent C (2013) A long-term, high-resolution wetland data set over the Amazon Basin, downscaled from a multi-wavelength retrieval using SAR data. J Hydrometeorol 14(2):594–607
43. Aires F, Papa F, Prigent C, Crétaux JF, Berge-Nguyen M (2013) Characterization and space/time downscaling of the inundation extent over the Inner Niger Delta using GIEMS and MODIS data. J Hydrometeorol 15(1):171–192. doi:10.1175/JHM-D-13-032.1
44. Entekhabi D, Njoku EG, O'Neill PE, Kellogg KH, Crow WT, Edelstein WN, Entin JK, Goodman SD, Jackson TJ, Johnson J, Kimball J, Piepmeier JR, Koster RD, Martin N, McDonald KC, Moghaddam M, Moran S, Reichle R, Shi JC, Spencer MW, Thurman SW, Tsang L, Van Ziel J (2010) The Soil Moisture Active Passive (SMAP) mission. Proc IEEE 98:704–716
45. Piles M, Entekhabi D, Camps A (2009) A change detection algorithm for retrieving high-resolution soil moisture from SMAP radar and radiometer observations. IEEE Trans Geosci Remote Sens 47:4125–4131
46. Anderson MP (2007) Introducing groundwater physics. Phys Today 60:42–47
47. Younger PL (2007) Groundwater in the environment: an introduction. Blackwell, Oxford, p 318
48. Hutti B, Nijagunappa R (2011) Application of geoinformatics in water resources management of semi-arid regions, North Karnataka, India. Int J Geomatics Geosci 2:373–382
49. Purkis S, Klemas V (2011) Remote sensing and global environmental change. Wiley-Blackwell, Oxford, p 367
50. Pool DR, Eychaner JH (1995) Measurements of aquifer storage change and specific yield using gravity surveys. Ground Water 33:425–432
51. Ramillien G, Frappart F, Cazenave A, Güntner A (2005) Time variations of the land water storage from an inversion of 2 years of GRACE geoids. Earth Planet Sci Lett 235:283–301
52. Swenson S, Wahr J, Milly PCD (2003) Estimated accuracies of regional water storage variations inferred from the Gravity Recovery and Climate Experiment (GRACE). Water Resour Res 39:12–23
53. Schmidt R, Schwinzer P, Flechtner F, Reigber C, Guntner A, Doll P, Ramillien P, Cazenave A, Petrovic S, Jochmann H, Wunsch J (2006) GRACE observations of changes in continental water storage. Global Planet Change 50:112–126

54. Rodell M, Famiglietti JS (2002) The potential for satellite-based monitoring of groundwater storage changes using GRACE: the High Plains aquifer, Central US. J Hydrol 263:245–256
55. Yirdaw SC, Snelgrove KR, Agboma CO (2008) GRACE satellite observations of terrestrial moisture changes for drought characterization in the Canadian Prairie. J Hydrol 356:84–92
56. Li B, Rodell M, Zaitchick BM, Reichle RH, Koster RD, Van Dam TM (2012) Assimilation of GRACE terrestrial water storage into a land surface model: evaluation and potential value for drought monitoring in western and central Europe. J Hydrol 446–447:103–115
57. Watkins MM (2004) Bowie lecture: time variable gravity measurements come of age. Eos 85 (47): Fall Meeting Supplement, Abstract G24A-01
58. Machiwal D, Jha MK, Mal BC (2011) Assessment of groundwater potential in a semi-arid region of India using remote sensing, GIS and MCDM techniques. Water Resour Manag 25:1359–1386
59. Gramling C (2013) Kenyan find heralds new era in water prospecting. Science 341:1327
60. Fetter CW (2001) Applied hydrogeology, 4th edn. Prentice-Hall, Upper Saddle River, p 598
61. Klemas V (2011) Remote sensing of sea surface salinity: an overview with case studies. J Coastal Res 27:830–838
62. Klemas V (2012) Remote sensing of coastal plumes and ocean fronts: overview and case study. J Coastal Res 28:1–7
63. Kolokoussis P, Karathanassi V, Rokos D, Argialas D, Karageorgis AP, Georgopoulos D (2011) Integrating thermal and hyperspectral remote sensing for the detection of coastal springs and submarine groundwater discharges. Int J Remote Sens 32:8231–8251
64. Loheide S (2009) A thermal remote sensing tool for mapping spring and diffuse groundwater discharge to streams. U.S. Geological survey report. http://water.usgs.gov/wrri/o8grants/2008WI192B.html. Accessed 15 Oct 2014
65. Thomson KPB, Nielsen G (1980) Groundwater discharge detection along the coasts of the Arabian Gulf and the Gulf of Oman using thermal infrared imagery. In: Proceedings of the 14th international symposium on remote sensing of environment, San Jose, Costa Rica, 23–30 Apr 1980, pp 835–843
66. Klemas V (2013) Airborne remote sensing of coastal features and processes: an overview. J Coastal Res 29:239–255
67. Di Martino G, Tonielli R (2010) Freshwater runoff effects on shallow-water multibeam surveys: using multibeam data processing to characterize submarine freshwater springs. Sea Technology, May 2010, pp 10–13
68. Jensen JR (2007) Remote sensing of the environment: an earth resource perspective. Prentice-Hall, Englewood Cliffs, p 608
69. Klemas V (2013) Remote sensing of wetland biomass: an overview. J Coastal Res 29:1016–1028
70. Cihlar J, St. Laurent A, Dyer JA (1991) Relation between the normalized difference vegetation index and ecological variables. Remote Sens Environ 35:279–298
71. Goward SN, Markham B, Dye DG, Dulaney W, Yang J (1991) Normalized difference vegetation index measurements from the advanced very high resolution radiometer. Remote Sens Environ 35:257–277
72. Young SS, Wang CY (2001) Land-cover change analysis of China using global-scale Pathfinder AVHRR Landcover (PAL) data, 1982–92. Int J Remote Sens 22:1457–1477
73. Yuan D, Elvidge CD, Lunetta RS (1998) Survey of multispectral methods for land cover change analysis. In: Lunetta RS, Elvidge CD (eds) Remote sensing change detection: environmental monitoring methods and applications. Ann Arbor, Chelsea, pp 21–40
74. Dong J, Kaufmann RK, Myneni RB, Tucker CJ, Kauppi PE, Liski J, Buermann W, Alexeyev V, Hughes MK (2003) Remote sensing estimates of boreal and temperate forest woody biomass: carbon pools, sources, and sinks. Remote Sens Environ 84:393–410
75. Gower ST, Kucharik CJ, Norman JM (1999) Direct and indirect estimation of leaf area index, fAPAR and net primary production of terrestrial ecosystems. Remote Sens Environ 70:29–51

76. Ku NW, Popescu SC, Ansley RJ, Perotto-Baldivieso HL, Fillippi AN (2012) Assessment of available rangeland woody plant biomass with a terrestrial lidar system. Photogramm Eng Remote Sens 78:349–361
77. Peregon A, Maksyutov S, Kosykh NP, Mironycheva-Tokareva NP (2008) Map-based inventory of wetland biomass and net primary production in Western Siberia. J Geophys Res 113:1–12
78. Riegel B (2012) A comparison of remote sensing methods for estimating above-ground carbon biomass at a wetland restoration area in the southeastern coastal plain. http://dukespace.lib.duke.edu/dspace/handle/10161/5164. Accessed 15 Oct 2012
79. Running SW, Nemani RR, Heinsch FA, Zhao M, Reeves M, Hashimoto H (2004) A continuous satellite-derived measure of global terrestrial primary production. Bioscience 54:547–560
80. Lucas R, Armston J, Fairfax J, Fensham R, Dwyer J, Bowen M, Eyre T, Laidlaw M, Shimada M (2010) An evaluation of the ALOS PALSAR L-band backscatter- above ground biomass relationship over Queensland, Australia. IEEE J Sel Top Earth Obs Remote Sens 3:576–593
81. Graham S (2000) Drought: the creeping disaster. NASA Earth Observatory, August 28, 2000. http://earthobservatory.nasa.gov/Features/DroughtFacts/. Accessed 11 Apr 2014
82. Weier J, Herring D (2000) Measuring Vegetation (NDVI & EVI). NASA Earth Observatory, August 30, 2000. http://earthobservatory.nasa.gov/Features/MeasuringVegetation/. Accessed 11 Apr 2014
83. Hao Z, AghaKouchak A (2014) A nonparametric multivariate multi-index drought monitoring framework. J Hydrometeorol 15:89–101
84. Momtaz F, Nakhjiri N, AghaKouchak A (2014) Toward a drought cyber infrastructure system. Eos 95(22):182–183
85. Leibowitz SG (2003) Isolated wetlands and their functions: an ecological perspective. Wetlands 23:517–531
86. Semlitsch RD, Bodie JR (1998) Are small, isolated wetlands expendable? Conserv Biol 12:1129–1133
87. Winter TC, Labaugh JW (2003) Hydrologic considerations in defining isolated wetlands. Wetlands 23:532–540
88. Dahl TE (2006) Status and trends of wetlands in the conterminous United States 1998 to 2004. U.S. Department of the Interior, Fish and Wildlife Service, Washington, DC, p 112
89. Kelly M, Tuxen K (2009) Remote sensing support for tidal wetland vegetation research and management. In: Yang X (ed) Remote sensing and geospatial technologies for coastal ecosystem assessment and management. Springer, Berlin, pp 341–363
90. Ozesmi SL, Bauer ME (2002) Satellite remote sensing of wetlands. Wetlands Ecol Manag 10:381–402
91. Prigent C, Matthews E, Aires F, Rossow WB (2001) Remote sensing of global wetland dynamics with multiple satellite data sets. Geophys Res Lett 28:4631–4634
92. Tiner RW (1996) Wetlands. In: Manual of photographic interpretation, 2nd edn. American Society for Photogrammetry and Remote Sensing, Falls Church, Virginia, p 2440
93. Lunetta RS, Balogh ME (1999) Application of multi-temporal Landsat 5 TM imagery for wetland identification. Photogramm Eng Remote Sens 65:1303–1310
94. Baker C, Lawrence R, Montagne C, Patten D (2006) Mapping wetlands and riparian areas using Landsat ETM+ imagery and decision-based models. Wetlands 27:465–474
95. De Roeck ER, Verhoest NEC, Miya MH, Lievens H, Batelaan O, Thomas A, Brendonck L (2008) Remote sensing and wetland ecology: a South African case study. Sensors 8:3542–3556
96. Frohn RC, Reif M, Lane C, Autrey B (2009) Satellite remote sensing of isolated wetlands using object-oriented classification of Landsat-7 data. Wetlands 29:931–941
97. Tiner RW (2003) Geographically isolated wetlands of the United States. Wetlands 23:494–516

98. Klemas V (2013) Remote sensing of emergent and submerged wetlands: an overview. Int J Remote Sens 34:6286–6320
99. Wulder MA, Hall RJ, Coops NC, Franklin SE (2004) High spatial resolution remotely sensed data for ecosystem characterization. Bioscience 54:511–521
100. McCoy R (2005) Field methods in remote sensing. Guilford, New York, p 161
101. Ellis JM, Dodd HS (2000) Applications and lessons learned with airborne multispectral imaging. In: Fourteenth international conference on applied geological remote sensing, Las Vegas, Nevada, 6–8 Nov 2000
102. Lyon JG, McCarthy J (1995) Wetland and environmental applications of GIS. Lewis, New York, p 400
103. Hays RL (2009) Vegetation patterns and nutrient cycling in Delaware Bay salt marshes, Great Marsh (Lewes) and Webbs Marsh (South Bowers), Delaware. PhD Dissertation, University of Delaware, Lewes, p 384
104. Jensen RR, Mausel P, Dias N, Gonser R, Yang C, Everitt J, Fletcher R (2007) Spectral analysis of coastal vegetation and land cover using AISA+ hyperspectral data. Geocarto Int 22:17–28
105. Schmid T, Koch M, Gumuzzio J (2005) Multisensor approach to determine changes of wetland characteristics in semiarid environments in central Sapin. IEEE Trans Geosci Remote Sens 43:2516–2525
106. Schmidt KS, Skidmore AK, Kloosterman EH, Van Oosten H, Kumar L, Janssen JAM (2004) Mapping coastal vegetation using an expert system and hyperspectral imagery. Photogramm Eng Remote Sens 70:703–716
107. Yang C, Everitt JH, Fletcher RS, Jensen JR, Mausel PW (2009) Mapping black mangrove along the south Texas gulf coast using AISA+ hyperspectral imagery. Photogramm Eng Remote Sens 75:425–436
108. Yang J, Artigas FJ (2009) Mapping salt marsh vegetation by integrating hyperspectral and LiDAR remote sensing. In: Wang J (ed) Remote sensing of coastal environments. CRC, Boca Raton, pp 173–187
109. Gilmore MS, Civco DL, Wilson EH, Barrett N, Prisloe S, Hurd JD, Chadwick C (2009) Remote sensing and in situ measurements for delineation and assessment of coastal marshes and their constituent species. In: Wang J (ed) Remote sensing of coastal environments. CRC, Boca Raton, pp 261–280
110. Adam E, Mutanga O, Rugege D (2010) Multispectral and hyperspectral remote sensing for identification and mapping of wetland vegetation: a review. Wetlands Ecol Manag 18:281–296
111. Simard M, Fatoyinbo LE, Pinto N (2009) Mangrove canopy 3D structure and ecosystem productivity using active remote sensing. In: Wang J (ed) Remote sensing of coastal environments. CRC, Boca Raton, pp 61–78
112. Wang Y (2009) Remote sensing of coastal environments: an overview. In: Wang J (ed) Remote sensing of coastal environments. CRC, Boca Raton, pp 1–24
113. Baghdadi N, Bernier M, Gauthier R, Neeson I (2001) Evaluation of C-band SAR data for wetlands mapping. Int J Remote Sens 22:71–88
114. Lang MW, McCarty GW (2008) Remote sensing data for regional wetland mapping in the United States: trends and future prospects. In: Russo RE (ed) Wetlands: ecology, conservation and restoration. Nova Science, Hauppauge, pp 73–112
115. Novo EMLM, Costa MPF, Mantovani JE, Lima IBT (2002) Relationship between macrophyte stand variables and radar backscatter at L and C band, Tucurui reservoir, Brasil. Int J Remote Sens 23:1241–1260
116. Rosenqvist A, Finlayson CM, Lowry J, Taylor D (2007) The potential of long-wavelength satellite-borne radar to support implementation of the Ramsar Wetland Convention. Aquat Conserv Mar Freshw Ecosyst 17:229–244
117. Townsend PA (2000) A quantitative fuzzy approach to assess mapped vegetation classifications for ecological applications. Remote Sens Environ 72:253–267

118. Townsend PA (2002) Relationships between forest structure and the detection of flood inundation in forested wetlands using C-band SAR. Int J Remote Sens 23:443–460
119. Hall DK (1996) Remote sensing applications to hydrology: imaging radar. Hydrol Sci J 41:609–624
120. Kasischke E, Melack J, Dobson M (1997) The use of imaging radars for ecological applications: a review. Remote Sens Environ 59:141–156
121. Kasischke E, Bourgeau-Chavez L (1997) Monitoring South Florida wetlands using ERS-1 SAR imagery. Photogramm Eng Remote Sens 63:281–291
122. Lang MW, Kasischke ES (2008) Using C-band synthetic aperture radar data to monitor forested wetland hydrology in Maryland's Coastal Plain, USA. IEEE Trans Geosci Remote Sens 46:535–546
123. Phinn SR, Stow DA, Van Mouwerik D (1999) Remotely sensed estimates of vegetation structural characteristics in restored wetlands, Southern California. Photogramm Eng Remote Sens 65:485–493
124. Rao BRM, Dwivedi RS, Kushwaha SPS, Bhattacharya SN, Anand JB, Dasgupta S (1999) Monitoring the spatial extent of coastal wetlands using ERS-1 SAR data. Int J Remote Sens 20:2509–2517
125. Wilson BA, Rashid H (2005) Monitoring the 1997 flood in the Red River Valley using hydrologic regimes and RADARSAT imagery. Can Geogr 49:100–109
126. Toyra JA, Pietroniro A, Martz W, Prowse TD (2002) A multi-sensor approach to wetland flood monitoring. Hydrol Process 16:1569–1581
127. Costa MPF, Telmer KH (2007) Mapping and monitoring lakes in the Brazilian Pantanal wetland using synthetic aperture radar imagery. Aquat Conserv Mar Freshw Ecosyst 17:277–288
128. Dwivedi R, Rao B, Bhattacharya S (1999) Mapping wetlands of the Sundarban delta and its environs using ERS-1 SAR data. Int J Remote Sens 20:2235–2247
129. Kasischke ES, Smith KB, Bourgeau-Chavez LL, Romanowicz EA, Brunzell S, Richardson CJ (2003) Effects of seasonal hydrologic patterns in south Florida wetlands on radar backscatter measured from ERS-2 SAR imagery. Remote Sens Environ 88:423–441
130. Harris J, Digby-Argus S (1986) The detection of wetlands on Radar imagery. In: Proceedings of the tenth Canadian symposium on remote sensing, Edmonton, Alberta, May 1986
131. Wdowinski S, Hong SH (2014) Wetland InSAR. In: Tiner R, Klemas V, Lang M (eds) Advances in wetland mapping. CRC, Boca Raton
132. Wdowinski S, Amelung F, Miralles-Wilhelm F, Dixon TH, Carande R (2004) Space-based measurements of sheet-flow characteristics in the Everglades wetland, Florida. Geophys Res Lett 31:L15503
133. Wdowinski S, Kim SW, Amelung F, Dixon TH, Miralles-Wilhelm F, Sonenshein R (2008) Space-based detection of wetlands' surface water level changes from L-band SAR interferometry. Remote Sens Environ 112:681–696
134. Deng M, Di L, Han W, Yagci AL, Peng C, Heo G (2013) Web-service-based monitoring and analysis of global agricultural drought. Photogramm Eng Remote Sens 79:926–943
135. Mu Q, Zhao M, Kimball JS, McDowell MG, Running S (2013) A remotely sensed global terrestrial drought index. Bull Am Meteorol Soc 94:83–98
136. Narasimhan B, Srinivasan R (2005) Development and evaluation of soil moisture deficit index (SMDI) and evapotranspiration deficit index (ETDI) for agricultural drought monitoring. Agr Forest Meteorol 133:69–88
137. Dutta D, Kundu A, Patel NR (2013) Predicting agricultural drought in eastern Rajasthan of India using NDVI and standardized precipitation index. Geocarto Int 28:192–209
138. NOAA/CPC (2014) Drought: the creeping disaster. NASA earth observatory feature article, http://earthobservatory.nasa.gov/Features/DroughtFacts/drought_facts_4.php. Accessed 28 July 2014

Imaging Spectrometry of Inland Water Quality in Italy Using MIVIS: An Overview

Claudia Giardino, Mariano Bresciani, Erica Matta, and Vittorio E. Brando

Contents

Abstract Airborne imaging spectrometry is a powerful tool to investigate key biophysical parameters in inland waters. High spectral resolution data forms a contiguous spectrum that enables the detection and identification of a variety of key water quality indicators (e.g. cyanobacteria pigments). High spatial resolution imagery is suitable for fine-scale observation (e.g. the patchy spatial distribution of

C. Giardino (✉) • M. Bresciani • E. Matta
Optical Sensing Group, Institute for Electromagnetic Sensing of the Environment, National Research Council of Italy, via Bassini 15, 20133 Milan, Italy
e-mail: giardino.c@irea.cnr.it

V.E. Brando
Optical Sensing Group, Institute for Electromagnetic Sensing of the Environment, National Research Council of Italy, via Bassini 15, 20133 Milan, Italy

Aquatic Remote Sensing Group, Commonwealth Scientific and Industrial Research Organisation (CSIRO) Oceans and Atmosphere, GPO Box 1666, Canberra, ACT 2601, Australia

T. Younos, T.E. Parece (eds.), *Advances in Watershed Science and Assessment*, The Handbook of Environmental Chemistry 33,
DOI 10.1007/978-3-319-14212-8_3

phytoplankton in productive waters). Airborne observations ensure flexible flight paths that allow observations of unexpected events to be acquired promptly. In this chapter, we present an overview of remote sensing techniques, by focusing on imaging spectrometry, for assessing water quality parameters in inland waters such as lakes, streams, rivers, reservoirs and ponds (defined 'Case-2 waters' according to a traditional remote sensing terminology). Then, we present examples of applications by using airborne Multispectral Infrared and Visible Imaging Spectrometer (MIVIS) images of Italian inland waters acquired at a spatial resolution varying from 3 to 5 m. Those examples include the retrieval of water quality parameters (i.e. chlorophyll-a, suspended particulate matter and coloured dissolved organic matter), the detection and monitoring of submerged vegetation, the observation of a cyanobacteria bloom in productive lakes and the investigation of the signal reflected by floating materials of terrestrial origin (i.e. pollens and oil).

Keywords Airborne • Cyanobacteria • Hyperspectral data • Lakes • Rivers • Water quality

1 Introduction

Inland natural waters are complex physical–chemical–biological systems including living and non-living materials that may be present in aqueous solutions or in aqueous suspensions. Together with air bubbles, foams and scum besides inhomogeneity resulting from small-scale water eddies, these components determine the bulk optical properties of inland waterbodies [1]. Such a complexity can be optically defined as 'Case-2' waters according to water classification established by Morel and Prieur [2]. These waters are influenced not just by phytoplankton and related particles (e.g. organic particles from death and decay of phytoplankton) but also by other substances introduced from outside the water column that vary independently from phytoplankton (e.g. resuspension of bottom particles in shallow areas, inorganic and organic suspended matter from land drainages and tributary) [3].

Balance and interaction of water components determines the quality of these delicate inland water ecosystems, whose quality is threatened by substances and factors of different origin: for instance, the content of nutrients, suspended particulate matter (SPM) originating from soil erosion, the presence of heavy metals and pesticides continuously added by anthropogenic sources. The quality of surface water in lakes, rivers and reservoirs is a major concern around the world. Eutrophication of surface waters from human and agricultural wastes and nitrification of groundwater from agricultural practices have affected large parts of the world, with unpredictable consequences on the quality and preservation of ecosystem goods and services [4].

When deterioration of inland water quality is caused by optically active substances, the effect of these changes can be observed with optical remote sensing

instruments. The nature and magnitude of these changes are controlled by the total amount of absorption and scattering occurring into the water volume that may be attributable to each optically significant organic and inorganic, suspended and dissolved, living and non-living component contained in the natural waterbody. At present, a variety of water quality parameters have been identified in literature as detectable by modern passive sensors onboard satellites: e.g. chlorophyll-a (chl-a) [5, 6] and phycocyanin (PC) [7, 8], SPM [9, 10], coloured dissolved organic matter (CDOM or yellow substances) [11, 12] or the diffused attenuation coefficient as measure for water transparency [13].

Floating materials such as oils (e.g. [14]), cyanobacteria scum (e.g. [15]), pollen or vegetation (e.g. [16]) can also be detected from remotely sensed imagery. The capacity of remote sensing in detecting those materials is relevant, because whatever is floating on the water surface might be the consequence of unusual events (e.g. oil spill, massive blooms of cyanobacteria) and might have relevant impacts on the landscape (e.g. [17]). Furthermore, when water transparency allows light to reach the bottom, the backward signal reaching the sensor also includes spectral information about the substrate. In such cases, the spectral signature of the bottom and the water depth are detectable from remote sensors. From these measures, the next ecological relevant information may be derived: total area of plant coverage, broadness of the littoral zone covered by macrophytes, growth cycle of the macrophytes or species compositions (e.g. [18–22]).

2 Methods: An Overview

Conceptually, remote sensing of water quality is simple: sunlight, whose spectral properties are known, enters a natural waterbody. The sunlight's spectral character is then altered, contingent upon the absorption and scattering properties of the waterbody (which, of course, depends on type and concentration of the various constituents composing that particular waterbody). Part of the altered sunlight eventually makes its way back out of the water and can be detected from a sensor aboard an aircraft or satellite. Knowing how different substances spectrally alter sunlight, for example, by wavelength-dependent absorption/scattering or by fluorescence, makes it possible to assess which substances are present in the water and in what concentration.

When spectral characteristics of the parameters of interest are known, semi-empirical methods are generally used. This knowledge is included in the statistical analysis by focusing on well-chosen spectral areas and appropriate wavebands used as correlates. Recently, Odermatt et al. [23] provided a review of the remote sensing algorithms, currently adopted to retrieve water quality parameters. They distinguished semi-empirical [24, 25] from spectral inversion procedures, the latter built on matching spectral measurements with bio-optical forward model-derived signatures by means of inversion techniques.

As an example, semi-empirical methods are widely used in productive waters to assess chl-a concentration. These methods employ band ratios between the secondary chl-a absorption maximum (at around 675 nm) and adjacent spectral bands not affected by phytoplankton absorption, such as the near-infrared reflectance peak near 700 nm [26, 27]. In other cases they use a combination of bands in the same red near-infrared regions [28, 29]. Matthews et al. [15] implemented an algorithm named 'Maximum Peak Height' in order to map the chl-a concentrations from remotely sensed images in hypertrophic conditions created by cyanobacteria proliferation.

Spectral inversion procedures are more generic and might be applicable independently of ground measurements and sensor characteristics. In the analytical approach, the concentrations of water quality parameters are related to the bulk inherent optical properties (IOPs) via the specific inherent optical properties (SIOPs). The IOPs of the water column are then related to the water reflectance and, hence, to the top-of-atmosphere radiance, such as described by the radiative transfer theory [30, 31]. The analytical method involves inverting all those associations to determine the water quality from remotely sensed data. Approaches used to invert bio-optical models may include matrix inversion methods [32, 33], neural networks [34, 35], look-up tables [36, 37], optimisation techniques [38–42] or classification-based approaches whose end-members are created by forward runs of the bio-optical model [43]. An example of such approach, using hyperspectral satellite data, Hyperion, acquired in Case-2 waters for chl-a, tripton and CDOM retrieval can be found in Brando and Dekker [32] and Giardino et al. [44]. In their work a linear matrix inversion method was used to invert a bio-optical model, which was parameterised according to the SIOPs in both study areas, starting from the atmospherically corrected Hyperion reflectance.

Quantitatively, the relationships developed to assess water quality in lakes within semi-empirical approaches are often site dependent and can be only applied to those images from which relationships are derived. Well-calibrated and validated spectral inversion procedures are instead applicable to every site acquired over the selected waterbody (presuming constant SIOPs), giving the opportunity to assess water quality independently from ground measurements. The procedure is also transferable to other systems, for which the optical characterisation of the waterbody is known. Nonetheless, they are used less because of the difficulties, or inaccuracies, in obtaining the parameters and the efforts required in calibrating the model [45].

Whatever approach is chosen, the assessment of water quality in inland water, from remote sensing, usually requires the transformation from sensor radiance to surface reflectance values to remove the atmospheric effect. The atmospheric effect is a dominant disturbance in remote observation of water quality, and imprecise corrections may produce large errors in obtaining water reflectance and consequently in retrieving concentrations of water quality parameters [33]. As a minimum, bidirectional effects of scattering and absorption in the atmosphere under varying aerosol optical depth are usually accounted for. Then to retrieve the water reflectance, correction for adjacent scattering from land into the light path, and/or

multiple scattering of light on water surface, might need to be accomplished. As inland waters are typically delimited by land, the contribution of reflections from the surrounding environment on the water surface might interfere with the estimations of signals coming from water. The remotely sensed signals coming from water might be finally affected by the illumination and acquisition geometries. The effect of wave-induced sun glint may happen and obscure the radiance originating from the water. Such glint, which is particularly noticeable with high spatial resolution sensors, hence hindering the mapping of water quality and benthic features, can be corrected according to published procedures [46–49].

3 Imaging Spectrometry

Algorithms for assessing water quality in optically complex waters perform best if they can make use of hyperspectral data. Hyperspectral remote sensing, or imaging spectroscopy, provides measurements across numerous discrete narrow bands, forming a contiguous spectrum that enables detection and identification of key biophysical properties of water column and bottom. For example, in case the chl-a concentration is estimated according to band ratio which makes use of red (680 nm) to near-infrared (700 nm) bands, the advantage of having a signal on a contiguous spectrum relies on the ability to define the algorithm according to the shift of the near-infrared reflectance band to be used [3]. Figure 1 shows the subsurface water reflectance computed from forward run of the bio-optical model [50] for chl-a concentration changing from 5 to 50 mgm^{-3}. With increasing chl-a concentrations,

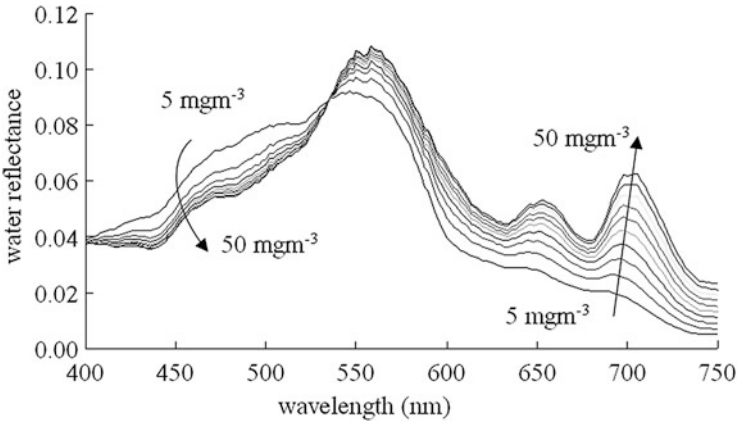

Fig. 1 Subsurface water reflectance provided by a bio-optical model [50] run for concentration of chl-a varying from 5 to 50 mgm^{-3} (shown by the *arrows*). In the near-infrared region, the wavelength position of the peak, adopted in band-ratio algorithms for chl-a estimation, shifts from 694 to 706 nm

both the appearance and intensification of peak around 700 nm and the shift of reflectance peak wavelength position from 694 to 706 nm are noticeable.

However, for spectral inversion procedures, a hyperspectral dataset could facilitate a physics-based modelling approach to quantitatively retrieve multiple constituents of interest (e.g. PC, chl-a, SPM, CDOM, phytoplankton functional types and benthic composition) ([51] and references therein). In fact, hyperspectral remote sensing provides essential data to de-convolve the remotely sensed signal and, thence, to detect the water components that could be missed by multispectral instruments, e.g. if the dataset contains many narrow spectral bands, then hyperspectral measurements can make the direct detection of the PC pigment easier ([52] and references therein).

Modern space-borne hyperspectral sensors (e.g. Hyperion, Hyperspectral Imager for the Coastal Ocean (HICO)) showed increasing capabilities in water quality [53–55], but they still present some inaccuracies in monitoring environments that are highly variable in space, e.g. especially in inland and near coastal waters. Özesmi and Bauer [56] observed how spatial resolution is one of the primary limiting factors in the application of satellite remote sensing to freshwater ecosystems. High spatial and spectral resolution data are essential attributes to provide accurate retrieval of water quality in both optically deep and shallow waters (e.g. [22]). The signal-to-noise ratio of the sensor is also critical in making accurate measurements of water quality parameters but, for the sake of brevity, will be not discussed in this chapter. In this context, high-resolution airborne hyperspectral sensors (e.g. Airborne Imaging Spectrometer for Applications (AISA), MIVIS, Airborne Visible/InfraRed Imaging Spectrometer (AVIRIS), Compact Airborne Spectrographic Imager (CASI), HYperspectral MAPper (HYMAP)) represent enhanced mapping tools (e.g. [16, 38, 39]) and also preliminary tests to design satellite-based systems (e.g. PRecursore IperSpettrale della Missione Applicativa (PRISMA), Environmental Mapping and Analysis Programme (EnMAP), Hyperspectral Infrared Imager (HyspIRI)). For example, in previous years, Koponen et al. [57] and Giardino et al. [58] used airborne AISA and MIVIS images, respectively, for simulating MERIS data on lakes.

4 MIVIS Applications in Italian Inland Waters

Generally inland waters include freshwater bodies as lakes, streams, rivers, reservoirs and ponds. In this study some Italian natural lakes, one fluvial lake and one river were considered. Italy has the highest number of lakes among Mediterranean countries; its most important lacustrine region is located in Northern Italy and includes deep subalpine lakes and some small–medium lakes. These lakes represent more than 90 % of the total Italian freshwater volume [59, 60]. The largest Italian subalpine lakes have morphometric characteristics in common: they are narrow, with north–south elongated shapes, and their floors lie below sea level.

The Italian subalpine lakes have high ecological and environmental value and are valuable resources of water within densely inhabited areas. Management and conservation of water quality and maintenance of biodiversity currently represent topics of major importance because of the need for technical support and scientific data for planning needed interventions. Within such a frame, imaging spectrometry definitely

represents a modern technology. In particular, since late 1990s airborne MIVIS hyperspectral data have been mainly used in Italy to assess inland water quality [61].

The hyperspectral Multispectral Infrared Visible Imaging Spectrometer (MIVIS) sensor [62, 63] is a Daedalus modular system composed of four imaging spectrometers which simultaneously record radiation coming from the Earth in 102 spectral channels from the visible to thermal infrared red spectral range (wavelengths ranging between 0.43 and 12.7 μm). MIVIS has been demonstrated to be a powerful instrument for mapping purposes in many different natural contexts, including lakes, lagoons and wetlands (e.g. [64, 65]). Results showed the great potential of the MIVIS sensor to clarify complex dynamics between primary producers [66], track their evolution [67], evidence complex patterns in the distribution of submerged aquatic vegetation and SPM [68], map macrophyte distribution and changes [67, 69, 70] and finally provide useful information to ecologists and environmental managers.

Figure 2 shows the location of the waterbodies considered in this study: three natural lakes (Garda and Idro in northern Italy and Trasimeno in central Italy), a system of three small fluvial lakes in Mantua and the Po River (where it receives the

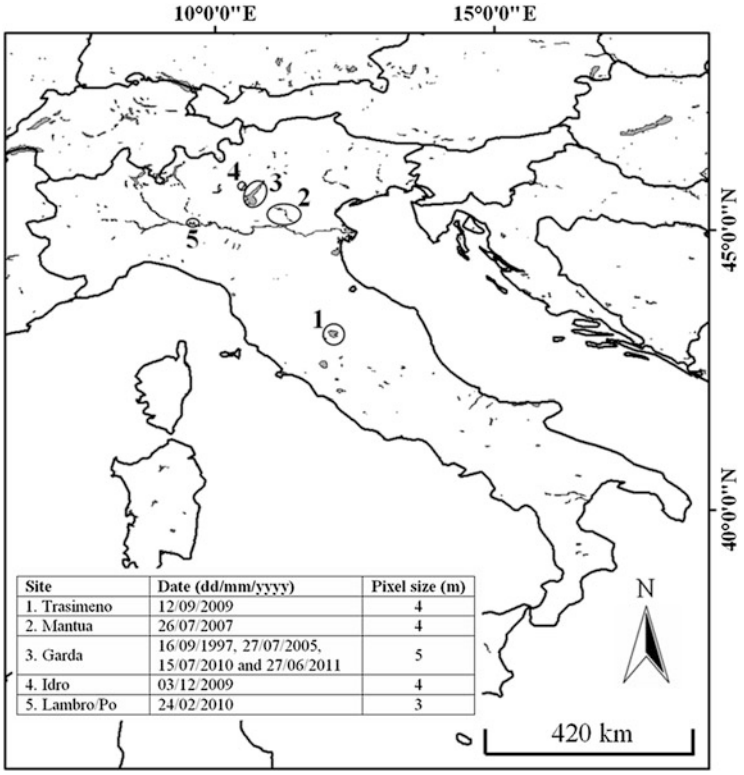

Site	Date (dd/mm/yyyy)	Pixel size (m)
1. Trasimeno	12/09/2009	4
2. Mantua	26/07/2007	4
3. Garda	16/09/1997, 27/07/2005, 15/07/2010 and 27/06/2011	5
4. Idro	03/12/2009	4
5. Lambro/Po	24/02/2010	3

Fig. 2 Position and names of waterbodies and MIVIS imagery data shown in the table (*map source*: Global Lakes and Wetlands Database)

waters from Lambro River). For those sites, MIVIS imagery has been acquired (cf. the table in Fig. 2) and analysed to investigate their water quality, as discussed in the following paragraphs.

4.1 Data Processing

The processing of MIVIS imagery, used in this study, is performed to correct data for atmospheric effects and subsequently, for some applications, to retrieve water quality parameters, substrate types and bottom depth.

The atmospheric correction was achieved with either ATCOR-4 [71] or 6S (Second Simulation of a Satellite Signal in the Solar Spectrum, vector version n. 1) [72] codes. ATCOR-4 is an atmospheric correction code used for the atmospheric correction of small and wide Field Of View (FOV) airborne sensors. ATCOR-4 uses look-up tables generated by MODerate resolution atmospheric TRANsmission (MODTRAN) [73, 74], relating sensor radiances and albedo for various atmospheric and geometric conditions. The 6S code is a basic radiative transfer code which enables accurate simulations of satellite and plane observation, accounting for elevated targets, use of anisotropic and Lambertian surfaces and calculation of gaseous absorption. The 6S also performs the atmospheric correction that, starting from the top-of-atmosphere radiance (or reflectance), allow the atmospherically corrected reflectance to be computed.

The retrieval of the optical properties of water column and bottom from atmospherically corrected imagery was achieved with BOMBER (Bio-Optical Model Based tool for Estimating water quality and bottom properties from Remote sensing images), a software package [75] based on the works from [41, 76, 77], which makes a spectral inversion of bio-optical models for optically deep and optically shallow waters. Several menus allow the user to choose the model type, to specify the input and output files and to set all of the variables involved in the model parameterisation and inversion. The inversion is performed with an optimisation technique [78] that simultaneously produces the maps of chl-a, SPM, CDOM and, in case of shallow waters, bottom depth and distributions of up to three different types of substrate. For both deep and shallow water models, a map of the relative error involved in the inversion procedure is also given.

In this study, both ATCOR-4 and 6S were run with rural and continental aerosol models, respectively, and by setting the target's altitude and the solar-target geometry; in all cases the aerosol concentration (or the visibility range) was derived from in situ measurements of the aerosol optical thickness. Then, the parameterisation of the bio-optical model implemented in BOMBER was carried out based on in situ measurements collected in the study areas.

4.2 Water Quality in Lake Trasimeno

Lake Trasimeno, a post-tectonic lake situated in central Italy, is the fourth largest Italian lake (124 km^2). The lake is almost round with a diameter of about 11 km, three small islands and an open bay colonised by aquatic vegetation in the south-eastern part. Tourism, agriculture and livestock breeding are the most important activities in the Trasimeno area: cultivated lands cover about 70 % of its catchment area (intensive agriculture with irrigational needs is only present in 28 % of the area). Lake Trasimeno is a closed lake, with shallow unstratified waters (average bottom depth is 4.5 m; maximum depth is 6 m). The lake shows from mesotrophic to eutrophic conditions, where principal critical parameters are phosphorous and chl-a, despite biological evidence of eutrophic–hypertrophic conditions. Important ecological constraints are recurring sediment resuspension phenomena and phytoplankton blooms, including those of cyanobacteria [79].

The concentrations of chl-a, SPM and CDOM were estimated using MIVIS data acquired on 12 September 2009 in the eastern portion of Lake Trasimeno. The atmospheric correction of MIVIS data was carried out using ATCOR-4. Then, the conversion of water reflectance into concentrations was based on a spectral inversion procedure implemented in BOMBER. The bio-optical model implemented in BOMBER was parameterised with data gathered from fieldwork activities performed in 2008 and 2009.

Figure 3 shows the BOMBER-retrieved products in the optically deep waters describing the concentrations of SPM, chl-a and $a_{CDOM}(440)$. The average values of SPM, chl-a and CDOM were, respectively, 5.9 gm^{-3} (standard deviation (SD) = 1.0 gm^{-3}), 1.1 mgm^{-3} (SD = 0.5 mgm^{-3}) and 0.35 m^{-1} (SD = 0.06 m^{-1}). These values are reliable for the season, as in late spring lake waters have acceptable quality that degrades from mid-summer until mid-autumn, when the lake is affected by phytoplankton blooms [80]. Figure 4 shows the scatter plots of chl-a vs. SPM, chl-a vs. CDOM and SPM vs. CDOM. The correlation is poor for each pair of water quality parameters, confirming that Lake Trasimeno is typical Case-2 water.

4.3 Cyanobacteria Bloom in Lakes of Mantua

The lakes of Mantua are three small and shallow lakes surrounding the city of Mantua; the Upper Lake is 3.7 km^2 and has a mean depth of 3.6 m, the Middle Lake is 1.1 km^2 with a mean depth of 3.0 m and the Lower Lake is 1.5 km^2 with a mean depth of 3.3 m. The system of lakes is fed by the Mincio River, the emissary of Lake Garda that was dammed during the twelfth century. The average flow of the Mincio River usually decreases in summer (up to −90 %) from the combination of upstream water deviation for irrigation purposes and less frequency of rain, with consequent water stagnation and increased residence time [81].

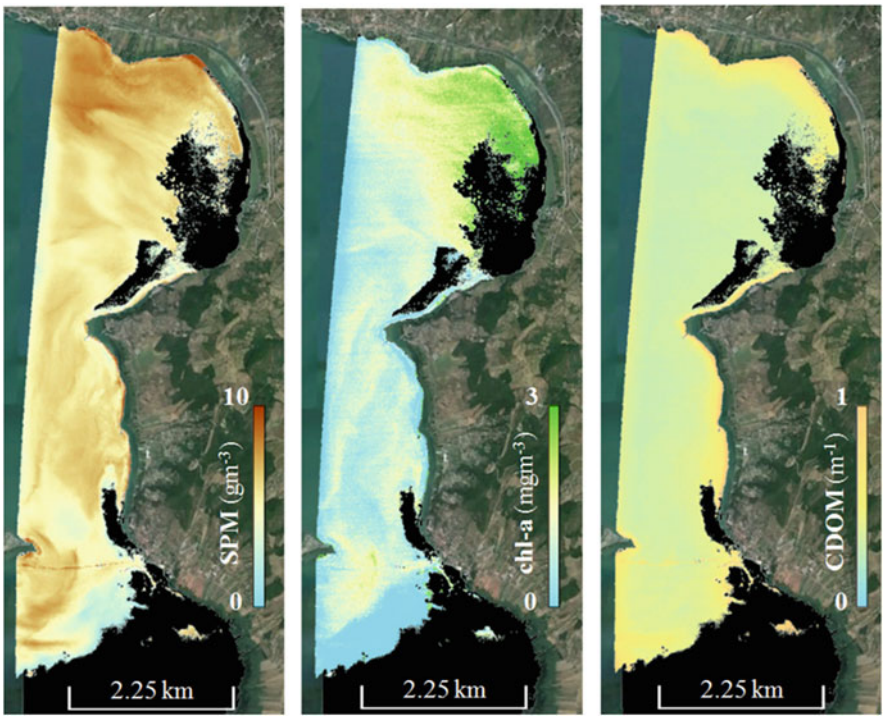

Fig. 3 Three BOMBER-retrieved products obtained from MIVIS data acquired on 12 September 2009 (the shallow waters are masked and printed in *black*)

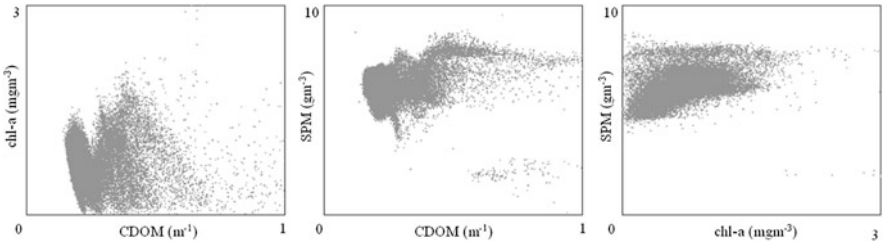

Fig. 4 Moving from left to right scatter plots of chl-a vs. CDOM, SPM vs. CDOM and SPM vs. chl-a (each point is a MIVIS pixel)

The water column hosts phytoplankton communities typical of eutrophic and/or hypertrophic systems rich in organic matter (e.g. diatoms in spring, cyanobacteria and chlorophytes in summer and autumn; [81]). Water stagnation favours phytoplankton blooms and chl-a can peak up to 200 mgm^{-3} in conjunction with the minimum river flows (~2 m^3s^{-1}). The presence of cyanobacteria is a major concern of the study area due to the potentiality of containing or releasing toxins into the water when the algae die and decay.

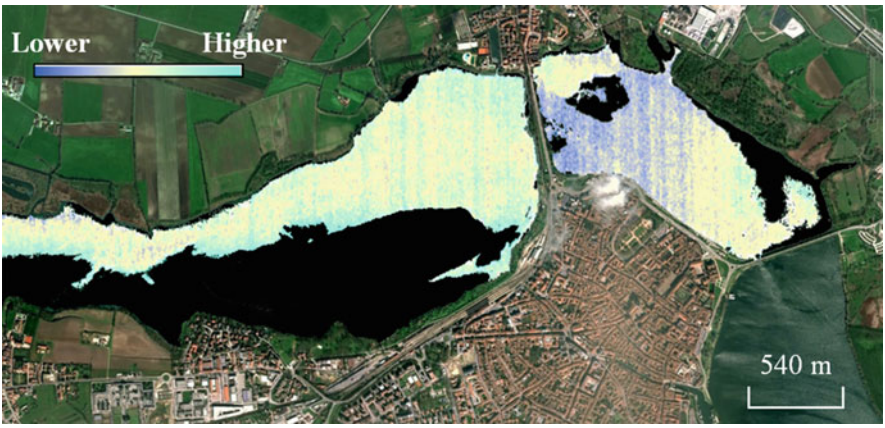

Fig. 5 Cyanobacteria abundance map of Mantua lakes derived from MIVIS data (glinted areas are masked in *black*)

Kutser [52] made a review of passive optical remote sensing methods and techniques for assessing cyanobacteria and other intense phytoplankton blooms in coastal and inland waters. Most of the methods used to detect cyanobacteria are based on the spectral characteristics of their accessory pigments (e.g. phycocyanins, phycoerythrin) associated with different algal species (e.g. *Microcystis* spp., *Planktothrix* spp.). According to Kutser [43], MIVIS bands 10 (620 nm) and 11 (640 nm) allow PC absorption feature near 630 nm and a small peak in reflectance spectra near 650 nm characteristic to cyanobacteria containing PC to be detected.

MIVIS data were acquired on 26 July 2007, with a sun elevation of 63° and an orientation of the sensor that unfortunately produced wave-induced sun glint patterns in some parts of the image (for the purposes of this study, those glint patterns were masked). Glint-free data were transformed into water reflectance using the empirical line method calibrated with in situ water reflectance collected during the MIVIS overpass as described in Bresciani et al. [82] and Giardino et al. [83]. MIVIS data were further elaborated to assess the spatial distribution of cyanobacteria. Figure 5 shows the map depicting the relative abundance of cyanobacteria (according to filed observation, it was mainly composed of *Oscillatoria* sp., *Microcystis* sp. and *Aphanizomenon* sp.).

4.4 Macrophyte Beds in Lake Garda

Lake Garda, located in the subalpine lake district, is the largest Italian lake (368 km^2). Its water volume is 49 km^3 and has an average depth of 133 m (to a maximum of 350 m). Lake Garda represents a valuable renewable resource,

because of the multiple uses of its waters. Similar to other subalpine lakes (e.g. Maggiore, Como, Iseo and Idro), it represents an essential strategic water supply for agriculture, industry, fishing and drinking. In its southern part, Lake Garda is characterised by gentle slopes which facilitate the growth of submerged macrophytes and the emergent *Phragmites australis* in the coastal zone. This ecosystem is highly vulnerable to anthropogenic perturbations (e.g. water level variations for agriculture and energy use and navigation), and according to the European rules [84] rigorous monitoring of the lake is required. In this context, high spatial and high spectral resolutions provide opportunities for cost-effective qualitative and quantitative analyses of the macrophyte distribution and change.

MIVIS imagery was acquired on 16 September 1997, 27 July 2005, 15 July 2010 and 27 June 2011 for the southern part of Lake Garda (Sirmione Peninsula). During the airborne campaign performed on 27 June 2011, a flight plan consisting of 12 runs was successfully accomplished covering the entire coastline of Lake Garda. The airborne campaigns were always performed synchronously with fieldwork activities aiming to gather data for the calibration of a bio-optical model and assessing the MIVIS-derived products.

MIVIS data were corrected for atmospheric effects with either 6S or ATCOR-4, the latter used in the latest acquisitions. The classification of submerged macrophytes and uncolonised sandy substrates was achieved by the spectral inversion of the atmospherically corrected MIVIS reflectances. Similarly to Lake Trasimeno, the spectral inversion was achieved with BOMBER where the implemented bio-optical model for shallow waters was parameterised with data gathered from fieldwork activities—in excess of 60 days over 10 years of in situ measurements. The bottom cover identification has been mapped considering bottom depths (i.e. those estimated with BOMBER synchronously with retrieval of bottom types) lower than 7 m, according to Giardino et al. [69], which is the limit of sensitivity of the model in Lake Garda waters.

Figure 6 shows the distribution of macrophytes in the whole Lake Garda: in the northern and in the central parts, the presence of macrophytes is small because the morphological characteristics (slopes descending fast to the lake) are not suitable for the growth of macrophytes; conversely depth gradients in the southern Lake Garda facilitate the growth of macrophytes. About 20.5 km^2 of shallow waters (i.e. bottom depth <7 m) has been mapped: approximately 17 km^2 is characterised by the presence of macrophytes, even if in some cases sparse.

Figure 7 shows the histogram depicting the height of the water column above the canopy in the Sirmione Peninsula area (cf. Fig. 6, zoom with the red frame) as derived by the MIVIS data collected from 1997 to 2011, according to the procedure described above (for more details refer to Bresciani et al. [67] and Giardino et al. [69]). The height of the water column above macrophytes is plotted together with water level fluctuation and water clarity (both derived from in situ measurements); the macrophyte distribution along the littoral zone of the Sirmione Peninsula might be linked to those two physical parameters; thus, the macrophyte change is then a consequence of both the anthropogenic pressure and meteo-climatic variations.

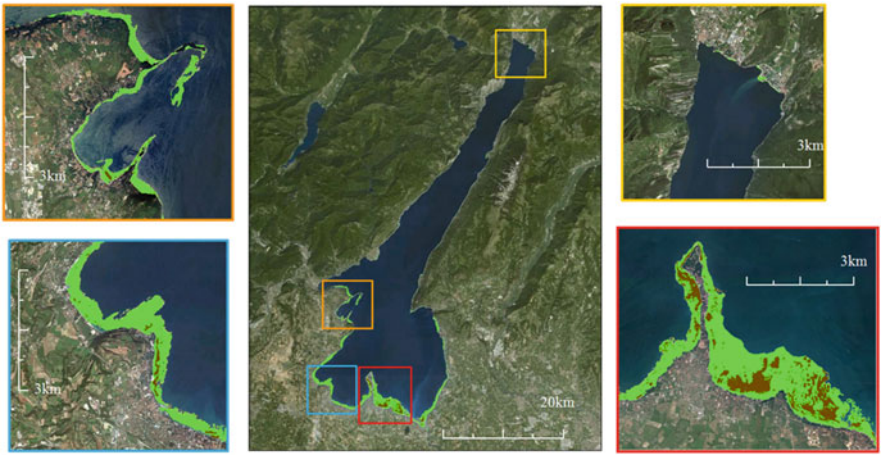

Fig. 6 Macrophytes (in *green*) cover map, up to 7 m depth, as estimated from MIVIS imagery acquired on 27 June 2011

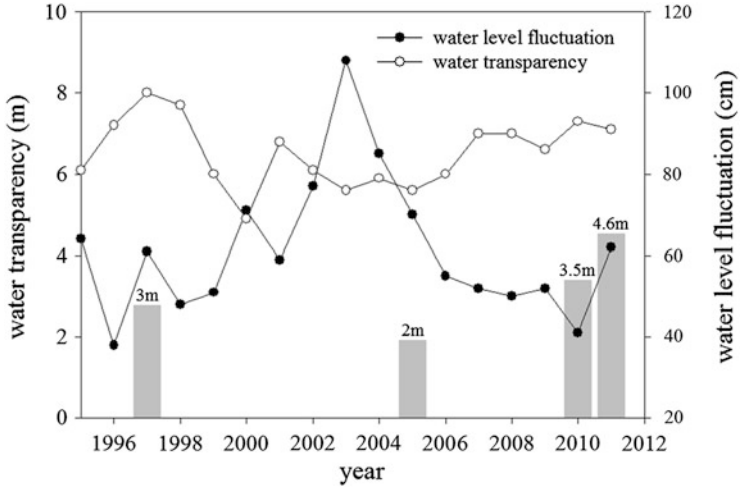

Fig. 7 The *histogram bars* show the height of the water column above the macrophyte bed in the Sirmione Peninsula area (cf. Fig. 6, *red box*) as derived by the MIVIS data collected from 1997 to 2011. The *two lines* show water level fluctuation and water clarity for the same period

4.5 Floating Materials in Lake Idro

Lake Idro is located in the subalpine district, west of Lake Garda, at an altitude of 368 m above sea level. The lake surface area is 11.03 km^2, maximum depth about 124 m and lake volume approximately 0.85 km^3. According to its trophic status, the

lake is meso-eutrophic and belongs to the meromictic type of circulation. The lake provides an important economic source for the local population mainly in terms of tourism recreation. It is the first Italian natural lake entirely transformed to a hydroelectric reservoir in 1929. Throughout the past decade, the progressive stabilisation of the water levels has enhanced the development, maintenance and proliferation of dense macrophyte stands all around the littoral zone, as a probable consequence of nutrient and organic matter accumulation in surface sediments. The steep slopes surrounding the lake are colonised by a mixed deciduous forest. Depending on the season, pollens, dead leaves and other terrestrial material might be easily transported into the air and deposited in the lake.

Beyond the reproductive function, the role of pollen in ecosystems, including Lake Idro, is poorly investigated. There are few evidences for its trophic function [85] or for its ability to convey harmful substances and/or toxins. There are numerous species, genera and families characterised by the production of allergenic pollen, among these the Pinaceae. The family Pinaceae includes many genera distributed throughout the Italian territory, anticipated pollen production in late autumn. An example is represented by *Cedrus* (such as *C. libani* and *C. deodara*), in the basin of Lake Idro, that during windy days is likely to be also transported on the water surface.

The accumulation of floating materials on the water surface might lead to complications for water-related interpretation and studies due to potential problems of specular reflection and other influences on colour and brightness. Since floating materials (e.g. plants) might have a significantly different spectra signal from that of water, the detection of those materials can be remotely sensed. Commonly, the algorithms which allow those materials to be detected from passive remote sensing make use of the near-infrared wavelength as it is expected that in this region the signal coming from water is usually relatively low. Villa et al. [86] showed how good floating vegetation monitoring capabilities are ensured by the use of simple and straightforward approaches based on vegetation indices.

Figure 8 shows a deposition phenomenon of terrestrial origin on Lake Idro observed by MIVIS data acquired on 3 December 2009: because it was early December, most likely the *Cedrus* species are responsible for the observed phenomenon. The atmospherically corrected reflectance obtained with ATCOR-4 shows (cf. pasted graph in Fig. 8) the different behaviour of the signal coming from the Lake Idro waters with respect to those where the pollen was floating. The spatial dimension of the phenomenon underlines the possible local impact of the dispersion of pollen and the role it may have in ecosystems, especially aquatic ecosystems.

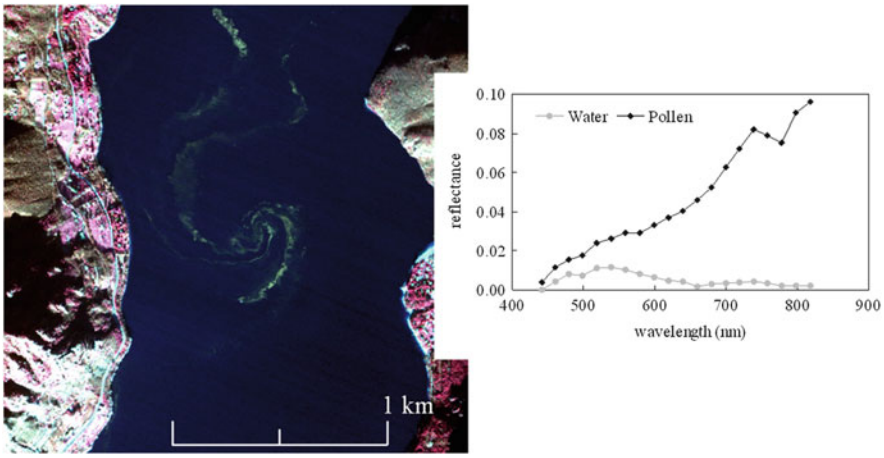

Fig. 8 The false colour MIVIS image of Lake Idro clearly shows floating materials of terrestrial origin (i.e. pollen from *C. libani* and *C. deodara*). The graph shows the atmospherically corrected MIVIS reflectance derived from the lake surface from pixels where the pollen is floating (i.e. *black line*) or absent (*gray line*)

4.6 Oil Spill in Confluence of Lambro and Po Rivers

The Po River, 652 km in length, is the main Italian river. The Po watershed drains 70,000 km^2, and land use is both industrial and agricultural. The Lambro River, a tributary of the Po River (ca. 350 km from the mouth), flows through the most heavily industrialised and densely populated portion of the Po River basin. The stretch of the Po River, located immediately downstream from the confluence of the Lambro River, does not receive any other major tributary for about 21 km along its course. The approximate annual mean flow of the two waterbodies is ~70 m^3s^{-1} for the Lambro River and ~580 m^3s^{-1} for the Po River in its middle reach [87]. Despite the implementation of a sewage treatment plant built in 2002, the Lambro River water quality remains poor [88].

On 23 February 2010, the contents of several silos containing oil and other hydrocarbons poured into the river north of Milano. This oily mass (estimated over 2.5 million litres) flowed down the entire length of the Lambro River, and despite both local authorities' and civil defence's efforts to stop the flow, on 24 February the oil entered the Po River. This disaster, of course, caused considerable damage to wildlife and vegetation in both rivers.

Airborne human observations can meet the primary need to identify an oil spill but, when airborne observations are combined with imaging spectrometry, a detailed map of the oil spill can be generated. Leifer et al. [89] made a substantial review on oil spill remote sensing, including a segment on airborne imaging spectrometry (cf. Table 2 in [89]). The electromagnetic spectrum, almost entirely, from the ultraviolet toward the thermal infrared wavelengths (and further beyond the microwave region), can be used for deriving information on oil spill events.

Within the visible near-infrared wavelengths, the detection of areas affected by a floating oil spill can make use of spectral differences between oil and water [90]. With respect to satellite, airborne hyperspectral and thermal infrared data have free-overcast collection and free-scheduling advantages. In particular, the timeframe for collecting and processing the data is important for oil spill surveillance and monitoring; data should be available in real-time and permit easy interpretation and use. Time is particularly critical for an oil spill occurring in rivers as water current can rapidly spread the oil over a long area in a short time.

We mapped the distribution of the oil spill flows from MIVIS data acquired on 24 February 2010; the flight was undertaken in the study area due to the alert status happening in Lambro River the day before. MIVIS data were collected from an altitude of 1,500 m with a spatial resolution of 3 m. Figure 9 shows a true colour

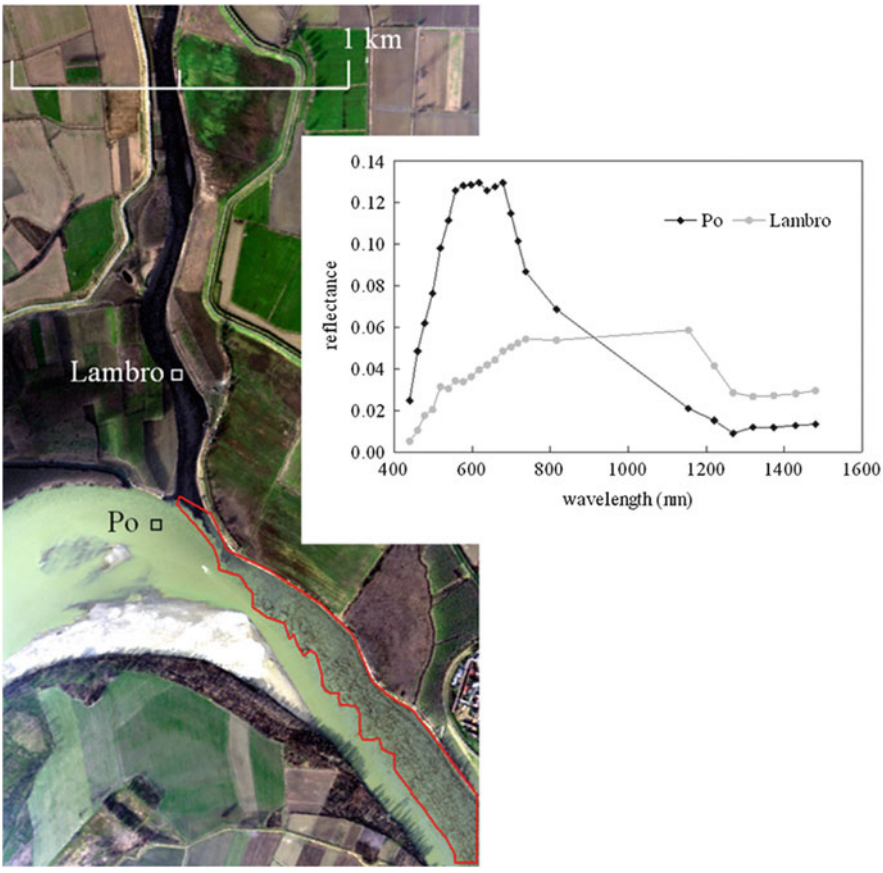

Fig. 9 The true colour MIVIS image clearly shows the transport of oil from Lambro into Po, where the *red line* outlines the oil flow in the Po River. The graph shows the atmospherically corrected MIVIS reflectance of the two rivers from pixels outlined in the image (*white* and *black squares* for Lambro and Po, respectively)

composition of the oil flowing from Lambro into Po River. The atmospherically corrected reflectance achieved with ATCOR-4 shows the different behaviour of the signal coming from the very turbid Po River waters with respect to those of Lambro River, where the oil film produce a spectral signature that is comparable to literature data [89].

In this application, the clear advantages of MIVIS were the flexibility of timing of flight and its spatial resolution. Further studies would need to better investigate the hyperspectral signal coming from oil in order to fully exploit the capabilities of this sensor which spans from visible to near-short wave and thermal infrared.

5 Conclusions

The quality of surface water in lakes, streams and reservoirs is a major concern around the world. Inland waters might be often strongly affected by changes due to the increasing anthropogenic pressure and meteo-climatic variations [91, 92]. These ecosystems are inestimable renewable natural resources for biodiversity and may also represent an essential strategic water supply for agriculture, industry, fishing and drinking water. In many countries lakes are an important resource for recreation and tourism with attractive landscape, mild climate and safe water quality. Therefore, any effort placed for preserving and/or improving the quality of these resources is justified.

In such a framework, remote sensing offers a useful tool for a variety of studies which need multi-scale analyses. Because imaging spectrometry provides a continuous signal of reflected radiation from visible to infrared wavelengths, it provides a means to investigate a variety of key bio-physical parameters such as phytoplankton pigments or bottom substrata types. In particular, airborne imaging spectrometry gathers data with a spatial resolution often more suitable for the fine-scale studies developed for freshwater aquatic ecology [93].

This chapter presented an overview of imaging spectrometry for Case-2 optically complex waters that, besides marine coastal zones, also include inland waters. The case studies of Italian lakes and rivers show how data acquired from the airborne MIVIS sensors can be used to: (1) assess chl-a, SPM and CDOM concentrations; (2) detect cyanobacteria bloom; and (3) map submerged macrophyte colonisation patterns and their recent changes. Two applications using MIVIS to recognise floating materials are presented by focusing on the advantages of a fine spatial scale and a flexible flight path, which are mandatory to monitor water quality in rivers and streams because of temporally dynamic conditions [94].

Hyperspectral airborne observations will keep contributing to freshwater aquatic ecology studies and water quality monitoring as a very efficient means to extend laboratory and ground-based measurements at local and regional scales. To fill the gap in scale from regional to global, satellite missions that deploy imaging spectrometers for regular acquisitions (e.g. Landsat) are instead required (e.g. HyspIRI).

Future research priorities that improve the exploitation of airborne imagery for water quality purposes might include: (1) a need to investigate the improvements gained from the synergistic use of different sensors in shallow waters (e.g. the use of aerial LiDAR bathymetry adds data on geomorphic features for the benthic habitat mapping achieved by imaging spectrometry); (2) a need of advanced spectral inversion techniques to simultaneously retrieve the concentrations of phytoplankton pigments (e.g. chl-a, phycocyanin and phycoerythrin); (3) a need of unmanned aerial vehicles equipped with hyperspectral sensors to make the tool more cost-effective and thence routinely used technique for water quality at local scale.

Acknowledgements MIVIS data presented in this chapter were provided by A. Cavazzini, G. Pizzaferri (Blom CGR Parma), C. Defrancesco (APPA Trento) and A. Martinelli (ARPA Lazio). This study would have not been possible without contributions provided by M. Bartoli and R. Bolpagni (University of Parma), M. Musanti (CNR-IREA) and G.L. Fila (CRA Municipality of Sirmione) during these years. This study was co-funded by European Union (FP7-People Co-funding of Regional, National and International Programmes, GA n. 600407) and the CNR RITMARE Flagship Project.

References

1. Bukata RP, Jerome JH, Kondratyev KY, Pozdnyakov DV (1995) Optical properties and remote sensing of inland coastal waters. CRC, Boca Raton, p 384
2. Morel A, Prieur L (1977) Analysis of variations in ocean color. Limnol Oceanogr 22(4): 709–722
3. Schalles JF (2006) Optical remote sensing techniques to estimate phytoplankton chlorophyll a concentrations in coastal waters with varying suspended matter and CDOM concentrations. In: Richardson LL, LeDrew EF (eds) Remote sensing of aquatic coastal ecosystem processes: science and management applications. Springer, Dordrecht, pp 27–79
4. Viaroli P, Lasserre P, Campostrini P (2007) Lagoons and coastal wetlands in the global change context: impacts and management issues. Hydrobiologia 577:1–168
5. Moses WJ, Gitelson AA, Perk RL, Gurlin D, Rundquist DC, Leavitt BC, Barrow TM, Barkhage P (2012) Estimation of chlorophyll-a concentration in turbid productive waters using airborne hyperspectral data. Water Res 46(4):993–1004
6. Gower J, King S (2007) Validation of chlorophyll fluorescence derived from MERIS on the west coast of Canada. Int J Remote Sens 28:625–635
7. Song K, Li L, Li Z, Tedesco L, Hall B, Shi K (2013) Remote detection of cyanobacteria through phycocyanin for water supply source using three-band model. Ecol Inform 15:22–33
8. Simis SGH, Peters SWM, Gons HJ (2005) Remote sensing of the cyanobacterial pigment phycocyanin in turbid inland water. Limnol Oceanogr 50:237–245
9. Knaeps E, Dogliotti AI, Raymaekers D, Ruddick K, Sterckx S (2012) In situ evidence of non-zero reflectance in the OLCI 1020 nm band for a turbid estuary. Remote Sens Environ 120:133–144
10. Eleveld MA (2012) Wind-induced resuspension in a shallow lake from Medium Resolution Imaging Spectrometer (MERIS) full-resolution reflectances. Water Resour Res. 48(4). doi:10.1029/2011WR011121

11. Doxaran D, Cherukuru RCN, Lavender SJ (2006) Inherent and apparent optical properties of turbid estuarine waters: measurements, modelling and application to remote sensing. Appl Optics 45:2310–2324
12. Kutser T, Pierson DC, Kallio K, Reinart A, Sobek S (2005) Mapping lake CDOM by satellite remote sensing. Remote Sens Environ 94:535–540
13. Lee ZP, Darecki M, Carder KL, Davis CO, Stramski D, Rhea WJ (2005) Diffuse attenuation coefficient of downwelling irradiance: an evaluation of remote sensing methods. J Geophys Res 110:C02017
14. Adamo M, De Carolis G, De Pasquale V, Pasquariello G (2009) Detection and tracking of oil slicks on sun-glittered visible and near infrared satellite imagery. Int J Remote Sens 30: 6403–6427
15. Matthews MW, Bernard S, Robertson L (2012) An algorithm for detecting trophic status (chlorophyll-a), cyanobacterial-dominance, surface scums and floating vegetation in inland and coastal waters. Remote Sens Environ 124:637–652
16. Hunter PD, Gilvear DJ, Tyler AN, Willby NJ, Kelly A (2010) Mapping macrophytic vegetation in shallow lakes using the Compact Airborne Spectrographic Imager (CASI). Aquat Conserv 20:717–727. doi:10.1002/aqc.1144
17. Hu C (2009) A novel ocean color index to detect floating algae in the global oceans. Remote Sens Environ 113:2118–2129
18. Klemas V (2013) Remote sensing of emergent and submerged wetlands: an overview. Int J Remote Sens 34(18):6286–6320
19. Fearns PRC, Klonowski W, Babcock RC, England P, Phillips J (2011) Shallow water substrate mapping using hyperspectral remote sensing. Cont Shelf Res 31:1249–1259
20. Alberotanza L, Cavalli RM, Pignatti S, Zandonella A (2006) Classification of submersed aquatic vegetation of the Venice lagoon using MIVIS airborne data. Ann Geophys-Italy 49(1):271–276
21. Marani M, Belluco E, Ferrari S, Silvestri S, D'Alpaos A, Lanzoni S, Feola A, Rinadlo A (2006) Analysis, synthesis and modelling of high-resolution observations of salt-marsh eco-geomorph ological patterns in the Venice lagoon. Estuar Coast Shelf Sci 69:414–426
22. Dekker AG, Brando VE, Anstee JM (2005) Retrospective seagrass change detection in a shallow coastal tidal Australian lake. Remote Sens Environ 97:415–433
23. Odermatt D, Gitelson A, Brando VE, Schaepman M (2012) Review of constituent retrieval in optically deep and complex waters from satellite imagery. Remote Sens Environ 118:116–126
24. Dekker AG, Malthus TJ, Hoogenboom HJ (1995) The remote sensing of inland water quality. In: Danson FM, Plummer SE (eds) Advances in environmental remote sensing. Wiley, Hoboken, pp 123–142
25. Cracknell AP, Newcombe SK, Black AF (2001) The ADMAP (algal bloom detection, monitoring and prediction) concerted action. Int J Remote Sens 22:205–247
26. Gons HJ, Hakvoort H, Peters SWM, Simis SGH (2005) Optical detection of cyanobacterial blooms. In: Huisman J, Matthijs HCP, Visser PM (eds) Harmful cyanobacteria. Springer, Dordrecht, pp 177–199
27. Gons HJ, Rijkeboer M, Ruddick KG (2002) A chlorophyll retrieval algorithm for satellite imagery (Medium Resolution Imaging Spectrometer) of inland and coastal waters. J Plankton Res 24:947–951
28. Gitelson AA, Schalles JF, Hladik CM (2007) Remote chlorophyll-a retrieval in turbid, productive estuaries: Chesapeake Bay case study. Remote Sens Environ 109:464–472
29. Thiemann S, Kaufman H (2000) Determination of chlorophyll content and tropic state of lakes using field spectrometer and IRS-IC satellite data in the Mecklenburg Lake Distract, Germany. Remote Sens Environ 73:227–235
30. Mobley CD (1994) Light and water-radiative transfer in natural waters. Academic, San Diego, p 591

31. Vermote EF, Tanrè D, Deizè JL, Herman M, Morcrette JJ (1997) Second simulation of the satellite signal in the solar spectrum, 6S: an overview. IEEE Trans Geosci Remote Sens 35(3): 675–686
32. Brando VE, Dekker AG (2003) Satellite hyperspectral remote sensing for estimating estuarine and coastal water quality. IEEE Trans Geosci Remote Sens 41:1378–1387
33. Keller PA (2001) Comparison of two inversion techniques of a semianalytical model for the determination of lake water constituents using imaging spectrometry data. Sci Total Environ 268:189–196
34. Schaale M, Fischer J, Olbert C (1998) Quantitative estimation of substances contained in inland water from multispectral airborne measurements by neural networks. In: Proceedings of the ASPRS-RTI annual conference, Tampa, Florida, 30 March–3 April 1998, pp 1345–1356
35. Schroeder T, Schaale M, Fischer J (2007) Retrieval of atmospheric and oceanic properties from MERIS measurements: a new case-2 water processor for BEAM. Int J Remote Sens 28: 5627–5632
36. Mobley CD, Sundman LK, Boss E (2002) Phase function effects on oceanic light fields. Appl Optics 41:1035–1050
37. Peters SWM, Eleveld M, Pasterkamp R, van der Woerd HJ, DeVolder M, Jans S, Ruddick K, Block T (2005) Atlas of chlorophyll-a concentration for the North Sea based on MERIS imagery of 2003. Vrije Universiteit, Amsterdam, p 121. http://www.brockmann-consult.de/revamp. Accessed 25 July 2014
38. Dekker AG, Phinn SR, Anstee J, Bissett P, Brando VE, Casey B, Fearns P, Hedley J, Klonowski W, Lee ZP, Lynch M, Lyons M, Mobley C, Roelfsema C (2011) Intercomparison of shallow water bathymetry, hydro-optics, and benthos mapping techniques in Australian and Caribbean coastal environments. Limnol Oceanogr 9:396–425
39. Heege T, Bogner A, Pinnel N (2004) Mapping of submerged aquatic vegetation with a physically based process chain. In: Proceedings SPIE 5233, remote sensing of the ocean and sea ice 2003, 43
40. Gege P (2004) The water color simulator WASI: an integrating software tool for analysis and simulation of optical in situ spectra. Comput Geosci 30:523–532
41. Lee Z, Carder KL, Mobley CD, Steward RG, Patch JS (1999) Hyperspectral remote sensing for shallow waters: 2. Deriving bottom depth sand water properties by optimization. Appl Optics 38:3831–3843
42. Lee Z, Carder KL, Chen RF, Peacock TG (2001) Properties of the water column and bottom derived from Airborne Visible Infrared Imaging Spectrometer (AVIRIS) data. J Geophys Res 106(11):639–651
43. Kutser T (2004) Quantitative detection of chlorophyll in cyanobacterial blooms by satellite remote sensing. Limnol Oceanogr 49:2179–2189
44. Giardino C, Brando VE, Dekker AG, Strömbeck N, Candiani G (2007) Assessment of water quality in Lake Garda (Italy) using Hyperion. Remote Sens Environ 109:183–195
45. IOCCG (2006) Remote sensing of inherent optical properties: fundamentals, tests of algorithms, and applications. In: Lee ZP (ed) Reports of the International Ocean-Colour Coordinating Group. IOCCG, Dartmouth, p 122
46. Mustard JF, Staid MI, Fripp WJ (2001) A semianalytical approach to the calibration of AVIRIS data to reflectance over water application in a temperate estuary. Remote Sens Environ 75:335–349
47. Vahtmäe E, Kutser T (2008) Sun glint correction of airborne AISA images for mapping shallow-water benthos. In: IEEE/OES Us/EU-Baltic international symposium: US/EU-Baltic international symposium, IEEE, Tallinn, 2008, pp 239–246
48. Cavalli RM, Pignatti S, Zappitelli E (2006) Correction on sun glint effect on MIVIS data of the Sicily campaign in July 2000. Ann Geophys-Italy 49(1):277–286
49. Hochberg EJ, Andrefouet S, Tyler MR (2003) Sea surface correction of high spatial resolution IKONOS images to improve bottom mapping in near-shore environments. IEEE Trans Geosci Remote Sens 41:1724–1729

50. Dekker AG, Peters SWM, Vos RJ, Rijkeboer JCJ (2001) Remote sensing for inland water quality detection and monitoring: state-of-the-art application in Friesland waters. In: Van Dijk A, Bos MG (eds) GIS and remote sensing technology in land and water management. Kluwer, Dordrecht, pp 17–38
51. Devred E, Turpie K, Moses W, Klemas VV, Moisan T, Babib M, Toro-Farmer G, Forget MH, Jo YH (2013) Future retrievals of water column bio-optical properties using the Hyperspectral Infrared Imager (HyspIRI). Remote Sens 5:6812–6837
52. Kutser T (2009) Passive optical remote sensing of cyanobacteria and other intense phytoplankton blooms in coastal and inland waters. Int J Remote Sens 30(17):4401–4425
53. Braga F, Giardino C, Bassani C, Matta E, Candiani G, Strömbeck N, Adamo M, Bresciani M (2013) Assessing water quality in the northern Adriatic Sea from HICO™ data. Remote Sens Lett 4(10):1028–1037
54. Gitelson AA, Gao BC, Li RR, Berdnikov S, Saprygin V (2011) Estimation of chlorophyll-a concentration in productive turbid waters using a Hyperspectral Imager for the Coastal Ocean—the Azov Sea case study. Environ Res Lett 6(2). doi:10.1088/1748-9326/6/2/024023
55. Lee Z, Casey B, Arnone R, Weidemann A, Parsons R, Montes MJ, Gao BC, Goode W, Davis C, Dye J (2007) Water and bottom properties of a coastal environment derived from Hyperion data measured from the EO-1 spacecraft platform. J Appl Remote Sens 1(1):011502. doi:10.1117/1.2822610
56. Özesmi SL, Bauer ME (2002) Satellite remote sensing of wetlands. Wetl Ecol Manag 10: 381–402
57. Koponen S, Pulliainen J, Kallio K, Hallikainen M (2002) Lake water quality classification with airborne hyperspectral spectrometer and simulated MERIS data. Remote Sens Environ 79: 51–59
58. Giardino C, Candiani G, Zilioli E (2005) Detecting chlorophyll-a in Lake Garda (Italy) using TOA MERIS radiances. Photogramm Eng Remote Sens 71(9):1045–1052
59. Salmaso N, Mosello R (2010) Limnological research in the deep southern subalpine lakes: synthesis, directions and perspectives. Adv Oceanogr Limnol 1:1–47
60. Rossaro B, Boggero A, Lencioni V, Marziali L, Solimini A (2006) Tools for the development of a benthic quality index for Italian lakes. J Limnol 65(1):41–51
61. Lindell T, Pierson D, Premazzi G (1999) Manual for monitoring European lakes using remote sensing techniques. EUR Report n.18665 EN. Office for Official Publications of the European Communities, Luxembourg, p 164
62. Bianchi R, Marino CM, Pignatti S (1994) Airborne hyperspectral remote sensing in Italy. In: Proceeding SPIE 2318, recent advances in remote sensing and hyperspectral remote sensing, 29. doi:10.1117/12.197243
63. Gianinetto M, Lechi G (2006) A new methodology for in-flight radiometric calibration of the MIVIS imaging sensor. Ann Geophys-Italy 49(1):65–70
64. Belluco E, Camuffo M, Ferrari S, Modenese L, Silvestri S, Marani A, Marani M (2006) Mapping salt-marsh vegetation by multispectral and hyperspectral remote sensing. Remote Sens Environ 105(1):54–67
65. Alberotanza L, Brando VE, Ravagnan G, Zandonella A (1999) Hyperspectral aerial images. A valuable tool for submerged vegetation recognition in the Orbetello Lagoons, Italy. Int J Remote Sens 20:523–533
66. Bolpagni R, Bresciani M, Laini A, Pinardi M, Matta E, Ampe EM, Giardino C, Viaroli P, Bartoli M (2014) Remote sensing of phytoplankton-macrophyte coexistence in shallow hypereutrophic fluvial lakes. Hydrobiologia 737:67–76
67. Bresciani M, Bolpagni R, Braga F, Oggioni A, Giardino C (2012) Retrospective assessment of macrophytic communities in southern Lake Garda (Italy) from in situ and MIVIS (Multispectral Infrared and Visible Imaging Spectrometer) data. J Limnol 71(1):180–190
68. Giardino C, Bresciani M, Valentini E, Gasperini L, Bolpagni R, Brando VE (2014) Airborne hyperspectral data to assess suspended particulate matter and aquatic vegetation in a shallow and turbid lake. Remote Sens Environ. doi:10.1016/j.rse.2014.04.034

69. Giardino C, Bartoli M, Candiani G, Bresciani M, Pellegrini L (2007) Recent changes in macrophyte colonisation patterns: an imaging spectrometry-based evaluation of southern Lake Garda (northern Italy). J Appl Remote Sens 1:011509. doi:10.1117/1.2834807
70. Villa P, Laini A, Bresciani M, Bolpagni R (2013) A remote sensing approach to monitor the conservation status of lacustrine Phragmites australis beds. Wetl Ecol Manag 21:399–416
71. Richter R (2009) Atmospheric/topographic correction for satellite imagery. DLR report DLR-IB 565-01/09, Wessling, Germany
72. Kotchenova SY, Vermote EF, Matarrese R, Klemm FJ Jr (2006) Validation of a vector version of the 6S radiative transfer code for atmospheric correction of satellite data. Part I: path radiance. Appl Optics 45:6762–6774
73. Berk A, Anderson GP, Acharya PK, Bernstein LS, Muratov L, Lee J, Fox M, Adler-Golden SM, Chetwynd JH, Hoke ML, Lockwood RB, Gardner JA, Cooley TW, Borel CC, Lewis PE, Shettle EP (2006) MODTRAN5: 2006 update. Proc SPIE 6233:62331F
74. Berk A, Bernstein LS, Anderson GP, Acharya PK, Robertson DC, Chetwynd JH, Alder-Golden SM (1998) MODTRAN cloud and multiple scattering upgrades with application to AVIRIS. Remote Sens Environ 65:367–375
75. Giardino C, Candiani G, Bresciani M, Lee Z, Gagliano S, Pepe M (2012) BOMBER: a tool for estimating water quality and bottom properties from remote sensing images. Comput Geosci 45:313–318
76. Albert A, Mobley CD (2003) An analytical model for subsurface irradiance and remote sensing reflectance in deep and shallow case-2 waters. Opt Express 11(22):2873–2890
77. Lee Z, Carder KL, Mobley CD, Steward RG, Patch JS (1998) Hyperspectral remote sensing for shallow waters: 1. A semi analytical model. Appl Optics 37:6329–6338
78. Lasdon LS, Waren AD (1978) Generalized reduced gradient software for linearly 708 and non linearly constrained problems. In: Greenberg HJ (ed) Design and 709 implementation of optimization software. Sijthoff & Noordhoff, Alphen aan den Rijn, pp 335–362
79. Cingolani L, Padula R, Di Brizio M, Ciccarelli E (2007) Eutrofizzazione del Lago Trasimeno: il problema delle fioriture algali. In: 14th Conference on Igiene Industriale, Corvara, Italy
80. Giardino C, Bresciani M, Villa P, Martinelli A (2010) Application of remote sensing in water resource management: the case study of Lake Trasimeno, Italy. Water Resour Manag 24: 3885–3899
81. Pinardi M, Bartoli M, Longhi D, Viaroli P (2011) Net autotrophy in a fluvial lake: the relative role of phytoplankton and floating-leaved macrophytes. Aquat Sci 73:389–403
82. Bresciani M, Giardino C, Longhi D, Pinardi M, Bartoli M, Vascellari M (2009) Imaging spectrometry of productive inland waters. Application to the lakes of Mantua. Ital J Remote Sens 41:147–156
83. Giardino C, Bresciani M, Longhi D, Bartoli M, Vascellari M (2009) Application of semianalytical modelling to imaging spectrometry of productive turbid lake waters. In: Proceeding 33rd 'International Symposium on Remote Sensing of Environment (ISRSE)', May 2009, Stresa (VB), Italy, pp 4–80
84. Directive 2000/60/EC (2000) Water framework directive of the European parliament and of the council of 23 October 2000 establishing a framework for Community action in the field of water policy. Official Journal L 327, 22 Dec 2000
85. Eggs B, Sanders D (2013) Herbivory in spiders: the importance of pollen for orb-weavers. PLoS One 8(11):e82637. doi:10.1371/journal.pone.0082637
86. Villa P, Bresciani M, Braga F, Bolpagni R (2014) Comparative assessment of broadband vegetation indices over aquatic vegetation. IEEE J Sel Top Appl Earth Obs Remote Sens 7(7):3117–3127. doi:10.1109/JSTARS.2014.2315718
87. Queirazza G, Martinotti W, Guzzi L (1992) Influenza degli apporti del fiume Lambro sulla distribuzione di elementi tra acqua e materiale sospeso del fiume Po. In: Marchetti R, Cotta Ramusino M (eds) Atti V Cong. Naz. S.It.E, pp 757–762
88. Viganò L, Bassi A, Garino A (1996) Toxicity evaluation of waters from a tributary of the River Po using the 7-day Ceriodaphnia dubia test. Ecotoxicol Environ Saf 35(3):199–208

89. Leifer I, Lehr WJ, Simecek-Beatty D, Bradley E, Clark R, Dennison P, Hu Y, Matheson S, Jones CE, Holt B, Reif M, Roberts DA, Svejkovsky J, Swayze G, Wozencraft J (2012) State of the art satellite and airborne marine oil spill remote sensing: application to the BP Deepwater Horizon oil spill. Remote Sens Environ 124:185–209
90. Andreou C, Karathanassi V, Kolokoussis P (2011) Spectral library for oil types. In: Proceedings of the 34th international symposium on remote sensing of environment, Sydney, 10–15 Apr 2011
91. Kaiblinger C, Anneville O, Tadonleke R, Rimet F, Druart JC, Guillard J, Dokulil MT (2009) Central European water quality indices applied to long-term data from peri-alpine lakes: test and possible improvements. Hydrobiologia 633:67–74
92. Nõges P, Nõges T, Ghiani M, Sena F, Fresner R, Friedl M, Mildner J (2011) Increased nutrient loading and rapid changes in phytoplankton expected with climate change in stratified South European lakes: sensitivity of lakes with different trophic state and catchment properties. Hydrobiologia 667(1):255–270
93. Giardino C, Bartoli M (2009) Introduction to the special issue AIT-SItE: "The contribution of remote sensing to the analysis and evaluation of ecological systems at different scales". Ital J Remote Sens 41:61–63
94. Olmanson LG, Brezonik PL, Bauer ME (2013) Airborne hyperspectral remote sensing to assess spatial distribution of water quality characteristics in large rivers: the Mississippi River and its tributaries in Minnesota. Remote Sens Environ 130:254–265

Using Remote Sensing to Assess the Impact of Human Activities on Water Quality: Case Study of Lake Taihu, China

Paolo Villa, Hongtao Duan, and Steven Arthur Loiselle

Contents

Abstract An integrated assessment of water quality stressors at watershed scale is the basis for timely and effective management actions. The capacity of remote sensing to deliver spatial and temporal information about fundamental environmental dynamics makes it an ideal tool for determining the causes of water quality

P. Villa (✉)
Institute for Electromagnetic Sensing of the Environment, National Research Council (IREA-CNR), Milan 20133, Italy
e-mail: villa.p@irea.cnr.it

H. Duan
State Key Laboratory of Lake Science and Environment, Nanjing Institute of Geography and Limnology, Chinese Academy of Sciences, Nanjing 210008, China

S.A. Loiselle
Dipartimento Farmaco Chimico Tecnologico, CSGI, University of Siena, 53100 Siena, Italy

T. Younos, T.E. Parece (eds.), *Advances in Watershed Science and Assessment*, The Handbook of Environmental Chemistry 33,
DOI 10.1007/978-3-319-14212-8_4

deterioration. This chapter focuses on harmful algal blooms in Lake Taihu (China), as a case study, demonstrating the potential of remote sensing for integrated assessment of watershed dynamics. The temporal and spatial variability of the conditions in Lake Taihu and its watershed were derived from satellite data to produce a monthly time series of algal bloom coverage, aquatic vegetation extent, and land cover from 2000 to 2013. Environmental features related to nutrient loading, climate conditions, and agricultural practices were also used to analyze the driving forces of algal blooms. Two distinct temporal patterns were identified. Prior to 2006, bloom initiation date was sensitive to agricultural activities (winter crop productivity and nutrient loading). After 2006–2007, an inversion of this relationship was observed, suggesting nutrient saturation with a shift to other watershed scale stressors, mainly climate related. After 2009, a return to pre-2006 conditions was shown. These results demonstrate how remote sensing can be used to monitor watershed dynamics as a whole, especially in conjunction with in situ environmental data.

Keywords Algal blooms • Aquatic vegetation • Lake Taihu • Land cover • Remote sensing • Water quality

1 Introduction

Inland water quality and consequently human health can be strongly affected by human activities on a watershed scale. An integrated assessment and identification of water quality stressors are needed to understand interactions and relations between land use, human activities, and water quality. Remote sensing can deliver a wide range of spatial–temporal information on environmental dynamics, making it a fundamental tool for monitoring and management of complex ecosystems [1].

Lake Taihu, the third largest freshwater lake in China, serves as a primary drinking water source for 40 million people in the Jiangsu and Zhejiang provinces as well as the Shanghai municipality [2]. However, the Taihu watershed has undergone tremendous change (driven by anthropic activities) during the past two decades. In 1990, algal blooms caused the closure of 116 factories and the cessation of water supplies to three million people in Wuxi [3]. In May 2007, a massive cyanobacterial bloom of *Microcystis* led to water supply problems for over one million people. These events brought the algal blooms of Lake Taihu to both national and international attention [2, 4–6].

The increased occurrence of harmful algal blooms (HABs), mainly caused by cyanobacteria, is a global issue and a serious threat to inland freshwater ecosystems. Many genera of cyanobacteria produce toxins with adverse effects on human health and aquatic life [7] and posing a threat to drinking and irrigation water supplies [8]. Algal blooms have often been associated with eutrophication due to excessive inputs of nutrients [9–11]. Nutrient inflow management actions have been put into

place in many areas, often focusing on phosphorous (P) load limitations. But the spread of non-nitrogen-fixing cyanobacteria (e.g., *Microcystis*, as in our case study of Lake Taihu) and the influence of climatic variables (mainly temperature and solar radiation) on bloom formation have introduced new factors, which need to be taken into account when setting up management strategies aimed at reducing the impact of HABs [12, 13].

The integration of remote sensing information about changes in both the aquatic and terrestrial compartments can provide new insights into the assessment of inland water bodies and coastal areas ecosystems. The objective of this chapter is to demonstrate the capabilities of remote sensing in providing multi-temporal information for water color and water quality (e.g., bio-optical parameters) as well as for environmental drivers of water quality threats, such as HABs. Specifically, the chapter focuses on HABs in Lake Taihu (China) to demonstrate the potential of remote sensing for integrated assessment of watershed dynamics.

2 Study Area

The Lake Taihu watershed is located in one of the most important developing areas of China and has experienced enormous changes in land use and land cover over the past three decades. From 1990 to 2010, the population of Taihu watershed has more than doubled, and economic growth brought along an increasing number of industries. The GDP of the area has seen a sharp increase, from 847 billion Yuan (RMB) in 1998 to 2,662 billion Yuan (RMB) in 2007 [2].

The Taihu watershed occupies the southern part of Jiangsu Province (Sunan), part of Zhejiang Province and Shanghai Municipality (Fig. 1). The Eastern China lake region (around 36,900 km^2), along the course of the lower Yangtze River, is currently one of the most densely populated areas in the world and therefore subject to significant anthropogenic pressures. More than 150 million people live in the three provinces of this region, Anhui, Jiangsu, and Shanghai, where a large part of national GDP is produced through industrial and agricultural activities. The local per capita GDP is three times the national average and the population density (averaging 600 per km^2) is seven times higher than national average.

This region contains one of the most abundant surface water resources in China. Hundreds of large and small lakes exist in the region, but most have undergone significant eutrophication over the past three decades. Lake Taihu is the largest and most endangered lake in the region, suffering from high nutrient loads and eutrophic condition, low water level, and frequent problems of massive anoxia and algal blooms. These issues jeopardize basic ecosystem services for local population and water resources for drinking water supplies, agriculture, fishing, fish farming, and aquaculture.

High water levels in Lake Taihu generally occur during late August to September, at the end of monsoon season, while low levels occur during November to May (winter and spring), the dry season. Lake sediment cores have shown that

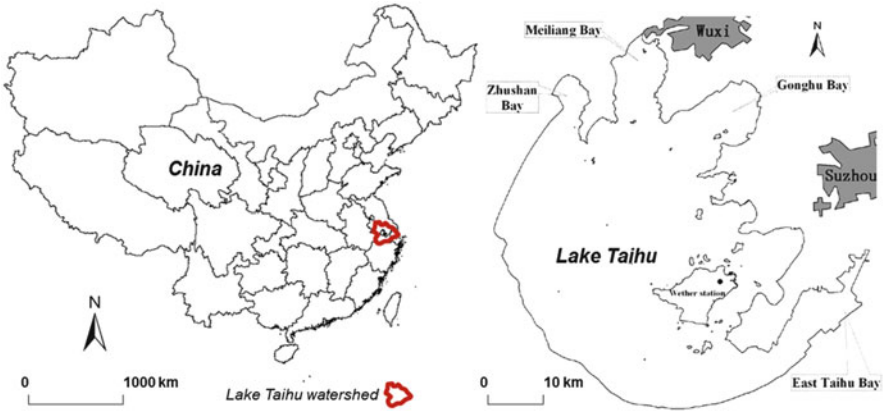

Fig. 1 Study area, Lake Taihu, and its surrounding areas, with the location of Meiliang Bay, Gonghu Bay, and Zhushan Bay

sediment particle size has become coarser over the last century [14]. The concentration of heavy metals, total organic carbon, and nutrients in the lake has also increased since 1970s [14]. The largest nutrient inflow into Lake Taihu originates from the southwestern sub-basin area (40–50 % of incoming TN and 60–70 % of TP) and the northwestern sub-basin area (15–20 % of incoming TN and 15–20 % of TP) [15].

The phytoplankton community during spring and summer seasons is dominated by the presence of *Microcystis* cyanobacteria. This dominance has been attributed to nutrient (N/P) ratios, underwater light availability, temperature, and zooplankton grazing [16]. Cyanobacteria blooms occur on a regular basis with the highest intensity in the northwestern bays (Meiliang Bay, in particular) where N-limiting conditions (and excess P) are frequent [16]. Light availability was found to be important in the deeper and more turbid central part of the lake on phytoplankton composition and biomass [17].

For *Microcystis*, the dominant cyanobacterial species in Lake Taihu, Liu et al. [18] assessed a high correlation between temporal dynamics and total nitrogen-to-total phosphorus ratio (TN:TP), nitrogen composition, water temperature, and pH. Under such conditions, phytoplankton composition shows signs of rapid replacement of chlorophyta (mainly *Ulothrix*) by cyanobacteria (mainly *Microcystis*) [19]. These phenomena are more critical in the northern parts of the lake (e.g., Meiliang Bay, near Wuxi city) than in the central part of the lake, because of low water level, favorable currents, and boat traffic [17].

The effects of climatic variables and nutrient loading on formation and characteristics of HABs in Lake Taihu have been studied by several research groups. These researchers assessed the influence of increased temperature and decreased concentration of nitrogen during the hot season on cyanobacteria biomass [19], considering the dual control of both climate factors and nutrients on the risk of bloom events [20]. In an earlier study, Chen et al. [21] identified temperature, wind,

and turbidity as the main driving factors for the formation of short-term phytoplankton blooms, while longer-term algal biomass dynamics were mostly correlated with the level of nutrients available.

In 2007, an extraordinary algal bloom event occurred in Lake Taihu. It was preceded by an anomalously mild winter season, which resulted in favorable conditions for overwintering of phytoplankton biomass and cyanobacterial blooms [17]. The 2007 bloom led to a drinking water shortage for more than one million people when HABs caused temporary closure of water treatment facilities in northern Lake Taihu. This event further raised the awareness of public authorities to the elevated environmental and human costs of HABs [22].

In this framework, remote sensing approaches were developed to map algal bloom spatial–temporal dynamics and their relation with environmental variables, to better understand those phenomena and mitigate their effects [2, 13, 23, 24]. A retrospective analysis by remote sensing and in situ measured data, focusing on bloom duration and dating back to 1987, was carried out by Duan et al. [2, 25]. Their study showed three distinct trends: from 1987 to 1997, blooms occurred later each year, while from 1997 to 2007 the trend was reversed, with blooms starting earlier each year, and after the 2007 bloom event, initiation occurred later each year. Bloom initiation date was found to correlate well with winter temperature minima and TN:TP ratios [23].

More recently, black water blooms, occurring in particular conditions of dissolved organic matter and phytoplankton combination in water column, and favored during springtime conditions in the macrophyte-dominated areas of the lake's hypereutrophic bays, were studied using remote sensing [25]. From this preliminary study, the authors conclude that this phenomenon and its connection with cyanobacteria and other algal blooming events needs to be further investigated.

Eutrophication and algal blooms have been partially attributed to climatic influences, such as the increasing temperature, and anthropogenic influences such as nutrient loading, but quantitative exploration of the main drivers has not been performed on a watershed scale. An integrated assessment of water quality stressors is fundamental to understand the relationship between land use, human activities, and ecosystem degradation, with the ultimate goal of promoting a more sustainable lake environment.

3 Remote Sensing of Lake Taihu Watershed

3.1 Dataset and Derived Features

In our study, the relationship between human activities and water quality of Lake Taihu was investigated through remote sensing to better understand the links between driving forces and dynamics of algal blooms. This was achieved by using low to mid-resolution multi-temporal and multi-seasonal satellite images

Table 1 Satellite datasets used and their characteristics

Sensor	Product	Spatial resolution	No. of scenes	Dates	Data content
Landsat 5 TM	L1G (TOA calibrated)	30 m	7	2000 (13 June, 31 July, 17 September, 04 November, 06 December)	Multispectral reflective bands (VIS-NIR-SWIR, 6 bands)
				2010 (24 May, 21 September)	
Landsat 7 ETM+	L1G (TOA calibrated)	30 m	5	2000 (01 March, 17 March, 04 May, 20 May, 11 October)	Multispectral reflective bands (VIS-NIR-SWIR, 6 bands)
HJ-CCD 1A-1B	L2 (TOA calibrated)	30 m	10	2010 (22 February, 26 March, 30 April, 12 May, 06 June, 31 July, 13 August, 17 October, 27–29 November, 09 December)	Multispectral reflective bands (VIS-NIR, 4 bands)
Terra MODIS	MOD13Q1	250 m	318	February 2000–November 2013	Vegetation Indices (16-day composites)

covering the period 2000–2013, specifically Landsat TM-ETM+, HJ-CCD 1A-B, and Terra MODIS data and products. Table 1 provides an overview of remotely sensed images used in the study.

Landsat 5 TM data acquired in September 2000 and September 2010 were used to explore macrophytes' spatial distribution and to assess aquatic vegetation changes during the decade 2000–2010. Multi-seasonal Landsat TM-ETM+ and HJ-CCD 1A-B data were used to assess phenological characteristics of aquatic vegetation for the same decade.

MODIS vegetation indices covering February 2000 to November 2013 were used to identify environmental features related to land cover and water quality. MODIS 16-day Normalized Difference Vegetation Index (NDVI) composites were summarized into a time series of NDVI monthly mean scores. These data were used to create three sets of environmental features, i.e., products related to algal bloom, winter crop phenology, and land cover of the Lake Taihu watershed.

Using the multi-temporal remotely sensed images, three products were derived for the monitoring of Lake Taihu and its watershed: (1) algal bloom spatial and temporal dynamics (2000–2013), described in Sect. 3.2; (2) aquatic vegetation distribution (2000–2010), described in Sect. 3.3; and (3) land cover evolution in the watershed (2000–2013), described in Sect. 3.4.

For algal bloom multi-temporal features, we derived (1) the maximum areal extent of algal blooms, (2) the mean annual areal extent of algal blooms, and (3) the starting date of bloom events (for which the mapped algal bloom area is >50 km^2) (Fig. 2).

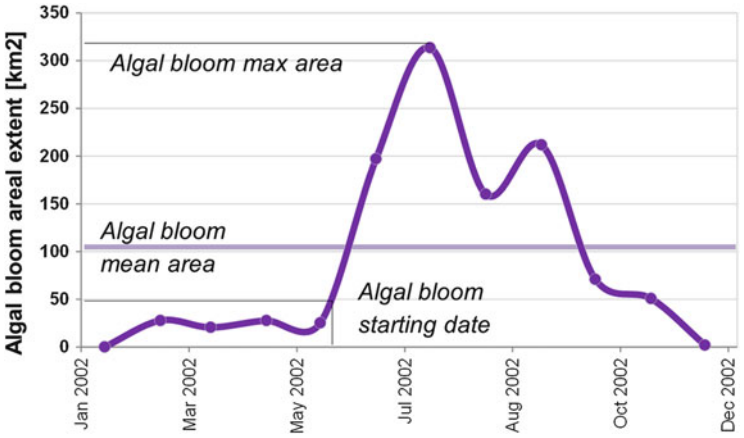

Fig. 2 Areal extent derived from monthly satellite time series for 2002 algal blooming features

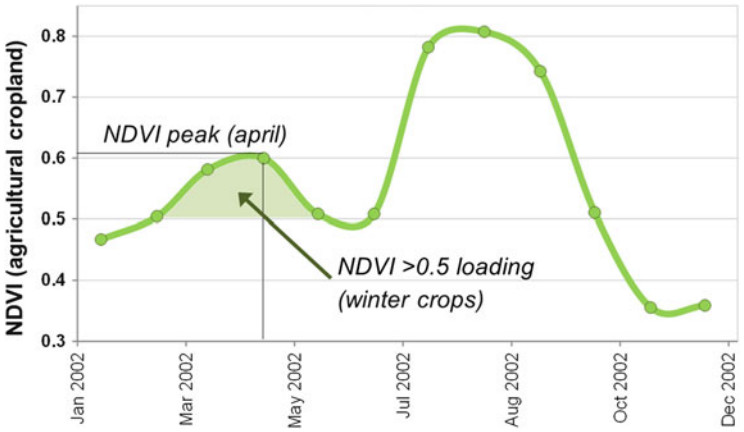

Fig. 3 NDVI peak as derived from monthly satellite time series for 2002 winter crop conditions

For winter crop seasonality and phenology, we derived (1) the NDVI peak value for agricultural winter crop season (April mean value) and (2) the NDVI loading as an accumulated value of NDVI greater than 0.5 during winter season, as a proxy of crop productivity (Fig. 3).

For features related to temporal land cover evolution, the multi-temporal evolution of five main land cover classes was taken into account—urban dense, urban sparse, agricultural medium intensity, agricultural high intensity, and natural vegetation—for each year from 2000 to 2013.

In addition to the environmental features derived from satellite data described above, in situ datasets were collected to characterize the environmental dynamics of

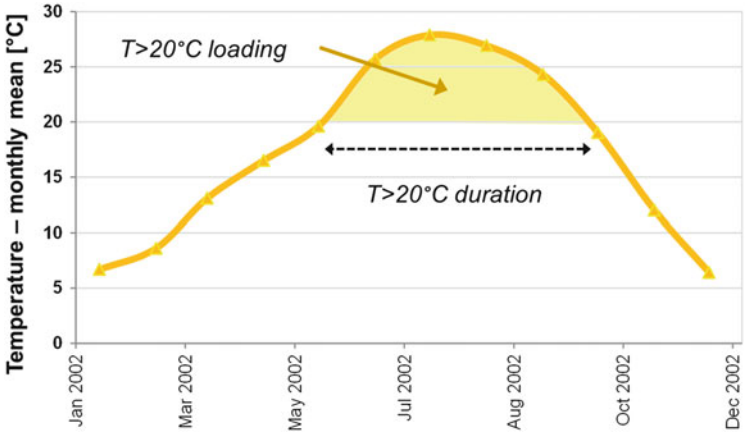

Fig. 4 Mean temperature derived from monthly in situ time series for 2002

the Lake Taihu watershed, including information about climatic condition and nutrient loadings.

Monthly mean air temperature data from 2000 to 2012 were collected from the weather station situated on Xishan Island, located on Lake Taihu. Previous studies have determined that a critical water temperature for cyanobacterial blooms ranges from 18 to 25 °C [18, 26, 27]. In studies of vegetation growth, crop dynamics and insect outbreaks, measures of accumulated temperature, expressed as the sum of degrees by which temperature changes in relation to a fixed level over a prolonged period, have been often used [28, 29]. In the present study, we used the effective accumulated temperature [20] during the hot season, expressed as follows: (1) the temperature >20 °C, a sum of mean monthly temperature minus 20 °C for the hottest months (May to September) of each year, and (2) the duration of the period for which monthly mean temperature was over 20 °C (Fig. 4).

Total phosphorus (TP) and total nitrogen (TN) concentrations were determined from monthly water samples collected from the center of two Lake Taihu sections (Central and Meiliang Bay) at a depth of 0.5 m, from 2000 to 2010. TP and TN in water samples were measured using combined persulfate digestion and spectrophotometric analysis for soluble reactive phosphorus and nitrate at the Taihu Laboratory for Lake Ecosystem Research (TLLER) [25].

Results of previous studies have demonstrated that the Lake Taihu system goes from a P-limited condition in winter months to an N-limited condition during the spring and summer seasons, when N-fixing cyanobacteria blooms occur [30]. Nutrient loading during the year is generally characterized by a spring peak in TN concentrations, which is probably linked to agricultural runoff (winter crops and paddy rice starting season) [31]. For characterization of yearly nutrient loading dynamics, we used in situ data of nutrient concentrations for deriving two distinct features: (1) total nitrogen (TN) concentration accumulated during winter and early

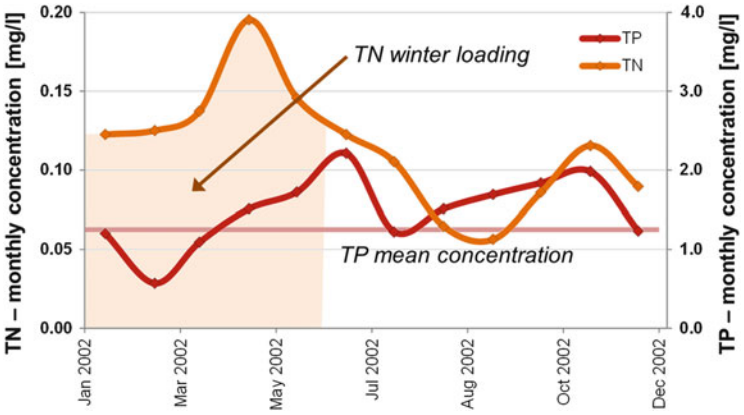

Fig. 5 Total nitrogen (TN) and total phosphorus (TP) derived from monthly in situ time series for 2002

spring, before bloom events generally start (around May), and (2) total phosphorus (TP) annual mean concentration (Fig. 5).

3.2 Algal Bloom Monitoring

In past studies, the mean areal extent of algal bloom events from February 2000 to November 2013 was determined using the Floating Algae Index (FAI) algorithm [24, 25] with MODIS Level-0 data. Bloom initiation date was defined as the first observation of surface bloom area larger than 150 km^2. Considering Lake Taihu as a whole, the spatial extent of the yearly maximum algal bloom extent was shown to remain relatively constant from 2000 to 2003 (~400 km^2), increased to 900 km^2 in 2005, and reached a maximum of 1,500 km^2 in 2006. The maximum area remained relatively stable at 1,000–1,200 km^2 for each year in the period 2007–2011, with the exception of 2009 when it dropped to 550 km^2.

Bloom extension of individual lake sections demonstrated a high heterogeneity. In general, open lake areas showed lower bloom extent until 2006, while the bays maintained a high spatial extent throughout the study period. The bloom extent dynamics of Gonghu Bay were more similar to those of the open waters than the eutrophic bays.

Algal blooms were first observed in Meiliang Bay and Gonghu Bay in June, 1987. In each year over the past two decades, the algal blooms were first observed 14 times in Meiliang Bay and 6 times in Zhushan Bay. The initial algal blooms were seen simultaneously in Meiliang Bay and Zhushan Bay in 1991, 1994, 1997, and 2003. Since 2000, the initial algal blooms were found in the western and northern bays and appear to begin to spread out in southward direction (see Fig. 1 for Meiliang, Zhushan, and Gonghu Bays' location).

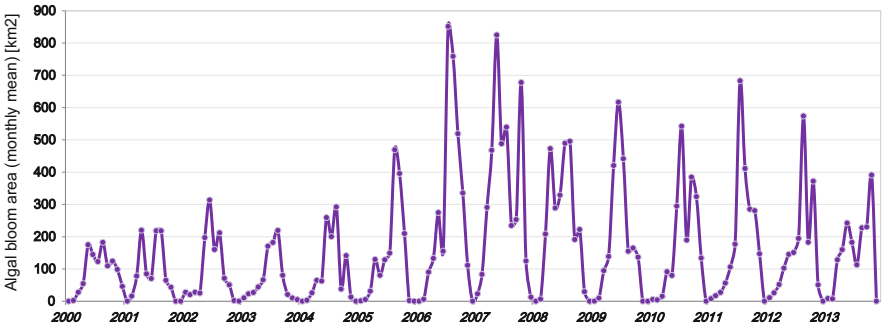

Fig. 6 Algal bloom mean monthly extent series for 2000–2013

In our study, algal blooms were derived from NDVI monthly mean from preprocessing of MODIS 16-day NDVI composites. By exploiting sensitivity of NDVI to vegetation spectral features [32], an area within Lake Taihu is identified as algal bloom in a specific month through a simple threshold approach separating clear water, characterized by strongly negative NDVI values, by very high phytoplankton concentration (mean monthly NDVI > 0.05). Note that these are surface accumulations and initiation date is not intended to identify the start of cyanobacteria bloom within a water column.

Figure 6 shows the complete monthly time series of algal bloom areal extent derived from algal bloom maps produced from 2000 to 2013. Algal blooms usually start during spring season (April–May) and extend into late summer and early autumn (September–November). The time series shows limited bloom extent for years 2000 to 2005 and highlights the exceptional 2007 event, which was preceded by a shorter 2006 bloom with a similar spatial extent. The overall intensity for 2008 to 2013 was less than 2007 but higher than pre-2006 conditions. The annual peak distribution area of algal blooms was relatively constant around 62 km^2 in 1987–2000, with a significant increase to 317 km^2 in 2005 and 806 km^2 in 2006. The 2007 peak of 979 km^2 occurred in late June, with a second peak with 855 km^2 in September [2].

Figures 7 and 8 show the spatiotemporal variation of algal blooms across Lake Taihu (blooms are represented by purple color in Fig. 7 and cyan in Fig. 8), derived from MODIS NDVI data at 250 m spatial resolution for 2 years with very different characteristics: 2001, characterized by a low-intensity blooms, and the extreme HAB event of 2007. From these figures, we can observe some distinct spatiotemporal patterns; the 2001 bloom occurred in spring (May) and summer season (August–September) and was particularly concentrated in the northern part of the lake, where blooms have frequently occurred. The 2007 bloom started earlier (between March and April) and lasted longer (almost until December). In 2007, the maximum area covered by algal blooms was 900 km^2 (nearly 40 % of the entire Lake Taihu surface) extending from the northern bays to the central and even southern part of the lake, which had been free from blooms in the past.

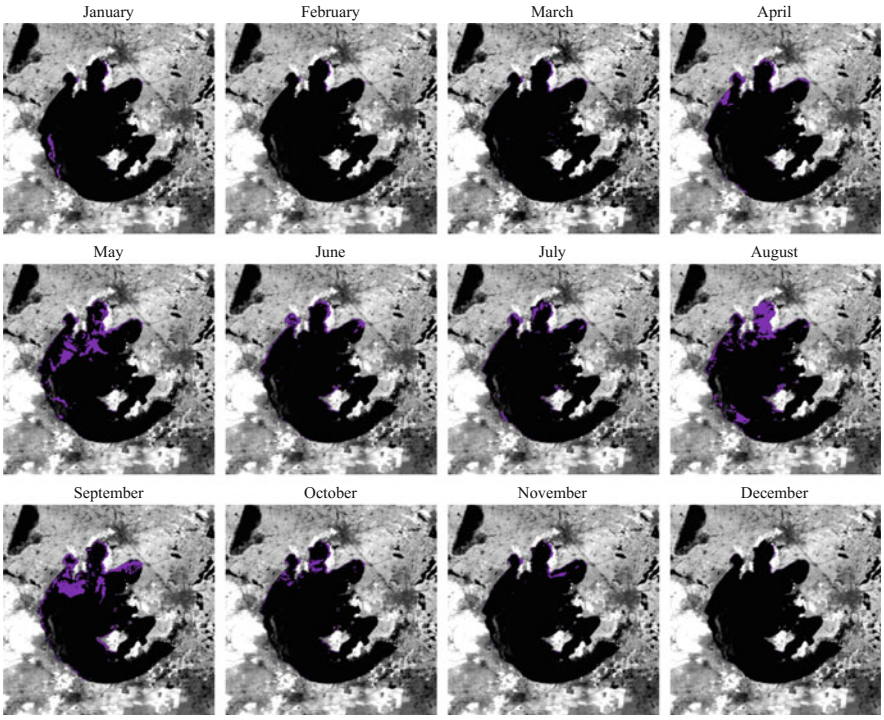

Fig. 7 Algal bloom mean monthly extent maps for year 2001 (low-level blooming example)

3.3 Aquatic Vegetation Mapping and Changes

Aquatic vegetation or macrophytes are fundamental components of aquatic ecosystems, providing numerous ecological functions. Littoral vegetation, mainly constituted by common reed beds (*Phragmites* sp.) in Lake Taihu, provides nitrogen transformation and nitrogen loss functions [33], while floating macrophytes (in particular *Trapa* sp.), present in abundance in eastern Lake Taihu, control sediment resuspension and influence the lake's phosphorous cycle [34]. Ma et al. [35] mapped the extent and temporal changes of aquatic vegetation communities throughout Lake Taihu by remote sensing, identifying a reduction of 90 km^2 between 2001 and 2007, with a loss of nearly 20 % of total macrophytes biomass in the lake [35]. Remote sensing can provide crucial information about specific land cover change features from multi-temporal datasets [e.g., 36].

In this case study, we explored changes in macrophytes coverage in 2000 and 2010, using data from the peak macrophytes extent in 2000 and 2010: Landsat 5 TM, acquired on 17 September 2000, and Landsat 7 ETM+, acquired on 21 September 2010.

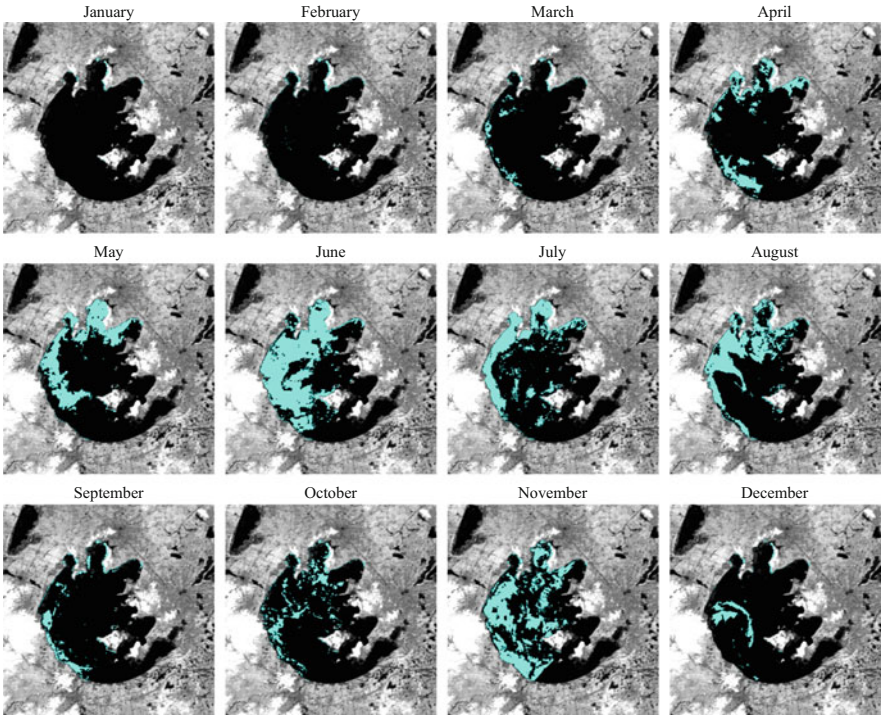

Fig. 8 Algal bloom mean monthly extent maps for year 2007 (peak event of the decade)

Aquatic vegetation present in the Lake Taihu was classified into four macro-classes: (1) emergent macrophytes, (2) floating macrophytes (including floating-leaved plants), (3) submerged macrophytes, and (4) algal bloom, to which an open water class was finally added. The approach adopted was a binary cascade decision tree with expert-based threshold and input features using multispectral satellite data described below:

- *NDAVI*—Normalized Difference Aquatic Vegetation Index: aquatic vegetation greenness and vigor spectral index [37]
- *SVI*—Soil and Vegetation Index: terrain land cover perviousness index [38]
- *NDWI*—Normalized Difference Water Index: vegetation water content index [39]
- *Chl-a*: concentration value according to the algorithm derived from the work of Ma and Dai [40], calibrated using in situ data of two monitoring stations

The results indicate dramatic changes in the spatial distribution and abundance of macrophytes during the decade, especially in eastern Taihu Lake (Fig. 9). Some of these changes were associated to the increased activities of aquaculture and fish farming in this region of the lake since 2000. Significant changes in the areal

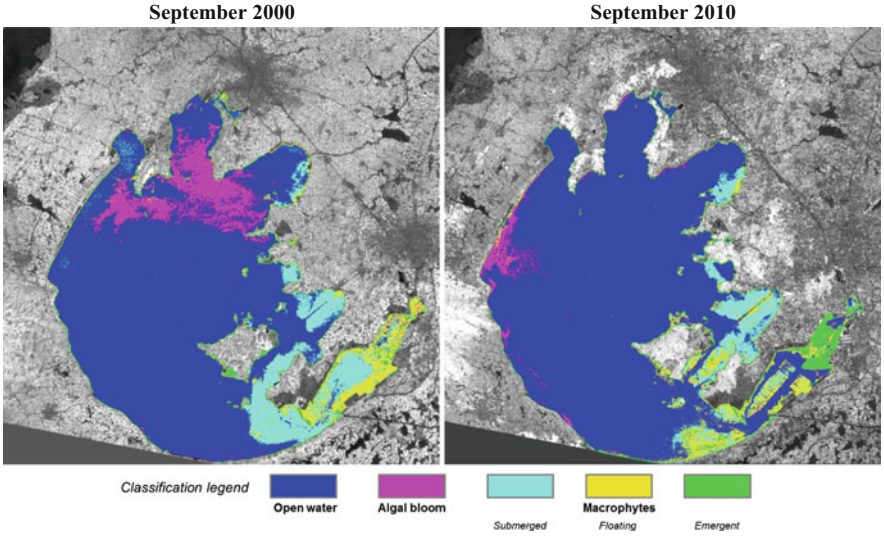

Fig. 9 Aquatic vegetation classification in Lake Taihu, derived from Landsat TM-ETM+ for the years 2000 (*left*) and 2010 (*right*), in peak vegetation season (September)

coverage of submerged and floating vegetation classes occurred in the eastern part of the lake (Table 2). The analysis of algae class was found to be strongly dependent on algal bloom seasonality for the specific year (2000–2010) and was not considered in the aquatic vegetation analysis focusing on macrophytes.

Multi-temporal data were also used for the reconstruction of a time series for phenology of different aquatic vegetation types. An example is given in Fig. 10, where multi-seasonal profiles for 2000 and 2010 are shown for different macrophytes classes (identified through classification of satellite features). Using Landsat TM-ETM+ (2000) and HJ-CCD 1A-1B (2010) datasets, we derived vegetation greenness and vigor expressed as NDAVI scores [37] and chlorophyll-*a* (Chl-*a*) content in water background calculated according to Ma and Dai [40].

3.4 Land Cover Change Assessment

Land cover change in the Lake Taihu watershed plays an important role in the environmental dynamics of the area. The primary pollution source of the Lake Taihu is related to wastewater discharge and nonpoint source nutrients from agricultural activities [41]. The main agricultural crops in the Taihu watershed are wheat and rapeseed during winter and paddy rice during summer [42]. Aquaculture is common in areas near the lake shore, and even in the lake itself, especially in eastern and southeastern regions. The development of aquaculture activities, which has grown considerably in the past 15 years (with the swamping of East

Table 2 Aquatic vegetation change detection (2000–2010), represented in last line as the difference in areal extension of aquatic vegetation mapped from 2010 with respect to 2000 situation

	Area (km^2)	September 2000					
		Open water	Algal bloom	Submerged	Floating	Emergent	2010 Total
September 2010	Open water	**1,594.67**	**222.72**	**106.35**	**39.60**	**3.04**	*1,966.40*
	Algal bloom	**60.31**	**1.36**	**2.95**	**6.09**	**1.48**	*151.90*
	Submerged	**65.47**	**0.43**	**77.26**	**7.71**	**1.02**	*142.52*
	Floating	**33.75**	**1.66**	**56.65**	**38.41**	**12.04**	*72.21*
	Emergent	**13.06**	**2.09**	**13.02**	**36.49**	**58.27**	*122.95*
	2000 Total	*1,767.28*	*228.27*	*256.25*	*128.31*	*75.87*	
	Changes 2000–2010	***172.60***	***226.91***	***178.99***	***89.90***	***17.60***	

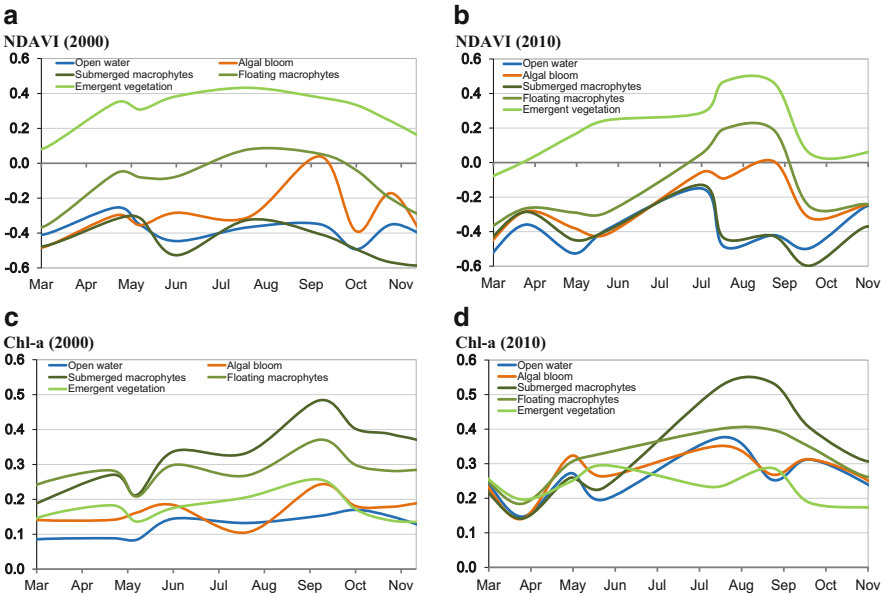

Fig. 10 Aquatic vegetation seasonal phenology assessment (2000–2010), using Landsat TM-ETM+ for the year 2000 and HJ-CCD 1A-1B for the year 2010: (**a**) NDAVI series for 2000, (**b**) NDAVI series for 2010, (**c**) Chl-*a* series for 2000, (**d**) Chl-*a* series for 2010

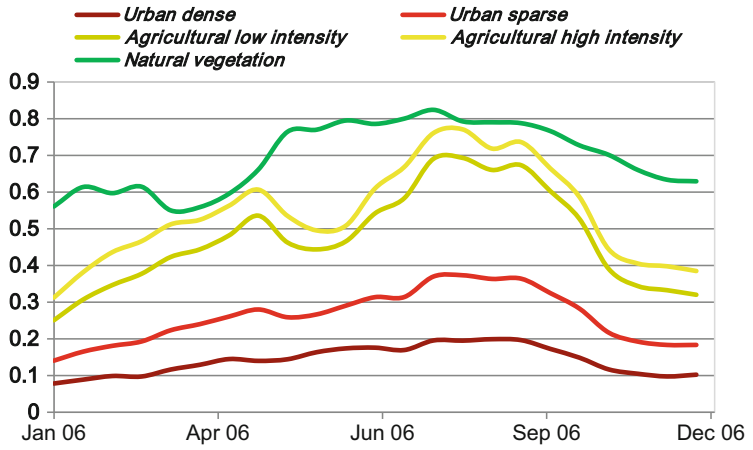

Fig. 11 Multi-temporal profiles of NDVI derived from MODIS satellite data for different land cover classes, showing the seasonal patterns characteristics of natural vegetation, agricultural crops, and more temporally stable target such as urban areas (example based on 2006)

Taihu Bay), has resulted in eutrophication and water supply problems and a reduction in the flood control capabilities of the Lake Taihu system [41].

Remote sensing is an effective tool for assessing land cover change in the watershed [36, 43]. In this study, multi-temporal (yearly) land cover maps were

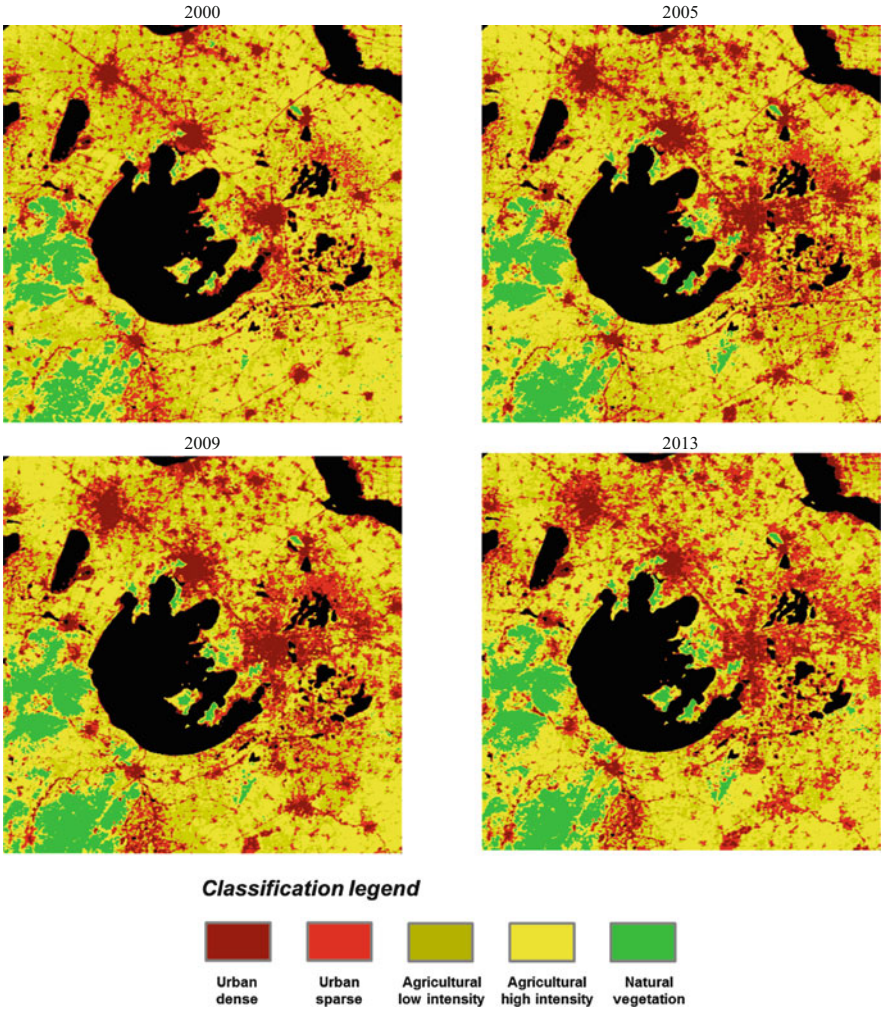

Fig. 12 Land cover maps produced starting from MODIS composites for specific years in the range 2000–2013

produced at a 250 m spatial resolution, covering the Taihu watershed area from 2000 to 2013. The interannual temporal dynamics (Fig. 11) for five land cover macro-classes were chosen as classification targets (urban dense, urban sparse, agricultural low intensity, agricultural high intensity, natural vegetation). For each year, two synthetic multi-temporal features were extracted: NDVI annual mean value and NDVI annual standard deviation of the monthly mean. Annual NDVI features ($NDVI_{mean}$ and $NDVI_{stdev}$) were clustered into the five categories using ISODATA algorithm and were subsequently labeled according to this classification scheme.

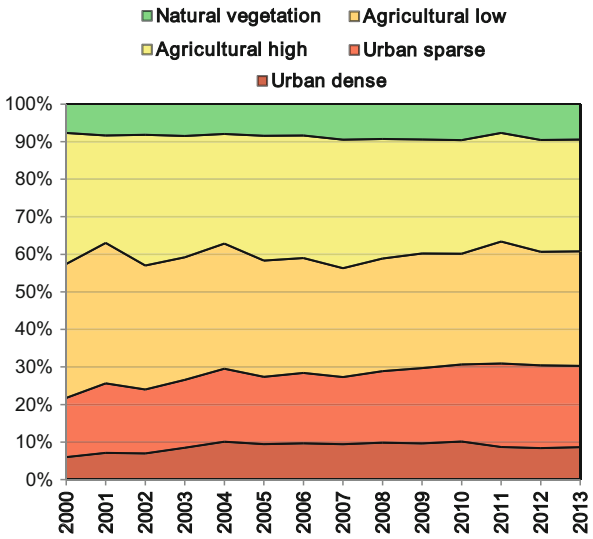

Fig. 13 Land cover evolution (in % cover of Taihu watershed) from 2000 to 2013

The expansion of the three main cities (Changzhou, Wuxi, and Suzhou) in the region was particularly significant (Fig. 12). Changes in land cover (Fig. 13) show a stable natural vegetation class, while the two urban cover classes increased from little more than 20 % in 2000 to around 30 % of the entire basin (in particular for sparse urban fabric) in 2013. Cropland, as the sum of the two agricultural land cover classes, was reduced from about 70 % in 2000 to 60 % in 2013.

4 Algal Blooms Driving Forces

Algal blooms in Lake Taihu have been studied in the past, but most of the scientific literature focused on specific areas, or specific drivers (e.g., nutrients). Globally, bloom events have been shown to be influenced by multiple factors, including pH level and CO_2 concentration [44], salinity [45, 46], light intensity [47–49], and temperature [13, 22, 50, 51]. Among the environmental factors that favor HABs in Lake Taihu, studies have shown that factors such as water temperature, winter climate, nutrient composition, nutrient loading, internal nutrients cycling, water level, thermal stratification, reduced water transparency, and pH influence bloom events [e.g., 18, 47, 52–54]. Among these factors, three are considered the most important in Lake Taihu: temperature (climate factor), nutrient loading (nutrient availability factor), and human activities (anthropogenic factor).

4.1 Temperature

Temperature, for both air and water, is a major environmental factor for phytoplankton growth. A positive correlation was found between initial bloom date and winter season air temperature when the previous year's winter temperature was

examined [2, 22]. The correlation of initial blooms was most significant when compared to minimum temperature ($P = 0.048$). These results were consistent with another study [55] in which temperature was reported as a major factor in the growth of phytoplankton. In addition, a tight correlation between algal recruitment and cumulative temperatures during winter and spring was reported both in laboratory and field studies in Lake Taihu [27]. The correlation between algal blooms and temperature is related to enzymatic activities responsible for algal blooms [56], as well as the stimulus effects of winter temperature on algal recruitment, one of the important stages for algal blooms in the following year [57]. The winter of 2007 was one of the warmest winters, and the mean temperature from January to March was higher than the mean monthly temperature in the preceding 25 years, with increments of 0.36 °C in January, 2.78 °C in February, and 1.98 °C in March; this increase may explain the massive algal blooms occurring in the summer of 2007 [4].

4.2 Nutrient Loading

Algal blooms have been attributed to excessive nutrient loading, mainly nitrogen and phosphorus. It is hypothesized that Lake Taihu HAB events are associated with the nutrient loading resulting from human activities. For the time period, 1991–1996, the annual average of total nitrogen concentration increased from 1.18 to 3.62 mg/L, and total phosphorus concentration increased from 0.10 to 0.18 mg/L [58]. Moreover, the concentrations of total nitrogen and total phosphorus in 2006 were found to be 200 and 150 % higher than the prior decade. Inputs of total nitrogen and total phosphorus from the Taihu watershed area increased from around 43,150 and 1,750 metric tons in 2002 to around 44,700 and 1,850 metric tons in 2003, respectively. The spatial dynamics of algal blooms indicated the influence of nutrients on algal blooms. The increased coverage of algal blooms in the south part of the Lake Taihu was likely a result of the declining gradient of nutrient concentration from nutrient loading in the northwest area of Lake Taihu. For example, the total phosphorus loading from the northwest catchments area accounted for 55 % in 2002 and 53 % of the total lake loading in 2003, and the total nitrogen loading accounted for 65 % in 2002 and 72 % in 2003. A southward flow of nutrients would help explain the increasing occurrences of algal blooms in the center and south of Lake Taihu. Previous studies confirm that Meiliang Bay and Zhushan Bay are the most eutrophic bays of the Lake Taihu [16].

4.3 Human Activities

Elevated nutrient loading is most often the result of a combination of human activities, e.g., sewerage, livestock waste drainage, and fertilizer runoff from agricultural lands [59, 60]. For example, Duan et al. [2] used human population and gross domestic production (GDP) per capita to establish a relationship between

anthropogenic activities and algal blooms in Lake Taihu, where GDP was found to be strongly correlated to the initial bloom date ($R^2 = 0.99$), and GDP per capita was correlated to annual bloom duration ($R^2 = 0.75$). These findings imply that anthropogenic factors may substantially outweigh climatic factors. The GDP in the Lake Taihu watershed increased from 848 billion Yuan (RMB) in 1998 to 2,662 billion Yuan (RMB) in 2007 and the GDP per capita from 2×10^4 to 6×10^4 Yuan (RMB) (not adjusted for inflation) [2]. Correspondingly, the number of months of detected algal blooms increased from two in 1998 to ten in 2007, and the initial bloom date advanced more than 100 days. Given the expected growth in human activity in this area in the coming decades, urgent efforts are needed to better identify the causes of Lake Taihu's degradation.

4.4 Integrated Assessment

Integrating remotely sensed and in situ data of the Taihu watershed, a multi-temporal analysis of HAB dynamics (maximum bloom area, mean bloom area, and bloom starting date) was performed. In situ data (temperature, nutrients, and chlorophyll-*a* concentration) and remotely sensed environmental factors (land cover change and agricultural practices as a proxy of anthropogenic influence) were used.

The available data covered two periods: for 2000–2010, a full set of environmental data was available (including in situ data on nutrient concentrations); and for the 2011–2013 temporal range, only features derived from satellite data and meteorological data. Figure 14 shows the mean monthly profiles of Lake Taihu covering the temporal range of 11 years, from 2000 to 2010, for some environmental parameters derived from in situ data—mean monthly air temperature (T), chlorophyll-*a* concentration (Chl-*a*), dissolved total nitrogen (TN), and dissolved total phosphorus (TP)—compared with corresponding mean monthly profiles of information extracted from MODIS satellite data for agricultural crop phenology (in terms of NDVI monthly mean) and mean monthly algal bloom areal extent.

From monthly profiles, the environmental dynamics in Lake Taihu and its watershed indicate that:

- Temperature cycles were characterized by very hot summers (mean monthly temperature for July and August ~30 °C) and relatively cold winters (mean monthly temperature for January ~5 °C), with a notable variability in spring temperature and in hot season duration ($T > 20$ °C).
- TN concentrations were highest in the winter (maximum loadings observed from 2004 to 2008), with decreasing TN concentrations in the late spring (May–June) and increasing TN concentrations in the autumn (October–November); TP concentrations increased in the summer (July–September), with particular maxima in recent years (2004, 2005, 2006, 2009).
- Chl-*a* concentrations, as a proxy of phytoplankton abundance, were lowest in the winter (December to March) and highest in the spring and summer, which in some cases could be attributed to cyanobacterial blooms.

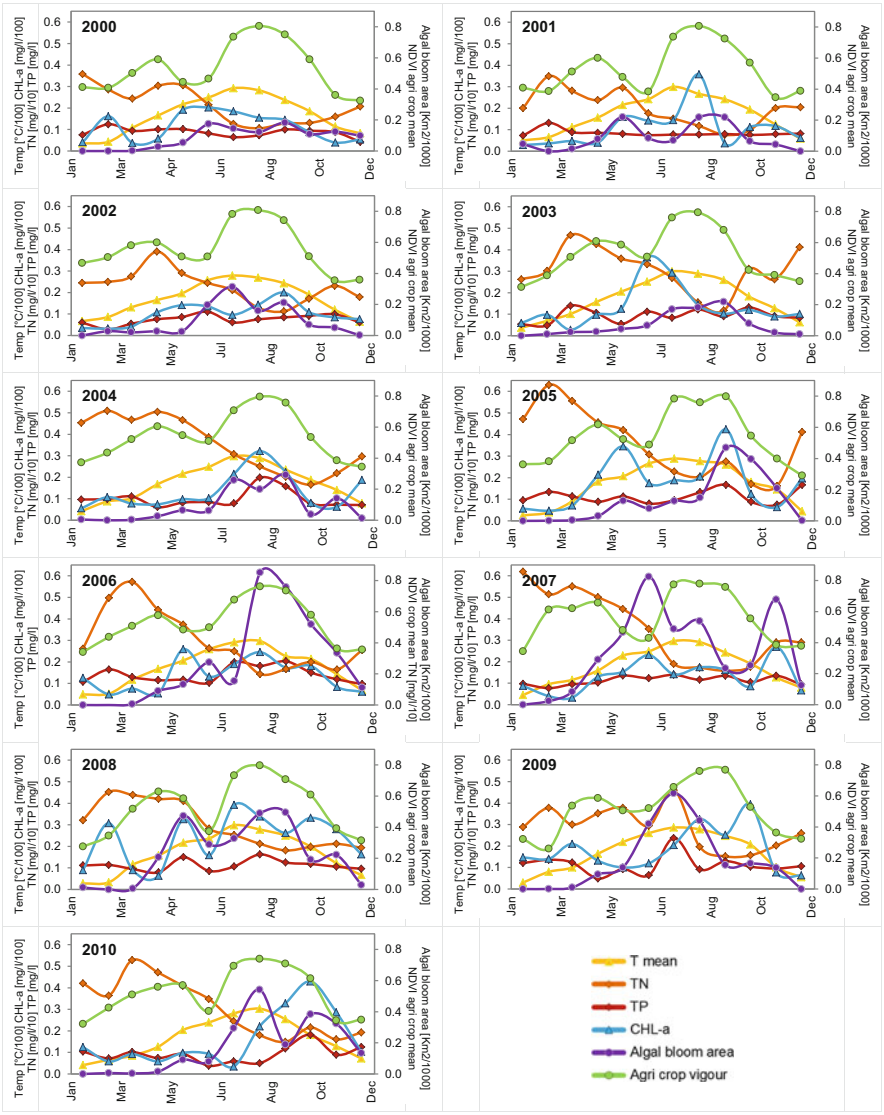

Fig. 14 Monthly profiles of Lake Taihu area covering 11 years (2000–2010): mean temperature (°C/100), Chl-*a* (10e−2 μg/L), TN (10e−1 mg/L), TP (mg/L), compared with agricultural crop phenology dynamics (NDVI) and algal bloom extent derived from MODIS data

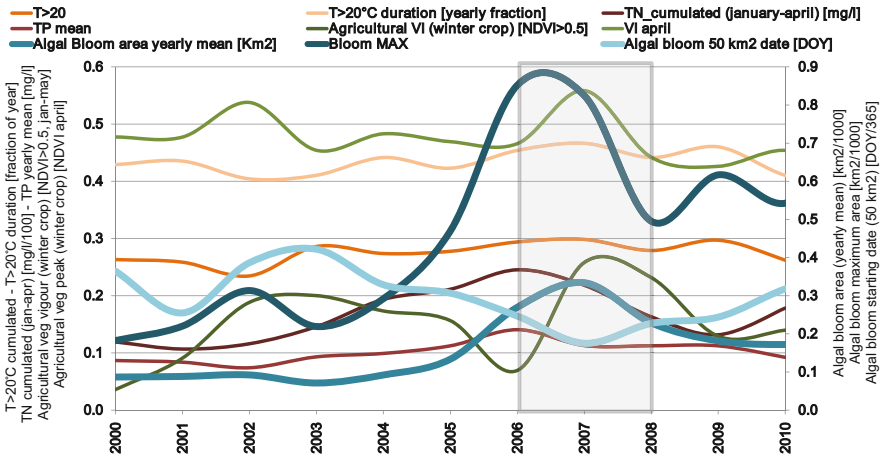

Fig. 15 Yearly variations of environmental features of Lake Taihu area covering 11 years (2000–2010), derived from monthly profiles shown in Fig. 12: duration of hot season ($T > 20$ °C), nitrogen (TN) accumulation during the winter–spring season (from January to April), algal bloom areal extent (yearly average, mapped from MODIS), agricultural vegetation productivity for winter crops at peak of season (cumulated NDVI > 0.5 in February–May range, from MODIS), algal bloom starting date (lake area covered by algae >50 km^2, derived from MODIS)

- A double cropping agricultural practice, with wheat as dominant winter crop (mean monthly NDVI peak occurring in early spring, from April to May), followed by a summer crop mainly consisting of paddy rice agriculture (mean monthly NDVI peak occurring in summer, from July to September depending on the year). Intensity and position of crop peak conditions were variable in relation to meteorological conditions as well as agricultural practices (i.e., differences in crop varieties and fertilization practices).
- Algal bloom extent generally initiated in the spring and extended into the late summer and autumn (see Fig. 6). Algal blooms coverage was relatively low from 2000 to 2005, followed by elevated and long-lasting HABs in 2006 and in 2007; after which, a more stable condition occurred, with bloom extent higher than pre-2006.

Yearly features described in Sect. 3.1 were derived from mean monthly profiles (Fig. 14) and temporal series of environmental variables from 2000 to 2011 (Fig. 15). The environmental time series included the following: the effective accumulated monthly temperature ($T > 20$ °C), the duration of the high temperature season (with $T > 20$ °C), total nitrogen (TN) accumulation during the winter–spring season (January to April) in lake water, total phosphorus mean concentration throughout the year, the agricultural vegetation productivity for winter crops at the peak of season (accumulated NDVI > 0.5 in February–May range, derived from MODIS), and winter crop vigor and greenness intensity at the peak of season (NDVI value for April, derived from MODIS). These environmental factors were

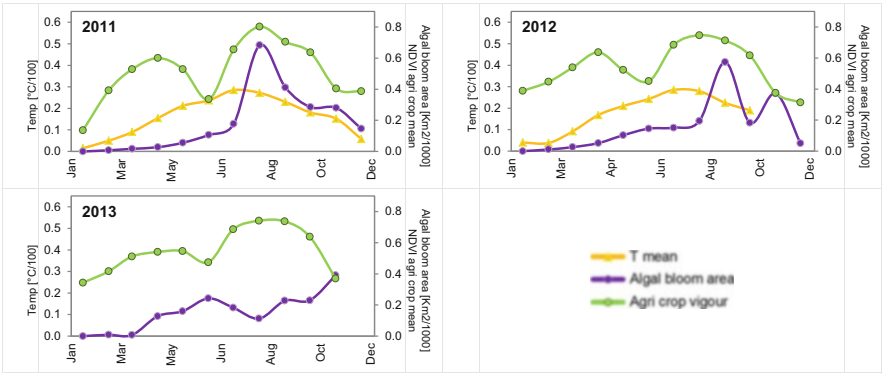

Fig. 16 Monthly profiles of Lake Taihu area covering the last 3 years (2011–2013), derived from MODIS data: agricultural crop phenology dynamics (NDVI) and algal bloom extent

compared to algal bloom dynamics extracted from the MODIS temporal series data. These included the algal bloom starting date (lake area covered by algae $>50\ km^2$), the algal bloom mean areal extent as yearly average, and the maximum monthly area bloom extent for each year.

The temporal series (Fig. 15) shows the anomalous behavior of 2006–2007, which marked a turning point for the Lake Taihu environmental system. This turning point was preceded by continuous increase of TN loading during winter and spring and an anomalous winter cropping season for 2006 (with a clear drop in NDVI >0.5 accumulated value, compared to 2005 and pre-2005 conditions), followed by a strong rebound in the winter crop productivity in 2007. Two distinct patterns emerged from the analysis of environmental factors shown in Fig. 15: one preceding the extreme blooms of 2007 and one following it. Before 2006, the algal bloom starting date was correlated to the winter crop productivity, an increase in winter productivity corresponded to a later HAB start. Starting with the 2006–2007 blooms, the relationship reverses (Fig. 15) and an increase in winter crop productivity corresponds to an earlier HAB start. This may be related to a shift from nutrient-limiting conditions (TN, in particular), which controlled pre-2006 algal blooms, to conditions of nutrient saturation (due to the simultaneous increase of both TN and TP from 2000 to 2006), where climatic and anthropic factors (temperature and winter crop seasonality) controlled algal dynamics. After the two extreme blooms of 2006–2007, the system appears to have stabilized, but a decrease in TN concentrations or another extended hot season like that of 2006 could lead to a new shift.

Some signs of the shift after 2010 were evident in temperature data (up to November 2012), as well as remotely sensed winter crop phenology and algal bloom characteristics, as mean and maximum extent, or starting date (Fig. 16).

The time series after 2011 indicated that HAB events were less intense than those of previous years, both in terms of mean and maximum extent, even if the

starting date demonstrated an earlier bloom initiation. Bloom behavior may be realigning to pre-2006 dynamics (bloom starting date is influenced by winter crop season productivity). Therefore, 2010–2011 could be identified as another turning point for the environmental system, after the 2006–2007 event, connected to a drop in accumulated temperature and hot season duration in 2011 compared to previous years (2009 and 2008).

5 Conclusions

Remote sensing provides crucial information on inland water quality, as well as the environmental factors that cause changes in water quality and ecosystem dynamics. Algal bloom events are strongly connected to human activities within a watershed, such as agriculture, demographic change, and economic development. Water quality and algal bloom management can no longer be limited to nutrient discharge control, but needs to take into account indirect factors related to watershed management (e.g., agriculture and aquaculture), as well as local and regional short-term climatic effects [30]. It is important that more complex scenarios are taken into account, requiring an integrated approach to data acquisition and information availability on finer spatial and temporal scales.

In this case study, we used an integrated watershed approach, based on remote sensing, to gather information about the environmental dynamics of a complex lake watershed (Lake Taihu), where algal blooms have caused a significant loss of ecosystem services and other uses of water. Our integrated analysis identified two distinct temporal patterns of algal bloom events, with an associated change in land use and environmental conditions. Prior to 2006, algal bloom initiation date was linked to land cover, in particular to winter crop productivity and the subsequent nutrient loading into the lake. After 2007, there was an inversion in this relationship between land cover and algal bloom dynamics, suggesting that nutrient saturation had occurred and other environmental factors, such as temperature and winter crop seasonality, became more important. After 2008, the situation seems to have returned to pre-2006 conditions with less intense bloom events up to 2013.

Our results indicate not only that remote sensing can provide crucial information for monitoring Lake Taihu watershed dynamics but also provides new insights into an integrated approach to monitoring and managing inland water bodies. Future research on the integrated assessment at a watershed scale could build on this approach by including additional environmental features: hydrology (e.g., water level, inflowing river regimes), meteorology (e.g., winds, precipitation time series), and sediment biogeochemistry. Additional information would provide further insights when placed within a comprehensive framework for watershed assessment. Eventually, a sub-watershed scale of analysis of environmental features within the watershed would help to identify localized phenomena.

References

1. Giardino C, Bresciani M, Villa P, Martinelli A (2010) Application of remote sensing in water resource management: the case study of Lake Trasimeno, Italy. Water Resour Manage 24(14): 3885–3899
2. Duan HT, Ma RH, Xu XF, Kong FX, Zhang SX, Kong WJ, Hao J, Shang L (2009) Two-decade reconstruction of algal blooms in China's Lake Taihu. Environ Sci Technol 43:3522–3528
3. Xu H, Paerl HW, Qin BQ, Zhu GW, Gao G (2010) Nitrogen and phosphorus inputs control phytoplankton growth in eutrophic Lake Taihu, China. Limnol Oceanogr 55:420–432
4. Guo L (2007) Doing battle with the green monster of Taihu Lake. Science 317:1166
5. Qin BQ, Zhu GW, Gao G, Zhang YL, Li W, Paerl HW, Carmichael WW (2010) A drinking water crisis in Lake Taihu, China: linkage to climatic variability and lake management. Environ Manage 45:105–112
6. Wang M, Shi W (2008) Satellite-observed algae blooms in China's Lake Taihu. Eos Trans Am Geophys Union 89:201–202
7. Chorus I, Bartram J (1999) Toxic cyanobacteria in water: a guide to their public health consequences, monitoring, and management. Spon, London
8. Paerl HW, Huisman J (2009) Climate change: a catalyst for global expansion of harmful cyanobacterial blooms. Environ Microbiol Rep 1:27–37
9. Carpenter SR, Caraco NF, Correll DL, Howarth RW, Sharpley AN, Smith VH (1998) Nonpoint pollution of surface waters with phosphorus and nitrogen. Ecol Appl 8:559–568
10. Huang C, Li Y, Yang H, Sun D, Yu Z, Zhang Z, Chen X, Xu L (2014) Detection of algal bloom and factors influencing its formation in Taihu Lake from 2000 to 2011 by MODIS. Environ Earth Sci 71:3705–3714
11. Schaeffer BA, Hagy JD, Conmy RN, Lehrter JC, Stumpf RP (2012) An approach to developing numeric water quality criteria for coastal waters using the seaWiFS satellite data record. Environ Sci Technol 46:916–922
12. Paerl HW, Xu H, McCarthy MJ, Zhu G, Qin B, Li Y, Gardner WS (2011) Controlling harmful cyanobacterial blooms in a hyper-eutrophic lake (Lake Taihu, China): the need for a dual nutrient (N & P) management strategy. Water Res 45(5):1973–1983
13. Zhang M, Duan H, Shi X, Yu Y, Kong F (2012) Contributions of meteorology to the phenology of cyanobacterial blooms: implications for future climate change. Water Res 46:442–452
14. Xue B, Yao S, Xia W (2007) Environmental changes in Lake Taihu during the past century as recorded in sediment cores. In: Qin B, Liu Z, Havens K (eds) Eutrophication of shallow lakes with special reference to Lake Taihu, China. Springer, Dordrecht, pp 117–123
15. Yu G, Xue B, Lai G, Gui F, Liu X (2007) A 200-year historical modeling of catchment nutrient changes in Taihu basin, China. Hydrobiologia 581(1):79–87
16. Chen Y, Qin B, Teubner K, Dokulil MT (2003) Long-term dynamics of phytoplankton assemblages: Microcystis-domination in Lake Taihu, a large shallow lake in China. J Plankton Res 25(4):445–453
17. James RT, Havens K, Zhu G, Qin B (2009) Comparative analysis of nutrients, chlorophyll and transparency in two large shallow lakes (Lake Taihu, PR China and Lake Okeechobee, USA). Hydrobiologia 627(1):211–231
18. Liu X, Lu X, Chen Y (2011) The effects of temperature and nutrient ratios on Microcystis blooms in Lake Taihu, China: An 11-year investigation. Harmful Algae 10(3):337–343
19. Ke Z, Xie P, Guo L (2008) Controlling factors of spring–summer phytoplankton succession in Lake Taihu (Meiliang Bay, China). Hydrobiologia 607(1):41–49
20. Cai LL, Zhu GW, Zhu MY, Xu H, Qin BQ (2012) Effects of temperature and nutrients on phytoplankton biomass during bloom seasons in Taihu Lake. Water Sci Eng 5(4):361–374
21. Chen Y, Fan C, Teubner K, Dokulil M (2003) Changes of nutrients and phytoplankton chlorophyll-*a* in a large shallow lake, Taihu, China: an 8-year investigation. Hydrobiologia 506:273–279

22. Chen Y, Chen H, Wu Y, Li Z, Sun L, Qu M, Kong Z (2007) Toxicity evaluation of Meiliang Bay, Lake Taihu, China—a drinking water source. In: Qin B, Liu Z, Havens K (eds) Eutrophication of shallow lakes with special reference to Lake Taihu, China. Springer, Dordrecht, pp 297–303
23. Duan H, Ma R, Loiselle SA, Shen Q, Yin H, Zhang Y (2014) Optical characterization of black water blooms in eutrophic waters. Sci Total Environ 482–483:174–183
24. Hu C, Lee Z, Ma R, Yu K, Li D, Shang S (2010) Moderate Resolution Imaging Spectroradiometer (MODIS) observations of cyanobacteria blooms in Taihu Lake, China. J Geophys Res 115:C04002
25. Duan H, Ma R, Zhang Y, Loiselle SA (2014) Are algal blooms occurring later in Lake Taihu? Climate local effects outcompete mitigation prevention. J Plankton Res 36:866–871
26. Karlsson-Elfgren I, Brunberg AK (2004) The importance of shallow sediments in the recruitment of Anabaena and Aphanizomenon (Cyanophyceae). J Phycol 40(5):831–836
27. Cao HS, Tao Y, Kong FX, Yang Z (2008) Relationship between temperature and cyanobacterial recruitment from sediments in laboratory and field studies. J Freshwater Ecol 23:405–412
28. Bunting ES (1976) Accumulated temperature and maize development in England. J Agric Sci 87(03):577–583
29. Ma LQ, Gao SJ, Wen JB, Zong SX, Xu ZC (2008) Effective accumulated temperature and developmental threshold temperature for Semanotus bifasciatus (Motschulsky) in Beijing. For Stud China 10(2):125–129
30. Paerl HW, Hall NS, Calandrino ES (2011) Controlling harmful cyanobacterial blooms in a world experiencing anthropogenic and climatic-induced change. Sci Total Environ 409(10): 1739–1745
31. Gao C, Zhu JG, Zhu JY, Gao X, Dou YJ, Hosen Y (2004) Nitrogen export from an agriculture watershed in the Taihu Lake area, China. Environ Geochem Health 26(2):199–207
32. Rouse JW, Haas RH, Schell JA, Deering DW (1974) Monitoring vegetation systems in the Great Plains with ERTS. NASA special publication 351, p 309
33. Wang H, Lu J, Wang W, Huang P, Yin C (2007) Spatio-temporal distribution of nitrogen in the undulating littoral zone of Lake Taihu, China. Hydrobiologia 581(1):97–108
34. Huang P, Han B, Liu Z (2007) Floating-leaved macrophyte (Trapa quadrispinosa Roxb) beds have significant effects on sediment resuspension. In: Qin B, Liu Z, Havens K (eds) Eutrophication of shallow lakes with special reference to Lake Taihu, China. Springer, Dordrecht, pp 189–193
35. Ma R, Duan H, Gu X, Zhang S (2008) Detecting aquatic vegetation changes in Taihu Lake, China using multi-temporal satellite imagery. Sensors 8(6):3988–4005
36. Gianinetto M, Villa P (2011) Mapping Hurricane Katrina's widespread destruction in New Orleans using multisensor data and the normalized difference change detection (NDCD) technique. Int J Remote Sens 32(7):1961–1982
37. Villa P, Mousivand A, Bresciani M (2014) Aquatic vegetation indices assessment through radiative transfer modeling and linear mixture simulation. Int J Appl Earth Obs Geoinf 30: 113–127
38. Villa P (2012) Mapping urban growth using Soil and Vegetation Index and Landsat data: the Milan (Italy) city area case study. Landscape Urban Plan 107(3):245–254
39. Gao BC (1996) NDWI—a normalized difference water index for remote sensing of vegetation liquid water from space. Remote Sens Environ 58(3):257–266
40. Ma R, Dai J (2005) Investigation of chlorophyll-*a* and total suspended matter concentrations using Landsat ETM and field spectral measurement in Taihu Lake, China. Int J Remote Sens 26(13):2779–2795
41. Qin B, Xu P, Wu Q, Luo L, Zhang Y (2007) Environmental issues of lake Taihu, China. Hydrobiologia 581(1):3–14

42. Reidsma P, Feng S, van Loon M, Luo X, Kang C, Lubbers M, Kanellopoulos A, Wolf J, van Ittersum MK, Qu F (2012) Integrated assessment of agricultural land use policies on nutrient pollution and sustainable development in Taihu Basin, China. Environ Sci Policy 18:66–76
43. Villa P, Lechi G, Gomarasca MA (2009) Multivariate differencing techniques for land cover change detection: the normalized difference reflectance approach. In: Ho PG (ed) Geoscience and remote sensing. InTech, Rijeka, pp 277–299
44. Shapiro J (1990) Current beliefs regarding dominance by blue-greens: the case for the importance of CO_2 and pH. Verh Int Ver Limnol 24:38–54
45. Laamanen MJ, Forsström L, Sivonen K (2002) Diversity of Aphanizomenon flos-aquae (cyanobacterium) populations along a Baltic Sea salinity gradient. Appl Environ Microbiol 68:5296–5303
46. Sellner KG, Lacouture RV, Parrish CR (1988) Effects of increasing salinity on a cyanobacteria bloom in the Potomac River estuary. J Plankton Res 10:49–61
47. Dokulil MT, Teubner K (2000) Cyanobacterial dominance in lakes. Hydrobiologia 438(1–3): 1–12
48. Gustavs L, Eggert A, Michalik D, Karsten U (2010) Physiological and biochemical responses of green microalgae from different habitats to osmotic and matric stress. Protoplasma 243: 3–14
49. Zevenboom W (1982) N_2-fixing cyanobacteria: why they do not become dominant in shallow hypertrophic lakes. Aquat Ecol 16:289–290
50. Kosten S, Huszar VLM, Becares E, Costa LS, van Donk E, Hansson LA, Jeppesen E, Kruk C, Lacerot G, Mazzeo N, De Meester L, Moss B, Lurling M, Noges T, Romo S, Scheffer M (2012) Warmer climates boost cyanobacterial dominance in shallow lakes. Global Change Biol 18: 118–126
51. O'Neil JM, Davis TW, Burford MA, Gobler CJ (2012) The rise of harmful cyanobacteria blooms: the potential roles of eutrophication and climate change. Harmful Algae 14:313–334
52. Schindler DW (1977) Evolution of phosphorus limitation in lakes. Science 195(4275): 260–262
53. Jacoby JM, Collier DC, Welch EB, Hardy FJ, Crayton M (2000) Environmental factors associated with a toxic bloom of Microcystis aeruginosa. Can J Fish Aquat Sci 57(1):231–240
54. Oliver RL, Ganf GG (2000) Freshwater blooms. In: Potts M, Whitton BA (eds) The ecology of cyanobacteria. Springer, Dordrecht, pp 149–194
55. van Beusekom JEE, Loebl M, Martens P (2009) Distant riverine nutrient supply and local temperature drive the long-term phytoplankton development in a temperate coastal basin. J Sea Res 61:26–33
56. Kutser T, Metsamaa L, Strombeck N, Vahtmae E (2006) Monitoring cyanobacterial blooms by satellite remote sensing. Estuar Coast Shelf Sci 67:303–312
57. Latour D, Sabido O, Salencon MJ, Giraudet H (2004) Dynamics and metabolic activity of the benthic cyanobacterium Microcystis aeruginosa in the Grangent reservoir (France). J Plankton Res 26:719–726
58. Fay P (1988) Viability of akinetes of the planktonic cyanobacterium Anabaena circinalis. Proc R Soc Lond B Biol Sci 234(1276):283–301
59. Lai G, Yu G (2006) A numerical simulation of nutrient transport in Taihu Basin. In: Proceedings of the International Conference on Hydrology and Management of Forested Wetlands, New Bern, NC, 8–12 April 2006. doi:10.13031/2013.20329
60. Lu J, Wang H, Wang W, Yin C (2007) Vegetation and soil properties in restored wetlands near Lake Taihu, China. Hydrobiologia 581(1):151–159

Remote Sensing for Regional Lake Water Quality Assessment: Capabilities and Limitations of Current and Upcoming Satellite Systems

Leif G. Olmanson, Patrick L. Brezonik, and Marvin E. Bauer

Contents

Abstract Remote, satellite-based sensing is a cost-effective way to gather information needed for regional water quality assessments in lake-rich areas. A major advantage is that it enables retrieval of current and historic information on lakes that were not part of ground-based sampling programs. Advances over the past decade have enabled the use of satellite imagery for regional-scale measurement of lake characteristics, such as clarity and chlorophyll. For example, in the Midwest USA,

L.G. Olmanson (✉) • M.E. Bauer
Department of Forest Resources, University of Minnesota, St. Paul, MN, USA
e-mail: olman002@umn.edu

P.L. Brezonik
Department of Civil, Environmental, and Geo-Engineering, University of Minnesota, Minneapolis, MN, USA

T. Younos, T.E. Parece (eds.), *Advances in Watershed Science and Assessment*, The Handbook of Environmental Chemistry 33,
DOI 10.1007/978-3-319-14212-8_5

historic and recent Landsat water clarity assessments have been conducted on more than 20,000 lakes to investigate spatial and temporal patterns and explore factors that affect water quality. The spatial characteristics of Landsat imagery allow for the assessment of all lakes larger than ~4 ha, but the broad nature and placement of its spectral bands have limited assessments largely for water clarity. European Space Agency (ESA) MERIS imagery with spectral bands that were selected for water has been used to assess chlorophyll for about 900 of Minnesota's large lakes (those > 150 ha). Improvements of the recently launched Landsat 8 and upcoming ESA Sentinel-2 satellites will expand our capabilities further enabling assessment of other optically related water quality characteristics, such as chlorophyll, colored dissolved organic matter (CDOM), and mineral suspended solids for all lakes, and upcoming Sentinel-3 will continue these capabilities for large lakes.

Keywords CDOM • Chlorophyll *a* • Lake water quality • Satellite imagery Landsat • Secchi depth • Sentinel

1 Introduction

Inland water bodies, such as lakes and reservoirs, are important natural resources for sustenance, recreation, and aesthetic enjoyment, and they add to the economic vitality and quality of life of regions where they occur. Water quality properties, such as chlorophyll *a*, total suspended matter, turbidity, colored dissolved organic matter (CDOM), and nutrients, are used by regulatory and resource management agencies to guide management and public safety decisions. In situ point sampling is the conventional method for collecting information on water quality variables. For effective lake management, it is important to have long-term water quality information on a synoptic scale. The "big picture" view of water quality allows managers to take into account not only differences among lakes but also changes through time for the whole lake and surrounding water bodies within a watershed or typically much larger areas. Unfortunately, only a small percentage of inland waters are regularly monitored by conventional methods, and historical water quality data are lacking for most inland waters. The "big picture" view of water quality is not practical with conventional point sampling methods due to limited resources, and historic water quality data are sparse. Satellite remote sensing has become a viable option for current synoptic measurements and historic assessments of important water quality variables due to improved computer software and hardware, as well as the availability of free or inexpensive satellite imagery.

2 Rationale for Optical Remote Sensing Using Satellite Imagery

Satellite remote sensing has the potential to provide synoptic and frequent water quality measurements of inland waters. Remote sensing satellites such as the Landsat series have been collecting and archiving imagery regularly since the early 1970s, which allows for the assessments of some historic water quality information even on inland waters lacking historical ground-based data. Satellite systems planned for launch in the next few years will allow better characterization of inland water quality on regional-to-global scales.

Optical remote sensing (ORS) using satellite imagery can be used to measure water quality of inland, marine, and coastal waters. Although there are many similarities between ORS applied to inland waters and ORS applied to marine systems, there also are profound differences. For example, spatial resolution requirements are much lower for the broad expanses of the oceans and most coastal areas than are needed for small inland water bodies. Several generations of satellite sensors acquire images with large pixel sizes (~0.3–1 km) that provide adequate spatial resolution for oceanic and most coastal studies but are too coarse for small inland water bodies. For perspective, the smallest water body that can be measured by a satellite sensor with a pixel size of 1 km is ~1,000 ha [1]. The spatial resolution of Landsat satellites, 30 m, generally allows measurements on water bodies larger than ~4 hectares (ha). As pixel size increases, the likelihood decreases that an image will have at least one pixel (preferably four or more) focused solely on open water and not affected by terrestrial and shallow near-shore areas. The smaller pixel size also allows for better characterization of bays and narrow portions of complex lake systems

A second difference relates to the optical complexity of inland waters. Remote sensing scientists focusing on marine systems are able to use increasingly sophisticated instrumentation such as the Moderate Resolution Imaging Spectroradiometer (MODIS) aboard the Aqua and Terra satellites to develop analytical and semi-analytical algorithms that retrieve chlorophyll levels from the oceans, and this has become a routine, global-scale operation [2, 3]. Remote sensing scientists focusing on inland waters have had to develop procedures primarily using other satellites like Landsat, which have adequate spatial resolution but at the same time have critical deficiencies in spectral and temporal resolution. The blue and green spectral bands used to retrieve chlorophyll levels from oceanic waters are not so useful for such purposes in optically complex inland waters [4–7]. These deficiencies have limited development of retrieval algorithms for inland water quality variables by satellite imagery mostly to empirical and semiempirical (described in Sect. 3.1) approaches. More sophisticated ground-based and aircraft-mounted spectroradiometers also have been used in recent years to advance the science of inland water ORS. In summary, the requirements for spatial resolution, most effective spectral bands, ability to use analytical (versus empirical) approaches, and ranges of interest for water quality variables like chlorophyll and CDOM are different between inland

waters and marine systems; these differences resulted in the development of two closely related but separate fields of study (e.g., also see [8]).

2.1 Inherent and Apparent Optical Properties and the Radiative Transfer Equation

When a photon of light interacts with matter, it can either disappear (energy converted to heat or a chemical bond), which is called absorption, or it can change its direction and/or energy, which is called scattering. The absorption and scattering properties of natural waters are the basis for use of ORS in measurement of inland water quality and can be expressed in terms of inherent optical properties (IOPs) and apparent optical properties (AOPs). IOPs depend only on the water medium and are independent of the available light field. Three important IOPs relative to ORS are the absorption coefficient, volume scattering function, and beam attenuation coefficient, all of which are wavelength dependent. The beam attenuation coefficient "c" is the sum of terms for the absorption "a" and scattering "b" of light in the medium:

$$c(\lambda) = a(\lambda) + b(\lambda) \tag{1}$$

where (λ) means a term is a function of wavelength; both $a(\lambda)$ and $b(\lambda)$ are functions of the nature and concentrations of substances in natural waters.

AOPs depend on the IOPs and also on the directional structure of the ambient light field in the medium. The most important AOPs relative to ORS are the irradiance reflectance and various diffuse attenuation coefficients. Signals received by satellite sensors for ORS ultimately get converted to irradiance reflectance values and to a closely related property called "remote sensing reflectance," hereafter referred to as R_{rs}. Radiative transfer theory provides the connection between IOPs and the AOPs [9] and thus is the basis for relating R_{rs} to concentrations of substances in water that affect light absorption and/or light scattering. The basic radiative transfer equation is [10, 11]:

$$R_{rs} = G(\lambda)\frac{b_b(\lambda)}{a(\lambda) + b_b(\lambda)} \tag{2}$$

where

$$a(\lambda) = a_w + a^*_{ph}(\lambda)C_{chla} + a_{CDOM}(\lambda) + a^*_{NAP}(\lambda)C_{NAP} \tag{3}$$

and

$$b_b(\lambda) = 0.5b_w(\lambda) + b^*_{b,ph}(\lambda)C_{chla} + b^*_{b,NAP}(\lambda)C_{NAP} \quad (4)$$

$G(\lambda)$ is a scaling factor accounting for geometrical conditions (e.g., solar zenith angle) and the state of the air-water interface; $a(\lambda)$ is the total absorption coefficient, which is the sum of absorption coefficients for water itself, phytoplankton, CDOM, and non-algal particles (NAP); $a^*_{ph}(\lambda)$ is a chlorophyll-specific absorption coefficient for phytoplankton; C_{chla} is the concentration of chlorophyll *a*; $a^*_{NAP}(\lambda)$ is the specific absorption coefficient for NAP; C_{NAP} is the concentration of NAP; and $b_b(\lambda)$ is the total backscattering coefficient, which similarly is composed of scattering terms for water itself, phytoplankton, and NAP. The backscattering coefficient for pure water is equal to one-half of the total scattering coefficient of pure water; it is assumed that there is equal probability of scattering in the forward and backward directions [11]. Equations (2)–(4) assume that the absorption and scattering properties of a water body depend on contributions from four components: pure water, phytoplankton, CDOM, and NAP. Ultimately, analytical and semi-analytical models for retrieval of water quality information on these variables are based on these equations.

2.2 *Water Quality Variables Amenable to Measurement by Optical Remote Sensing*

2.2.1 Currently Measured Variables

To be measurable by ORS, a water quality constituent must affect at least one of the two principal optical properties that control the amount of light reflected back to a sensor from the water body: absorption and scattering. Because pure water strongly absorbs incoming radiation in the ultraviolet (UV) range and also (but to a somewhat lesser extent) in the infrared (IR) range, the portion of the electromagnetic spectrum useful for remote sensing of water quality is limited to the visible range (~400–700 nm) plus the near UV (roughly 360–400 nm) and the near IR (~700–900 nm). Beyond this range, absorption of incoming radiation is so strong that essentially nothing is reflected back into the atmosphere. Consequently, the water quality constituents amenable to measurement by ORS must absorb or scatter light within this wavelength range.

Constituents like plant pigments, especially chlorophyll *a*, and humic substances, which constitute much of the CDOM in water bodies, are the most important examples of light-absorbing substances amenable to measurement by ORS. CDOM is usually reported by limnologists and remote sensing scientists in terms of its light absorptivity at specific wavelengths, commonly 420 and 440 nm, e.g., a_{440} (m^{-1}), but chloroplatinate units (CPU) are still used by some water quality

scientists and engineers. Although many synthetic organic compounds used in modern society are colored (i.e., absorb light in the visible range), they do not occur in natural waters at sufficient concentrations, except in very rare pollution events, to be measurable by ORS. Similarly, a variety of metal ions and metal-ion complexes are visibly colored (e.g., species of Cr, Cu, and Mn), but their concentrations in natural waters, especially in forms that are colored, are far too low to affect reflectance spectra. A possible exception, iron (Fe), is discussed below in the context of CDOM measurements.

Suspended particles, including phytoplankton, organic detritus derived from microbial decomposition and secondary production, and mineral suspended solids such as aluminosilicate clays and soil particles (SS_{min}), are the primary constituents in natural waters that affect scattering. Because the spectral characteristics of light scattering by various types of suspended particles are not sufficiently unique, ORS techniques generally are not able to distinguish among the types of suspended particles causing scattering and thus affecting reflectance. Phytoplankton cells, because of their chlorophyll content, are an exception, but results normally are presented in terms of chlorophyll concentrations and not cell counts or cell volume. Light-scattering water quality constituents measured by ORS thus are "lumped parameters" like total suspended solids (TSS) and turbidity. Light scattering depends on a complicated set of factors, including particle numbers, sizes, shapes, and surface properties; no universal relationship between the reflectance of light and TSS (in mg/L) thus should be expected. Rather, such relationships are time and place specific depending on the properties of the suspended particles, as mentioned above. Because turbidity measured by a laboratory turbidimeter or nephelometer is directly related to the scattering of light in water bodies that produces the reflected light measured by optical remote sensors, development of universal or quasi-universal ORS relationships for turbidity may be possible. A few studies have reported on the measurement of turbidity by ORS and are discussed further in Sect. 2.2.4.

Secchi depth (SD), an important optical property of natural waters, is affected by both light scattering and light absorption. In most water bodies, scattering caused by phytoplankton and plankton-derived particles controls SD, and thus it serves as a common and simple measure of lake trophic status. Many studies have shown strong correlations between SD^{-1} and chlorophyll levels (or log SD versus log [chlorophyll]) in lakes [1, 12]. CDOM and SS_{min} also affect SD in some waters, and proper interpretation of SD data depends on what factors are affecting water clarity. Brezonik [13] quantified the influence of CDOM on SD using in situ experiments in which a concentrated source of CDOM-like material was added incrementally to low-CDOM and low turbidity lake water in mesocosm-scale "limnobags." At a measured CDOM of 200 CPU, equivalent to $a_{440} \approx 20\ m^{-1}$, representative of highly colored bog lakes, and negligible SS_{min}, the SD was ~1.5 m; at CDOM = 70 CPU ($a_{440} \approx 7\ m^{-1}$), representative of moderately colored lakes, the SD was 4.5 m. Preisendorfer [14] showed that SD^{-1} is proportional to the sum of two fundamental optical properties: $\alpha + K_d$, where α is the beam attenuation coefficient (measured by an underwater transmissometer) and K_d, the diffuse attenuation coefficient

(determined by measuring the amount of incident light remaining as a function of depth with an underwater light meter). K_d and α are spectrally and depth averaged values for a given water body.

Values of K_d at specific wavelengths, most commonly $K_{d,490}$, have been retrieved from ORS data by marine scientists as part of efforts to develop analytical methods to retrieve water quality information from satellite imagery (e.g., [10, 15, 16]). Plug-in algorithms to compute $K_{d,490}$ were developed for several MERIS processors in the BEAM software system, including the Case 2 Regional and Boreal lakes processors [17–19]. K_d is not a common water quality variable in inland waters, however, and there seems to have been little interest among freshwater remote sensing scientists in using the algorithms for K_d in inland lakes. This situation is likely to change when improved satellite sensors (see Sect. 2) that allow for more analytical retrieval methods become available for inland water ORS measurements.

In summary, only a few water quality variables are amenable to direct measurement by ORS, but they include two variables, chlorophyll *a* and CDOM, that are critically important for understanding lake metabolism and carbon cycling. A third variable, SD, probably is the most widely measured lake water quality parameter because its simplicity and low cost facilitates use by citizen monitoring programs. SD also is important because it is related directly to water quality as perceived by lake users and to trophic conditions and chlorophyll levels. TSS and turbidity round out the common water quality variables amenable to measurement by ORS.

2.2.2 Potential Variables with Improved Spectral Characteristic Sensors

As noted above, a few other variables could become important in applications of ORS to regional-scale measurements of inland lake water quality when sensors with improved spectral characteristics and adequate spatial resolution become available. These include SS_{min}, K_d, and specific plant pigments indicative of various classes of algae (e.g., see [10]), such as phycocyanin for cyanobacteria. Identification and measurement of the abundance of submerged and emergent aquatic plants also can be achieved using ORS [20–22], but details of this topic are beyond our scope.

2.2.3 Non-optical Variables Sometimes Correlated with Variables Having Optical Properties

Many examples can be found in the remote sensing literature that claim the ability to measure water quality variables that do not directly affect light reflectance or are present in natural waters at such low concentrations that they do not affect reflectance signals measured by satellite sensors. Examples include mercury, bacteria (e.g., *Escherichia coli*) [23], and total phosphorus (TP) [24, 25]. In all cases, the reported relationships involve empirical regression equations. Despite the fact that

high r^2 values sometimes are reported, the relationships "work" only because the "non-optical" variable is correlated in the water bodies used to develop the relationship with an optical variable that affected reflectance. For example, the bacterial indicator of fecal contamination, *E. coli*, is found in waters contaminated by human activities, and correlation of *E. coli* abundance with TSS and turbidity might be expected. Similarly, phosphorus often is the limiting nutrient for algal growth in lakes, and correlations between chlorophyll and TP or SD and TP thus are common (e.g., [12]). Such relationships cannot be applied reliably beyond the database from which they were derived because no intrinsic or causative relationship exists between the non-optical and optical variables or between the non-optical variable and reflectance.

The use of empirical relationships that depend on secondary correlations has led to criticisms that remote sensing scientists are "overselling" their technology (e.g., [8, 26]). A more transparent and defendable approach is to develop relationships between reflectance data and variables that directly affect reflectance and then separately determine whether a sufficiently close relationship exists between the optical variable retrieved from imagery and a non-optical variable of interest. Applications of such empirical relationships still should be limited to the data sets on which they are based, but situations exist in which useful information can be obtained by this approach. For example, evaluation of a suite of environmental conditions retrieved from satellite imagery was found useful in predicting outbreaks of waterborne diseases even though the disease-causing microorganisms do not directly affect satellite imagery signals [27]. Similarly, atmospheric scientists have estimated transport of specific pollutants like mercury (Hg) from Asia across the Pacific Ocean to North America by tracking atmospheric dust using satellite imagery and independent measurements of the pollutant (e.g., Hg) concentrations in atmospheric dust over the Pacific.

Relationships between DOC (dissolved organic carbon) and reflectance also have been reported (e.g., [28]), but insofar as DOC per se is not an optical variable and does not itself affect reflectance, these also are the results of indirect correlations. To the extent that such relationships work, they rely on the fact that a fraction of DOC (CDOM) affects reflectance. For some waters good correlations exist between CDOM and DOC, but as Brezonik et al. [29] recently showed, no single DOC-CDOM relationship applies across a broad spectrum of surface waters. Some sources of DOC, e.g., autochthonous organic matter and anthropogenic organic matter derived from wastewater, have low color per unit of carbon. As a result, CDOM and DOC are poorly correlated in many natural waters. For example, Spencer et al. [30] found that r^2 values for DOC-CDOM relationships were ≤ 0.5 in 11 of 30 large North American rivers, and four rivers (the Colorado, Columbia, Rio Grande, and St. Lawrence) had $r^2 < 0.2$. Factors giving rise to poor DOC-CDOM relationships include the extent to which the DOC is autochthonous or anthropogenic and the extent to which allochthonous DOC has been photodegraded.

The following three sections summarize the spectral basis for retrieval of the three most important water quality characteristics—clarity, chlorophyll, and CDOM—from remote sensing imagery.

2.2.4 Water Clarity Variables

Three water clarity variables discussed here include Secchi depth (SD), turbidity, and TSS.

Water clarity, whether measured as light scattering in laboratory turbidimeters, as the in situ depth of disappearance of a white disk (SD), or as the slope of the logarithm of light attenuation with depth (K_d) in a water body, provides critically important information to both users of water bodies and to water resource managers. Fortunately, because of their close relationship to both IOPs and AOPs of water, clarity parameters are well suited to measurement by ORS.

In part because of the widespread availability of calibration data from citizen and agency monitoring programs, SD has been the subject of many ORS studies (see Sect. 4 for details). Retrieval of SD from satellite imagery also is facilitated by the fact that the broad Landsat bands are suitable for SD retrieval. Numerous studies have yielded good relationships for SD that involve bands 1 and 3 in two-term equations like $\ln(\mathrm{SD}) = a(\mathrm{TM1}/\mathrm{TM3}) + b\mathrm{TM1} + c$ [31], where ln(SD) is the natural logarithm of Secchi depth; a, b, and c are regression coefficients; and TM1 and TM3 are reflectance values for thematic mapper bands 1 and 3. As SD decreases, reflectance in the red band (TM3) increases. The blue band (TM1) tends to normalize brightness in the red and improves algorithm performance. R^2 values for such equations are in the range 0.71–0.96 for lakes in Minnesota [32]; others [33] reported similar ranges of fit. Olmanson et al. [1] found that MERIS and Landsat imagery worked equally well for SD, but the coarser spatial resolution of MERIS allowed assessment of only about 8 % of the Minnesota lakes accessed by Landsat.

Models for turbidity and TSS in optically complex waters, where phytoplankton, CDOM, and $\mathrm{SS}_{\mathrm{min}}$ all may affect IOP features, should avoid the absorption characteristics of chlorophyll in the red and CDOM in the blue region and use the scattering peak at ~705 nm or band combinations in the NIR or green regions (where plant pigments have minimal absorption). For example, Gitelson et al. [34] found that a difference ratio algorithm $(R560 - R520)/(R560 + R520)$ was highly correlated with TSS in lakes and rivers with TSS values < 66 mg/L. Phytoplankton absorption is at a minimum near 560 nm, but reflectance at this wavelength is sensitive to TSS; in contrast, reflectance at 520 nm is relatively insensitive to changes in TSS [35].

Numerous studies have shown the usefulness of NIR bands for turbidity and TSS (for reviews, see [10, 35]). The scattering peak at ~700 nm was found to be strongly correlated with TSS by many studies (e.g., [36–38]), and Senay et al. [39] reported a good relationship for turbidity. The difference in reflectance at 710 and 740 nm was

found useful by Shafique et al. [40]. The scattering peak at ~700 by itself also was found to work well for NVSS (nonvolatile SS, essentially equivalent to SS_{min}) [41].

Olmanson et al. [42] found strong relationships between reflectance at 705 nm and both turbidity and TSS ($r^2 = 0.77–0.93$ for both) using airborne hyperspectral imagery to assess water quality in the optically complex waters of the Minnesota, Mississippi, and St. Croix Rivers in the Minneapolis-St. Paul region. Depending on location and time, CDOM, phytoplankton, and/or SS_{min} all may dominate the optical properties of these rivers. They also found a predictive equation ($r^2 = 0.80–0.90$) for volatile suspended solids, VSS, a measure of organic suspended matter, using the ratio of reflectance at 705 to 670 nm. For SS_{min} they found that using band at 705 nm and the ratio of reflectance at 705 to 670 nm, a combined model (TSS and chlorophyll *a*), yielded an r^2 of 0.85–0.97 for SS_{min}. The resulting maps clearly distinguished phytoplankton-based turbidity from SS_{min} (Fig. 1 [42]: reprinted with permission from the publisher). The transition from phytoplankton-dominated water at location "a" (Fig. 1B) to inorganic sediment-dominated water at location "e" is captured in the reflectance spectra extracted from the imagery (Fig. 2). Absorption characteristics of chlorophyll are distinctly visible at location "a" but become more moderate toward location "e." This example demonstrates the massive quantity of information obtainable from a single image that would have been missed by traditional monitoring, which would probably involve only one sample for the entire area.

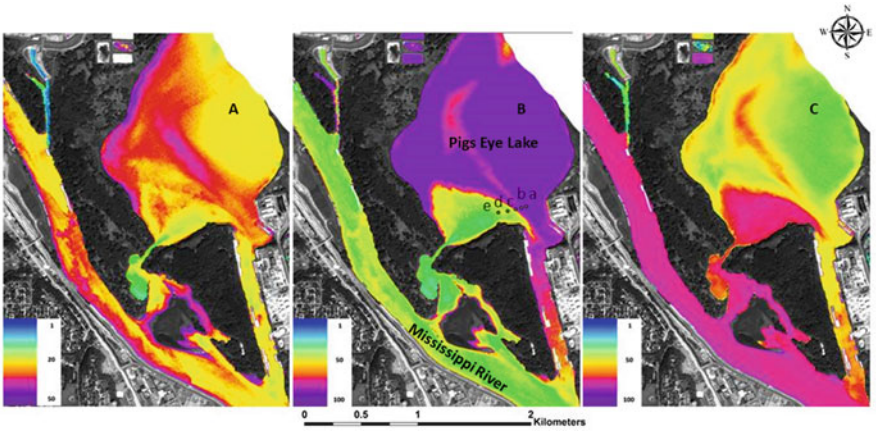

Fig. 1 Maps of Pig's Eye Lake, St. Paul, Minnesota, showing transition from conditions dominated by inorganic sediment to conditions dominated by phytoplankton: (**A**) turbidity, (**B**) chlorophyll *a*, and (**C**) NVSS/TSS (% SS_{min}); August 30, 2007. Reprinted from Olmanson et al. [42] with permission of the publisher

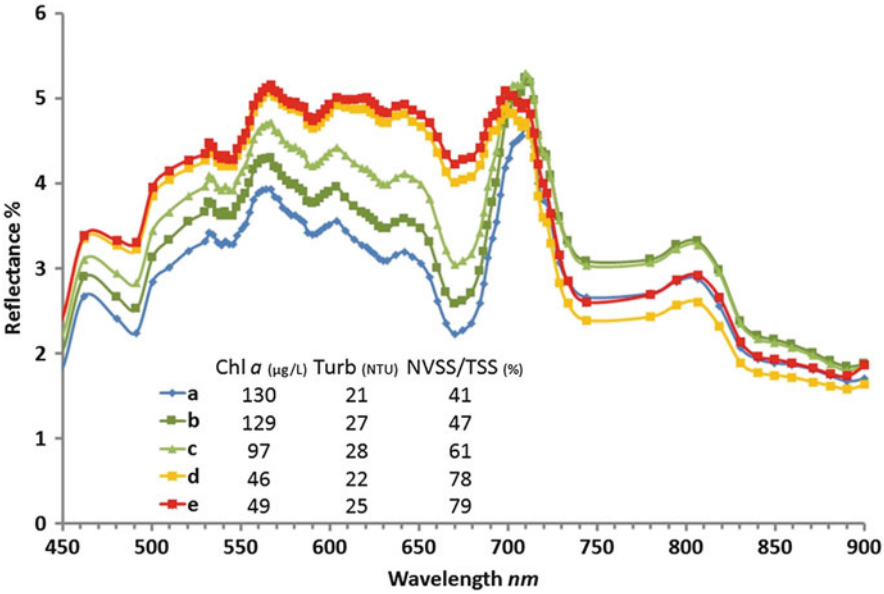

Fig. 2 Reflectance spectra of the transition zone for conditions dominated by inorganic sediment in the Mississippi River to conditions dominated by phytoplankton in Pig's Eye Lake, August 30, 2007 (Fig. 1b). Tabulated chl *a*, turbidity, and NVSS/TSS values were calculated from reflectance spectra using the best predictive models. Reprinted from Olmanson et al. [42] with permission of the publisher

2.2.5 Chlorophyll and Other Pigments

Predictive models that use ORS to estimate a water quality variable should use wavelengths that identify key spectral characteristics of the variable without interference from competing optical features of other variables. For chlorophyll, this means that algorithms commonly used for the open oceans, which involve reflectance in the blue and green regions, do not work well for inland waters because these waters are influenced by TSS and CDOM. This makes them optically more complex [43] than open ocean waters, where chlorophyll and chlorophyll-related properties are the primary factors affecting reflectance. CDOM and SS_{min} have overlapping absorption features with chlorophyll *a* in the blue region.

Successful chlorophyll models for inland waters thus use absorption characteristics in the red wavelengths—a reflectance trough at ~670 nm caused by a peak in absorption by chlorophyll *a* and a reflectance peak at the red edge (~700–710 nm) caused by scattering by phytoplankton; absorption by CDOM and suspended solids is minimal at these wavelengths [44, 45]. Many studies (e.g., [34, 46–50]) have reported strong relationships between chlorophyll *a* and the reflectance ratio for ~700 nm and ~670 nm in a variety of inland waters and over a wide range of concentrations (e.g., 0.1–350 µg/L; [35]). The usefulness of the red-edge signal for chlorophyll *a* estimation in optically complex river waters also was shown by

Olmanson et al. [42] using airborne hyperspectral imagery on waters of the Minnesota, Mississippi, and St. Croix Rivers. For chlorophyll *a*, the ratio of reflectance at 705 to 670 nm yielded r^2 values of 0.75–0.93. Of the recently or currently available and forthcoming satellite sensors, only MERIS and the Sentinel-2 and Sentinel-3 satellites have appropriately narrow red-edge bands.

Despite the above comments, it must be noted that many studies have reported strong empirical relationships between the broad bands of Landsat sensors and chlorophyll *a* (e.g., [1]); typical predictive equations involve the ratio of TM or ETM+ bands 1 and 3. Absorption by chlorophyll *a* is strong in bands 1 (450–520 nm) and 3 (630–690 nm). Nonetheless, increased scattering by phytoplankton cells counteracts some of the absorption effects and leads to increased reflectance with increasing chlorophyll *a* levels in band 1 and even larger increases in band 3. If it is known that the optical properties of the water bodies being studied are dominated by phytoplankton, the use of these empirical relationships may be considered acceptable. However, for regional assessments where specific water quality characteristics are not known, lakes with high CDOM and/or SS_{min} may be misclassified.

As an example, when we used Landsat 8 imagery to estimate chlorophyll *a* and SD in lakes of northeastern Minnesota for August 31, 2013, we found strong relationships for both variables ($r^2 = 0.70$ and 0.77; RMSE 0.758 and 0.406, respectively). Calibration data (±3 days) for the images are from the Minnesota Pollution Control Agency (for chlorophyll *a*, $n = 99$; for SD, $n = 258$) [51]. For most Minnesota lakes, the results are believed accurate because phytoplankton dominates their optical properties. When we used the same models for the St. Louis River Estuary (SLRE), where optical properties of the waters are dominated by CDOM and SS_{min}, however, the resulting maps misrepresented SS_{min} as chlorophyll (Fig. 3 zoomed into Duluth, MN & Superior, WI area: SLRE at the western edge of Lake Superior). Consequently, we believe it is best to limit regional-scale assessments using Landsat to water clarity or turbidity, which is appropriate for the spectral characteristics of the Landsat sensors, unless independent data are available to verify that SS_{min} and CDOM are not important factors in the lakes being assessed.

The characteristics of Landsat, MERIS, and MODIS sensors for regional water quality measurements were analyzed by Olmanson et al. [1]. Imagery from the three sensors was compared for spatial and spectral characteristics, and empirical models were developed for chlorophyll *a* using various bands and band ratio combinations as dependent variables. MERIS provided a better fit for chlorophyll *a* ($R^2 = 0.85$, $n = 90$) than Landsat and MODIS ($R^2 = 0.79$ for both, $n = 177$ and 42, respectively). The red-edge band at 708 nm improved the fit and allowed discrimination between phytoplankton and SS_{min}, but the Landsat and MODIS results misclassified high SS_{min} levels as chlorophyll *a*, similar to Fig. 3.

Phycocyanin, a pigment occurring in cyanobacteria (formerly known as blue-green algae), can serve as a marker for the presence of these microorganisms in surface waters and is amenable to measurement by ORS. Cyanobacteria are common in eutrophic water bodies, and some species produce substances that are toxic

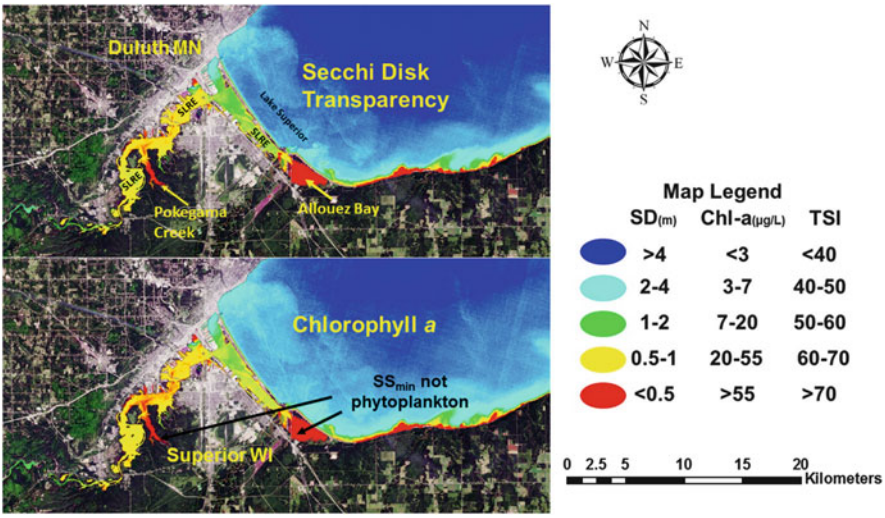

Fig. 3 Maps of chlorophyll *a* and SD in the St. Louis River Estuary (SLRE) at west end of Lake Superior created from an Aug. 31, 2013, Landsat 8 image. Spectral characteristics of the OLI sensor do not allow discrimination of phytoplankton from SS_{min} in optically complex waters. The SS_{min} dominated waters of Pokegama Creek and Allouez Bay are misclassified as having high chlorophyll *a*. Models were developed for the entire path 27 row 27 Landsat image using available lake data, $n = 260$ for SD, 71 for chlorophyll *a* within 3 days of the image

to animals. Thus, there has been much interest by water resource managers in methods for real- or near real-time assessment of the abundance and spatial distribution of cyanobacterial blooms. Phycocyanin has a strong absorption peak near 620 nm, which leads to a characteristic dip in reflectance spectra around 600–630 nm for water bodies with cyanobacteria blooms (e.g., Fig. 4). Several researchers have reported empirical algorithms for cyanobacterial abundance using hyperspectral measurements and reflectance ratios around this wavelength range [52, 53]. Unfortunately, this wavelength range represents a gap in coverage by the sensors of the Landsat satellites (for OLI of Landsat 8, band 3 has a range of 530–590 nm and band 4 a range of 640–70 nm). Vincent et al. [54] claimed to be able to measure phycocyanin and trace cyanobacterial blooms in Lake Erie using Landsat. They reported an r^2 of 0.77 for the relationship, but this is thought to be an example of indirect correlation (e.g., [35]). The retrieval equation probably was responding to chlorophyll signals; cyanobacteria were the dominant algae in the lake at the time of the measurements, and a high correlation could be expected between phycocyanin and chlorophyll levels. Several groups (e.g., [55–58]) have found that the narrower bands of MERIS are suitable for retrieval of phycocyanin concentrations. In these cases, the fluorescence of phycocyanin at ~681 nm is detected using a semiempirical second derivative function that also uses reflectance data for nearby bands at 709 and 665 nm.

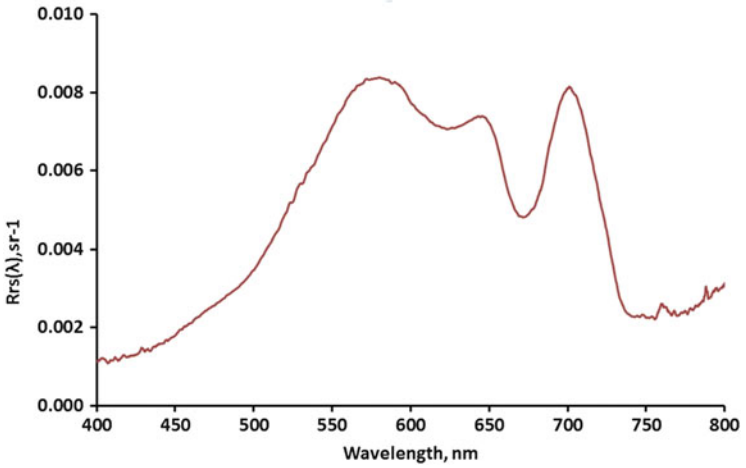

Fig. 4 Reflectance spectra for a eutrophic stretch of the Mississippi River downstream of St. Paul, Minnesota. Data redrawn from Brezonik et al. [29]

2.2.6 Colored Dissolved Organic Matter

Interest among aquatic scientists has increased greatly over the past decade in ORS applications to measure CDOM in surface waters. In part, this reflects a growing interest in quantifying the role of lakes and other surface water bodies in the global carbon cycle, along with the understanding that CDOM represents a large fraction of the total DOC in many aquatic systems.

A wide range of approaches, including analytical, semi-analytical, matrix inversion, and empirical techniques, have been used to retrieve CDOM values for fresh and marine waters by satellite imagery. The most successful algorithms for marine conditions (including coastal waters) involve semi-analytical matrix inversion methods (e.g., [59–61]); but such approaches have been used only a few times for freshwaters (e.g., [11, 62]). The most common retrieval methods for lakes are empirical reflectance-ratio equations that involve nonlinear (power) equations. For example, the equation of Kutser et al. [4] uses the ratio of Advanced Land Imager (ALI) band 2 (525–605 nm) to band 3 (630–690 nm): $a_{420} = 5.13(\mathrm{ALI2/ALI3})^{2.67}$. ALI bands 2 and 3 have approximately the same wavelength ranges as Landsat TM and ETM+ bands 2 and 3 and Landsat 8 OLI bands 3 and 4. Menken et al. [49] independently found a similar relationship using ground-based hyperspectral reflectance data, $a_{440} = 146.4(R_{670}/R_{550})^{2.08}$, and Ficek et al. [63] also used a similar equation.

Using in situ reflectance hyperspectra and associated water quality measurements on ~30 Minnesota and Wisconsin lakes with wide ranges of CDOM, chlorophyll, and TSS, Brezonik et al. [29] recently found that the best band ratio models used similar wavelengths for Landsat 8 bands. With the larger selection of Sentinel-2 and Sentinel-3 bands, a different ratio using ~500 nm:~750 nm worked best.

Simulated Landsat 8, Sentinel-2, and Sentinel-3 bands calculated from the hyperspectra yielded $r^2 = 0.84$–0.86 for a_{440}. The broader Landsat 8 bands worked nearly as well as the narrower Sentinel bands and hyperspectral bands, probably because CDOM lacks specific peaks or troughs in absorbance or reflectance. These r^2 values generally are considered very good for remote sensing predictive equations. Nonetheless, the average for absolute values of percent difference between measured and predicted CDOM across the four best predictive models was 31 %. Although some of the differences can be attributed to sampling variability and measurement uncertainty, the largest source likely is model error. Such large uncertainties should serve as a cautionary note to limnologists and remote sensing scientists.

The effectiveness of predictive equations based on longer wavelengths is counterintuitive given that CDOM absorptivity increases quasi-exponentially with decreasing wavelength and is increasingly diminished in the green and red regions. Although the physical basis for the relationships is still uncertain, the higher band (ALI3, OLI4) centered at 670 nm probably corrects for effects of chlorophyll on reflectance, and the lower band (ALI2, OLI3) centered at ~560 nm probably measures the influence of CDOM. It is important to realize that the small absorbance values measured in laboratory spectrophotometers involve much shorter light paths (1–10 cm) than those of interest in lakes. For example, as noted earlier, a CDOM level of $a_{440} = 20\ \mathrm{m}^{-1}$ implies a Secchi depth of ~1.5 m. Based on UV-visible absorbance spectra we have measured on similar waters, such a sample would have an absorbance (A) of ~0.022 at 560 nm in a 1 cm cell. Given that the Beer-Lambert law applies, the value of A that would apply to a light path of 1.5 m would be ~3.3, and converting to percent of incident light at 560 nm remaining at a depth of 1.5 m yields a value of ~3 %. Light reflected back to the air-water interface from the white surface of the Secchi disk again must travel 1.5 m through the absorbing medium, and thus much less than 1 % of the incident light at 560 nm arrives back at the water surface. Clearly, even small absorbance values measured in the laboratory have large effects on reflectance when the long light paths of lake water columns are considered.

Brezonik et al. [29] found a CDOM-dependent difference in slopes of reflectance spectra in the range of ~570–650 nm. For low-CDOM waters, reflectance decreased with increasing wavelength, but for high-CDOM waters reflectance increased with increasing wavelength. Even though CDOM absorbance is low in this range, it does affect reflectance, as the calculation in the preceding paragraph demonstrated. Other constituents that affect reflectance spectra (notably plant pigments) have minimal effects in this wavelength region.

CDOM levels are much lower in marine waters than in freshwaters; absorptivity at 412 nm, a_{412}, generally is $< 1\ \mathrm{m}^{-1}$ in coastal waters and $< 0.1\ \mathrm{m}^{-1}$ in the open ocean. In contrast, a_{440} values $< \sim 2\ \mathrm{m}^{-1}$ in lakes generally are considered negligible, although remote sensing scientists are starting to take interest in measuring CDOM in low-CDOM lakes [29]. Values in lakes that are considered "humic colored" commonly are in the range of ~5–20 m^{-1} and may range up to 40 m^{-1} or even more in highly colored bogs. Concentrations of TSS and chlorophyll also

tend to be higher in freshwaters than in the oceans, and most freshwaters thus are optically very complex. As noted earlier for chlorophyll, remote sensing methods used for marine waters are not always applicable to freshwaters, and this situation also applies to CDOM. For example, marine scientists interested in CDOM look forward to using a band in the near UV (~380 nm) that will be available on a forthcoming NASA sensor for ocean CDOM. Plant pigment absorbance decreases greatly below ~400 nm, but CDOM absorbance continues to increase exponentially. This band thus avoids interference between the absorbance of plant pigments and CDOM that precludes using bands in the blue region for CDOM retrieval. Bands in the near UV likely would not be useful for inland waters, however, because light absorption by the typically higher levels of CDOM is so strong that there is essentially no reflectance signal (all incoming light is absorbed).

Finally, one of the main reasons for measuring CDOM by ORS is the possibility of using the values to estimate DOC in lakes at regional-to-global scales. As discussed in Sect. 2.2.3, this is not straightforward because DOC-CDOM correlations are not always high. Even when they are, a relationship that works well for one set of lakes may not be the same for a different set of lakes. A further complication in DOC-CDOM relationships is the recent finding that complexation of DOM by dissolved iron enhances the color intensity of the organic substances [64, 65]. Scientists interested in using CDOM to estimate DOC at regional-to-global scales should recognize that DOC-CDOM relationships are site specific and perhaps time specific [29]. Additional predictor variables likely will be needed to develop more robust predictive relationships between CDOM and DOC. In addition to a possible need to account for the iron content of the water, water residence time would help account for photobleaching of CDOM [66], the CDOM spectral slope (S) would help define the quality or structural nature of CDOM [67, 68], and various climatic and landscape metrics [69, 70] may account for DOC loadings to lakes.

3 Current and Upcoming Remote Sensing Systems for Regional Water Quality Assessment

A large number of airborne and space-borne sensors are potentially available for remote sensing of water resources (Table 1), but none is ideally suited for monitoring inland waters, especially regarding our primary interest for this chapter—water quality assessments of all lakes (above some nominal size) at regional scales. Systems that are expensive, need to be tasked to collect specific imagery, cover only small areas, or have coarse spatial resolution may be suitable for special projects but not for routine synoptic lake monitoring. Moreover, sensors with only a few broad bands do not provide reflectance data useful for accurate retrieval of water quality measures like chlorophyll across a broad range of water quality conditions, i.e., for optically complex inland waters. Characteristics of systems suitable for regional aquatic assessments include spatial resolution appropriate for lakes > 4 ha (i.e., spatial resolution or pixel size of 5–50 m^2), regular collection of imagery

Table 1 Potential space-borne sensors for remote sensing of water resources

		Resolution						
Satellite/ sensor	Period of operation	Spatial (m)	Spectral (no. bands) (Vis/RE/ NIR/SWIR/TIR)[a] (no.)	Radiometric (bits)	Temporal (days)	Swath width (km)	Image cost ($)	Limitations
Landsat class								
Landsat 5	1984–2012	30/120	3/0/1/2/1 (7)	8	16	180	Free	Spectral, temporal
Landsat 7	1999–present	30/60	3/0/1/2/1 (7)	8	16	180	Free	Spectral, temporal
Landsat 8	2013–present	30/100	4/0/1/2/2 (10)	12	16	180	Free	Spectral, temporal
Spot-5	2002–present	10/20	3/0/1/0/0 (4)	8	26 nadir, 2–3	60	$	Spectral, cost
Spot-6	2012–present	6	3/0/1/0/0 (4)	12	26 nadir, 2	60	$$	Spectral, cost
Spot-7	2014–present	6	3/0/1/0/0 (4)	12	26 nadir, 2	60	$$	Spectral, cost
RapidEye	2008–present	5	3/1/1/0/0 (5)	12	5.5 nadir, 1	77	$	Spectral, cost
High resolution								
IKONOS	1999–present	3.2	3/0/1/0/0 (4)	11	3.5	11.3	$$	Spectral, cost
QuickBird	2001–present	2.44	3/0/1/0/0 (4)	11	3	16.5	$$	Spectral, cost
GeoEye-1	2008–present	1.65	3/0/1/0/0 (4)	11	26 nadir, 4–5	15.2	$$	Spectral, cost
WorldView-2	2009–present	1.85	5/1/2/0/0 (8)	11	1.1 off nadir	16.4	$$$	Cost, swath
WorldView-3	2014–present	1.24/ 3.7/30	9/1/5/13/0 (28)	11	4.5 off nadir	66 (5 strips)	$$$$	Cost

(continued)

Table 1 (continued)

		Resolution						
Satellite/ sensor	Period of operation	Spatial (m)	Spectral (no. bands) (Vis/RE/ NIR/SWIR/TIR)[a] (no.)	Radiometric (bits)	Temporal (days)	Swath width (km)	Image cost ($)	Limitations
Oceanographic								
CZCS	1978–1986	825	4/0/1/1/0 (6)	8	Varies	1,566	Free	Spatial, spectral
SeaWiFS	1997–2010	1,100	6/0/1/1/0 (8)	10	1	2,801	Free	Spatial, spectral
MODIS Terra	1999–present	250/ 500/ 1 km	10/0/6/14/6 (36)	12	1	2,330	Free	Spatial, spectral
MODIS Aqua	2002–present	250/ 500/ 1 km	10/0/6/14/6 (36)	12	1	2,330	Free	Spatial, spectral
Hyperspectral								
HICO	2009–present	~90	52/2/33/0/0 (87)	12	Varies	42 × 192	Free	Experimental, limited images
Hyperion	2000–present	30	34/2/43/163/0 (220)	12	Varies	7.5 × 100	Free	Experimental, limited images
Approaching ideal								
MERIS	2002–2012	300	8/1/6/0/0 (15)	12	3	1,200	Free	Spatial, no SWIR for atm corr
Sentinel-2	Planned 2015	12/20/ 60	4/1/5/3/0 (13)	12	5	290	Free	Spectral but has red edge
Sentinel-3 (OLCI)	Planned 2015	300	10/1/10/0/0 (21)	12	2.8	1,269	Free	Spatial

This is not an exhaustive list of satellite sensors that provide monitoring capabilities for aquatic resources but includes the ones that have been used most widely or show the greatest promise for future use

[a]*Vis* visible, *RE* red edge, *NIR* near infrared, *SWIR* shortwave infrared, *TIR* thermal infrared

(preferably at least weekly but every 2–3 days is better), appropriate spectral bands (discussed further below), and images that are inexpensive or available for free. As Table 1 indicates, all current sensors fail to meet one or more of these criteria. The Medium Resolution Imaging Spectrometer (MERIS) sensor on the European satellite Envisat came closest to meeting the above criteria, but it has not been operational since 2012, and its pixel size (300 m^2) limited it to moderately large lakes (> 150 ha [~370 ac]). For Minnesota, its spatial resolution provided measurements for only ~8 % of the state's lakes [1].

This situation leaves Landsat and related satellites (Table 1) as the current "default systems" for inland lake monitoring by ORS. The Landsat series was designed primarily for land features and has been hugely important for land use/land cover analyses, vegetation condition, and agricultural applications, but Landsat sensors also have been used for over 30 years to estimate some water quality variables on inland lakes [71–76]. The biggest drawback of the Landsat sensors, aside from low temporal resolution (repeat coverage every 16 days), is their limited and coarse spectral resolution (only 3–4 bands in the visible range (e.g., for Landsat 5 and 7: band 1, 450–520 nm; band 2, 520–600 nm; band 3, 630–690 nm; Landsat 8 added a new band 1, 430–450 nm, and slightly narrowed the ranges for the earlier three bands, which now are designated band 2 through band 4). As described in Sect. 2.2.5, this may hinder the accurate retrieval of data on important variables like chlorophyll in waters with complex optical properties and also limits the types of algorithms applicable to Landsat data.

A class of multispectral sensors with high spatial resolution (Table 1) could be used for more locally based regions, such as city-scale projects. This imagery can be fairly expensive, but for important areas and projects, it has the advantage of being able to monitor smaller water bodies than Landsat can. For example, Sawaya et al. [21] found that IKONOS imagery worked as well as Landsat for water clarity (SD) assessment, and a single image was able to assess the clarity of 236 lakes and ponds as small as 0.08 ha in the City of Eagan, Minnesota. In contrast, Landsat imagery was able to assess only 48 of the water bodies (minimum size of 1.5 ha). The spatial resolution of IKONOS and QuickBird images has made them particularly useful for aquatic plant surveys [21, 22]. Several high-resolution systems are now operational (Table 1), but WorldView-2 and WorldView-3 with 8 and 28 spectral bands, respectively, may be particularly useful for water quality assessments.

Launched in February 2013 with a new Operational Land Imager (OLI) sensor, Landsat 8 has several improvements over the Thematic Mapper (TM) and Enhanced Thematic Mapper (ETM+) instruments on previous Landsat satellites. The OLI sensor has improved signal-to-noise ratio, radiometric resolution (12-bit vs. 8-bit for Landsat 5 and 7), and two new spectral bands—a shorter wavelength blue band (see above) and a shortwave infrared band positioned to detect cirrus clouds. These advancements should improve the ability to map variables like water clarity and CDOM but may not improve the discrimination of chlorophyll from SS_{min}. Landsat 7 launched in 1999 continues to collect imagery and can be used for water clarity assessments.

US government agencies have made significant investments in systems like the Coastal Zone Color Scanner (CZCS), Sea-viewing Wide Field-of-view Sensor

(SeaWiFS), and MODIS, to monitor oceans and coastal areas. Each sensor yielded advances in sensor technology, and as noted earlier, they provide useful information on chlorophyll and other optically related variables using analytical and semi-analytical algorithms. Their spatial resolutions, however, are suitable only for large lakes (> 900, 1,100, and 400 ha, respectively). MODIS has been used effectively for water quality studies on some of the Laurentian Great Lakes [77, 78]. Another important problem regarding inland lake applications of these sensors is that their spectral bands were designed for marine waters. They lack a critically important red-edge band needed for most inland water studies.

The next advancement for remote sensing of regional water quality of lakes will come from the European Space Agency (ESA) Sentinel-2 satellites, which at the time of this writing are scheduled for launch in April 2015 (Sentinel-2A) and approximately one year later for Sentinel-2B. Although these satellites were designed primarily for land observations, their improved spatial resolution (10, 20, and 60 m), spectral bands (narrower green and red, red edge, and 3 NIR bands), and temporal coverage (every 3–5 days) will greatly enhance the capabilities to assess optically related water quality characteristics (e.g., chlorophyll, CDOM, SS_{min}) in inland lakes. Landsat 8 and Sentinel-2 have specific SWIR bands selected for atmospheric corrections and cloud screening that will greatly enhance their use for routine monitoring.

An example of water quality maps for chlorophyll *a* and CDOM created from Sentinel-2 bands is shown in Fig. 5 for the SLRE. In this case, the band information

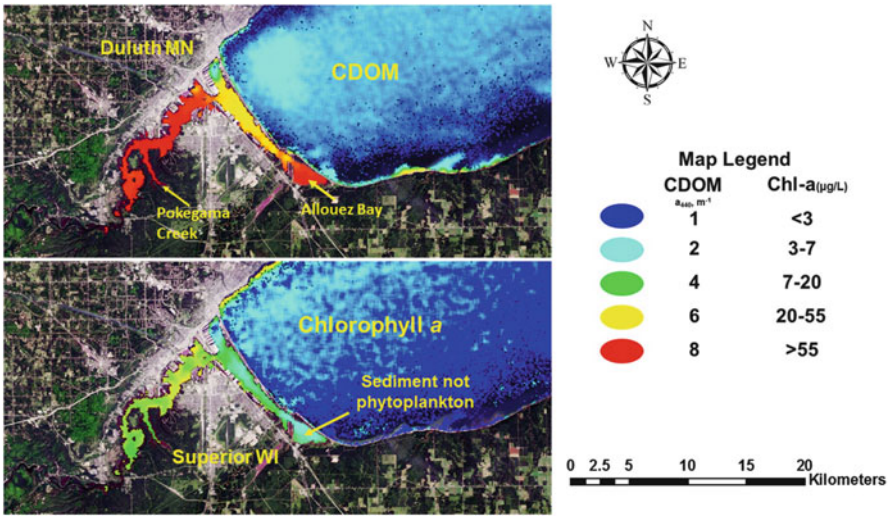

Fig. 5 CDOM and chlorophyll *a* maps for the St. Louis River Estuary at west end of Lake Superior created from an Aug. 31, 2013, HICO image using simulated Sentinel-2 bands. Spectral characteristics of Sentinel-2 sensor allow discrimination of phytoplankton from SS_{min} in optically complex waters. The SS_{min} dominated waters of Pokegama Creek and Allouez Bay are classified correctly as having low chlorophyll *a* and high CDOM. Models were developed using data from the St. Louis River Estuary and Lake Superior. Background imagery: Aug 31, 2013, Landsat 8 image

was simulated from imagery obtained by the Hyperspectral Imager for the Coastal Ocean (HICO) on the International Space Station. The spectral characteristics of the simulated Sentinel-2 imagery allowed for accurate measurements of chlorophyll in optically complex waters in contrast to the limitations encountered with Landsat 8 bands (Fig. 3; see Sect. 2.2.5) which misrepresented SS_{min} as chlorophyll *a*.

3.1 Empirical and Semi-analytical Approaches to Lake Water Quality Assessment

The algorithms used to retrieve water quality data for inland waters from satellite imagery are empirical to semi-analytical. Empirical algorithms statistically model relationships between measured water quality variables and spectral bands and/or combinations of spectral bands. Strictly empirical algorithms require no understanding of the physics required to model atmospheric and underwater optical properties. Thus, they are relatively simple to perform and are well represented in the literature. This approach is also where many have "oversold" what can be sensed with remote sensing (i.e., when imagery is used for measurements of variables that have no optical properties, such as phosphorus, DOC, or bacteria [23, 24, 79, 80]).

A better approach involves semi-empirical methods, which use bands that are selected based on knowledge of how optically active parameters affect reflectance in various spectral bands. Once such models are identified, they can be applied and used for routine monitoring, as has been done for water clarity assessments of over 20,000 lakes in Minnesota [32], Wisconsin [81], and Michigan [82, 83]. These assessments used field data within a few days of the Landsat image acquisition to calibrate models using the ratio of the Landsat TM1/TM3 bands plus band TM1 as predictor variables. Matthews [35] recently provided a thorough review of the literature on empirical and semi-empirical methods using ORS to measure inland water quality, and that paper should be accessed for further details.

Theoretically, once systemic and atmospheric correction is accurately applied to imagery allowing for a true water-leaving reflectance product, universal algorithms could be developed for specific sensors and water quality variables, which would reduce the need for contemporaneous field data. Unfortunately, accurate atmospheric correction for inland water quality is difficult on a regional basis and needs further development to be operational [1, 84].

Analytical methods are theoretically derived and use complex approaches such as radiative transfer or bio-optical modeling, and semi-analytical methods use analytical techniques that are empirically parameterized with in situ data. Semi-analytical methods to estimate water quality variables are thought by some to be the pathway to global water quality products using ORS [84]. However, many challenges remain with parameterization of the algorithms, and at present there are no successful validated regional assessments using semi-analytical methods in the

literature. Semi-analytical methods are typically region specific and applied to one lake or a few lakes. They require ground-based measurements of the IOPs of each lake for proper model calibration. More recent "adaptable" inversion algorithms [59, 85] are more robust and have the potential to be able to be applied for regional assessments of hundreds to thousands of lakes [84].

4 Regional Lake Water Quality Assessment: Case Studies

4.1 Water Quality of Inland Lakes

Early studies using Landsat imagery for water quality assessment were largely exploratory and involved only one or a few lakes [71–76]. An exception is the work of Martin et al. [86], who used semiautomated procedures to assess the trophic status of around 3,000 lakes in Wisconsin using Landsat Multispectral Scanner (MSS) imagery. The first regional assessment using Landsat TM imagery was completed in the Twin Cities Metropolitan Area (Minnesota, USA) on the water clarity of over 500 lakes [87]. Kloiber et al. [31, 88] followed with a temporal assessment and statistical analysis of SD in those same lakes for the 1973 to 1998 period. A decrease in imagery costs corresponding with the launch of Landsat 7 in April 1999, and the establishment of a NASA-funded Upper Midwest Regional Earth Science Applications Center (RESAC) also in 1999, allowed for statewide SD assessments for Minnesota, Wisconsin, and Michigan by the University of Minnesota, University of Wisconsin-Madison, and Michigan State University.

After RESAC funding ended in 2003, Olmanson et al. [32] continued the remote sensing for SD in Minnesota over eight periods from 1975 to 2008. A statistical analysis of the spatial and temporal trends was recently published [89] (see Sect. 4.2). Minnesota lake water clarity data can be accessed in the Lake Browser [90].

The Wisconsin Department of Natural Resources also continued statewide Landsat water clarity assessments on approximately 8,000 Wisconsin lakes annually [81]. All available clear late summer images are being processed for water clarity assessment on an interannual basis (S. Greb, Wisconsin Department of Natural Resources, personal communication, 2014). Wisconsin lake water clarity data can be accessed in the Lakes and AIS Mapping Tool [91].

Since the original water clarity assessment of Michigan lakes in 2002 [82], the United States Geological Survey (USGS) has continued statewide water clarity assessments for ~3,000 lakes. The 2003–2005 and 2007–2008 assessments were documented by Fuller et al. [83]. Since then, the USGS has conducted annual assessments of water clarity in Michigan with 2009–2010 and 2011 completed and 2013–2014 and 2000 assessments underway. Michigan water clarity data can be accessed in the Michigan Lake Water Clarity Interactive Map Viewer [92].

In Maine, McCullough et al. [93] combined watershed characteristics with Landsat data to assess the water clarity of ~1,500 lakes. This approach was also used to investigate temporal trends in water clarity [94], which found that water clarity declined in Maine's lakes during the 1995–2010 period.

4.1.1 Remote Sensing of Great Lakes Water Clarity

The Great Lakes are a good example of water resources for which remote sensing has been used to compensate for the paucity of in situ data. Binding et al. [95] showed the advantage of remote sensing over ground-based monitoring with substantial increase in spatial and temporal coverage. Results using CZCS for the 1979–1985 period and the SeaWiFS for the 1998–2006 period showed seasonal and interannual variability in SD due to phytoplankton blooms, resuspension of bottom sediments, and whiting events. The satellite observations document how long-term impacts can be monitored. The findings indicate that the reduction of nutrient loading and particulate removal by the introduction of zebra mussels through filter feeding significantly changed water clarity for Lake Erie and Lake Ontario. For Lake Erie, SD increased in the eastern basin but decreased in the western basin. SD in Lake Ontario more than doubled to > 4 m after the introduction of zebra mussels. The study also indicated a reduction in the frequency and intensity of whiting events due to the effects of calcium uptake by increased mussel populations.

4.2 Geospatial and Temporal Analysis of Minnesota's 10,000 Lakes

Landsat imagery provides a reliable method to obtain comprehensive spatial and temporal coverage of an important water quality variable, water clarity. Traditional ground-based monitoring programs generally target larger recreational lakes and thus are not randomly selected. Using such data to extrapolate to the larger population could lead to biased conclusions [89]. Fortunately, the use of such data to calibrate Landsat imagery for regional assessments allows for the entire population to be studied.

In Minnesota the water clarity database for more than 10,500 lakes for time periods centered around 1985, 1990, 1995, 2000, and 2005 was analyzed statistically for spatial distributions, temporal trends, and relationships with morphometric and watershed factors that potentially affect lake clarity [89]. The analysis found that water clarity is lower in southern and southwestern Minnesota and clearer in the northern and northeastern portions of the state. Temporal trends were detected in ~11 % of the lakes with 4.6 % having improving clarity and 6.2 % decreasing clarity. Small and shallow lakes appeared to be more susceptible to decreasing clarity trends than large and deep lakes. Deep lakes generally had higher clarity

than shallow lakes overall and when grouped by watershed land cover percentages. Lakes in agriculturally dominated ecoregions in southern and western Minnesota were more susceptible to decreasing clarity than the rest of the state. Statewide water clarity remained stable from 1985 to 2005 but decreased in ecoregions where agricultural is the main land use. Water clarity decreased as agriculture and/or urban percentages increased and forested land was associated with higher water clarity.

5 Conclusions

ORS using satellite imagery can be used to measure water quality of inland, marine, and coastal waters. ORS in marine waters is well established with a large investment in several generations of increasingly sophisticated satellite sensors acquiring images with large pixel sizes that are ideal for oceanic and most coastal studies but are too coarse for most inland water bodies. With these systems sophisticated analytical and semi-analytical algorithms have been developed that retrieve chlorophyll levels from the oceans on a routine, global-scale basis.

Remote sensing scientists focusing on inland waters have had to rely on other satellites like Landsat, which have adequate spatial resolution but critical deficiencies in spectral and temporal resolution. The spectral bands used to retrieve chlorophyll levels from oceanic waters do not work in optically complex inland waters. These deficiencies have limited development of retrieval algorithms for inland water quality variables by satellite imagery mostly to empirical and semi-empirical approaches.

Therefore, use of remote sensing for regional inland water quality has progressed slowly since the launch of the first Landsat satellite in 1972. Although there have been many successful regional water quality assessments, these have largely been limited to water clarity due to the available spectral bands and/or to only very large lakes (due to the large pixel size of sensors designed to study the oceans). Landsat 8 (launched in 2013) has some significant improvements over its predecessors, but its spectral and temporal characteristics remain largely unchanged, except for a shorter wavelength blue band. The next big advancement for remote sensing of regional water quality of lakes will come from the ESA Sentinel-2 and Sentinel-3 satellites. Improvements in spectral and temporal characteristics of these satellites will allow for better characterization of chlorophyll, CDOM, and SS_{min} in optically complex waters.

For effective lake management, it is essential to have long-term water quality information on a synoptic scale. Combining Landsat and Sentinel satellite imagery will greatly improve the ability to acquire imagery when needed and should significantly improve the utility and usefulness of ORS for water resource managers. Landsat 8 and Sentinel-2 imagery can be used for the assessment of all lakes, and Sentinel-3 can be used for large lakes more often with its higher temporal resolution. Once reliable water quality products can be produced in a timely fashion

on a regional basis, their adoption and use by resource managers should increase significantly. The increased use of remote sensing will greatly improve the management of our water resources and should ultimately lead to better remote sensing systems for monitoring these important natural resources.

Acknowledgments We gratefully acknowledge the support from the University of Minnesota Agricultural Experiment Station, project MIN-042-056, and the "U-Spatial" project. P.L.B. received support from a Professional Development for Retirees grant from the University of Minnesota Office of the Vice President for Research and Retirees Association.

References

1. Olmanson LG, Brezonik PL, Bauer ME (2011) Evaluation of medium to low resolution satellite imagery for regional lake water quality assessments. Water Resour Res 47(9), W09515. doi:10.1029/2011WR011005
2. O'Reilly JE, Maritorena S, Mitchell BG, Siegel DA, Carder KL, Garver SA, Kahru M, McClain C (1998) Ocean color chlorophyll algorithms for SeaWiFS. J Geophys Res 103: 24937–24953
3. Franz BA, Bailey SW, Eplee RE, Feldman GC, Kwiatkowska E, McClain C, Meister G, Patt FS, Werdell PJ (2005) The Continuity of ocean color measurements from SeaWiFS to MODIS. In: Butler JJ (ed) Earth observing systems: X. Proceedings SPIE, vol 5882, The International Society for Optical Engineering, pp 49–60
4. Kutser T, Pierson DC, Kallio KY, Reinart A, Sobek S (2005) Mapping lake CDOM by satellite remote sensing. Remote Sens Environ 94:535–540
5. GEO (2007) Inland and nearshore coastal water quality remote sensing. In: Bauer M, Dekker A, DiGiacomo P, Greb S, Gitelson A, Herlevi A, Kutser T (eds) GEO Group on Earth Observation Workshop Final Report, 27–29 March 2007, Geneva, p 32
6. Gitelson AA, Gurlin D, Moses WJ, Barrow T (2009) A bio-optical algorithm for the remote estimation of the chlorophyll a concentration in case 2 waters. Environ Res Lett 4(4):5. doi:10.1088/1748-9326/4/4/045003
7. Moore GF, Aiken J, Lavender SJ (1999) The atmospheric correction of water colour and the quantitative retrieval of suspended particulate matter in Case II waters: application to MERIS. Int J Remote Sens 20(9):1713–1733
8. Bukata RP (2013) Retrospection and introspection on remote sensing of inland water quality: "Like Déjà Vu all over again". J Great Lakes Res 39(Suppl):2–5
9. Mobley CD (1994) Optical properties of water. In: Bass M (ed) Handbook of optics. McGraw-Hill, New York, p 1152
10. Devred E, Turpie KR, Moses W, Klemas VV, Moisan T, Babin M, Toro-Farmer G, Forget MH, Jo YH (2013) Future retrievals of water column bio-optical properties using the Hyperspectral Infrared Imager (HyspIRI). Remote Sens 5:6812–6837. doi:10.3390/rs5126812
11. Kutser T, Herlevi A, Kallio K, Arst H (2001) A hyperspectral model for interpretation of passive optical remote sensing data from turbid lakes. Sci Total Environ 268:47–58
12. Carlson RE (1977) A trophic state index for lakes. Limnol Oceanogr 22:361–369
13. Brezonik PL (1978) Effect of organic color and turbidity on Secchi disk transparency. J Fish Res Board Can 35:1410–1416
14. Preisendorfer RW (1986) Secchi disk science: visual optics of natural waters. Limnol Oceanogr 31:909–926
15. Austin RW, Petzold T (1981) The determination of the diffuse attenuation coefficient of sea water using the Coastal Zone Color Scanner. Oceanogr Space 13:239–256

16. Fichot C, Sathyendranath S, Miller WL (2008) SeaUV and SeaUVC, algorithms for the retrieval of UV/Visible diffuse attenuation coefficients from ocean colour. Remote Sens Environ 112: 1584–1602
17. Doerffer R, Schiller H (2008) MERIS lake water algorithm for BEAM ATBD, GKSS Research Center, Geesthacht, Version 1.0, 10 June 2008
18. Doerffer R, Schiller H (2008) MERIS regional, coastal and lake case 2 water project—atmospheric correction ATBD, GKSS Research Center, Geesthacht, Version 1.0, 18 May 2008
19. The European Space Agency Envisat Project (2014) Brockmann Consult: BEAM earth observation toolbox and development platform, documentation pages. http://www.brockmann-consult.de/cms/web/beam/documentation. Accessed 28 Aug 2014
20. Klemas V (2013) Remote sensing of emergent and submerged wetlands: an overview. Int J Remote Sens 34(18):6286–6320. doi:10.1080/01431161.2013.800656
21. Sawaya K, Olmanson L, Heinert N, Brezonik PL, Bauer ME (2003) Extending satellite remote sensing to local scales: land and water resource monitoring using high-resolution imagery. Remote Sens Environ 88:144–156
22. Chipman JW, Olmanson LG, Gitelson AA (2009) Remote sensing methods for lake management: a guide for resource managers and decision-makers. Developed by the North American Lake Management Society in collaboration with Dartmouth College, University of Minnesota, University of Nebraska and University of Wisconsin for the United States Environmental Protection Agency, p 132
23. Vincent RK, McKay RM, Al-Rshaidat MMD, Czajkowski K, Bridgeman T, Savino J (2005) Mapping the bacterial content of surface waters with Landsat TM data: importance for monitoring global surface sources of potable water. In: Proceedings ASPRS Pecora 16: global priorities in land remote sensing, Oct 23–27, 2005, Sioux Falls, SD, p 6
24. Torbick N, Hession S, Hagen S, Wiangwang N, Becker B, Qi J (2013) Mapping inland lake water quality across the Lower Peninsula of Michigan using Landsat TM imagery. Int J Remote Sens 34(21):7607–7624. doi:10.1080/01431161.2013.822602
25. Blue Water Satellite, Inc. (2013) White paper: total phosphorus water monitoring using satellite imagery. http://bluewatersatellite.com/resources/js/tinymce/jscripts/tiny_mce/plugins/uploaded/How%20Satellite%20Images%20Provide%20Total%20Phosphorus%20Monitoring%20White%20Paper.pdf. Accessed 28 Aug 2014
26. Bukata RP (2005) Satellite monitoring of inland and coastal water quality retrospection, introspection, future directions. CRC, Boca Raton, p 272
27. Ford TE, Colwell RR, Rose JB, Morse SS, Rogers DJ, Yates TL (2009) Using satellite images of environmental changes to predict infectious disease outbreaks. Emerg Infect Dis 15(9): 1341–1346. doi:10.3201/eid1509.081334. http://wwwnc.cdc.gov/eid/article/15/9/08-1334
28. Vertucci FA, Likens GE (1989) Spectral reflectance and water quality of Adirondack Mountain region lakes. Limnol Oceanogr 34:1656–1672
29. Brezonik PL, Olmanson LG, Finlay JC, Bauer ME (2014) Factors affecting the measurement of CDOM by remote sensing of optically complex inland waters. Remote Sens Environ 155. doi:10.1016/j.rse.2014.04.033
30. Spencer RGM, Butler KD, Aiken GD (2012) Dissolved organic carbon and chromophoric dissolved organic matter properties of rivers in the USA. J Geophys Res 117, G03001. doi:10.1029/2011JG001928
31. Kloiber SM, Brezonik PL, Olmanson LG, Bauer ME (2002) A procedure for regional lake water clarity assessment using Landsat multispectral data. Remote Sens Environ 82:38–47
32. Olmanson LG, Bauer ME, Brezonik PL (2008) A 20-year Landsat water clarity census of Minnesota's 10,000 lakes. Remote Sens Environ 112(11):4086–4097. doi:10.1016/j.rse.2007.12.013
33. Chipman JW, Lillesand TM, Schmaltz JE, Leale JE, Nordheim MJ (2004) Mapping lake water clarity with Landsat images in Wisconsin, USA. Can J Remote Sens 30:1–7

34. Gitelson A, Garbuzov G, Szilagyi F, Mittenzwey K, Karnieli A, Kaiser A (1993) Quantitative remote sensing methods for real-time monitoring of inland waters quality. Int J Remote Sens 14:1269–1295
35. Matthews MW (2011) A current review of empirical procedures of remote sensing in inland and near-coastal transitional waters. Int J Remote Sens 32:6855–6899
36. Härmä P, Vepsalainen J, Hannonen T, Pyhalahti T, Kamari J, Kallio K, Eloheimo K, Koponen S (2001) Detection of water quality using simulated satellite data and semi-empirical algorithms in Finland. Sci Total Environ 268:107–121
37. Kallio K, Kutser T, Hannonen T, Koponen S, Pulliainen J, Vepsalainen J, Pyhalahti T (2001) Retrieval of water quality from airborne imaging spectrometry of various lake types in different seasons. Sci Total Environ 268:59–77. doi:10.1016/S0048-9697(00)00685-9
38. Koponen S, Attila J, Pulliainen J, Kallio K, Pyhälahti T, Lindfors A, Rasmus K, Hallikainen M (2007) A case study of airborne and satellite remote sensing of a spring bloom event in the Gulf of Finland. Cont Shelf Res 27:228–244. doi:10.1016/j.csr.2006.10.006
39. Senay GB, Shafique NA, Autrey BC, Fulk F, Cormier SM (2001) The selection of narrow wavebands for optimizing water quality monitoring on the Great Miami River, Ohio using hyperspectral remote sensor data. J Spatial Hydrol 1:1–22
40. Shafique NA, Autrey BC, Fulk FA, Flotemersch JE (2003) Hyperspectral remote sensing of water quality parameters for large rivers in the Ohio River Basin. In: First interagency conference on research in the watersheds, Benson, Arizona, October 27–30, 2003. USDA Agricultural Research Service, Washington DC
41. Ammenberg P, Flink P, Lindell T, Pierson D, Strombeck N (2002) Bio-optical modelling combined with remote sensing to assess water quality. Int J Remote Sens 23(8):1621–1638. doi:10.1080/01431160110071860
42. Olmanson LG, Brezonik PL, Bauer ME (2013) Airborne hyperspectral remote sensing to assess spatial distribution of water quality characteristics in large rivers: the Mississippi River and its tributaries in Minnesota. Remote Sens Environ 130:254–265
43. Morel A, Prieur L (1977) Analysis of variations in ocean color. Limnol Oceanogr 22:709–722
44. Gitelson A (1992) The peak near 700 nm on reflectance spectra of algae and water: relationships of its magnitude and position with chlorophyll concentration. Int J Remote Sens 13(17): 3367–3373
45. Moses WJ, Gitelson AA, Perk RL, Gurlin D, Rundquist DC, Leavitt BC, Barrow TM, Brakhage P (2011) Estimation of chlorophyll-a concentration in turbid productive waters using airborne hyperspectral data. Water Res 46(4):993–1004. doi:10.1016/j.watres.2011.11.068
46. Duan HT, Zhang YZ, Zhan B, Song KS, Wang ZM (2007) Assessment of chlorophyll-a concentration and trophic state for Lake Chagan using Landsat TM and field spectral data. Environ Monit Assess 129:295–308. doi:10.1007/s10661-006-9362-y
47. Gons HJ (1999) Optical teledetection of chlorophyll a in turbid inland waters. Environ Sci Tech 33:1127–1132. doi:10.1021/es9809657
48. Mittenzwey K, Gitelson A, Ullrich S, Kondratiev K (1992) Determination of chlorophyll a of inland waters on the basis of spectral reflectance. Limnol Oceanogr 37:147–149
49. Menken K, Brezonik PL, Bauer ME (2006) Influence of chlorophyll and humic color on reflectance spectra of lakes: implications for measurement of lake-water properties by remote sensing. Lake Reserv Manag 22(3):179–190
50. Moses WJ, Gitelson AA, Berdnikov S, Povazhnyy V (2009) Satellite estimation of chlorophyll-a concentration using the red and NIR bands of MERIS—the Azov Sea case study. IEEE Geosci Remote Sens Lett 6:845–849. doi:10.1109/LGRS.2009.2026657
51. Minnesota Department of Natural Resources (2014) LakeFinder. http://www.dnr.state.mn.us/lakefind/index.html. Accessed 28 Aug 2014
52. Schalles J, Yacobi Y (2000) Remote detection and seasonal patterns of phycocyanin, carotenoid and chlorophyll pigments in eutrophic waters. Archives Hydrobiology, special issues. Adv Limnol 55:153–168

53. Randolph KL, Wilson J, Tedesco L, Li L, Pascual L, Soyeux E (2008) Hyperspectral remote sensing of cyanobacteria in turbid productive water using optically active pigments, chlorophyll a and phycocyanin. Remote Sens Environ 112:4009–4019
54. Vincent RK, Qin X, McKay RM, Miner J, Czajkowski K, Savino J, Bridgeman T (2004) Phycocyanin detection from Landsat TM data for mapping cyanobacterial blooms in Lake Erie. Remote Sens Environ 89(3):381–392
55. Wynne TT, Tomlinson MC, Warner RA, Tester PA, Dyble J, Fahnensteil GL (2008) Relating spectral shape to cyanobacterial blooms in the Laurentian Great Lakes. Int J Remote Sens 29: 3665–3672
56. Wynne TT, Stumpf RP, Tomlinson MC, Dybleb J (2010) Characterizing a cyanobacterial bloom in western Lake Erie using satellite imagery and meteorological data. Limnol Oceanogr 55:2025–2036
57. Wynne TT, Stumpf RP, Tomlinson MC, Fahnenstiel GL, Dybleb J, Schwab DJ, Joseph-Joshi S (2013) Evolution of a cyanobacteria bloom forecast system in western Lake Erie: development and initial evaluation. J Great Lakes Res 39:90–99. doi:10.1016/j.jgir.2012.10.003
58. Lunetta RS, Schaeffer BA, Stumpf RP, Keith D, Jacobs SA, Murphy MS (2014) Evaluation of cyanobacteria cell count detection derived from MERIS imagery across the eastern USA. Remote Sens Environ. doi:10.1016/j.rse.2014.06.008
59. Brando VE, Dekker AG, Park YJ, Schroeder T (2012) Adaptive semianalytical inversion of ocean color radiometry in optically complex waters. Appl Optics 51:2808–2833
60. Carder KL, Chen FR, Lee ZP, Hawes SK, Kamykowski D (1999) Semianalytic moderate-resolution imaging spectrometer algorithms for chlorophyll a and absorption with bio-optical domains based on nitrate-depletion temperatures. J Geophys Res Oceans 104:5403–5421
61. Hoge FE, Lyon PE (1996) Satellite retrieval of inherent optical properties by linear matrix inversion of oceanic radiance models: an analysis of model and radiance measurement errors. J Geophys Res Oceans 101:16631–16648
62. Zhu W, Yu Q, Tian YQ, Chen RF, Gardner GB (2011) Estimation of chromophoric dissolved organic matter in the Mississippi and Atchafalaya river plume regions using above-surface hyperspectral remote sensing. J Geophys Res 116, C02011. doi:10.1029/2010JC006523
63. Ficek D, Zapadka T, Dera J (2011) Remote sensing reflectance of Pomeranian lakes and the Baltic. Oceanologia 53:959–970
64. Xiao YH, Sara-Aho T, Hartikainen H, Vähätalo AV (2013) Contribution of ferric iron to light absorption by chromophoric dissolved organic matter. Limnol Oceanogr 58:653–662
65. Köhler SJ, Kothawala D, Futter MN, Liungman O, Tranvik L (2013) In-lake processes offset increased terrestrial inputs of dissolved organic carbon and color to lakes. PLoS ONE 8(8): e70598. http://dx.doi.org/10.1371/J.pone.0070598
66. Müller RA, Futter MN, Sobek S, Nisell J, Bishop K, Weyhenmeyer GA (2013) Water renewal along the aquatic continuum offsets cumulative retention by lakes: implications for the character of organic carbon in boreal lakes. Aquat Sci 75:535–545
67. Helms JR, Stubbins A, Ritchie JD, Minor EC, Kieber DJ, Mopper K (2008) Absorption spectral slopes and slope ratios as indicators of molecular weight, source, and photobleaching of chromophoric dissolved organic matter. Limnol Oceanogr 53:955–969
68. Williamson CE, Brentrup JA, Zhang J, Renwick WH, Hargreaves BR, Knoll LB, Overholt EP, Rose KC (2014) Lakes as sensors in the landscape: optical metrics as scalable sentinel responses to climate change. Limnol Oceanogr 59:840–850
69. Pace ML, Cole JJ (2002) Synchronous variation of dissolved organic carbon and color in lakes. Limnol Oceanogr 47:333–342
70. Sobek S, Tranvik LJ, Prairie YT, Kortelainen P, Cole JJ (2007) Patterns and regulation of dissolved organic carbon: an analysis of 7,500 widely distributed lakes. Limnol Oceanogr 52: 1208–1219
71. Brown D, Warwick R, Skaggs R (1977) Lake condition in east central Minnesota. Minnesota Land Management Information System Report 5022. Center for Urban and Regional Affairs, University of Minnesota, Minneapolis

72. Dekker AG, Peters SWM (1993) The use of the thematic mapper for the analysis of eutrophic lakes—a case-study in the Netherlands. Int J Remote Sens 14(5):799–821
73. Lathrop RG (1992) Landsat Thematic Mapper monitoring of turbid inland water quality. Photogramm Eng Remote Sens 58:465–470
74. Lathrop RG, Lillesand TM, Yandell BS (1991) Testing the utility of simple multidate Thematic Mapper calibration algorithms for monitoring turbid inland waters. Int J Remote Sens 12: 2045–2063
75. Lillesand TM, Johnson WL, Deuell RL, Lindstrom OM, Meisner DE (1983) Use of Landsat data to predict the trophic state of Minnesota lakes. Photogramm Eng Remote Sens 49: 219–229
76. Ritchie JC, Cooper CM, Schiebe FR (1990) The relationship of MSS and TM digital data with suspended sediments, chlorophyll and temperature in Moon Lake, Mississippi. Remote Sens Environ 33:137–148
77. Shuchman R, Leshkevich G, Hat C, Pozdnyakov D, Korosov A (2008) Development of a robust hydro-optical model for the Great Lakes for the extraction of chlorophyll, dissolved organic carbon and suspended minerals from MODIS satellite data. In: IAGLR 51st Annual Conference on Great Lakes Research, 19–23 May 2008, Petersborough, ON
78. Grimm A (2013) Satellite Remote Sensing-Based Coastal and Nearshore Monitoring Research at MTRI. Michigan Tech Research Institute, Michigan Technological University. http://glc.org/files/projects/lmmcc/lmmcc-20130418-Grimm-lmmccnemo1.pdf. Accessed 28 Aug 2014
79. Rogers RH (1975) Application of Landsat to the surveillance and control of lake eutrophication in the Great Lakes Basin. Type II Report for the Period of August 11 through November 11, 1975, Prepared for Goddard Space Flight Center, p 55
80. McKeon JB Rogers RH (1976) Water quality map of Saginaw Bay from computer processing of Landsat-2 data. Special Report Prepared for Goddard Space Flight Center, p 6
81. Greb SR, Martin AA, Chipman JW (2009) Water Clarity Monitoring of Lakes in Wisconsin, USA using Landsat. In: Proceeding of 33rd International Symposium of Remote Sensing of the Environment, 4–8 May 2009, Stresa
82. Fuller LM, Aichele SS, Minnerick RJ (2004) Predicting water quality by relating Secchi-disk transparency and chlorophyll a measurements to Satellite Imagery for Michigan Inland Lakes, August 2002: U.S. Geological Survey Scientific Investigations Report 2004–5086
83. Fuller LM, Jodoin RS, Minnerick RJ (2011) Predicting lake trophic state by relating Secchi-disk transparency measurements to Landsat-satellite imagery for Michigan inland lakes, 2003–05 and 2007–08: U.S. Geological Survey Scientific Investigations Report 2011–5007, p 36
84. Malthus TJ, Hestir EL, Dekker AG, Brando VE (2012) The case for a global inland water quality product. In: Proceedings, IEEE International Geoscience and Remote Sensing Symposium (IGARSS), 22–27 July 2012, 5234–5237. doi:10.1109/IGARSS.2012.6352429
85. Campbell G, Phinn SR, Dekker AG, Brando VE (2011) Remote sensing of water quality in an Australian tropical freshwater impoundment using matrix inversion and MERIS image. Remote Sens Environ 115:2403–2414
86. Martin RH, Boebel EO, Dunst RC, Williams OD, Olsen MV, Merideth RW Jr, Scarpace FL (1983) Wisconsin lakes—a trophic assessment using Landsat digital data. Wisconsin Lake Classification Survey Project, S00536601, p 294
87. Olmanson LG (1997) Satellite remote sensing of the trophic state conditions of lakes in the Twin Cities Metropolitan Area. University of Minnesota, St. Paul
88. Kloiber SM, Brezonik PL, Bauer ME (2002) Application of Landsat imagery to regional-scale assessments of lake clarity. Water Res 36:4330–4340
89. Olmanson LG, Brezonik PL, Bauer ME (2013) Geospatial and temporal analysis of a 20-year record of Landsat-based water clarity in Minnesota's 10,000 lakes. J Am Water Resour Assoc 50:748–761. doi:10.1111/jawr.12138
90. University of Minnesota (2011) Remote Sensing and Geospatial Analysis Laboratory. Remote Sensing of Water, Lake Browser. http://water.umn.edu/. Accessed 28 Aug 2014
91. Wisconsin Department of Natural Resources (2014) Lakes & AIS Mapping Tool. http://dnrmaps.wi.gov/SL/?Viewer=Lakes%20and%20AIS%20Viewer. Accessed 28 Aug 2014

92. U.S. Geologic Survey (2014) Michigan Water Science Center. Michigan Lake Water Clarity Interactive Map Viewer. http://miwebmapper.er.usgs.gov/cmilakesrs/. Accessed 28 Aug 2014
93. McCullough IM, Loftin CS, Sader SA (2012) Combining lake and watershed characteristics with Landsat TM data for remote estimation of regional lake clarity. Remote Sens Environ 123:109–115
94. McCullough IM, Loftin CS, Sader SA (2013) Landsat imagery reveals declining clarity of Maine's lakes during 1995–2010. Freshw Sci 32(3):741–752. doi:10.1899/12-070.1
95. Binding CE, Jerome JH, Bukata RP, Booty WG (2007) Trends in water clarity of the Lower Great Lakes from remotely sensed aquatic color. J Great Lakes Res 33:828–841. doi:10.3394/0380-1330(2007)33[828:TIWCOT]2.0.CO;2

Interactive Geospatial Analysis Tool for Estimating Watershed-Scale Consumptive Use: Potomac River Basin Case Study

Jan Ducnuigeen, Sarah N. Ahmed, Karin R. Bencala, Heidi L.N. Moltz, Andrea Nagel, and Cherie L. Schultz

Contents

Abstract Human water use around the globe continues to increase while available water supplies are threatened by contamination, climate change, and aging infrastructure. Effective management of water resources is essential to ensure that water is available when and where it is needed. A necessary first step is quantifying the

J. Ducnuigeen • S.N. Ahmed • K.R. Bencala • H.L.N. Moltz • A. Nagel • C.L. Schultz (✉)
Interstate Commission on the Potomac River Basin, Rockville, MD, USA
e-mail: cschultz@icprb.org

T. Younos, T.E. Parece (eds.), *Advances in Watershed Science and Assessment*, The Handbook of Environmental Chemistry 33,
DOI 10.1007/978-3-319-14212-8_6

amount of water needed and making this information readily available to decision-makers. Specifically, information is needed on both the total amount of water withdrawn and the portion of that water which is not returned to the source, at a spatial and temporal scale that will support management decisions. Quantifying this water loss (i.e., consumptive use) is important for gauging impacts to downstream water users and to maintaining functioning ecosystems. This effort can be challenging in large basins where water use data may be collected in various formats by numerous agencies utilizing different metrics. The objective of this chapter is to present a case study model developed for the Potomac River Basin in the United States. The model consists of a basin-wide analysis and mapping tool that incorporates monthly water use data from multiple political jurisdictions, estimates consumptive water use, displays raw and summary information in an interactive geospatial format, and shares information with stakeholders via an interactive web-based mapping tool. The developed tool is expected to assist in long-term local, state, and basin-wide comprehensive water resources planning; real-time drought management; and a better understanding of human impacts on water resources.

Keywords Consumptive use • Geospatial tool • Open source • Return flow • Water planning • Water use • Web-based mapping

1 Introduction

There are heightened concerns about water availability in many parts of the world in the face of population growth and changes in the global climate [1]. Approximately 20 % of the world's population deal with water shortages and another 25 % do not have sufficient supplies due to a lack of infrastructure [2]. As a result, tensions may arise between groups of water users with competing interests. Concurrently, human water withdrawals alter natural hydrology to a degree that causes adverse impacts on the health of aquatic communities [3, 4]. In the world's major river and lake systems, watersheds often span multiple governmental jurisdictions and include large and diverse groups of users and ecosystems dependent on adequate water supplies.

To balance a diverse array of needs, a collaborative approach can be an effective means for developing a water resources management plan [5–7]. Such an approach requires that stakeholders have confidence in the scientific methods used to formulate the plan and in the data upon which analyses are based [8]. In systems where water scarcity, actual or potential, is an issue, data on water use for human purposes is a key piece of information. Who is withdrawing water, in what quantity, and where? How much of a given water withdrawal is later returned to the system, and where is it returned? How have water withdrawals and return flows changed over time, and how are they projected to change in the future?

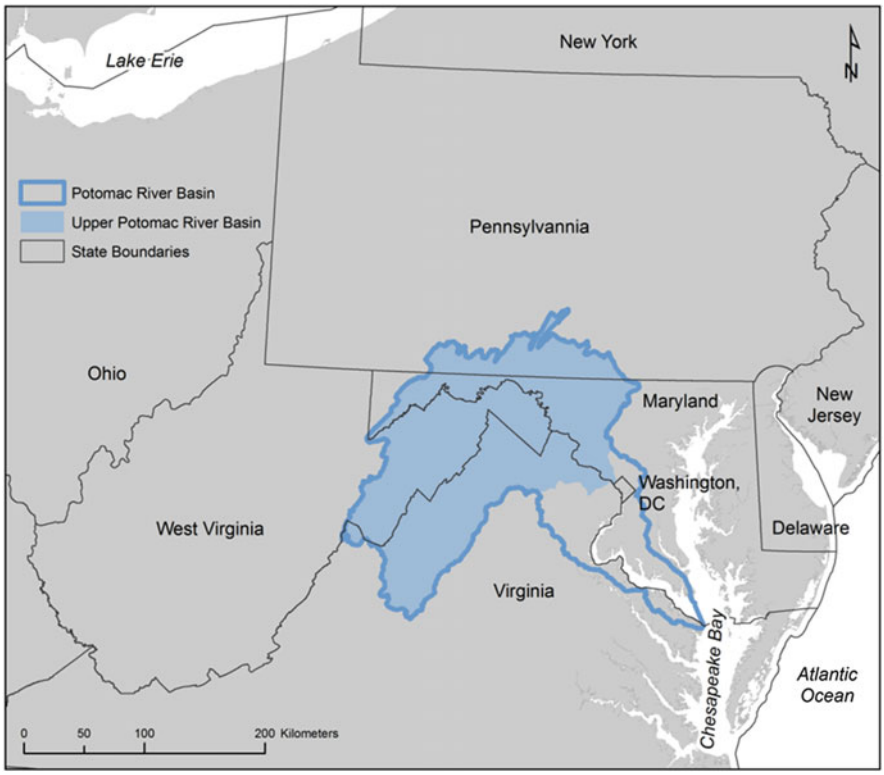

Fig. 1 Location of the Potomac River Basin and upper Potomac River Basin. *Sources*: Sub--basins—USDA/NRCS; river segments—Chesapeake Bay Program; rivers—USEPA/USGS; coastline—NOAA; state boundaries—US Census

Until recently, water use studies across the United States, and around the world, have been done at relatively coarse spatial and temporal resolutions, primarily because of data limitations. Temporal resolution has typically been annual or decadal, and spatial resolution has been generally at the national scale for global studies [9] and at the county or state scale for US studies [10]. However, water use analyses at finer scales are desirable because of the high variability of water availability in most regions [11, 12].

The Potomac River Basin (Fig. 1) spans multiple governmental (state) jurisdictions that include the states of Maryland, Pennsylvania, Virginia, and West Virginia and the District of Columbia (Washington, DC). Considering these complex and politically challenging environmental and water resource issues, stakeholders often rely on the Interstate Commission on the Potomac River Basin (ICPRB) to facilitate dialog and provide input on possible solutions. The question of how to gauge current and potential future impacts of consumptive use, i.e., net water withdrawals, at the watershed and sub-watershed levels has long challenged resource managers

in the basin. To support collaborative planning, ICPRB is developing an interactive, web-based geospatial–temporal water use analysis and mapping tool for the drainage area of the freshwater portion of the river, referred to in this study as the upper Potomac River Basin.

The objective of this chapter is to describe tools that will enable water resource managers to gather multiple governmental (state) jurisdictions' water withdrawal data, estimate watershed-scale consumptive use of water, and make the information available to water resource managers and stakeholders via an interactive web-based mapping tool.

2 Project Scope and Objective

2.1 Study Area

The Potomac River is the primary source of water for the Washington, DC, metropolitan area; the river and its tributaries supply many of the rapidly growing upstream communities. The region faces continuing population growth and potential changes in water availability from climate change [13–15]. Flow in the river is seasonal, typically dropping to its lowest levels of the year in summer and early fall. The river usually meets water supply and environmental needs. But over the past century, droughts have occurred which reduced the river's natural flow to levels that would not meet today's demands or those anticipated in the future.

The headwater streams of the Potomac River originate in Maryland, Pennsylvania, Virginia, and West Virginia. The freshwater portion of the river extends to the head of tide, located a few kilometers below Little Falls dam near Washington, DC. The drainage area for the upper Potomac River Basin, the nontidal portion (Fig. 1), is 29,950 square kilometers (km^2). Figure 2 shows major tributaries and sub-basins for the upper Potomac River Basin. The Potomac River flows past Washington, DC, through the Potomac Estuary and into the Chesapeake Bay, an ecologically rich and economically productive estuary on the eastern coast of the United States.

The Washington, DC, metropolitan area has a cooperative system of water supply management designed to assure adequate water supplies during drought. This system is governed by a set of agreements entered into by the region's major water suppliers in the early 1980s and includes shared storage facilities and coordinated operations during periods of low flows. It has served the metropolitan area well over the past 30 years, successfully meeting demands and environmental flow requirements during the two moderate droughts in 1999 and 2002. However, recent demand and water availability forecasts indicate that significant changes to this system will be needed by the end of the next 30-year planning horizon, 2040, because of anticipated growth in metropolitan area water demand and upstream consumptive use of water.

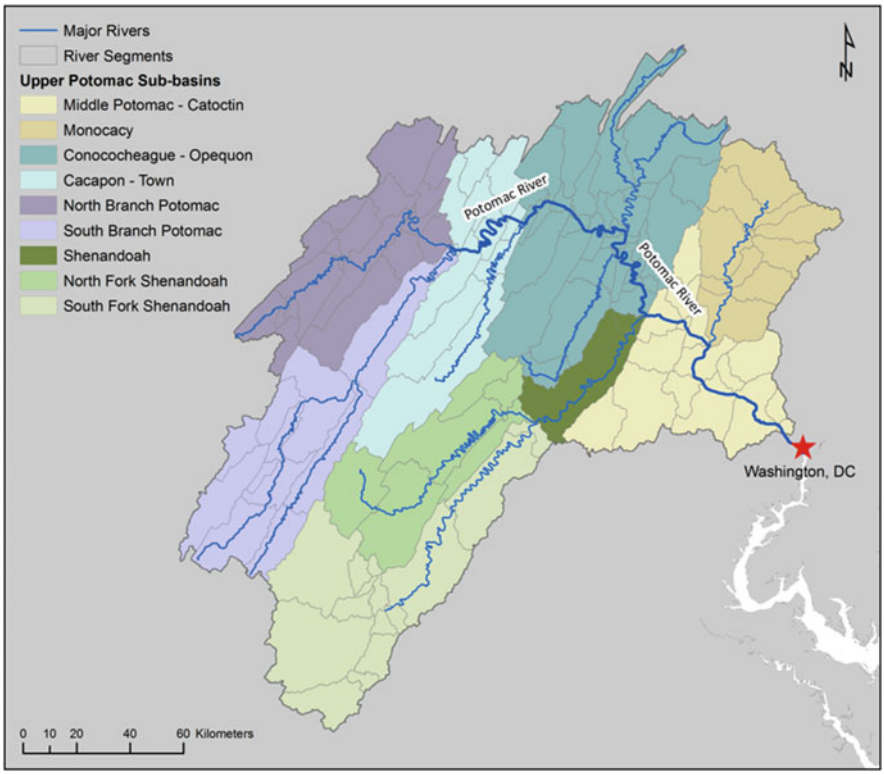

Fig. 2 Map of upper Potomac River Basin, showing sub-basins, river segments, and major rivers. *Sources*: Sub-basins—USDA/NRCS; river segments—Chesapeake Bay Program; rivers—USEPA/USGS; coastline—NOAA; state boundaries—US Census

Many small and mid-sized communities in the Potomac River Basin found their water supplies strained during the droughts of 1999 and 2002. This prompted new water supply planning initiatives in all four states within the basin. At the same time, studies are conducted throughout the basin to determine the relationship between stream flows and aquatic health and to develop environmental flow thresholds to inform water withdrawal permit decisions [16–18]. Such environmental flow thresholds could limit the amount of water available to public water suppliers and other users during low flow conditions. The renewed focus on water supply and stream flows in the basin by the four states, metropolitan area suppliers, upstream jurisdictions, and environmental organizations has prompted the ICPRB to propose a basin-wide approach to water supply management as an integral part of a new comprehensive water resources plan for the basin [19].

An important component of the data support necessary for this effort is information on water use. The states' new water supply planning initiatives have significantly increased the amount of available water use data in the basin. Though Maryland and Virginia have had water withdrawal data collection programs in

place since the 1980s, all four basin states now have reporting requirements for users whose withdrawals exceed specified thresholds.

2.2 Objective

The objective of the ICPRB project is to develop a comprehensive, flexible, and transparent analysis and mapping tool for water withdrawals and consumptive use in the upper Potomac River Basin to ultimately facilitate collaborative water resources planning in the region. The tool is being designed to support development of a basin-wide water supply management strategy, including existing water supply planning efforts. It will provide a long-term time series of monthly water use data and allow for analyses of seasonality and inter-annual variability as well as trends. The tool will make data, at the watershed scale, easily accessible to water managers in all basin states. It will also provide information on consumptive use in the upper Potomac Basin from 1985 to the present, in a monthly time step at the small watershed scale. The project comprises three components: (1) a relational database containing a compilation of available monthly water withdrawal data from basin states, supplemented by 5-year datasets of annual withdrawals aggregated to the county level by the US Geological Survey (USGS); (2) a Water Balance Conveyance Model which computes consumptive use, including the effects of inter-watershed transfers of water; and (3) an interactive web-based mapping tool to readily share information. Each of these components is discussed in subsequent sections of this chapter.

Such information will help governmental agencies evaluate the impact of potential water withdrawal permitting decisions in the sub-watersheds within the basin and those that cross state boundaries. It will improve estimates of cumulative consumptive use upstream of the Washington, DC, metropolitan area water suppliers' Potomac River intakes, an important input for the area's long-term planning and operational models. The information will also assist multiple stakeholders with local, state, and basin-wide planning.

3 Methods

The major focus of this chapter is on consumptive use of water. The analysis and mapping tool described here provides estimates of consumptive water use at a spatial and temporal resolution commensurate with planning needs in the Potomac River Basin. Details of the methods are provided below.

3.1 Chesapeake Bay Program Watershed Model

The spatial units of analysis for this ICPRB project are the watershed-based "river segments" (Fig. 2) developed for the Chesapeake Bay Program (CBP) Watershed Model [20, 21]. The CBP Watershed Model, an open-source modeling tool based on the Hydrologic Simulation Program—FORTRAN (HSPF), simulates flows and concentrations of nutrients and sediment in streams flowing within the Bay watershed, which includes the Potomac River Basin. Several organizations, including ICPRB, have adopted the CBP Watershed Model as a water supply planning tool [13, 18]. The CBP Watershed Model's streamflow and pollutant concentration estimates are provided by river segment, and some model inputs, including water supply withdrawals and wastewater treatment plant discharges, are also aggregated by river segment. The delineation of the river segments is based primarily on considerations of data availability. The choice of the river segments as spatial units of analysis for our project provides a convenient interface with the CBP Watershed Model.

3.2 Water Balance Conveyance Model

To compute consumptive use for a given spatial unit, a Water Balance Conveyance Model was constructed to route water flow from raw water withdrawal points to wastewater discharge points and to track consumptive losses and return flows along the way. This model was developed specifically to address the complexities often present in public water supply and wastewater treatment systems and the interactions of public systems with self-supplied facilities or with other public systems.

The tool for consumptive use relies on withdrawal data provided by each state within the Potomac Basin. However, the states' data differ in the time period of data availability, collection methods, and categorization of water uses. One benefit of this effort is the compilation of state data into a single location that allows Potomac water use to be understood as a whole.

The developed tool incorporates three features to facilitate a collaborative planning process: transparency, flexibility, and accessibility. The interactive mapping component of the tool will promote transparency by allowing stakeholders to view and access basin-wide water use data. The underlying database incorporates a flexible design that allows the addition of site-specific water consumption data as it becomes available, and in the absence of site-specific data, relies on regional and national data. Finally, the tool is being developed using open-source database and mapping software, making it widely accessible to all stakeholders. Section 3.6 provides details of the ICPRB Water Balance Conveyance Model configuration.

3.2.1 Data Identification

The data used include monthly time series of consumptive use estimates for 1985–2012 by water use type (e.g., public water supply, commercial, industrial). This captures the seasonal variation of water use in the basin and long-term trends and allows for comparisons of water use in drought and non-drought years. Streamflow from the upper basin is measured at the USGS gauge on the Potomac River at Little Falls.

3.3 Definition of Consumptive Use

For this effort, consumptive water use is defined as the amount of water associated with a withdrawal for water supplies (domestic, industrial, and agricultural uses) from a given resource that is not returned to the same resource and is thus unavailable to other users or aquatic communities [10, 22–26]. Return flows may be less than withdrawals for a variety of reasons: losses due to evaporation or transpiration, incorporation of water into products or crops, or consumption by humans or livestock [22]. This definition of consumptive water use includes all types of "blue" water (water present in aquifers, lakes, reservoirs, and streams) but excludes "green" water (water stored in the soil or within vegetation that is ultimately evaporated and transpired) [27, 28]. The definition is limited to blue water since its use in the Potomac Basin is subject to influence by management strategies. Consumptive use from blue water sources used for irrigation is also considered in this study. By the above definition of consumptive use, a withdrawal may also be consumptive if it occurs from a given resource and its associated return flow is discharged to a different resource (often referred to as an inter-basin transfer). Thus, the specification of spatial scale is integral to the concept of consumptive use.

For an individual facility, for example, a commercial or industrial facility that withdraws, uses, and discharges (return flow) water at the same location, consumptive use can be expressed by a simple water balance equation:

$$\mathrm{CU} = W - R \tag{1a}$$

where

CU = consumptive use
W = water withdrawn
R = water returned

Equation (1a) can be used to compute the facility's consumptive use when withdrawal and discharge data are available and under the assumption that inflows and outflows due to leakage are not significant. Consumptive use results computed

using Eq. (1a) are sometimes reported in terms of consumptive use coefficients, that is, consumptive loss as a percent of total withdrawal:

$$\text{CU coefficient } (\%) = 100 \times (W - R)/W \tag{1b}$$

More generally, for a given resource of interest, for example, a lake, aquifer, or river, consumptive use is the sum of all withdrawals from the resource minus the sum of all return flows to the same resource. In this study, consumptive use is estimated for each river segment in the upper Potomac Basin, that is,

$$\text{CU}_\text{A} = \sum\nolimits_{\text{all } i \text{ where } W_i \text{ is located in A}} W_i - \sum\nolimits_{\text{all } j \text{ where } R_j \text{ is located in A}} R_j \tag{2}$$

where

CU_A = consumptive use in river segment, A
W_i = withdrawal, i
R_j = return flow, j

Because watersheds are aggregates of river segments, calculation of consumptive use by river segment from Eq. (2) allows estimates of consumptive use to be made by watershed, thus providing information on the impact of upstream withdrawals on downstream users and ecosystems.

Application of Eq. (2) is straightforward if accurate data on withdrawals and return flows are available. However, this is generally not the case at the regional scale. Withdrawal and corresponding return flow data is often lacking for individual industrial facilities and commercial establishments and is rarely available for agricultural enterprises. Return flows from public systems are comingled with rainwater and groundwater that enter the networks of pipes that collect wastewater, as described in Sect. 3.5.2. Public supply or wastewater systems may have interconnections with other public systems or with industrial systems. The approaches used to address these problems are described in the following sections.

3.4 Water Withdrawal and Return Flow Data

Water withdrawal data for this project were obtained from four states in the Potomac Basin and compiled into a single relational database. Maryland and Virginia, which comprise 56 % of the upper Potomac Basin, have relatively continuous records of monthly withdrawals by large quantity users (for Maryland, beginning in 1979, and for Virginia, beginning in 1982). Pennsylvania has continuous records beginning in 2005 and West Virginia beginning in 2003.

Water withdrawal data are reported by water use type (categories of end uses). Although the various state datasets differ in their water use categories and definitions, sufficient overlap exists to provide values of water withdrawals for the

following nine use categories: aquaculture (AQU), self-supplied commercial facilities (COM), self-supplied industrial facilities (IND), crop and nursery irrigation (IRR-C), golf course irrigation (IRR-G), livestock production (LIV), mining (MIN), thermoelectric power generation (PP), and public water supply systems (PWS).

The withdrawal data available from the states has significant data gaps over the time period of the study, 1985–2012. To fill these gaps, annual water use data compiled by the USGS are used. Starting in 1985 and every 5 years thereafter, the USGS estimates total annual water use at the county level by water use type [29]. In addition to the eight water use categories given above, the USGS data provide estimates of self-supplied domestic water use (SSD). For this study, values of average annual withdrawals from the USGS datasets are interpolated to provide time series of monthly withdrawals at the county level, and these are disaggregated by river segment and weighted by area or in some cases by land use area to obtain monthly time series of average withdrawals by water use type by river segment.

Return flow (discharge) data for wastewater treatment plants (WWTPs) in the Chesapeake Bay watershed are available from the CBP. These data include monthly flows and nutrient concentrations from municipal and county wastewater treatment facilities and certain large industrial facilities. As described below, the CBP discharge dataset is used in this study to determine the locations of the WWTPs associated with public water supply systems and to estimate site-specific consumptive use coefficients for selected large industrial facilities for which paired withdrawal and discharge data are available.

3.5 Consumptive Use Estimate Methods

This study uses a variety of methods to estimate consumptive use in the upper Potomac Basin, depending on water use type and on data availability and quality. For selected industrial and commercial facilities for which both withdrawal and discharge data are readily available, site-specific consumptive use coefficients are computed from Eq. (1b). For all other cases, consumptive use is estimated from withdrawal data and non-site-specific consumptive use coefficients: (a) for public water supply systems, consumptive use coefficients are computed from upper Potomac Basin withdrawal data using the "winter base rate" method; (b) for other use types, coefficients from the published literature are used.

The relational database used in this study has been designed to facilitate the addition of site-specific consumptive use coefficients as more data becomes available. Details of consumptive use estimate methods are provided below.

3.5.1 Published Consumptive Use Coefficients

When available data to compute site-specific consumptive use coefficients are insufficient, consumptive use is often estimated using published coefficients calculated by other studies conducted in regions with similar climates and water use patterns [30]. This approach requires water withdrawal amounts categorized by end-use type (e.g., domestic, commercial, irrigation) and the related coefficients. The accuracy of this method is limited since the coefficients were originally calculated for a specific set of use categories and are then applied uniformly throughout the study area. Nonetheless, use of published coefficients does provide estimates for planning purposes that would not otherwise be available.

For non-PWS use types, this study incorporates calculated consumptive use coefficients available for three states in the Great Lakes region of the United States, i.e., Indiana, Ohio, and Wisconsin [22]. This is the largest scale study conducted to date in the United States that provides consumptive use coefficients at monthly time scale. Shaffer [22] compiled available monthly withdrawal and return flow data for water users in Ohio and withdrawal data for Indiana and Wisconsin for the years 1999–2004. Shaffer computed monthly and annual consumptive use coefficients using the water balance equation, Eq. (1b), for the Ohio water users that provided both withdrawal and return flow data. The dataset included 196 commercial records, 471 industrial records, 289 thermoelectric power records, 59 golf course records, 20 crop and 42 nursery irrigation user records, 18 livestock records, 33 aquaculture records, and 418 mining site records, where the number of records refers to a facility and year in which both monthly withdrawal and return flow data were available. This ICPRB study applies Shaffer's monthly coefficients to withdrawal time series that do not have site-specific consumptive use coefficients in the following use categories: AQU, COM, IND, IRR-GOLF, IRR-CROP, LIV, and PP. Because mining withdrawals in the upper Potomac Basin are primarily for dewatering purposes, consumptive use coefficients for the MIN use category are set equal to zero. Consumptive use for PWS is calculated from upper Potomac Basin data using methods described below.

3.5.2 Consumptive Use Estimates for PWS Systems

Shaffer [22] and others have noted that the simple water balance equation, expressed by Eqs. (1a) and (1b), does not provide meaningful estimates of consumptive use when used with withdrawal and discharge data from a public water supply system and associated wastewater treatment system. Municipalities and counties distribute potable water and collect wastewater via complex networks of pipes that are subject to losses and gains not typically measured and difficult to quantify. Gains and losses experienced by wastewater collection systems are particularly difficult to characterize because of the effects of inflow and infiltration (I/I). During wet weather periods, inflows from direct connections to a wastewater collection system, such as rooftop

downspouts, sump pumps, and unsealed manhole covers, or infiltration of stormwater via leaks in underground pipes, valves, and connections can cause peak flows which may be many times the typical dry weather flows [31–33]. During dry weather periods, collection systems may interact with groundwater, experiencing net infiltration or, alternatively, exfiltration [34], depending on the level of the water table in relation to the conveyance pipes. Inflow and infiltration (I/I), which is in part associated with deteriorating infrastructure, is an important and costly problem for the wastewater industry because it can cause sanitary sewer overflows that affect water quality in receiving streams. Also, any additional flow must be accounted for in the design capacity of wastewater treatment plants.

In the initial stages of this project, an effort was made to estimate the "wet weather" portion of I/I so that it could be accounted for in the estimate of PWS consumptive use from withdrawal and discharge data. Simple linear regressions demonstrated that monthly WWTP discharges from municipal facilities increase significantly with monthly precipitation. However, further analyses, using multiple regressions of monthly discharge on total monthly precipitation and on season, indicated that discharges are also strongly correlated with season. Results for two upper Potomac communities are plotted in Fig. 3. The graphs show that mean monthly discharge and estimated "dry weather discharge" both have a seasonal variation, with discharges highest in the winter months (December, January, and February) and lowest in the summer months (June, July, and August). Dry weather discharge is the estimated discharge not attributable to precipitation. In the examples shown, all model coefficients were significant at the 95 % confidence level. Note that without I/I, discharges would be expected to be relatively constant, reflective of indoor water use rates, and to be less than withdrawals, reflecting consumptive and nonconsumptive losses. The seasonal dependence evident in Fig. 3 can be attributed to the variation in dry weather infiltration/exfiltration into wastewater collection pipes due to fluctuating groundwater levels, which are significantly higher in the upper Potomac Basin in the winter than in the summer.

These analyses suggest that monthly discharge data from municipal WWTPs cannot be used to obtain estimates of consumptive use for Potomac Basin communities because water use return flows are comingled with wet weather inflows and groundwater infiltration/exfiltration. Though it might be feasible in some cases to estimate and account for the wet weather component of discharge, no procedure is currently available to estimate the effects of dry weather infiltration or exfiltration that appears to occur due to fluctuating groundwater levels.

Because municipal WWTP discharge data is not reflective of water use return flows, an alternative method for estimating consumptive use, the winter base rate (WBR) method, is often used [22, 35–38]. The method is applicable in regions with a temperate climate where it is reasonable to assume that consumptive use is primarily due to outdoor water use in non-winter months. This method does not rely on WWTP discharge data, but rather estimates consumptive use solely from monthly water withdrawal data. The winter base rate method is based on the following assumptions: (1) no significant consumptive use occurs in the winter months; and (2) the observed difference between wintertime withdrawals and

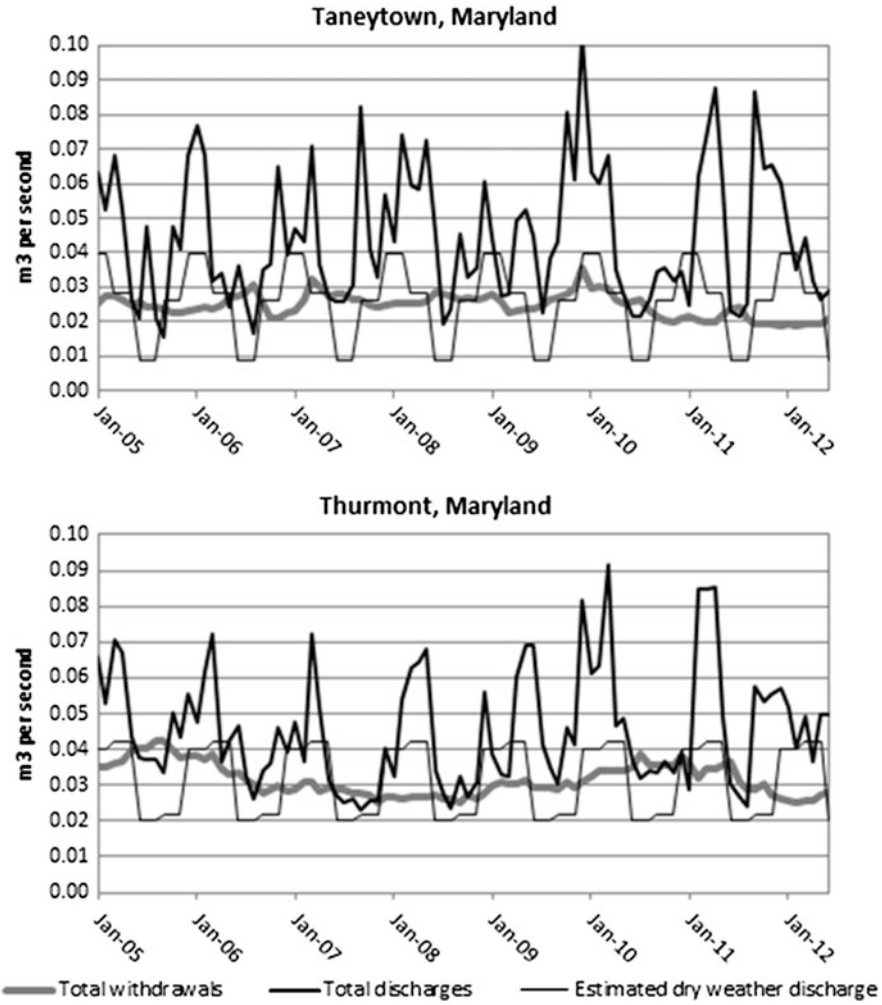

Fig. 3 Total monthly withdrawals and wastewater discharges are plotted for two small- to medium-sized communities in the upper Potomac Basin. Also plotted are dry weather discharges, estimated as the coefficients, b_1, b_2, b_3, and b_4, of the regression model, discharge $= b_1 \times x_1 + b_2 \times x_2 + b_3 \times x_3 + b_4 \times x_4 + b_5 \times$ precipitation. The x_i are binary variables which $=1$ if month is in Season i, or $=0$ otherwise

withdrawals in other months of the year is due to outdoor water use, which is completely or largely consumptive. The consumptive use coefficient from the winter base rate method is given by Eq. (3):

$$\text{CU coefficient } (\%) = (\text{monthly withdrawal} - \text{winter withdrawal})/ (\text{monthly withdrawal}) \times (\text{outdoor use CU coefficient}) \quad (3)$$

An appropriate definition of the winter withdrawal requires consideration of regional conditions and characteristics. For example, in an Illinois study by LaTour [35], winter withdrawals were computed as an average of November through April withdrawals and assumed outdoor use was 80 %. For Ohio, Indiana, and Wisconsin, Shaffer [22] defined the winter withdrawals as the average of December through February withdrawals and assumed that outdoor use is 100 % consumptive. In this study, because water main breaks are common in the winter months due to freezing conditions, a system's winter withdrawal in a given water year is computed as the minimum of the December, January, and February total withdrawal, with outdoor use assumed to be 100 % consumptive.

The winter base rate method has some obvious limitations. It ignores consumptive use that does not vary seasonally, as might occur for a public supply system that supplies a large industrial facility whose consumptive use is constant throughout the year. It would not give accurate results for a system with significant seasonal variations in user population, for example, a community that experiences a large influx of tourists during the summer months. In addition, no systematic evaluations of the method have been conducted, partly because an alternative methodology is not available for the PWS use type. However, Shaffer [22] did apply the method to commercial as well as public supply users, and for commercial facilities, she compared results from the winter base rate method with those obtained from the simple water balance approach, Eqs. (1a) and (1b). Shaffer found that the annual consumptive use coefficient for both Ohio and Indiana from the winter base rate method was 30 %, which fell between the median and average of the annual consumptive use coefficients for facilities in Ohio computed using Eq. (1b), which were 17 and 42 %.

3.6 Configuration of the Water Balance Conveyance Model

As described above, this study estimates consumptive use primarily by application of non-site-specific consumptive use coefficients to water withdrawal quantities rather than by using return flow data. The coefficients are obtained from literature values or, in the case of PWS, computed using the winter base rate method. In a few instances when sufficient data were available, the water balance equation, Eq. (1b), was used. However, return flows are often discharged at locations some distance away from original withdrawal points. Therefore, in order to estimate consumptive use by this study's spatial unit of analysis, the river segment, a means of representing the routing of water from withdrawal points to discharge points was needed. An available water routing model and database structure, the New England Water-Use Data System [39] was considered, but it was determined that its data needs were too intensive for a region the size of the upper Potomac Basin.

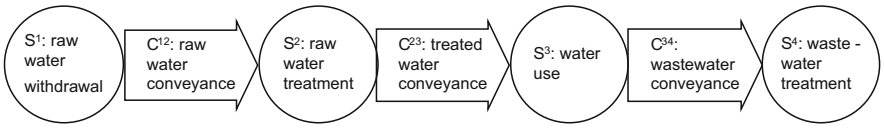

Fig. 4 Schematic of the components of the Water Balance Conveyance Model (*Source*: Authors)

The Water Balance Conveyance Model was developed for this project to capture the effects of inter-watershed transfers. The model can route water from withdrawal points to discharge points and represent evaporative and other consumptive losses and return flows occurring throughout a complex system. The model has sufficient flexibility to represent situations common in the upper Potomac Basin, such as interconnections between two or more water distribution systems or wastewater collection systems, and where self-supplied industrial and commercial users ultimately discharge to public wastewater collection/treatment systems. It can represent both consumptive loss and return to the resource which may occur at the point of water use. It can represent the losses that often take place at water treatment plants where the treatment process may involve consumptive evaporative losses and/or discharges of residual process water back to streams. Finally, it can represent consumptive losses that may occur at WWTPs in cases where a portion of discharge is reused for irrigation or other purposes.

The model structure is depicted in Fig. 4. It represents four types of sites, denoted S^m, where $m = 1$ to 4, and three types of conveyance structures that link the sites, $C^{m\ m+1}$, for $m = 1$ to 3:

- S^1—raw water withdrawal sites: surface water intakes and groundwater wells.
- C^{12}—raw water conveyances: pipes from withdrawal points to water treatment facilities.
- S^2—raw water treatment sites: this includes no treatment in some cases, onsite treatment at some groundwater wells, and industrial or municipal and county water treatment facilities.
- C^{23}—treated water conveyances: conveyance pipes from water treatment facilities to users.
- S^3—water users: water users may be represented as individual users, e.g., an individual industrial facility, or by a group of users, say, the residents, commercial establishments, and minor industrial facilities located within a town's water service area.
- C^{34}—wastewater conveyances: conveyance pipes of sanitary sewer systems from users to wastewater treatment facilities.
- S^4—wastewater treatment: this includes onsite septic systems of some users and municipal, commercial, and industrial wastewater treatment facilities.

Each site in the model has associated spatial data, and the model represents consumptive losses and return flows via time-dependent loss and return factors associated with each site. The model also includes conveyance factors that represent the fraction of water from a given site of type, S^m, that is conveyed to a

destination site of type S^{m+1}. The loss, return, and conveyance factors are estimated from available information, including county and municipal water and sewer planning documents.

Denoting the n_m sites of node type, S^m, as $S_1^m, S_2^m, \ldots, S_{n_m}^m$ at locations $x_{m1}, x_{m2}, \ldots, x_{mn_m}$, where the x may be points, or extended locational data types, that is, lines or polygons, then, for each node type, S^m, consumptive losses and return flows at each of the sites $S_{i_m}^m$ have time-dependent values,

$L_{i_m}^m(t) =$ consumptive loss fraction at site $S_{i_m}^m$ at time, t, $i_m = 1, 2, \ldots, n_m$
$R_{i_m}^m(t) =$ return flow fraction at site $S_{i_m}^m$ at time, t, $i_m = 1, 2, \ldots, n_m$

Each of the three conveyance types, $C^{m\ m+1}$, can have up to $(n_m \times n_{m+1})$ conveyances. For example, conveyance type $C^{2\ 3}$ comprises the systems conveying treated water from the treatment plants to users. It would be possible, in the case of a highly interconnected system, for each of the n_3 users to obtain some portion of their water from all of the n_2 treatment plants. Finally, the portion of the water from site $S_{i_m}^m$ that is conveyed to site $S_{i_{m+1}}^{m+1}$ at time, t, after losses and return flows at site $S_{i_m}^m$, is given by a conveyance factor, c, where $c_{i_m i_{m+1}}^{m\,m+1}(t)$ is the fraction of water leaving site $S_{i_m}^m$ that is conveyed to site $S_{i_{m+1}}^{m+1}$ at time, t, with $i_m = 1, 2, \ldots, n_m$ and $i_{m+1} = 1, 2, \ldots, n_{m+1}$ and where the condition is imposed that

$$\sum_{i_{m+1}=1}^{n_{m+1}} c_{i_m i_{m+1}}^{m\,m+1}(t) = 1 \tag{4}$$

that is, that 100 % of the water leaving site $S_{i_m}^m$, after losses and return flows at the site are subtracted, is accounted for.

$W_{i_1} = W_{i_1}(t)$ be the value of the withdrawal at withdrawal site $S_{i_1}^1$ at time, t, where $i_1 = 1, 2, \ldots, n_1$. Several withdrawal sites may contribute to water at a subsequent site, $S_{i_m}^m$, where $m = 2$, 3, or 4, and water from each W_{i_1} may have traveled through multiple conveyance paths before arriving at a subsequent site. The total amount of water arriving at $S_{i_m}^m$, where $m = 2$, 3, or 4, is the product of all conveyance factors, c, times the product of all factors representing water remaining after losses and return flows at sites or conveyances, summed over all potential withdrawal sites and all potential paths. Then the total loss and total return flows at site $S_{i_m}^m$, for $m = 1$ to 4, are given by

$$\text{Loss at } S_{i_m}^m = \sum_{i_1}^{n_1} \cdots \sum_{i_{m-1}}^{n_{m-1}} W_{i_1} \times \prod_{p=1}^{m-1} \left[\left(1 - L_{i_p}^p - R_{i_p}^p \right) \times C_{i_p\ i_{p+1}}^{p\ p+1} \right] \times L_{i_m}^m \tag{5}$$

$$\text{Return at } S_{i_m}^m = \sum_{i_1}^{n_1} \cdots \sum_{i_{m-1}}^{n_{m-1}} W_{i_1} \times \prod_{p=1}^{m-1} \left[\left(1 - L_{i_p}^p - R_{i_p}^p \right) \times C_{i_p\ i_{p+1}}^{p\ p+1} \right] \times R_{i_m}^m \quad (6)$$

If it is assumed that all of the water that reaches a wastewater treatment site, $S_{i_4}^4$, which represents an endpoint of the system, is accounted for, that is, that the sum of the fraction of loss and return at each of these endpoint sites is one,

$$L_{i_4}^4 + R_{i_4}^4 = 1 \quad \text{for } i_4 = 1 \text{ to } n_4 \quad (7)$$

then it can be verified that the expressions for system losses and return flows given in Eqs. (5) and (6) satisfy global water balance. The global water balance equation requires that the sum of all withdrawals is equal to the sum of all losses and returns, or, in terms of the quantities defined in Eqs. (5) and (6), that

$$\sum_{i_1=1}^{n_1} W_{i_1} = \sum_{m=1}^{4} \left[\sum_{i_m}^{n_m} \left(\text{Loss at } S_{i_m}^m + \text{Return at } S_{i_m}^m \right) \right] \quad (8)$$

Equation (8) can be shown to be satisfied by substituting Eqs. (5) and (6) and simplifying using the expressions given by Eqs. (4) and (7).

In developing the Water Balance Conveyance Model, an attempt was made to strike a balance between model complexity and data availability. For many of the Basin's municipal and county systems, information is publicly available in water and sewer planning documents on water and wastewater treatment facilities, water and sewer service areas, and on interconnections between systems. Information in these documents often allow estimates to be made of the approximate percentages of water routed from a given point in a system to a subsequent point, for example, from a water treatment plant to various water service areas. However, detailed measurements of flow between system components are generally not available.

Figure 5 shows sites and conveyance structures in a hypothetical inter-watershed system. This figure illustrates a number of complexities that can be represented by the Water Balance Conveyance Model: (1) a public supply stream intake and an associated WWTP located in different watersheds, resulting in an inter-watershed transfer, and (2) a public water service area with a boundary that does not match that of the sewer service area, resulting in a portion of users discharging wastewater to individual septic and some self-supplied industrial and commercial users discharging to the sewer service area for the public WWTP.

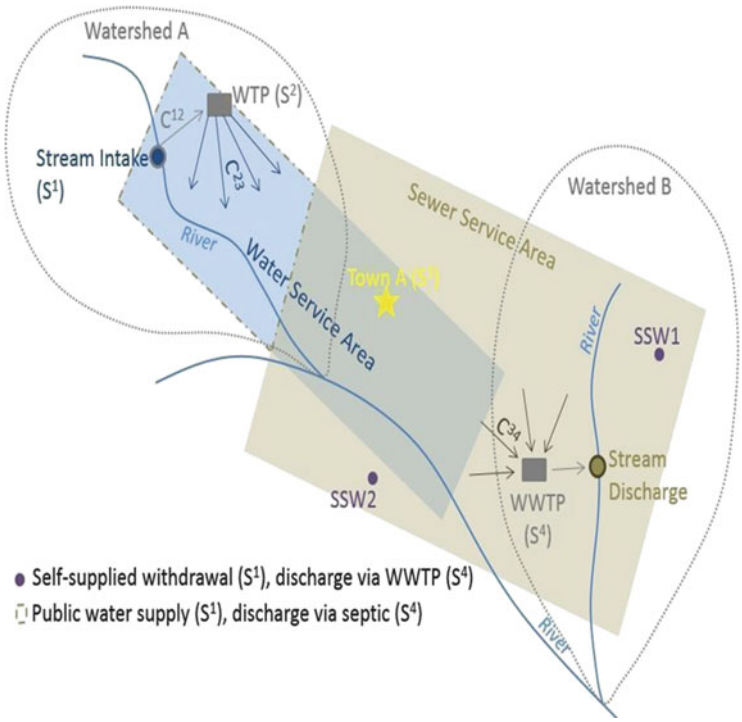

Fig. 5 Example application of the Water Balance Conveyance Model (*WTP* water treatment plant, *WWTP* wastewater treatment plant, *SSW* self-supplied withdrawal) (*Source*: Authors)

3.7 Interactive Mapping Tool

The tool under development for this project includes an online interactive map interface which displays time series of total monthly consumptive use in user-selected watersheds and also enables the users to access and review underlying data. Consumptive use in each watershed is computed according to Eq. (2), using spatial queries, as the sum of all withdrawals minus the sum of all estimated return flows occurring in the watershed. Return flows are estimated from withdrawal data and consumptive use coefficients and routed using the Water Balance Conveyance Model described in the previous section.

In order to meet budget constraints and provide a system that could be easily shared, open-source software was selected for the mapping tool architecture. Open-source software is generally defined as software that can be used, modified, and redistributed without any restrictions, limitations, or royalty payments and usually includes the source code for the software [40]. Using a variety of open-source software, a prototype system has been developed that is flexible in accommodating a wide array of data formats and spatial data types, but also scalable for large volumes of data.

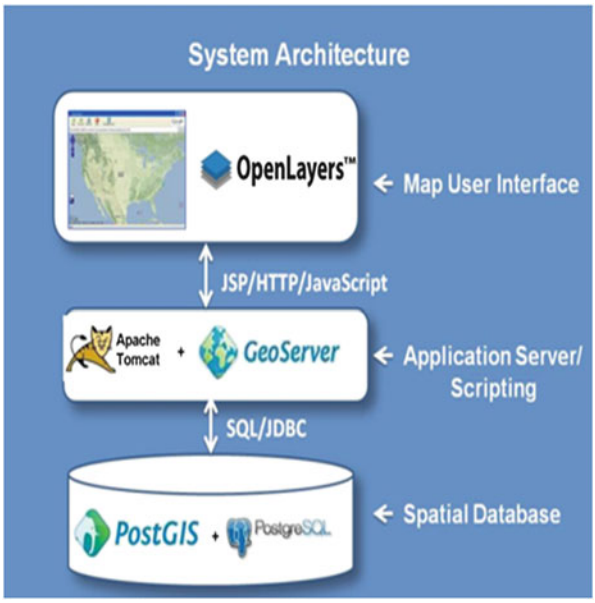

Fig. 6 Architecture of the interactive mapping tool (*Source*: Authors)

The mapping tool is designed to display estimates of cumulative consumptive water use at the terminus of predetermined watersheds upstream of a watershed of interest. The end user interacts with the system using a web browser and, upon first page load, is presented with a web-mapping interface. When the user clicks on a watershed, the system sends a query request to a backend database containing both spatial and nonspatial data. The query extracts withdrawal data and consumptive use estimates and returns a rendered map and summary calculations of withdrawals and consumptive use upstream of the selected watershed. These results are displayed to the end user in the form of a map with the upstream watersheds and withdrawal sites highlighted, tables of information on those withdrawal sites, and summary information on total water withdrawals and consumptive water use within the originally selected watershed. The returned display also includes a chart of withdrawals over time.

The architecture of this tool, shown in Fig. 6, consists of three main components: the map user interface, the application server and web server, and the spatial database. The map user interface is a browser-based JavaScript mapping library called OpenLayers [41]. This library is called from an html web page and displays background terrain data from a modified version of OpenStreetMap data (provided by Stamen Design [42] terrain tile server in an interactive frame) allowing the user to pan, scroll, or zoom the terrain view. The OpenLayers map also shows overlay polygon elements depicting the boundaries of watersheds, streams, and water withdrawal sites. These three elements are stored as geometry layers within the spatial database and are delivered to the OpenLayers map interface as tile overlays through a Web Map Service (WMS) from the rendering engine of the application

server, or GeoServer [43]. The Apache Tomcat [44] is a web server software which runs in conjunction with the application server to provide browser-based activity in the form of html web pages commonly found in any Internet-driven application. The spatial database consists of the robust and scalable PostgreSQL [45] relational database. Its capacity to store geometry for the watersheds and withdrawal points within the database is aided by an extension called PostGIS [46].

These three components of the system take user input in the form of map clicks, communicate with each other through a series of scripts to retrieve data from the spatial database, and deliver it back to the user interface in the form of map feature highlights, tabular data in tables, and interactive charts. While there are numerous methods and software architectures that can accomplish the same tasks as described in this section, this architecture was chosen for its use of open-source software and scalability.

4 Results and Discussion

4.1 Water Withdrawals in the Upper Potomac Basin

The tool developed for this project allows analysis of total withdrawals and consumptive use in the upper Potomac Basin, including trends in time and differences during drought and non-drought years. This is of interest to Washington, DC, metropolitan area water supply planners as water consumptively used upstream will not be available at their downstream intakes. As an example, Fig. 7 shows a graph of total withdrawals by public water suppliers, who are responsible for the majority of consumptive water use occurring in the upper basin during the summer months. The figure shows time series plots of withdrawals by the Washington, DC,

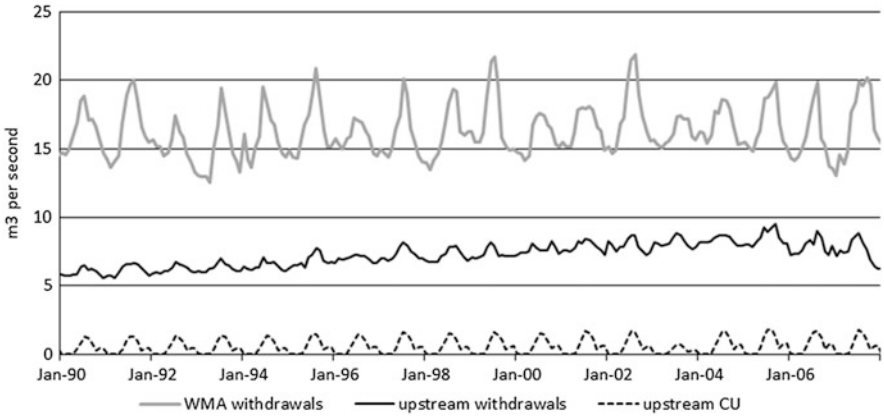

Fig. 7 Total upper Potomac Basin withdrawals for Washington, DC, metropolitan area (WMA) public water suppliers and withdrawals and consumptive use of upstream suppliers

metropolitan area suppliers and by the suppliers upstream of the metropolitan area. The graph also shows the consumptive use of the upstream suppliers.

4.2 Significance of Inter-Watershed Transfers

The significance of inter-watershed transfers in some parts of the Potomac Basin is illustrated in Fig. 8, which shows consumptive use in the Monocacy sub-basin computed by two different methods. The Monocacy sub-basin includes portions of Frederick and Carroll counties in Maryland and Adams County in Pennsylvania. Figure 8a shows consumptive use in August 2012 estimated assuming onsite return flow, i.e., assuming that any discharge of wastewater occurs in the same watershed as the associated withdrawal. Figure 8b shows consumptive use for the same month, computed using the Water Balance Conveyance Model described in Sect. 3.6. The results capture the significant transfers of water that occurs in this sub-basin. Municipalities and other users in Frederick County, who formerly relied upon the Monocacy River, are increasingly turning to the Potomac River as a more reliable water supply. However, most municipal WWTPs in the county still discharge to the Monocacy River and its tributaries.

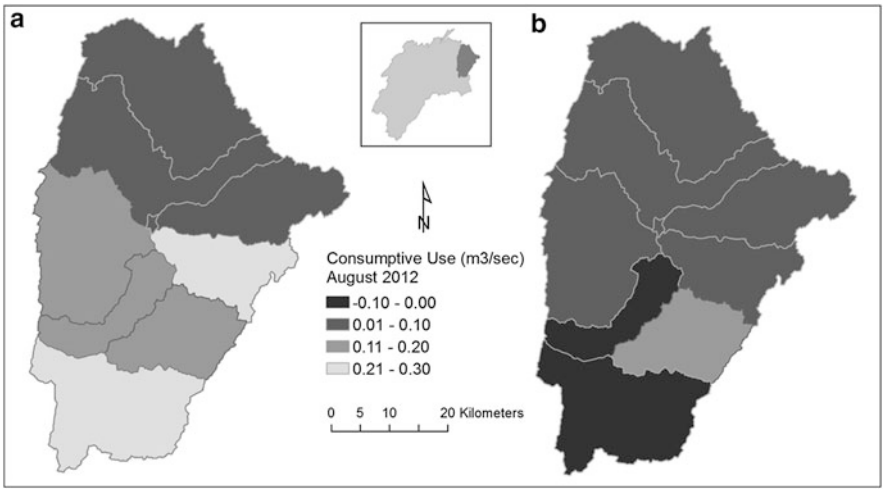

Fig. 8 Consumptive use in the Monocacy sub-basin by river segment, calculated assuming onsite return flow for all withdrawals (**a**) and by the Water Balance Conveyance Model (**b**). A negative consumptive use value indicates a net importation of water into the area (*Source*: River segments from CBP)

4.3 Prototype Version of Mapping Tool

A desktop prototype version of the interactive mapping tool was constructed to test methods for developing an Internet browser-based mapping application and backend relational database to hold and display withdrawal data and consumptive use estimates. In this prototype, sample data were used and onsite return flows were assumed for all withdrawals. Development of the tool has provided an opportunity to better understand the complexities of web-based interactive architectures and lays the groundwork for developing a more advanced tool to incorporate the full Water Balance Conveyance Model.

The tool provides the user with summary cumulative upstream withdrawal data and consumptive use estimates. Therefore, the system must be able to uniquely identify the watershed within which the user has clicked and the withdrawal points contained only within that selected watershed. When the user first loads the map user interface, OpenLayers, in a web browser, the watersheds and withdrawal point elements are loaded automatically onto the screen map using JavaScript programming within the html page. Figure 9 shows the boundary of several nested watersheds in red and overlaid on the Stamen terrain background. Withdrawal points are shown as white dots. The boundary of each of these watersheds is stored as an individual geometry within the PostgreSQL spatial database, with each containing an attribute table. The attribute table includes a unique watershed identification

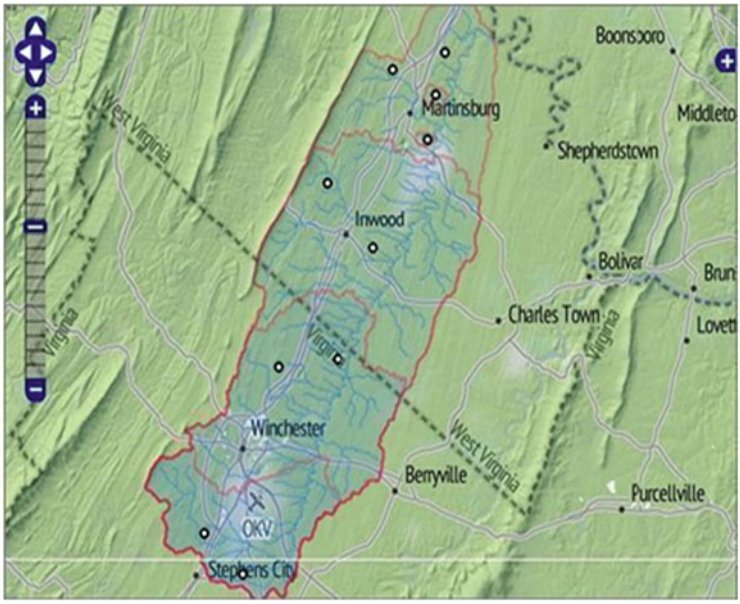

Fig. 9 Map user interface showing an OpenLayers map with a Stamen terrain background, overlaid by watershed boundaries in *red* and withdrawal points as *white dots* (*Sources*: watersheds—authors; map tiles and data—Stamen Design and OpenStreetMap)

number and the watershed area. Withdrawal points are also independent geometry elements stored in the spatial database.

A person utilizes the tool by clicking on a location of interest, such as a watershed with a potential future withdrawal, to obtain spatial and tabular outputs. When the user initiates the process by clicking in a watershed on the mapping interface, a series of scripts are run to perform two major tasks. In the first task, the system must correctly identify the watershed within which the user has clicked. This is accomplished through a series of actions that select the smallest nested watershed under the clicked point and the associated unique identification number.

The second task performed after a user clicks on the map is to return summary information to the user interface about withdrawal and consumptive use within the watershed. Using the unique ID of the selected watershed determined from the first task, a series of additional JavaScript functions, Java Server Page scripts, and Structured Query Language (SQL) statements are built and sent to the spatial database to perform a spatial query of the withdrawal points contained within the selected watershed and calculate the summary information. The spatial database responds to these queries by returning the geometry of the selected watershed, the geometry of the withdrawal points within the watershed, as well as the summary of consumptive use estimates. The information is displayed in the user interface in four different ways. First, the elements are highlighted on the map (Fig. 10). This onscreen display of the selected features is intended to provide the user with visual confirmation of which watershed and withdrawal points were selected.

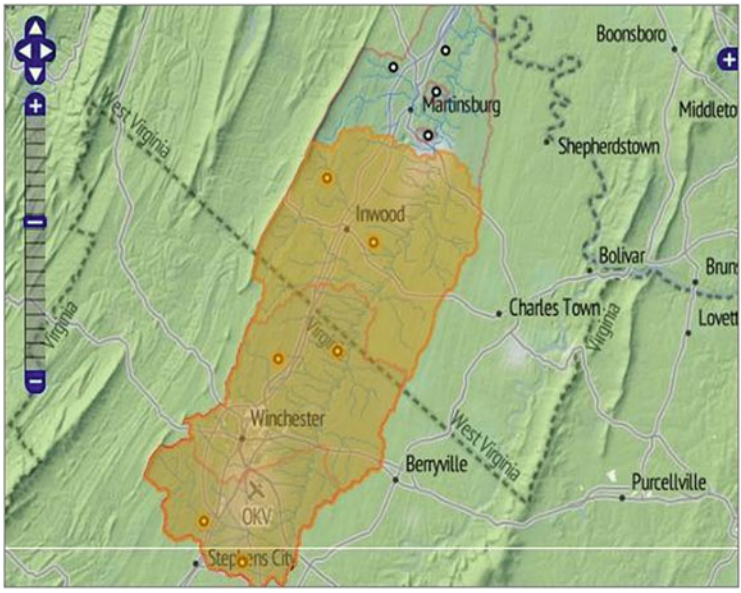

Fig. 10 The map user interface showing the highlighted watershed and withdrawal points as detected from the user's mouse click (*Sources*: watersheds—authors; map tiles and data—Stamen Design and OpenStreetMap)

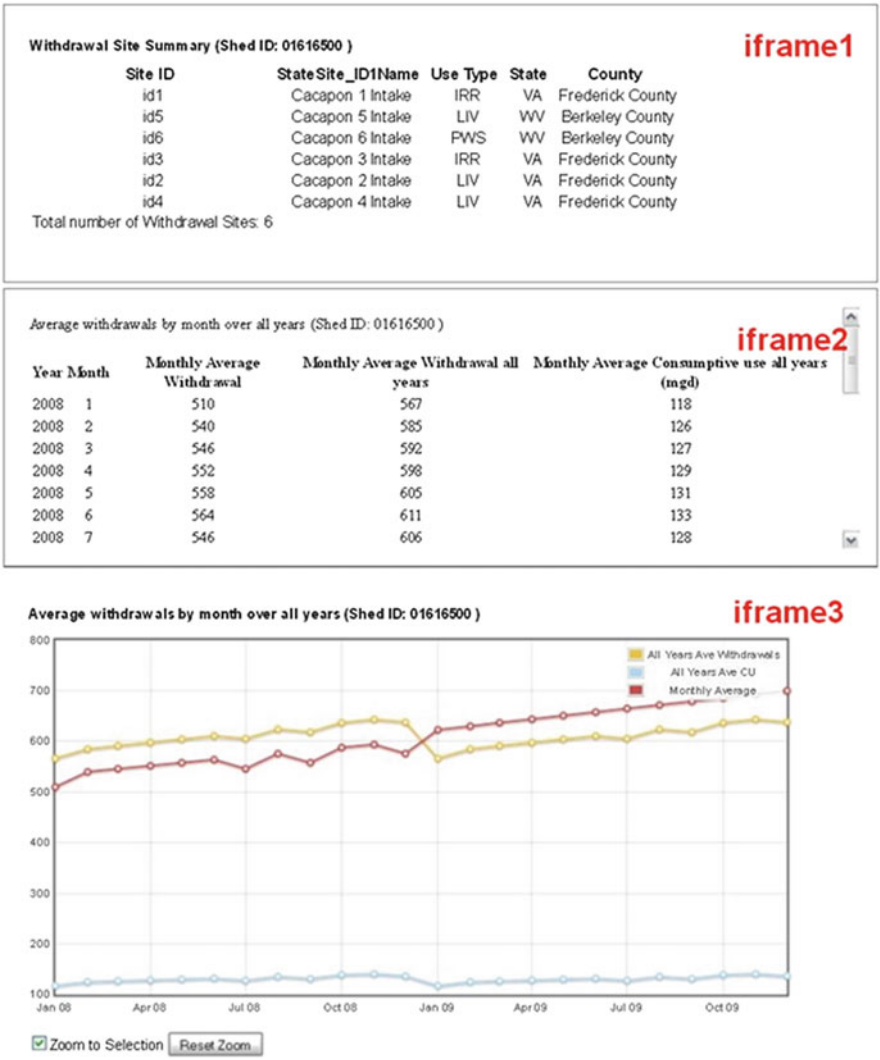

Fig. 11 Screenshot of three of the user interface elements (*Source*: Authors)

The queried information is also displayed in the user interface as a tabular and graphical summary of water use information for the withdrawal points contained within the selected watershed. An example tabular display is shown in Fig. 11, iframe 1. This table allows the user to see the names, county, and other attribute information for each withdrawal. Tabular summary information is also provided including monthly withdrawals and consumptive use for the selected watershed (Fig. 11, iframe 2). These same calculations are then plotted utilizing an open-source JavaScript plotting library, FLOT [47] (Fig. 11, iframe 3).

These four user interface responses (shown in Figs. 10 and 11) comprise the prototype interactive web elements designed to provide users with watershed-scale water use information. A user may further click any point on the screen within a watershed, and the system will (1) dynamically remove any results from the previous map click, (2) refresh the map, and (3) repopulate the three iframes with updated information and calculations.

4.4 Discussion

Quantifying water use, and the portion not returned to a resource after use, is an essential component of sustainably managing water resources. This information forms the basis for current decision-making as well as proactive planning efforts to ensure sustainable supplies under future environmental, economic, social, and technological conditions. Particularly in watersheds that span multiple jurisdictions, such as the Potomac, compiling and assessing data can have the added benefit of encouraging communication across political boundaries to manage a shared resource.

Many interactive watershed data analysis and/or mapping tools have been constructed in the United States, generally for individual states. Some, but not all, of these tools have a web-based component. The USGS StreamStats program has interactive maps either fully implemented or under development for most states [48]. StreamStats primarily provides streamflow statistics and watershed characteristics for user-delineated watersheds. The Maryland StreamStats application [49], constructed in collaboration with the Maryland Department of Environment, also provides information on withdrawals and discharges for a particularly vulnerable portion of the state, to select users only. Because of security concerns, water withdrawal data with associated locational information cannot be made publicly available in the United States, and web-based tools are generally password protected. Pennsylvania [50] and Virginia [51] also have water use mapping tools available to select users for data entry and data access. West Virginia [52] and Michigan [53] have online tools available to the public to help users assess the impact of potential withdrawals. Colorado's Decision Support System website [54] provides a suite of tools to access and analyze water availability and water use data.

A regional water resource planning effort has been underway for many years in the Great Lakes Basin, led by the Great Lakes Commission. For the Great Lakes Basin (including the Canadian portion), data collection is driven by ongoing resource concerns that have led to interstate and international agreements and significant financial support. The online Great Lakes Regional Water Use Database [55] does not have a visual map interface, but it does allow registered users to upload and manage data and the public to generate water use summary reports. Another regional-based effort in the United States has been initiated by the Susquehanna River Basin Commission, which is also developing an interstate web-based, consumptive use tool [56].

5 Conclusions

In the Potomac River Basin, the database, Water Balance Conveyance Model, and interactive mapping tool described in this chapter may be used for a number of purposes, and other basins may benefit from using a similar approach. Specifically, the Water Balance Conveyance Model is easily adaptable to an endless array of water use systems as well as spatial and temporal changes to those systems. This model was developed to provide consumptive use estimates at the watershed scale by representing transfers of water from withdrawal points to discharge points. The model structure, which represents four types of sites (water withdrawal sites, water treatment facilities, end users, and wastewater treatment facilities), is sufficiently flexible to address the level of complexity of interactions and water transfers present in the upper Potomac River Basin. But the water balance equations, Eqs. (5), (6), and (8), for $N = 4$ site types could be easily extended to a more general model with N site types to represent other situations. Also, it is relatively straightforward to add losses and return flows from conveyances to the equations if the model were applied to regions with data to support representation of these types of losses and returns.

The interactive mapping tool provides an easily understandable and readily accessible way to make complex datasets available to diverse stakeholder interests. Since these products are generated utilizing open-source software, the cost is negligible and the system can be developed to accommodate local complexities. Advances in technology that are available and usable by anyone are allowing water resource agencies with limited budgets to undertake more sophisticated analyses for use in decision-making and planning.

Select stakeholders may also utilize the tool to evaluate potential consequences of changing water use. For example, when coupled with water availability data (e.g., streamflows) from sources such as the Chesapeake Bay Program Watershed Model and USGS' StreamStats [48], the tool's water use summaries may be utilized to understand the water supply–water demand relationship. Similarly, the tool may also be used to inform local, state, and basin-wide water resources planning efforts.

Challenges faced during the development of this tool are not unique to the Potomac River Basin. They include (1) combining different water use datasets into a common database format, (2) incorporating flexibility into the conveyance model that is able to capture losses and returns to the system through various processes, and (3) accommodating the considerable staff time and effort required to obtain necessary programming skills to work with the open-source software components.

The pilot version of the Water Balance Conveyance Model is implemented with Microsoft Access for the Monocacy sub-basin. The next version will be implemented in PostgreSQL, to interface with the interactive mapping tool. The prototype mapping tool currently calculates consumptive water use using sample withdrawal data and consumptive use coefficients, with the assumption of onsite return flows. The next version of the mapping tool will make use of the withdrawal

and estimated return flow values computed by the Water Balance Conveyance Model and will be completed by extending the application of the geospatial tools beyond the test watershed to the entire basin. The functionality of the prototype system is readily scalable to the Potomac Basin by simply appending new watershed geometries and associated tables for withdrawals and consumptive use estimates. In addition, water availability metrics, which have been simulated by the Chesapeake Bay Program Watershed Model for the river segments, will be incorporated into the next version of the tool to allow users to assess the impact of consumptive use on streamflow.

References

1. Vorosmarty CJ, Green P, Salisbury J, Lammers RB (2000) Global water resources: vulnerability from climate change and population growth. Science 289:284–288
2. United Nations Development Programme (UNDP) (2006) Human development report 2006. Beyond scarcity: power, poverty and the global water crisis, p 388. http://hdr.undp.org/en/content/human-development-report-2006. Accessed 6 Oct 2014
3. Poff NL, Allan JD, Bain MB, Karr JR, Prestegaard KL, Richter BD, Sparks RE, Stromberg JC (1997) The natural flow regime. BioScience 47(11):769–784
4. Postel S, Richter B (2003) Rivers for life: managing water for people and nature. Island Press, Washington, DC, p 220
5. RCSE-Shinga University, ILEC (2011) Development of ILBM platform process: evolving guidelines through participatory improvement, p 502
6. Giuliani M, Castelletti A (2013) Assessing the value of cooperation and information exchange in large water resources systems by agent-based optimization. Water Resour Res 49(7): 3912–3926
7. Food and Agriculture Organization (2007) Coping with water scarcity. Challenge of the twenty-first century. UN-Water, p 29
8. Gerlak A, Lautze J, Giordano M (2011) Water resources data and information exchange in transboundary water treaties. Int Environ Agreements Polit Law Econ 11(2):179–199
9. Shiklomanov I (2000) Appraisal and assessment of world water resources. Water Int 25:11–32
10. Kenny JF, Barber NL, Hutson SS, Linsey KS, Lovelace JK, Maupin MA (2009) Estimated use of water in the United States in 2005. U.S. Geological Survey Circular 1344, p 52
11. Oki T, Kanae S (2006) Global hydrological cycles and world water resources. Science 313 (5790):1068–1072
12. Weiskel PK, Vogel RM, Steeves PA, Zarriello PJ, DeSimone LA, Ries KG (2007) Water use regimes: characterizing direct human interaction with hydrologic systems. Water Resour Res 43(4). doi:10.1029/2006WR005062
13. Ahmed SN, Bencala KB, Schultz CL (2013) 2010 Washington metropolitan area water supply reliability study, part 2: potential impacts of climate change. Interstate Commission on the Potomac River Basin. Publication number ICPRB 13-07
14. Stagge JH, Moglen GE (2013) A nonparametric stochastic method for generating daily climate-adjusted streamflows. Water Resour Res 49:6179–6193. doi:10.1002/wrcr.20448
15. Sheer DP, Rivera MW, Wright BA, Day J (2013) Dynamic reservoir operations: managing for climate variability and change. Water Research Foundation. http://www.waterrf.org/Pages/Projects.aspx?PID=4306. Accessed 6 Oct 2014
16. Apse C, DePhilip M, Zimmerman J, Smith MP (2008) Developing instream flow criteria to support ecologically sustainable water resource planning and management. The Nature Conservancy, p 196

17. Cummins J, Buchanan C, Haywood C, Moltz H, Griggs A, Jones RC, Kraus R, Hitt N, Villella-Bumgardner R (2010) Potomac basin large river environmental flow needs. Interstate Commission on the Potomac River Basin. Publication number ICPRB 10-03
18. U.S. Army Corps of Engineers, The Nature Conservancy, and Interstate Commission on the Potomac River Basin (2013) Middle Potomac River watershed assessment: Potomac River sustainable flow and water resources analysis. Available via ICPRB. http://www.potomacriver.org/pubs/pubs. Accessed 6 Oct 2014
19. Moltz H, Haywood C, Hoffman J (2011) Integrated water resources management in the Potomac River Basin paper. In: Integrated water resources management: the Emperor's new clothes or indispensable process? Summer specialty conference, American Water Resources Association, Baltimore, 27–29 June 2011
20. U.S. Environmental Protection Agency (2010) Chesapeake Bay Phase 5.3 Community Watershed Model. EPA 903S10002—CBP/TRS-303-10
21. Shenk G, Wu J, Linker L (2012) Enhanced HSPF model structure for Chesapeake Bay watershed simulation. J Environ Eng 138(9):949–957. doi:10.1061/(ASCE)EE.1943-7870.0000555
22. Shaffer KH (2009) Variations in withdrawal, return flow, and consumptive use of water in Ohio and Indiana, with selected data from Wisconsin, 1999–2004. U.S. Geological Survey Scientific Investigations Report 2009–5096, p 93
23. Gleick PH (2003) Water use. Annu Rev Environ Resour 28(1):275–314
24. Döll P, Kaspar F, Lehner B (2003) A global hydrological model for deriving water availability indicators: model tuning and validation. J Hydrol 270(1):105–134
25. Alcamo J, Döll P, Henrichs T, Kaspar F, Lehner B, Rösch T, Siebert S (2003) Development and testing of the WaterGAP 2 global model of water use and availability. Hydrol Sci J 48(3):317–337
26. Solley WB, Chase EB, Mann WB IV (1983) Estimated use of water in the United States in 1980. U.S. Geological Survey Circular 1001, p 56. http://pubs.er.usgs.gov/publication/cir1001. Accessed 6 Oct 2014
27. Savenije HHG (2000) Water scarcity indicators; the deception of the numbers. Phys Chem Earth Pt B 25(3):199–204
28. Falkenmark M, Rockström J (2004) Balancing water for humans and nature: the new approach in ecohydrology. Earthscan, London, p 247
29. USGS Water Use Data in the United States. http://water.usgs.gov/watuse/data/. Accessed 6 Oct 2014
30. Shaffer KH, Runkle DL (2007) Consumptive water-use coefficients for the Great Lakes basin and climatically similar areas. USGS Scientific Investigations Report, p 191
31. U.S. Environmental Protection Agency (1990) Rainfall induced infiltration into sewer systems. Report to Congress. EPA/430/09-90/005
32. U.S. Environmental Protection Agency (1996) Seminar publication: national conference on sanitary sewer overflows, Washington, DC, 24–26 April 1996, EPA/625/R-96/007
33. Swarner R, Thompson M (1996) Modeling inflow and infiltration in separate sewer systems. In: Seminar publication—national conference on sanitary sewer overflows (SSOs), Washington, DC, 24–26 April 1996
34. Rutsch M, Rieckermann J, Cullmann J, Ellis JB, Vollertsen J, Krebs P (2008) Towards a better understanding of sewer exfiltration. Water Res 42(10–11):2385–2394
35. LaTour JK (1991) Determination of water use in Rockford and Kankakee areas, Illinois: U.S. Geological Survey Water-Resources Investigations Report 90–4166, p 70
36. DeSimone LA (2002) Simulation of ground-water flow and evaluation of water-management alternatives in the Assabet River Basin, eastern Massachusetts. U.S. Geological Survey Scientific Investigations Report 2004–5114, p 133
37. Mullaney JR (2004) Water use, ground-water recharge and availability, and quality of water in the Greenwich area, Fairfield County, Connecticut and Westchester County, New York, 2000–2002: U.S. Geological Survey Water-Resources Investigations Report 03–4300, p 64

38. Horn MA, Moore RB, Hayes L, Flanagan SM (2008) Methods for and estimates of 2003 and projected water use in the Seacoast region, southeastern New Hampshire: U.S. Geological Survey Scientific Investigations Report 2007–5157, p 87
39. Tessler S (2002) Data model and relational database design for the New England water-use data system (NEWUDS). US Geological Survey Open File Report 1359. http://pubs.usgs.gov/of/2001/ofr01359/. Accessed 6 Oct 2014
40. The Open Source Initiative (OSI) (2013) The Open Source Definition. http://opensource.org/osd. Accessed 6 Oct 2014
41. Open Source Geospatial Foundation (OSGEO) (2013) OpenLayers. http://openlayers.org. Accessed 6 Oct 2014
42. Stamen (2014) Map tiles by Stamen Design, under Creative Commons BY 3.0. Data by OpenStreetMap under CC BY SA
43. OpenGeo (2013) GeoServer. http://geoserver.org/. Accessed 6 Oct 2014
44. Apache Software Foundation (2013) Apache Tomcat. http://tomcat.apache.org. Accessed 6 Oct 2014
45. PostgreSQL Global Development Group (PostgreSQL GDG) (2013) PostgreSQL. http://www.postgresql.org/about. Accessed 6 Oct 2014
46. Refractions Research (2008) PostGIS. http://refractions.net/products/postgis. Accessed 6 Oct 2014
47. IOLA (2013) Flot: attractive Javascript plotting for jQuery. http://www.flotcharts.org/. Accessed 6 Oct 2014
48. StreamStats. http://water.usgs.gov/osw/streamstats/. Accessed 6 Oct 2014
49. Maryland StreamStats. https://streamstatsags.cr.usgs.gov/md_swuds/Index.aspx. Accessed 6 Oct 2014
50. Pennsylvania: Department of Environmental Protection (2012). Yield analysis tool (version 2.0) [computer software]. Harrisburg, Pennsylvania
51. Virginia Water Supply Planning Program—Annual Water Withdrawal Reporting. http://www.deq.virginia.gov/Programs/Water/WaterSupplyWaterQuantity/WaterSupplyPWaterSu/AnnualWaterWithdrawalReporting.aspx. Accessed 3 Nov 2014
52. West Virginia Water Withdrawal Guidance Tool. http://www.dep.wv.gov/WWE/wateruse/Pages/WaterWithdrawal.aspx. Accessed 6 Oct 2014
53. Michigan's Water Withdrawal Assessment Tool. http://www.deq.state.mi.us/wwat/. Accessed 6 Oct 2014
54. Colorado Decision Support Systems: cdss.state.co.us/Pages/CDSSHome.aspx. Accessed 6 Oct 2014
55. Great Lakes Regional Water Use Database. http://projects.glc.org/waterusedata/. Accessed 6 Oct 2014
56. Susquehanna River Basin Commission. http://www.srbc.net/planning/cwuas.htm. Accessed 6 Oct 2014

Advances in Water Sensor Technologies and Real-Time Water Monitoring

Tamim Younos and Christopher J. Heyer

Contents

Abstract Measurements of natural water quality and water quantity are essential to make informed decisions for sustainable management of water resources and ecosystem protection. During the late nineteenth and early twentieth centuries, manual or discrete water monitoring techniques were developed and refined for water quality and quantity measurements, and many of these techniques are still used around the

T. Younos (✉)
The Cabell Brand Center for Global Poverty and Resource Sustainability Studies, Blacksburg, VA, USA
e-mail: tyounos@gmail.com

C.J. Heyer
Aquatic Informatics Inc., Vancouver, BC, Canada

T. Younos, T.E. Parece (eds.), *Advances in Watershed Science and Assessment*, The Handbook of Environmental Chemistry 33,
DOI 10.1007/978-3-319-14212-8_7

world. Discrete water quantity measurements and water quality sampling are conducted at regular time intervals (e.g., monthly) and do not provide sufficient data to capture temporal and spatial changes that occur during episodic events. In recent decades, there have been significant advances in water monitoring technologies that include sensor technologies, remote monitoring technologies, and data transfer technologies. These technologies allow water resource managers and researchers to capture real-time water quantity and quality data during episodic events such as major storms. Real-time and continuous water monitoring can capture temporal changes and provides broader spatial coverage of water quantity and quality in a watershed. Furthermore, it allows data collection when it is normally impractical with discrete sampling (e.g., during major storm events, nighttime, remote, and dangerous locations). This chapter presents an overview of advances in water sensor technologies. Topics discussed include various types of sensors for water quantity and water quality measurements, examples of commercially available water quantity and water quality monitoring devices, data collection and transport platforms, and data management and quality assurance/quality control for water monitoring.

Keywords Biosensors • Chemical sensors • Data platform • Optical sensors • Physical sensors • Telemetry • Water level sensors • Water monitoring

1 Introduction

Measurements of natural water quantity and water quality are essential to make informed decisions for sustainable management of water resources and ecosystem protection. Measurements of the quantity of water are required for drought and flood management; for estimating the availability of water supplies for municipal, industrial, and agricultural uses; and for estimating pollutant loads in surface waters. Water quality measurements are required to assess the overall health of a watershed, the suitability of the watershed to support living resources and provide ecosystem services, and to identify potential threats to human health.

During the late nineteenth and early twentieth centuries, manual or discrete water monitoring techniques were developed and refined for water quality and quantity measurements, and many of these techniques are still used around the world. Discrete water quantity measurements and water quality sampling conducted at regular time intervals (e.g., monthly) provide a broad view of seasonal changes of water quantity and quality but do not provide sufficient data to capture temporal and spatial changes that occur during episodic events such as precipitation and major storm events, pollutant discharges and spills, and harmful algal blooms. In order to capture the impacts of these episodic events, temporally and spatially intensive monitoring techniques need to be applied.

In recent decades, there have been significant advances in water monitoring technologies that include sensors technologies, remote monitoring technologies, and data transfer technologies [1]. These technologies allow regulatory agencies/water resources managers and researchers to capture real-time data for water

quantity and quality changes during episodic events. Real-time and continuous water monitoring programs can provide broader temporal and spatial coverage than discrete monitoring programs and allow for the collection of data during times when it is impractical (e.g., night) or dangerous (e.g., during storm events) to send sampling crews into the field. Some noted applications of real-time water monitoring technologies include flood forecasting, drinking water source protection, nonpoint source pollution control, ecosystem management, and real-time response to potentially catastrophic events.

This chapter presents an overview of advances in water sensor and real-time monitoring technologies. Topics discussed include various types of sensors for water quantity and water quality measurements, examples of commercially available water quantity and water quality monitoring devices, data collection and telemetry platforms, and data management and quality assurance/quality control for water monitoring.

2 Monitoring Water Quantity

Streamflow, also known as discharge, is one of the most commonly reported parameters in watershed monitoring programs and has origins dating to the late 1800s. Direct measurement of continuous streamflow is not practical. However, streamflow (Q) can be calculated from parameters that can be measured directly, i.e., water velocity (V) and stream cross-sectional area (A). Discrete water velocity in the stream cross section is measured using a velocimeter. The stream geometry (depth and width) is also measured at the same points to calculate the stream cross-sectional area. From these measures, discrete discharge can be calculated using the equation: $Q = A \times V$. In order to estimate streamflow continuously, these discrete discharge measurements need to be related to a parameter that can easily be measured continuously such as water level. Measurements of discrete discharge and water level are made over the entire flow regime in order to establish a good relationship between stage (surface water elevation above a datum) and streamflow (discharge). This relationship is known as a stage–discharge relationship or a rating curve. Once established, a rating curve can be applied to a station to continuously estimate discharge based on continuously measured water level (stage).

Stage–discharge relationships work well for unidirectional streamflows. However, when there are tidal influences, bidirectional flow or backflow, an accurate stage–discharge relationship cannot be established by water level measurements alone, and an index velocity rating needs to be developed. To establish an index velocity rating, continuous velocity and water level measurements are made with a deployed velocimeter and water level sensor at a stable location on a stream or river. Computing discharge using the index velocity method differs from the discrete stage–discharge method by separating velocity and area into two ratings—the index velocity rating and the stage-area rating. The outputs from each of these ratings, mean stream velocity (V) and cross-sectional area (A), are then

multiplied together to compute a streamflow. For the index velocity method, V is a function of such parameters as streamwide velocity, stage, and cross-stream velocity, and A is a function of stage and cross-sectional shape. These measurements are made over the entire flow regime in order to establish a good relationship between stage and area and between index velocity and mean velocity.

Technologies discussed in this section include water level sensors for continuous stage measurements in surface water applications and acoustic Doppler technology for measuring discrete and continuous water velocity to calculate discharge.

2.1 Water Level Sensors

Major sensor types for continuous water level measurements include submersible pressure transducers, shaft encoders, bubbler systems, or noncontact RADAR systems. Tables 1 and 2 describe major types of water level sensors, function mechanisms, typical sensor accuracy, and sensor suitability versus site characteristics. Major types of water level sensors are described in the following sections.

As a cautionary note, all sensors depicted in Table 2 can measure water level in brackish water. However, as stated earlier, it would be difficult to establish an accurate stage–discharge relationship for tidal bidirectional flows. In those situations, using an alternative method such as the index velocity rating is preferred.

Table 1 Continuous water level measurement sensor types and accuracies

Sensor type	Pressure sensor (transducers)	Bubbler system	Shaft encoder	RADAR level
Function mechanisms	Measures water level from pressure change in response to change in the water level	Measures pressure required to push air through the water and calculates water level from the measured pressure	Measures the rise and fall of water using a float, weight, and pulley	Measures water level by propagating microwave energy and calculates water level from pulse travel time
Onsite installation location	Pressure sensor is installed at a fixed depth in the water	Airline orifice tube is installed at a fixed depth in the water; bubbler, pressure sensor electronics, and DCP are installed above the water	Stilling well pipe is installed in the water, and shaft encoder is installed inside the stilling well	Installed on a bridge or other fixed structures spanning the water, using mounting arm
Typical accuracy (mm)	±2	±2	±0.073	±3

Table 2 Continuous water level measurement sensor-type capabilities and limitations

Site properties	Pressure sensor (transducers)	Bubbler system	Shaft encoder	RADAR level
Brackish water	o	o	o	o
Flash floods	o	o	*	*
Large debris in water	o	o	o	*
Snow/ice cover and flows	*	*	o	–
Migrating channels	o	o	o	*
Unstable banks	–	–	–	*
Stilling well	*	o	*	–
Bridge	*	*	*	*
Weir/flume	*	*	*	o

Symbols: (*) perfect match, (o) sensor will work, (–) limited

2.1.1 Submersible Pressure Transducers

Submersible pressure transducers are used extensively in groundwater level measurements, but their use has been expanded to surface water applications [2]. The submersible pressure transducer is deployed at a fixed depth—it measures pressure change in response to change in the water level and translates pressure change to water level through calibration. Submersible pressure transducers can be categorized as absolute sensors and vented sensors. Absolute sensors are not vented to the atmosphere, and therefore water level measurements can be biased by changes in atmospheric pressure.

Water level data collected with an absolute submersible pressure transducer should either be corrected in real time with measurements using an atmospheric barometric pressure sensor or post-corrected based upon logged atmospheric barometric pressure. In contrast to absolute sensors, vented submersible pressure transducers have a vent tube that vents the sensor to the atmosphere. This venting eliminates any potential bias on water level from changes in atmospheric pressure and therefore results in a higher accuracy sensor (Fig. 1).

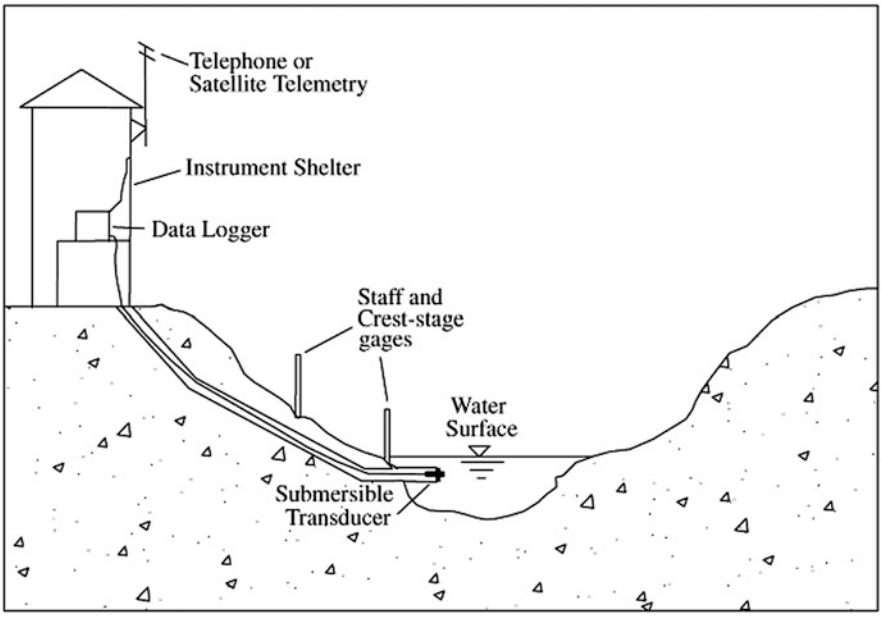

Fig. 1 Example of submersible pressure transducer for continuous water level measurement. *Source*: USGS [2] (public domain)

2.1.2 Bubbler Systems

Bubbler systems consist of three major components: a pressurized air source to push air through an orifice tube, an orifice tube whose open end is mounted at a fixed depth, and a pressure sensor (Fig. 2). Bubblers force a bubble or air through the orifice line and measure the pressure it takes to expel the air bubble out the submerged end of the line. The pressure required to move the air directly corresponds to water depth. Bubbler systems simultaneously compensate to changes in barometric pressure to ensure the highest accuracy measurement.

While bubbler systems have been in use for several decades, modern systems are self-contained and typically include a small compressor to generate the pressure needed and ensure a continuous flow of air through the orifice line. Some bubbler systems on the market today contain built-in data loggers, while others require connection to a separate data logger. Because only an orifice line is exposed to the water and the other major components can be protected in a gauge house, these sensors tend to last longer than submersible sensors.

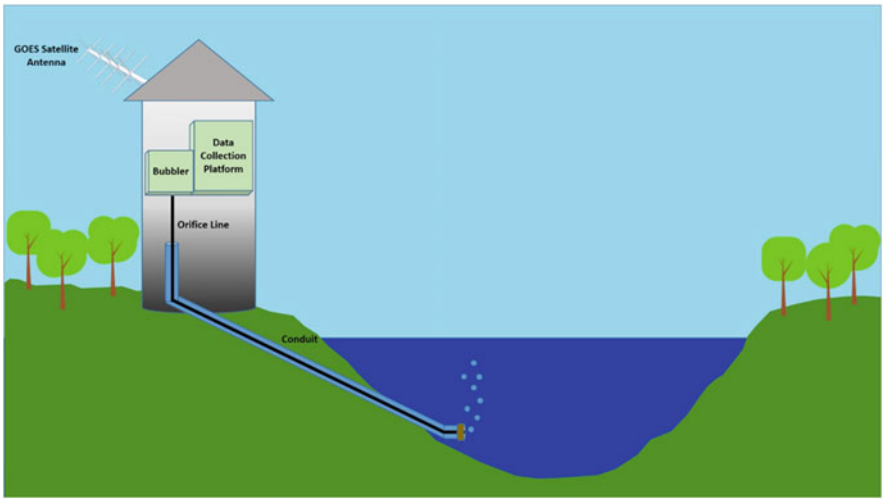

Fig. 2 Illustration of a typical bubbler system installation. *Source*: Second author

2.1.3 Shaft Encoders

Shaft encoders are deployed inside of stilling wells and consist of five major components: a pulley and shaft, an encoder which counts and interprets the shaft rotations, a float, a cable, or tape which passes over the pulley and is connected to the float on one end and a counterweight on the other end, and a counterweight (Fig. 3). As the water level in the stilling well changes, the float goes up and down which in turn rotates the pulley and the shaft. The shaft rotations are translated by the shaft encoder into meaningful water level values.

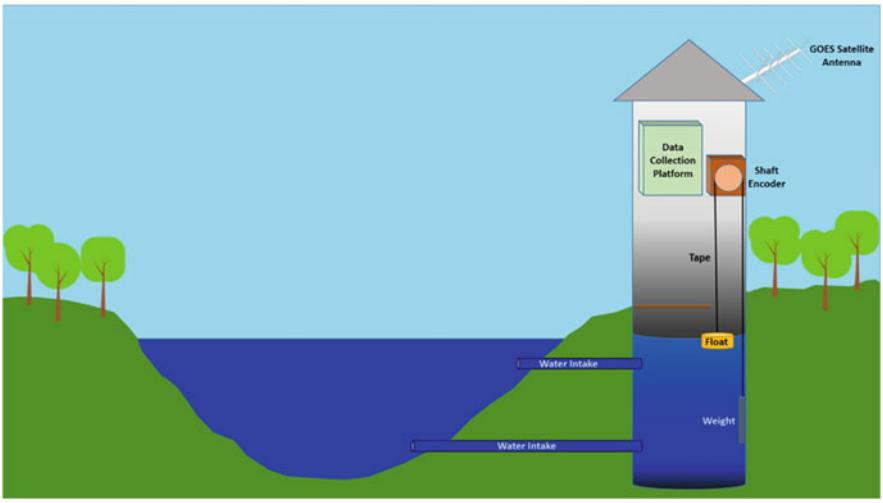

Fig. 3 Illustration of a typical shaft encoder installation. *Source*: Second author

2.1.4 Noncontact RADAR Sensors

A newer sensor technology for water level measurement available on the market is noncontact RADAR sensors. These sensors are mounted above the water on a bridge or other structures and have zero contact with the water. A microwave pulse is transmitted towards the water, and the time for the pulse echo to return is directly related to the distance from the sensor to the water surface.

Figure 4 shows a tide gauge RADAR-based water level sensor combined with a data logger installed on NOAA (National Oceanic and Atmospheric Administration) Pier in Scituate, Massachusetts (USA) [3]. Recently, NOAA published an updated version of the field installation and design analysis guide for microwave water level sensors [4]. Figure 5 shows the RADAR-based water level sensor system typical output. Water level measured values (blue) are plotted against the predicted (green). The tide gauge logs data every 6 min and posts to a website every 15 min.

Fig. 4 Tide gauge RADAR-based water level sensor mounted on a pier. Primary components: (*A*) RADAR sensor, (*B*) solar panel, (*C*) data collection platform (DCP). *Source*: NOAA [3, 4] (public domain)

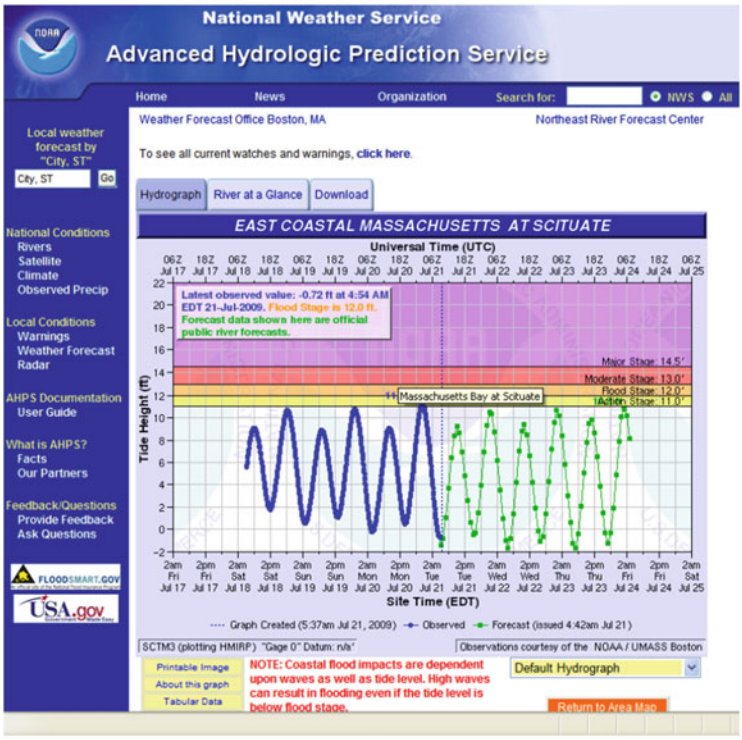

Fig. 5 Example data collected by a RADAR-based noncontact water level sensor system. *Source*: NOAA, National Weather Service [4] (public domain)

2.2 Acoustic Doppler Technology

Acoustic Doppler current profiler (ADCP) allows accurate measurements of streamflow from a boat, bridge, or cableway. The ADCP uses the Doppler effect to determine water velocity by sending a sound pulse into the water and measuring the change in frequency of the sound pulse reflected back to the ADCP by suspended sediment or other particulates transported in surface water. The change in frequency, or Doppler shift, measured by the ADCP, is translated into water velocity. The sound is transmitted into the water from a transducer to the bottom of the river and receives return signals throughout the entire depth (Fig. 6). The ADCP also uses acoustics to measure water depth by measuring the travel time for a pulse of sound that reach the river bottom and return back to the ADCP [5].

The river-bottom tracking capability of the ADCP acoustic beams is combined with a global positioning system (GPS) and real-time kinematic (RKT) survey to track the progress of the ADCP across the river and provide velocity and river width and depth measurements. The river flow (Q) is computed from A (cross-sectional area) $\times V$ (velocity) relationship. The use of ADCPs reduces time to determine discharge (flow rate) and makes it possible to measure river discharge under flooding conditions. Furthermore, the ADCP provides a detailed profile of water velocity and direction for the river cross section and increases accuracy of flow measurements. Figure 7 shows an example of using ADCP for velocity measurement and water turbidity.

The ADCPs can also be deployed in various configurations (upward-looking, side-looking, and downward-looking) to continuously measure water velocity, currents, and waves and calculate discharge. These instruments often utilize a built-in pressure transducer for secondary water level measurement and wave measurement (through the use of specialized software). Most ADCP instruments feature at least two beams, one beam for measuring water velocity and a second beam for measuring water level.

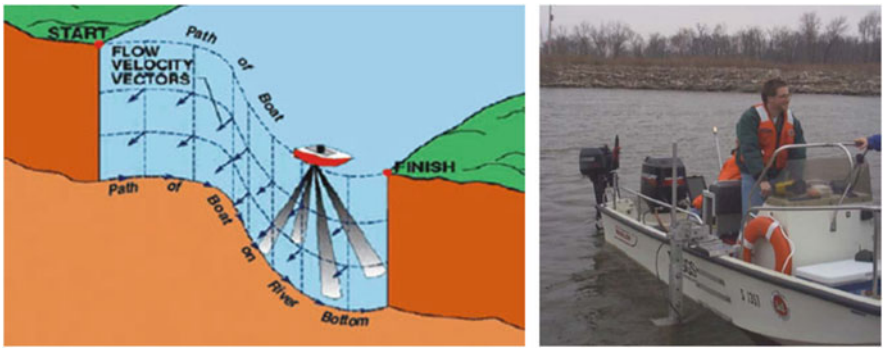

Fig. 6 Illustration of acoustic Doppler current profiler (ADCP) measurements (*left*) and photo of a moving boat measurement with an ADCP (*right*). *Source*: USGS [5] (public domain)

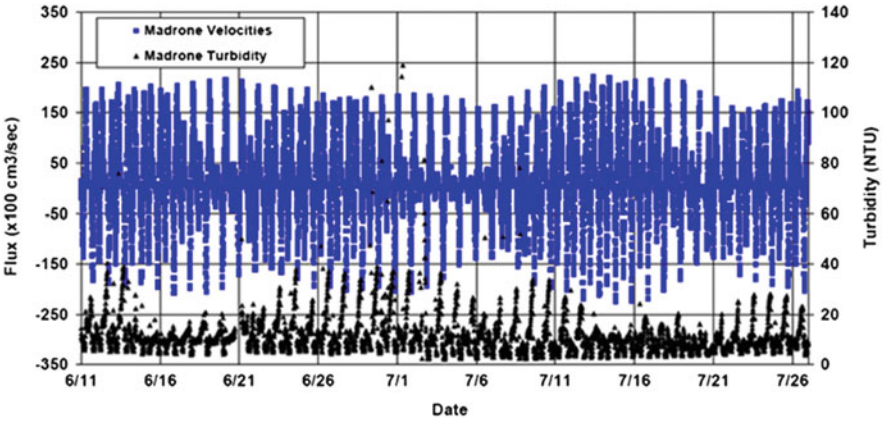

Fig. 7 Example time series plot of tidal channel discharge and turbidity measurements using ADCP, cross-sectional area, and real-time kinematic global positioning system (RTK-GPS) survey methods. *Source*: USGS [5] (public domain)

SonTek IQ+; Source: SonTek, a Xylem, Inc. brand

Teledyne RD Instruments ChannelMaster H-ADCP; Source: Teledyne RD Instruments

SonTek Argonaut SL; Source: SonTek, a Xylem, Inc. brand

Fig. 8 Various types of fixed ADCPs for continuous measurements of water velocity and continuous discharge calculation. *Source*: SonTek and Teledyne RD Instruments (with permissions from Xylem and Teledyne)

Several types of commercially available ADCPs are shown in Fig. 8. ADCPs are commonly used in monitoring locations where a stage–discharge relationship cannot be established because of bidirectional flow or a backwater situation (Fig. 9). Discharge is calculated from the continuously measured velocity which is used as an index of the mean velocity in a river or stream channel and the continuously measured water level. Most ADCPs can be preprogrammed using channel dimensions (depth and width) to continuously calculate channel cross-sectional area. These ADCPs can be configured to measure velocity at set sampling intervals with set averaging periods (for details, see [6]).

Fig. 9 Illustration of a side-looking ADCP deployed in a small tidal stream with bidirectional flow for continuous measurement of velocity and water level and continuous calculation of discharge. *Source*: SonTek, a Xylem Inc. (with permissions from Xylem)

2.3 Real-Time Flow Monitoring

Two examples of real-time water level sensor applications are illustrated below. The US Geological Survey (USGS) has established a network of real-time water level monitoring stations on rivers across the United States (Fig. 10). In these stations, real-time water level is typically recorded at 15- to 60-min intervals using a combination of the water level sensors described below. Data are stored on data loggers installed at each station and then transmitted to the USGS offices every 1–4 h via satellite, telephone, and/or radio telemetry. Typical weekly output is shown in Fig. 11.

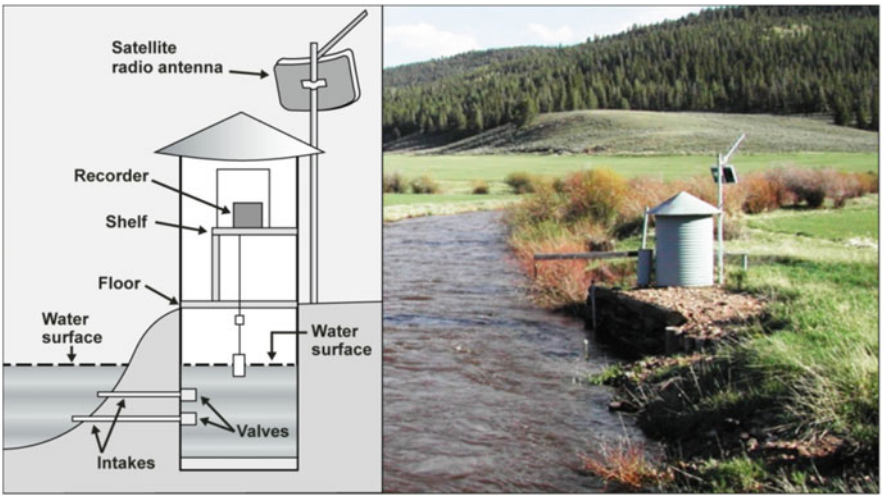

Fig. 10 Illustration and photo of a typical USGS water level monitoring station. *Source*: USGS [2] (public domain)

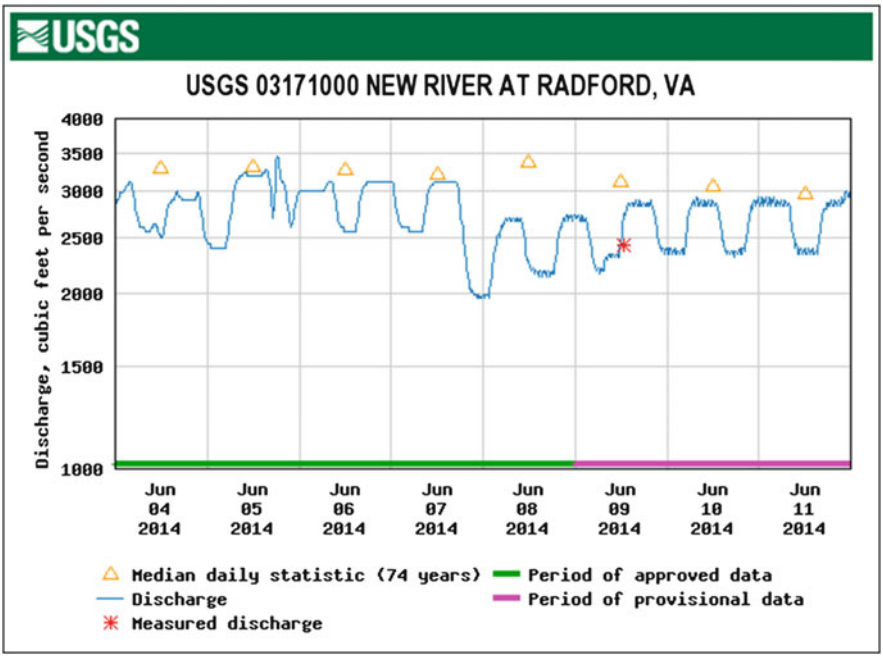

Fig. 11 Recorded water level data from the New River at Radford, Virginia (USGS Site: 03171000), for the period 4–11 June 2014. *Source*: USGS National Water Information Web Interface (public domain)

3 Monitoring Water Quality

Water quality sensors are used to measure parameters that indicate the symptoms of possible water degradation. For example, very low dissolved oxygen concentration is a good indicator of a possible anaerobic condition, which can have a detrimental impact on aquatic living resources. Diagnostic water quality monitoring is often performed to obtain baseline water quality information that identifies the possible causes of water quality degradation. Commonly monitored parameters include measurements of water temperature, pH and conductance, dissolved oxygen content, turbidity, and algal biomass. Results of diagnostic monitoring are usually used to plan more elaborate water monitoring programs for water pollution control purposes.

Discrete water quality monitoring involves limited onsite measurements, point water sampling, and laboratory analysis. Discrete water quality monitoring does not capture sudden temporal changes in water quality (e.g., spills). Furthermore, discrete measurements are usually implemented during the day when it is practical to deploy field crews. Because discrete water quality measurements are usually made during the day, problems such as nighttime changes in dissolved oxygen, hypoxia, or anoxia often go undetected.

Various types of water quality sensors have been developed for water quality monitoring. These include physical sensors, chemical sensors, optical sensors, and biosensors. Water quality sensors can be part of single- or multiparameter handheld instruments for discrete water quality monitoring, a component of a multiparameter data sonde which is typically used for continuous and unattended water quality monitoring, or they can be a single sensor connected to a data collection platform (DCP) for real-time monitoring. An overview of water quality sensors and their application is provided below.

3.1 Physical Sensors

Physical sensors can measure physical properties of water such as water temperature and electrical conductivity.

3.1.1 Water Temperature Sensors

Chemical and biological process rates in natural water are temperature dependent and affect the optimal health of living resources in water. The dissolved oxygen content of water, rates of photosynthesis and respiration, and living resource sensitivity to diseases, parasites, and toxins are all temperature dependent. Thermal stress on living resources can lead to the migration of living resources out of an area in search of more optimal conditions and in some cases death [7]. Water temperature is a not only a staple measurement for water resource managers, but it is also a critical sensor in most multiparameter instruments because other sensor measurements are temperature dependent and need to be temperature corrected.

Water temperature sensors measure temperature with a high-precision thermistor. Thermistors contain a resistor, whose resistance changes with temperature, housed inside a thin-walled sleeve of heat conductive, corrosion-resistant material (e.g., titanium). The change in resistance is directly proportional to the change in temperature and the resistivity of the resistor material, which is a constant. A low-voltage direct current (DC) is passed through the resistor to measure a voltage drop, and the related temperature is calculated from a manufacturer-specific algorithm. Since initial invention, the core sensing technology of thermistors has largely remained unchanged; however, advances in electronics and microprocessors have made today's sensors more accurate and stable than their predecessors.

3.1.2 Conductance Sensors

Conductance or electrical conductivity is a measure of water's ability to pass an electric current which can be used as an indicator of water quality. Streams and rivers usually have a constant range of baseline conductivity. The baseline conductivity in streams and rivers is affected by the chemical composition of the water, which is primarily determined by the geology of the stream/river bank and bed. Sediments which contain salts and inorganic dissolved solids that readily ionize in water result in high conductivity, while inert material, such as granite bedrock that does not ionize in water results in low conductivity. Change in baseline conductivity is an indicator of change in water quality that may be caused by evaporation, flooding, pollutant intrusion via stormwater runoff, or other contaminant discharges into surface water systems. For example, an oil spill would result in reduced conductivity levels because of the presence of hydrocarbons and alcohols, while an untreated sewage discharge would increase conductivity levels due to the presence of nitrates and phosphates [8].

Conductivity is directly related to water temperature, and therefore it is often expressed as conductivity at 25 °C, otherwise known as specific conductance. Conductivity sensors measure an electrical current flow through one or more pairs of electrodes and the water sample. A voltage is applied between a pair of electrodes that are a known distance apart from one another. The resistance of water and its chemical composition results in a voltage drop which is indirectly related to the conductivity of water, measured per centimeter, and expressed in units of μS/cm. Like thermistors, the core sensing technology of conductivity sensors has largely remained unchanged since the 1950s. However, these sensors have become more stable and accurate due to advances in electronics and microprocessors.

Other water quality parameters that can be calculated from conductivity are salinity and total dissolved solids (TDS). Salinity and conductivity are strongly correlated, and salinity is commonly calculated from conductivity and temperature measurements by manufacturer algorithms that follow Standard Methods for the Examination of Water and Wastewater (Standard Method #2520 [9]). TDS, commonly expressed in mg/L concentrations, is calculated from conductivity and a monitoring location-specific empirically determined coefficient (Standard Method #2510 [9]). Many sensor manufacturers provide capability to automatically

calculate TDS concentrations from that empirically determined coefficient that the user inputs into the instrument.

3.2 Chemical Sensors

Chemical sensors are used to measure chemical properties of water such as pH, dissolved oxygen, and some pollutants such as nitrate, ammonium, and chloride.

3.2.1 pH Sensors

By definition, pH is a measure of hydrogen ion concentration and indicates level of acidity or alkalinity in water. pH is measured on a log scale from 0 to 14; each whole pH unit represents a tenfold change in the concentration of hydrogen (H^+) and hydroxide (OH^-) ions. The pH of water has a direct impact on living resources and can affect the toxicity and solubility of chemicals, heavy metals, and other pollutants such as phosphorous and other nutrients [10]. In freshwater lakes, changes in pH can increase nutrient solubility and plant uptake, resulting in increased plant growth and ultimately eutrophic conditions. Fluctuations in pH levels are often caused by anthropogenic sources of pollution, such as the combustion of fossil fuels, smelting and mining operations, agricultural runoff, and wastewater and industrial discharge. In many fish species, reproduction is impacted at pH levels below 5.0, and death often occurs when levels drop below 4.0, while gill and skin damage can occur at higher pH levels [11].

Historically, pH sensors have consisted of a glass sensing bulb filled with a stable pH solution (usually 7) that experiences constant binding of H^+ ions, a reference electrode, and a potentiometer. When the sensor is placed into the water where the H^+ ions vary, the differential of H^+ ions creates an electrical potential (mV) which is compared to the stable potential of the reference electrode. The electrical potential is related to pH values through a form of the Nernst equation, a formula that describes the potential of the electrochemical cell as a function of the concentrations of the ions taking part in the reaction. Through the continued miniaturization of electronics and microprocessors, the signal processing electronics in today's sensors have been placed in very close proximity to the sensing element, resulting in decreased interference and increased sensitivity, accuracy, and stability.

3.2.2 Dissolved Oxygen Sensors

Dissolved oxygen is one of the most critical water quality parameters. Natural water systems produce and consume oxygen, and therefore, dissolved oxygen levels exhibit diurnal variability as well as seasonal variability. Atmospheric exchange and plant photosynthesis add oxygen to the system while respiration, decomposition,

and biochemical demand consume oxygen. Typical daily dissolved oxygen peak in natural waters occurs in the late afternoon at the height of photosynthesis and minimum level at dawn after a night of respiration. When algal blooms are fueled by nutrient enrichment, these daily variations in dissolved oxygen can be significant and can result in fish kills if dissolved oxygen level drops below critical thresholds. Seasonal variation of dissolved oxygen can result in hypoxic and anoxic conditions in natural waters during the warm summer months when water temperature reaches maximum levels and algal biomass peaks, which can stress and kill living resources.

The first practical dissolved oxygen sensor for field measurement was developed in the early 1960s. These early sensors required continuous replenishment of oxygen through the membrane which was achieved by either moving the sensor through the water column or by using an electric stirrer to move oxygen across the membrane. These sensors remained largely unchanged until the early 1990s when stirring-independent electrochemical dissolved oxygen sensors were developed, thereby enabling more efficient unattended continuous water quality monitoring.

Electrochemical dissolved oxygen sensors consist of a gold cathode and silver anode in an electrolyte solution that is trapped over the sensing elements by an oxygen permeable membrane. Oxygen molecules diffuse through the membrane at a rate proportional to the pressure difference across the membrane and are reduced at the gold cathode producing an electrical signal between the cathode and the anode. The partial pressure of oxygen in the water is proportional to the amount of oxygen diffusing through the membrane. The partial pressure of oxygen can be barometrically compensated to yield a percent saturation value, which can then be converted to a dissolved oxygen concentration value by compensating for temperature and salinity [12]. These electrochemical sensors require some level of flow in order to replenish the oxygen through the membrane resulting in electrochemical reduction of oxygen molecules. More advanced optical dissolved oxygen sensors which eliminate that problem are described under optical sensors.

3.2.3 Nitrate, Ammonium, and Chloride Ion-Selective Electrode Sensors

Nitrate, ammonium, and chloride are important measures of aquatic health and can have significant impacts on living resources. Excess levels of nitrate can lead to eutrophication, and excess levels of ammonium and chloride can lead to living resource toxicity. Additionally, excess levels of chloride can lead to impacts comparable to excessive TDS levels. Similar in design to pH sensors, there are a range of ion-selective electrodes (ISEs) available for the measurement of parameters, most commonly nitrate, ammonium, and chloride. These sensors work exactly like pH sensors except that a PVC membrane, selective for the analyte, is used rather than a glass bulb that is selective for H^+ ions. The sensor module contains a static concentration of the analyte, which binds to the inner membrane. The measured electrical potential is related to the analyte values through a form of the Nernst equation. These sensors only work in freshwater due to ion interferences. Optical nitrate sensors offer several advantages over ISEs and are described in Sect. 3.3.5.

3.3 Optical Sensors

Optical sensors, the most advanced technology for water monitoring, are used to measure water quality parameters such as dissolved oxygen, pH, turbidity, chlorophyll, cyanobacteria, dissolved organic matter, hydrocarbons, and nitrate. Figure 12 shows a typical optical sensor design. Optical sensors offer several advantages over electrochemical sensors, particularly in terms of calibration stability, antifouling capability, and long-term deployment capability. However, these sensors can be susceptible to optical interference and may require a high level of ground truthing which means more field technician involvement and verification. Additionally, results from these sensors are not always comparable between manufacturers, and universally recognized calibration standards may not be available [13]. Despite those challenges, optical sensors provide a significant opportunity for long-term monitoring and evaluating the status and trends of water quality at fixed water monitoring locations. Some typical optical sensor applications are described below.

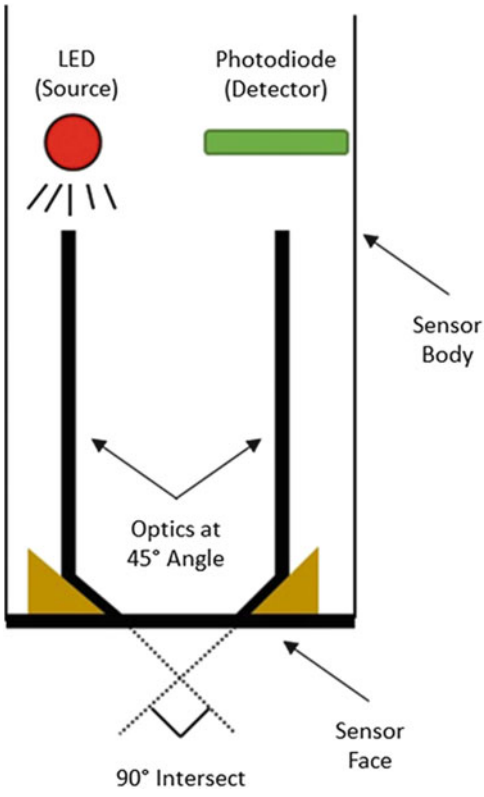

Fig. 12 Typical optical sensor design for multiparameter sondes showing the emitting light source (LED), optics, and the detector (photodiode). *Source*: Second author

3.3.1 Optical Dissolved Oxygen Sensors

In the mid-2000s, optical dissolved oxygen sensors became widely available. Optical dissolved oxygen sensors use a permeable membrane through which dissolved oxygen molecules diffuse without electrochemical reduction of oxygen molecules. These sensors utilize a special dye, light-emitting diodes (LEDs), and photoreceptors; the dye luminesces red when excited with a blue LED and is detected by the photoreceptor. The dye's ability to luminesce is quenched in the presence of oxygen. Stability and accuracy of the sensor is increased by using a secondary reference red LED which is reflected back to the photoreceptor. The partial pressure of oxygen in the water is proportional to the amount of oxygen diffusing through the membrane and can be measured by the lifetime of the luminescence from excitation by the blue light compared to that of the reference value (red light). The partial pressure of oxygen can be barometrically compensated to yield a percent saturation value, which can then be converted to a dissolved oxygen concentration value by compensating for temperature and salinity [11].

Optical dissolved oxygen sensors are almost exclusively smart sensors, each with their own microprocessor housed within the sensor. These sensors are also typically designed for use with antifouling systems such as wipers, making them an ideal solution for long-term monitoring. Optical sensors have significantly low maintenance requirement and increased support for long-term deployments. These sensors are incredibly stable and exhibit significantly less calibration drift than the electrochemical sensors.

3.3.2 Turbidity Sensors

Turbidity sensors measure the clarity of water and can be used as a surrogate for the amount of suspended material in the water (e.g., soil particles, plankton, and microbes). Increased levels of turbidity absorb more heat and can result in warmer water temperatures. Excess turbidity reduces light availability which can have an impact on submerged aquatic vegetation and photosynthesis and dissolved oxygen production. Suspended materials in the water column can also add stress to living resources through gill blockage and increased disease susceptibility. Benthic macroinvertebrates, fish eggs, and bivalves can be smothered as particles settle out of the water column. Common causes of high turbidity include runoff from urban stormwater, construction sites, agricultural practices, logging activity, and point source discharges [14].

Turbidity can be measured by one of the three main methods: transmissometer, backscatter, and nephelometer (Fig. 13). All of these methods measure turbidity by illuminating the water sample volume with a light source and measuring the intensity of light scattered by the particles in the water at a set angle with an optical detector (e.g., photodiode). Most multiparameter water quality sondes utilize sensors that measure turbidity via the nephelometric method. For this method, the light

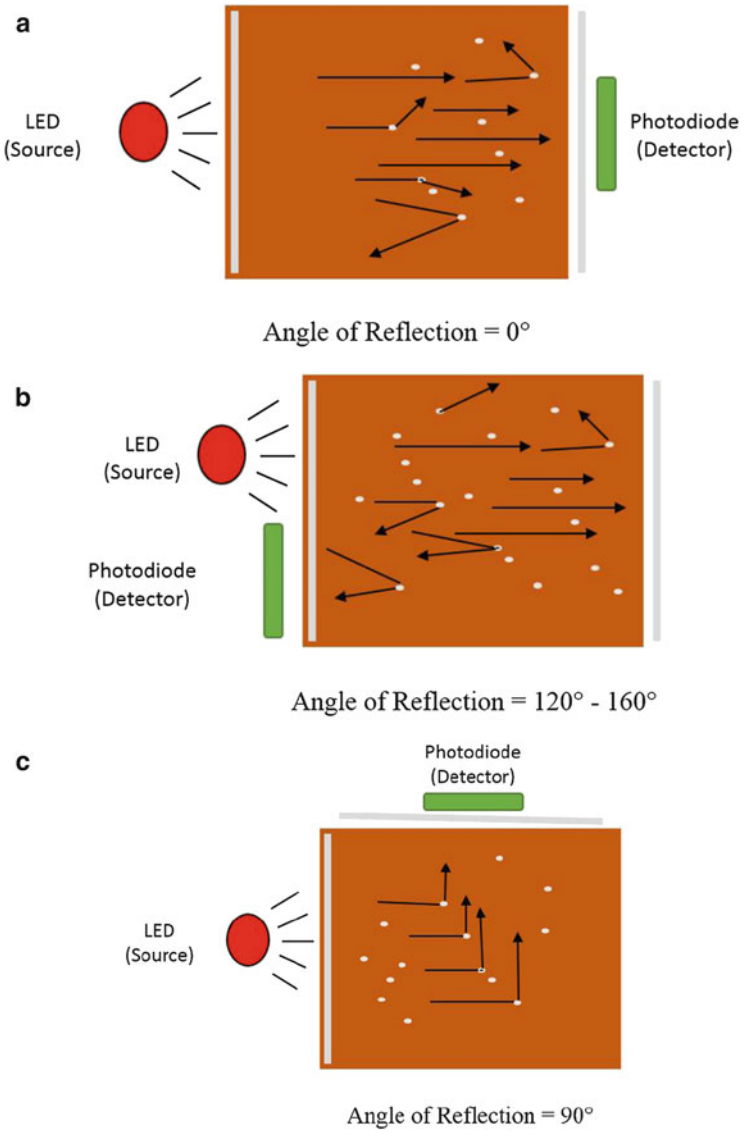

Fig. 13 Turbidity measurement methods: (**a**) transmissometer method, (**b**) backscatter method, and (**c**) nephelometric method. *Source*: Second author

source is typically infrared and the angle of particle reflection is 90°. The measurement units of these sensors are Nephelometric Turbidity Units (NTUs) or Formazin Nephelometric Units (FNUs).

3.3.3 Chlorophyll and Cyanobacteria Sensors

Chlorophyll and cyanobacteria sensors measure the amount of algal biomass in the water, which is an indication of the primary production capability of the system, and the overall health of the water body. Too little algae in the system can result in a lack of food for larger zooplankton and a lack of dissolved oxygen. An overabundance of algae in the system can be indicative of eutrophication and can result in reduced light penetration and sags in dissolved oxygen during peak periods of respiration or when the algae die off and are decomposed by the microbial loop. Some algal blooms can also produce toxins which may be harmful to living resources and/or human health. Algal biomass is measured by exciting the chlorophyll and phycobilin pigments in the algal cells with an LED of specific wavelengths and measuring the intensity of the emitted light, which is proportional to the concentration of the algal biomass. The excitation and emission wavelengths of these sensors vary for different manufacturers; as an example, for YSI EXO total algae sensors, the emission is 685 ± 20 nm, the chlorophyll excitation is 470 ± 15 nm, and the phycocyanin excitation is 590 ± 15 nm.

3.3.4 Optical Nitrate Sensors

Optical nitrate sensors operate on the principle that nitrate ions absorb ultraviolet (UV) light (wavelengths less than 220 nm) which is measured by a photometer and then converted to a nitrate concentration. Optical nitrate sensors are designed to convert spectral absorption properties measured to a nitrate concentration by using laboratory calibrations and integrated algorithms that account for interferences from other absorbing ions and organic matter. These sensors allow for real-time nitrate measurements without the need for chemical reagents and demonstrate good in-stream accuracy, typically within 3–5 % of laboratory data [15].

Optical sensors offer numerous advantages over ion-selective electrodes (ISEs) and wet chemistry analyzers including higher resolution, accuracy, precision, measurement range, chemical-free operation, faster response time, and the benefit of additional spectral information. However, these instruments are currently very power hungry and require some form of infrastructure for deployment (e.g., DCP station with solar power). Figure 14 illustrates the results of real-time nitrate concentrations measured by optical nitrate sensors (reported as nitrogen) and streamflow (discharge) in Smith Creek near New Market, Virginia (USGS Site 01632900).

Fig. 14 Real-time nitrate measurements (in mg/L as nitrogen) collected with an optical nitrate sensor and calculated discharge (cubic feet per second) from Smith Creek near New Market, VA, USA (USGS Site 01632900), for the period 27 March–23 April 2014. *Source*: USGS National Water Information Web Interface. *Source*: USGS (public domain)

3.3.5 CDOM Sensors

Fluorescence-based optical sensors are designed to measure the fluorescent fraction of colored dissolved organic matter (CDOM). Therefore, these sensors are typically referred to as FDOM sensors. FDOM sensors can be used to assess terrestrial influences in streams and rivers, to track pollution discharge, to map plumes of high or low dissolved organic carbon (DOC) in adjacent waters, to assess the amount of light absorbed by dissolved constituents in the water, and to assess the dispersion of point source pollution from anthropogenic wastes. Similar in design to chlorophyll and cyanobacteria sensors, FDOM sensors use a UV light source to excite organic matter particles and measure the emission. Some FDOM sensors are available that have been specifically tuned to both refined and crude hydrocarbons.

3.4 Biosensors

A biosensor is a device that detects, records, and transmits information regarding a physiological change or the presence of various chemical or biological materials in

the environment; it integrates a biological component, such as a whole bacterium or a biological product (e.g., an enzyme or antibody) with an electronic component to yield a measurable signal [16]. A biosensor system consists of bio-recognition layer or receptor, transducer, and electronic display system.

Biosensor systems are categorized according to the type of transducer used in the system: optical, electrochemical, and acoustic. Optical biosensors use fiber-optic probes that detect change in optical density for a range of wavelengths (~750 nm) that can be correlated to analyte concentration. Some optical sensors such as surface plasmon resonance (SPR) sensors use fluorescence to amplify the signal and increase the sensitivity of the sensor. Electrochemical biosensors use electrodes that measure the electric current produced by the oxidation or reduction of electroactive species. Electrodes are made of metals such as platinum, gold, silver and stainless steel, or carbon-based materials that are inert at the potentials at which the electrochemical reaction takes place. Acoustic biosensors use membranes made of chemically interactive material that detect changes in resonant frequency of an antigen. Acoustic sensors contain a crystal resonator, usually quartz, connected to an amplifier whose resonant frequency is a function of the properties of the membrane.

Biosensors are applied in a wide variety of fields such as medical diagnostics, bioweapons, agricultural and food processing industries, and environmental sciences. The integration of biosensor technology in real-time water quality monitoring is an upcoming technology. As typical applications, uses of biosensors to detect pathogens and toxins are discussed below.

3.4.1 Pathogen Detection

Technologies for early warning and rapid detection of pathogens are critical for human health protection. *E. coli*, a pathogenic microorganism, is often used as an indicator of fecal contamination in water. Several advanced techniques such as PCR (polymerase chain reactions) and RNA (ribonucleic acid) probes that identify *E. coli* DNA are developed to detect *E. coli* presence in water. However, these techniques can take up 1 or 2 days to obtain results. Only a few technologies have been developed that allow real-time or rapid detection of *E. coli*. Although there have been significant advances in biosensor technology during the last decade, there are still several shortcomings of biosensors. The most widespread problems include limited capability for real-time and spatial measurements, as well as durability, specificity, and the cost of the technology. Typical examples from available scientific literature are discussed below.

Radke and Alocilja [17] developed a technique for real-time detection of *E. coli* O157:H7 in water. The technique is called nucleic acid sequence-based amplification (NASBA) method. The system consists of a high-density gold microelectrode array biosensor fabricated from silicon with a 2-μm layer of thermal oxide as an insulating layer with an active area of 9.6 mm^2. To create a biological sensing surface, the sensor surface is functionalized for bacterial detection using heterobifunctional cross-linkers and immobilized polyclonal antibodies. Bacteria in the

water sample become attached to the immobilized antibodies, and the change in impedance caused by the bacteria is measured over a frequency range of 100 Hz–10 MHz. Heijnen and Medema [18] also developed a rapid real-time NASBA method for the detection of *E. coli* in water. In their method, a fragment of the clpB-mRNA is amplified, and a specific molecular beacon probe is used to detect the amplified mRNA fragment during the NASBA reaction. This method can produce results within 3–4 h. These studies demonstrate that the NASBA method has high potential as a rapid test for microbiological water quality monitoring.

Nanotechnology has opened new avenues of research for early warning and detecting pathogens in water. In the United States, NASA's exploratory efforts to detect water and biological traces on the planet Mars have delivered important discoveries that are applicable to developing ultrasensitive biosensors [19]. The major components of the biosensor are carbon nanotubes: tubes of graphite about 1/50,000th the diameter of a human hair. These biosensors use nucleic acids bound to *E. coli* or other pathogens of interest to create an electrical change and send a signal. Early Warning, Inc., a spin-off from NASA's Research Center, has developed a working version of the NASA biosensor calibrated to detect the bacteria strain *E. coli* O157:H7 in water, and its commercial Biohazard Water Analyzer can be configured to test for a suite of waterborne pathogens including *E. coli*, *Cryptosporidium*, *Giardia*, and other bacteria, viruses, and parasitic protozoa. The biosensor operates in the field via a wired or wireless network allowing for rapid detection of pathogenic contaminants [19].

3.4.2 Toxin Detection

Microorganisms are increasingly used as specific devices for sensing biologically relevant concentrations of pollutants [20]. For example, Fiorentino et al. [21] developed a whole-cell bacterial biosensor for measuring aqueous concentrations of aromatic aldehydes.

Recent research exploits the known characteristics of photosystems, which convert light energy into chemical energy, to detect changes in the process of photosynthesis of algae in water under environmental stress. Algae are sensitive to toxins in water. Using chlorophyll, a biological molecule found in photosynthetic organisms such as algae, fluorescence to detect toxins in water is a relatively new idea. The chlorophyll fluorescence detection provides information about the efficiency of photosynthesis as well as insight on how tolerant the organism is under certain environmental stresses and the effect of those stresses on the photosynthetic process.

Researchers at the Oak Ridge National Laboratory (ORNL) in the United States have utilized naturally free-living algae in water to investigate the impact on the chlorophyll fluorescence produced by algae in the presence of the chemicals [22]. Results are reported for paraquat, methyl parathion, potassium cyanide, diuron, and atrazine concentrations in water. The study shows that algae are capable of detecting very minute concentrations of the toxins in water.

3.4.3 Futuristic Biosensors

Research and development of innovative and real-time biosensor technologies are underway. For example, the system called TIGER (Triangulation Identification for the Genetic Evaluation of Risks) is a type of mass biosensor that detects microorganisms in the water and evaluates their potential risk [23]. Automated water analyser computer supported system (AWACSS) which is based on immunochemical technology can measure a variety of organic pollutants in water at the low nanogram per liter level in a single few-minutes analysis without the need of any pre-concentration or pretreatment steps [24]. AWACSS is equipped with a software package for remote control and web-based networking between the measurement and control stations, global management, trend analysis, and early warning applications. Lu et al. [25] reported on detecting *E. coli* O157:H7 in water that use a remote query (wireless) magnetoelastic sensor platform. Researchers are also developing robotic biosensors that imitate the appearance of fish and are capable of moving around in the water and sensing water properties (e.g., [26]).

4 Water Quality Monitoring Devices

Electronic handheld instruments for discrete water temperature and conductivity measurements have been around since the 1950s, but more advanced sensors such as dissolved oxygen and pH became available in the early 1960s. These instruments range the gamut from simple single parameter thermistors for measuring water temperature to more complex multiparameter instruments (described below) capable of being equipped with multiple physical, chemical, and optical sensors. Many of today's instruments are capable of being calibrated by the end user with known standards and feature digital displays, data logging capability, and in some cases built-in GPS for data georeferencing. Historically, these instruments have been used for fixed period measurement regimes (e.g., daily, weekly, or monthly) and have augmented water quality sample collection for subsequent laboratory analysis. As a result of electronic and sensor developments over the last 60+ years, these instruments have become extremely accurate and are standard for many monitoring programs today (Fig. 15).

The first multiparameter data sondes were introduced in the late 1960s, but their early use was primarily limited to discrete water quality measurements. It wasn't until the late 1980s/early 1990s that multiparameter data sondes advanced to the point that they were practical to use for continuous unattended water quality monitoring, providing temporally intensive data records (e.g., every 15 min).

Multiparameter water quality sondes are capable of being equipped with multiple physical, chemical, and optical sensors (Fig. 16). These instruments typically feature a built-in data logger, internal batteries for unattended deployment, antifouling capabilities (e.g., copper alloys and wipers) for increased deployment

Fig. 15 Examples of handheld water quality instruments for discrete measurements. *Source*: YSI and Xylem [with permissions from YSI and Xylem]

Fig. 16 Examples of multi-parameter water quality instruments and smart sensors for continuous monitoring. *Source*: YSI and Eureka [with permissions from YSI, Xylem and Eureka]

duration, and are capable of being calibrated by the end user with known standards. These instruments also feature multiple communication options for setup, calibration, deployment configuration, data downloading, and connection to a DCP or telemetry system (e.g., Bluetooth, RS-232, SDI-12, RS-485).

Over the past 60 years, electronics and sensor technology have advanced from analog to digital, resulting in more stable electronics and higher sensor accuracies. This in turn has resulted in instruments that are more accurate (due to reduced signal interference), hold their user calibration longer without drift, and have become more widely accepted as alternatives to laboratory analysis. These advances have also resulted in the advent of smart sensors. Smart sensors typically will have a microprocessor in the same sensor housing as the sensing electronics, making them digital instruments that store their own calibration, allowing them to be transferred from one multiparameter instrument to another without the need to recalibrate. Some of these smart sensors can even be connected directly to a DCP, in some cases negating the need for a multiparameter data sonde all together.

5 Data Collection and Transfer Platforms

Discrete water quality measurement programs only provide a snapshot in time much like a photograph. Continuous and unattended water quality monitoring programs provide a stream of data on conditions, similar to a movie, which results in a better understanding of environmental processes and the ability to capture data during episodic events, especially at times when it is impractical and dangerous to be in the field. Temporally intensive monitoring programs yield a wealth of data to water resource managers and provide valuable insight into the impacts of intense storms, low dissolved oxygen events, fish kills, and harmful algal blooms, among others.

Temporally intensive, continuous water monitoring programs are valuable for understanding and assessing water quality conditions and living resource habitats and guiding watershed restoration activities. A common observance among monitoring programs, after the implementation of continuous water quality monitoring, is the true magnitude of daily dissolved oxygen fluctuations. Many conventional shallow water monitoring programs sample dissolved oxygen during the day when it is practical to sample, often measuring at the peak of photosynthesis and find dissolved oxygen levels that are considered sufficient for supporting living resources. However, these programs miss measuring nighttime dissolved oxygen levels. With continuous monitoring, water resource managers have found that many of these shallow water systems have large daily swings in dissolved oxygen concentration and, actually, go hypoxic or anoxic at night when photosynthesis ceases and respiration significantly increases. These large fluctuations can lead to fish kills in waters affected by algal blooms due to excess nutrients. Figure 17 shows an example of daily dissolved oxygen fluctuations.

While some multiparameter water quality data sondes operate off of internal batteries and have their own internal data logger, many other sensors do not. Therefore, many monitoring stations utilize a DCP. The DCPs integrate multiple sensors together and provide power, data logging and control capability, and in many cases data telemetry. At their most basic level, DCPs consist of a data logger, one or more 12 VDC batteries, a solar regulator, and a telemetry module housed inside of a weatherproof enclosure, with one or more external solar panels, a telemetry antenna, and some form of lightning protection. The data logger is the heart of the system and initiates sensor measurements and controls functions based on time or events; controls external devices such as autosamplers, pumps, or valves; logs data; provides onboard data processing and computations; and interfaces with telemetry devices such as telephone modems (including cellular and voice synthesized), line-of-site radio transceivers, satellite transmitters, and Ethernet and Wi-Fi interfaces.

The data loggers, attached sensors, and telemetry devices are powered by 12 VDC batteries that are continuously charged by the external solar panels whose voltage is regulated by the solar regulator down to safe levels. The telemetry devices are connected to external antennas appropriate for the telemetry method.

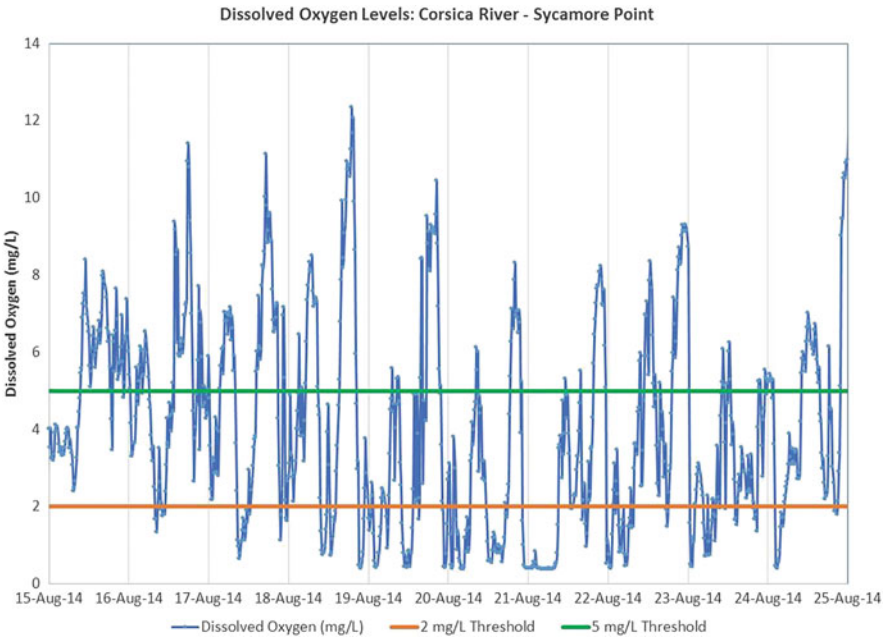

Fig. 17 Dissolved oxygen diurnal variability at Sycamore Point on the Corsica River in Centreville, Maryland (USA). Data were collected with a YSI 6600V2-4 data sonde and YSI ROX optical dissolved oxygen sensor suspended at 1 m below the surface (floating rig). *Source*: Maryland Department of Natural Resources (*Source*: Eyes on the Bay website [27]) (public domain)

The DCPs are grounded and protected to some extent from lightning strikes with the use of in-line lightning protectors in the telemetry antenna cables and in-line fuses in the sensor power feeds. Figure 18 shows a water quality monitoring station that includes a data logger, cellular telemetry system, solar panel, solar regulator, battery, water quality sensors, and meteorological sensors.

While standalone, temporally intensive monitoring programs provide a wealth of data and information not observed with discrete monitoring programs, they do not provide timely information. Telemetry is a great addition to any DCP because it provides real-time eyes on your data for quality assurance/quality control and for immediate decision support. Real-time data ensures that the user is collecting the highest quality data. For example, if a sensor drifts as a result of fouling, the user will know about it from observing the real-time data, and they can proceed to correct the problem by cleaning and recalibrating the sensor (or replace the drifting sensor with a freshly calibrated one) right away rather than waiting until the normal maintenance cycle only to find that some of the data are bad. It's inefficient and sometimes costly to deploy sensors (without real-time data) for a few weeks and then learn about a problem when the data is downloaded from the data logger. Telemetry also provides real-time alarming and alerting to changing conditions

Fig. 18 Example of real-time water quality and water level monitoring, DCPs for Watershed Monitoring. *Source*: Second author

(e.g., the onset of algal blooms or changes in water quality due to illicit discharges). Real-time alarming and alerting provides water resource managers with the information needed to make adaptive sampling and management decisions. For example, based on real-time data sampling, crews may be dispatched to collect additional data and water samples, or recreational water use bans may be implemented to protect public health from events such as harmful algal blooms.

6 Data Management and Quality Assurance/Quality Control

Data quality should be paramount above all else with a monitoring program. After all, in most cases monitoring programs are developed to collect data, so informed water resource management decisions can be made. Those management decisions will ultimately only be as good as the data they are based on. With all of the recent advancements in water sensor technology, it is easy to get heavily focused on the deployment, operations and maintenance of monitoring instrumentation, and the collection of massive amounts of temporally and spatially intensive data. Unfortunately, many monitoring programs get so focused on the physical collection of the

data; they fail to devote adequate time and effort required to quality assure (QA), quality control (QC), manage, and ultimately utilize those data.

Fortunately, advances in software to acquire, process, model, and publish water data have resulted in simplified data management, analysis, and information sharing to enable better decisions for the sustainable management of water resources. Common components of these software suites include capabilities for time series and discrete data analysis and management, rating curve development, modeling and forecasting, and data publishing with real-time alarming and alerting capability for changing conditions. Modern software systems can be deployed both in the cloud and in traditional enterprise environments (e.g., see Fig. 19). These software suites allow water resource managers to consolidate and protect their data, avoid inaccuracies, and facilitate adaptive management and collaboration. Users benefit from improved reporting and better decision making that will allow for the development of strategies and policies based on real-time checked and validated information. Additionally, water resource managers utilizing these software packages benefit from secure and QA/QC assured data that is auditable and defensible, giving stakeholders confidence in the decisions made based on those data. Water resource managers can use their resources wisely and efficiently and get the most from their sampling costs. Furthermore, these systems enable water resource managers to provide their stakeholders with information and insight, not just raw data.

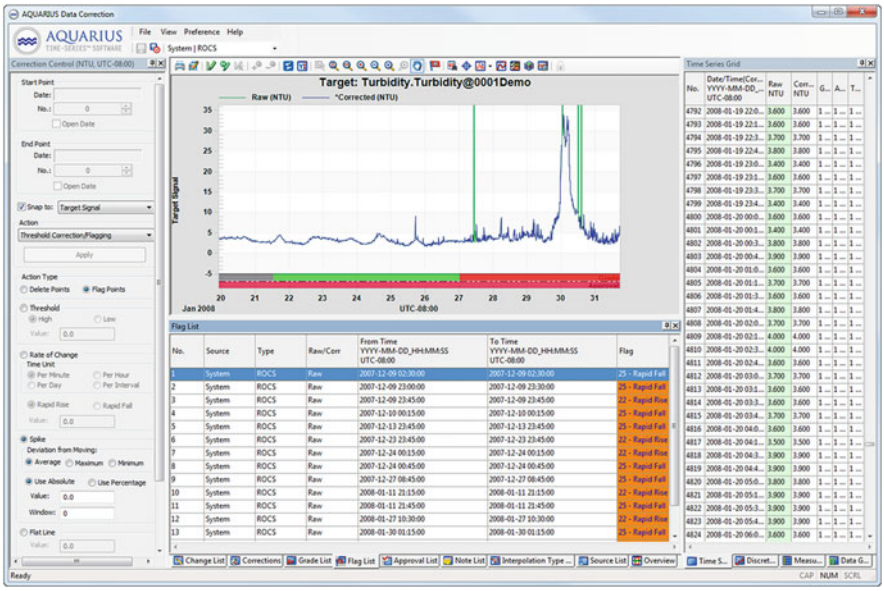

Fig. 19 Example of AQUARIUS Time-Series software for the acquisition, processing, quality assurance/quality control (QA/QC), modeling, and publishing of water data. *Source*: Second author

7 Limitations

Despite significant advances in technologies discussed in this chapter, not all water quality parameters of interest can be accurately and reliably measured with in situ sensor technology. In fact, most of the water quality parameters of interest still need to be analyzed in the laboratory from collected and processed water samples.

There are some instruments available that are a hybrid between in situ sensors and laboratory analyses. These instruments bring the laboratory to the field. Micro volumes of whole water samples are collected by these analyzers via pumps, and then the sample is mixed with analyte-specific reagents to induce a chemical reaction. A colorimetric measurement is then made by the analyzer to determine the concentration of the analyte in the water sample. These instruments are available from a handful of manufacturers to measure phosphate, nitrate, nitrite, ammonia, silicates, total phosphorous, total nitrogen, total dissolved iron, and sulfide. Many of these instruments measure only one parameter; however, some of these instruments can measure up to four parameters sequentially. The two largest drawbacks to these instruments are sample processing time and the necessity to deal with chemical reagents and wastes. For these reasons, these instruments have not been as widely accepted into monitoring programs as sensor technologies.

While this chapter covers advances in water monitoring technologies, it does not address topics such as which monitoring techniques are most appropriate for data collection needs or how to deploy and maintain monitoring technologies in the field. There are many resources available on these topics, particularly from sensor manufactures, state and federal monitoring organizations, and independent workgroups. One particularly useful resource is the Field Deployment Guide developed by the Aquatic Sensor Workgroup (ASW) which is part of the Advisory Committee on Water Information's (ACWI) Methods and Data Comparability Board [28].

8 Conclusions

This chapter provides an overview of advanced in water sensor and real-time monitoring technologies and associated applications. Technologies discussed include various types of sensors for water quantity and water quality measurements, examples of commercially available water quantity and water quality monitoring devices, data collection and transport platforms, and data management and quality assurance/quality control for water monitoring. These technologies allow water resource managers and researchers to capture real-time water quantity and quality data during episodic events such as major storms. Real-time and continuous water monitoring can capture temporal changes and provides broader spatial coverage of

water quantity and quality in a watershed. Furthermore, it allows data collection when it is normally impractical with discrete sampling. Telemetry is a great addition to sensor technologies and DCP because it provides to user real-time data and ensures that the user is collecting the highest quality data. Advances in software to acquire, process, model, and publish water data have resulted in simplified data management, analysis, and information sharing to enable better decisions for the sustainable management of water resources.

In conclusion, water sensor technologies, associated computer hardware/software, and telemetry technologies are evolving fields of research and technology development. New and advanced technologies, for example, biosensors and various integrated technologies, provide exciting opportunities and challenges for futuristic water monitoring programs and aquatic ecosystem preservation.

Disclaimer This chapter provides an overview of water sensor technologies and associated fields. References are provided for informational purposes only and do not constitute endorsement of any manufacturers, websites, or other sources cited in this chapter.

References

1. Younos T (ed) (2003) Advances in water monitoring research. Water Resources, Littleton, p 230
2. Freeman LA, Carpenter MC, Rosenberry DO, Rousseau JP, Unger R, McLean JS (2004) Use of submersible pressure transducers in water-resources investigations. Techniques of water-resources investigations 8-A3. U.S. Geological Survey, Reston, p 50
3. NOAA (2011) Test and evaluation report: limited acceptance of the design analysis WaterLog® H-3611i microwave radar water level sensor. National Oceanic and Atmospheric Administration (NOAA) technical report NOS CO-OPS 061. Silver Spring, MD, p 55
4. NOAA (2013) Field installation guide field installation procedures for design analysis WaterLog® H3611i microwave radar water level sensor using the Sutron Data Collection Platform version 1.0. National Oceanic and Atmospheric Administration (NOAA), Ocean Systems Test and Evaluation Program, p 52
5. Mueller DS, Wagner CR (2013) Measuring discharge with acoustic Doppler current profilers from a moving boat. Techniques and methods 3-A22. U.S. Geological Survey, Reston, p 64
6. Levesque VA, Oberg KA (2012) Computing discharge using the index velocity method. Techniques and methods 3-A23, U.S. Geological Survey, Reston, p 148
7. USEPA (2012) 5.3 Temperature. In: Water: monitoring and assessment. http://water.epa.gov/type/rsl/monitoring/vms53.cfm. Accessed 5 Sept 2014
8. USEPA (2012) 5.9 Conductivity. In: Water: monitoring and assessment. http://water.epa.gov/type/rsl/monitoring/vms59.cfm. Accessed 5 Sept 2014
9. APHA (2014) Standard methods for the examination of water and wastewater, 22nd edn. American Public Health Association, American Water Works Association & Water Environment Federation, Baltimore
10. USEPA (2012) 5.4 pH. In: Water: monitoring and assessment. http://water.epa.gov/type/rsl/monitoring/vms54.cfm. Accessed 5 Sept 2014
11. Fondriest Environmental, Inc. (2014) pH of water. Fundamentals of environmental measurements. http://www.fondriest.com/environmental-measurements/parameters/water-quality/ph/. Accessed 5 Sept 2014
12. YSI Incorporated, a Xylem, Inc. Brand (2009) The dissolved oxygen handbook. W39 0909

13. Pellerin BA, Bergamaschi BA, Horsburgh JS (2012) In situ optical water-quality sensor networks—workshop summary report. USGS open-file report 2012–1044. https://www.cuahsi.org/PageFiles/Pellerin%20et%20al%202012_OpticalSensorWorkshopSummary_OFR.pdf
14. USEPA (2012) Turbidity. In: Water: monitoring and assessment. http://water.epa.gov/type/rsl/monitoring/vms55.cfm. Accessed 5 Sept 2014
15. Pellerin BA, Bergamaschi BA, Downing BD, Saraceno JF, Garrett JD, Olsen LD (2013) Optical techniques for the determination of nitrate in environmental waters: guidelines for instrument selection, operation, deployment, maintenance, quality assurance, and data reporting. Chapter 5 of Section D, water quality book 1, collection of water data by direct measurement. Techniques and methods 1-D5. http://pubs.usgs.gov/tm/01/d5/pdf/tm1d5.pdf
16. De Corcuera JIR, Cavalieri RP (2003) Biosensors. Encyclopedia of agricultural, food, and biological engineering, pp 119–123. doi:10.1081/E-EAFE120007212
17. Radke SM, Alocilja EC (2005) High density microelectrode array biosensor for detection of E. coli O157:H7. Biosens Bioelectron 20(8):1662–1667
18. Heijnen L, Medema G (2009) Method for rapid detection of viable Escherichia coli in water using real-time NASBA. Water Res 43(12):3124–3132
19. NASA (2014) NASA Office of Chief Technologist and NASA Spinoff. http://spinoff.nasa.gov/Spinoff2009/ps_1.html. Accessed 5 Sept 2014
20. Lei Y, Chen W, Mulchandani A (2006) Microbial biosensors. Anal Chim Acta 568:200–210
21. Fiorentino G, Ronca R, Bartolucci S (2009) A novel E. coli biosensor for detecting aromatic aldehydes based on a responsive inducible archaeal promoter fused to the green fluorescent protein. Appl Microbiol Biotechnol 82:67–77. doi:10.1007/s00253-008-1771-0
22. Rodriguez M, Greenbaum E (2009) Detection limits for real-time source water monitoring using indigenous freshwater microalgae. Water Resour Res 81(11):2363–2371
23. Ecker DJ et al (2006) The Ibis T5000 universal biosensor: an automated platform for pathogen identification and strain typing. J Lab Autom 11:341–351
24. Proll G, Jens T, Kaiser J, Kraemmer P, Sacher F, Stien J, Gauglitz G (2006) Advanced environmental biochemical sensors for water monitoring—automated water analyser computer supported system (AWACSS). In: Twardowska I et al (eds) Soil and water pollution monitoring, protection and remediation. Springer, Heidelberg, pp 131–144
25. Lu QH, Lin SG, Luo S, Cai Q, Grimes CA (2009) Wireless, remote-query, and high sensitivity *Escherichia coli* O157:H7 biosensor based on the recognition action of concanavalin A. Anal Chem 81:5846–5850
26. Meinhold B (2009) Monitoring water pollution with robotic fish. http://inhabitat.com/monitoring-water-pollution-with-robotic-fish/. Accessed 25 Aug 2014
27. Maryland Department of Natural Resources: Continuous Monitoring Current Results (2014) http://mddnr.chesapeakebay.net/newmontech/contmon/current_results_fullyear_graph.cfm?param=DOC&station=corsicariver&choose_date=22809&choose_range=7. Accessed 5 Sept 2014
28. Advisory Committee on Water Information, Methods and Data Comparability Board, Aquatic Sensor Workgroup (2010) Field deployment guide. http://www.watersensors.org/pdfs/ASW-Field-Guide-Rivers-web.pdf. Accessed 8 Oct 2014

Instrumenting Caves to Collect Hydrologic and Geochemical Data: Case Study from James Cave, Virginia

Madeline E. Schreiber, Benjamin F. Schwartz, William Orndorff, Daniel H. Doctor, Sarah D. Eagle, and Jonathan D. Gerst

Contents

M.E. Schreiber (✉) • S.D. Eagle • J.D. Gerst
Department of Geosciences, Virginia Tech, Blacksburg, VA, USA
e-mail: mschreib@vt.edu

B.F. Schwartz
Department of Biology, Texas State University-San Marcos, San Marcos, TX, USA

W. Orndorff
Virginia Department of Conservation and Recreation, Richmond, VA, USA

D.H. Doctor
U.S. Geological Survey, Reston, VA, USA

T. Younos, T.E. Parece (eds.), *Advances in Watershed Science and Assessment*, The Handbook of Environmental Chemistry 33,
DOI 10.1007/978-3-319-14212-8_8

Abstract Karst aquifers are productive groundwater systems, supplying approximately 25 % of the world's drinking water. Sustainable use of this critical water supply requires information about rates of recharge to karst aquifers. The overall goal of this project is to collect long-term, high-resolution hydrologic and geochemical datasets at James Cave, Virginia, to evaluate the quantity and quality of recharge to the karst system. To achieve this goal, the cave has been instrumented for continuous (10-min interval) measurement of the (1) temperature and rate of precipitation; (2) temperature, specific conductance, and rate of epikarst dripwater; (3) temperature of the cave air; and (4) temperature, conductivity, and discharge of the cave stream. Instrumentation has also been installed to collect both composite and grab samples of precipitation, soil water, the cave stream, and dripwater for geochemical analysis. This chapter provides detailed information about the instrumentation, data processing, and data management; shows examples of collected datasets; and discusses recommendations for other researchers interested in hydrologic and geochemical monitoring of cave systems. Results from the research, briefly described here and discussed in more detail in other publications, document a strong seasonality of the start of the recharge season, the extent of the recharge season, and the geochemistry of recharge.

Keywords Cave • Dripwater • Epikarst • Karst • Recharge • Subsurface monitoring

1 Introduction

Karst aquifers form from dissolution of soluble rock, including limestone and dolostone, by groundwater. Dissolved carbon dioxide promotes dissolution of these rocks, which enlarges fractures to form conduits and caves. Karst aquifers are vital water resources, providing approximately 40 % of drinking water supplies in the United States [1]. An estimated 25 % of the global population uses freshwater derived in part or entirely from karst sources [2].

Characterizing how karst aquifers are recharged is crucial for sustaining this critical groundwater resource. However, recharge processes in karst systems are difficult to characterize due to heterogeneity of the epikarst. Epikarst is defined as the interval of weathered and fractured bedrock that extends from the base of the soil zone to less weathered bedrock below [2]. The epikarst is often called the "skin" of karst aquifers [3], as it is a critical zone that significantly influences karst hydrology, water quality, and ecosystems. The epikarst controls both the quantity and quality of autogenic (internal) recharge to karst aquifers and, as a result, is a particularly important component of the system.

Due to the highly variable flow velocities and residence times within the epikarst, traditional methods to determine recharge generally do not work in epikarst, thus requiring specialized techniques. Continuous monitoring of physical and chemical characteristics of cave dripwater is one approach that can be used to test hypotheses and answer a variety of scientific questions about the epikarst system, including the biodiversity of epikarst communities (e.g., [4]), epikarst

hydrologic properties (e.g., [5]), epikarst hydrogeochemical properties (e.g., [6–8]), the influence of drip rates on isotopic composition of speleothems used for paleoclimate interpretation (e.g., [9–11]), and the impact of seasonal climatic variations on cave dripwater (e.g., [12, 13]), among other topics.

Approaches to measure cave drip rates include manual measurement of the timing between water droplets (e.g., [6, 14]); automated counting of water droplets by some triggering mechanism, such as a drum (e.g., [15, 16]), or passage by an electroluminescent diode (e.g., [12]); manual timed volumetric measurement by collection into a vessel of known volume; and automated volumetric measurement using a tipping bucket style gauge, generally a modified rain gauge ([5], among many others). Drop-counting methods suffer from the assumption of known and consistent volume per drop. This has been shown experimentally to vary, but there is a general mathematical relation between drop mass and the radius of curvature of the drip point of detachment [17]. The tipping bucket gauge approach is preferred for moderate to high-flow dripwater, but may suffer from inaccuracies at very high discharges. Decisions to use one method over another should consider these limitations.

One major advantage of using automated methods for hydrologic research in karst systems is the ability to collect high-resolution datasets over long time periods, from years to decades. Automated methods have greatly expanded over the past several decades as sensor, data storage, and battery technologies have improved. Data loggers can hold millions of data points, allowing for deployment of equipment for months at a time, depending on temporal measurement frequency. Thus, automated equipment has allowed for both higher resolution and longer term monitoring. Researchers can address more detailed research questions and return to repeatedly "mine" the dataset as additional questions regarding data of varying temporal resolutions emerge.

In addition to cave drip rates, sensors that measure specific conductance can be deployed in caves and programmed to collect data as frequently as needed, depending on the research need and available data storage. For example, Baldini et al. [10] and Shade and Veni [18] collected data on the rate and specific conductance of cave dripwater to examine connections between discharge and geochemical composition. Sensors for temperature, relative humidity, and barometric pressure are also available, easily deployable, and relatively robust under cave conditions. Other sensors, such as those for dissolved oxygen and pH, are currently less robust for use in caves and, depending on sensor type, can require more frequent calibration and may be subject to fouling. Sensors for turbidity, a parameter of interest at many sites affected by surface water, are available and robust, but are generally an order of magnitude more expensive than the aforementioned sensors.

Many studies on epikarst and cave dripwater have included geochemical sampling of the dripwater for a variety of constituents, including major ions, alkalinity, trace elements, organic carbon, and isotopes of water, strontium, and dissolved inorganic and organic carbon (e.g., see [6, 8, 13, 16, 19, 20]). Methods for sample collection of cave dripwater for geochemical analysis in these studies vary depending on whether individual or groups of stalactites are being targeted for sampling, the time period of collection, and the analytes of interest, many of which

can require specialized methods of collection (e.g., dissolved gases require gas-tight sampling methods; unstable analytes may require pre-preservation with acids or chemicals).

Although there have been many advances in cave instrumentation over the past several decades, there are few detailed descriptions of the instrumentation and data collection, processing, and management, leaving each new researcher to "reinvent the wheel." The objective of this chapter is to describe instrumentation for continuous measurement of hydrologic and geochemical parameters of cave dripwater, other hydrologic inputs such as precipitation and soil water, and outfalls such as a cave stream or spring. The instrumentation described herein was designed and deployed in James Cave, located in the doline-dominated karst systems of the Appalachian Great Valley in southwestern Virginia (USA). The overall goal of the James Cave research program is to evaluate the quantity and quality of recharge in karst systems. More details about the James Cave program are included in graduate theses by S. Eagle [21] and J. Gerst [22].

2 Study Site

The case study site, James Cave, is located in Pulaski County, Virginia (USA) (Fig. 1). James Cave is an ideal study site for three primary reasons: it is representative of caves in the Appalachian Great Valley; it is a short drive from the Virginia Tech campus; and it is accessible for installation and maintenance of instruments. These are important factors in selection of a site where frequent visits and equipment maintenance may be required. The study area is in a temperate climate zone, with an average annual temperature of 11.3 °C and an average annual precipitation of 92.4 cm (period of record: 1969–2009) [23].

James Cave is developed in limestones and dolostones of the Cambro-Ordovician Conococheague Formation (Fig. 2) in the Valley and Ridge physiographic province. Bedrock fracturing/jointing developed primarily as a result of the Pulaski fault system, a complex series of ENE-trending low-angle thrust faults [24, 25]. Soils overlying the cave are composed of Lowell silt loam and the Wurno–Newbern–Faywood silt loam [26], derived from residuum from weathered limestone and shale. Soils range in thickness from 0.25 to 2 m and rest directly on relatively unweathered bedrock with little saprolite development.

James Cave consists of approximately 2.3 km of cave passage, with a smaller section instrumented for this project (Fig. 3). There are two entrances to the cave, both located within sinkholes (Fig. 4). The source of the stream within James Cave is not well known. Based on the lateral extent of limestone around the field site and the lack of perennial sinking surface streams on the sinkhole plain, it appears that the cave stream is derived entirely from autogenic sources (i.e., dripwaters). During large storm events, it has been observed that overland flow enters the two entrances as well as other sinkholes within the likely watershed of the cave stream.

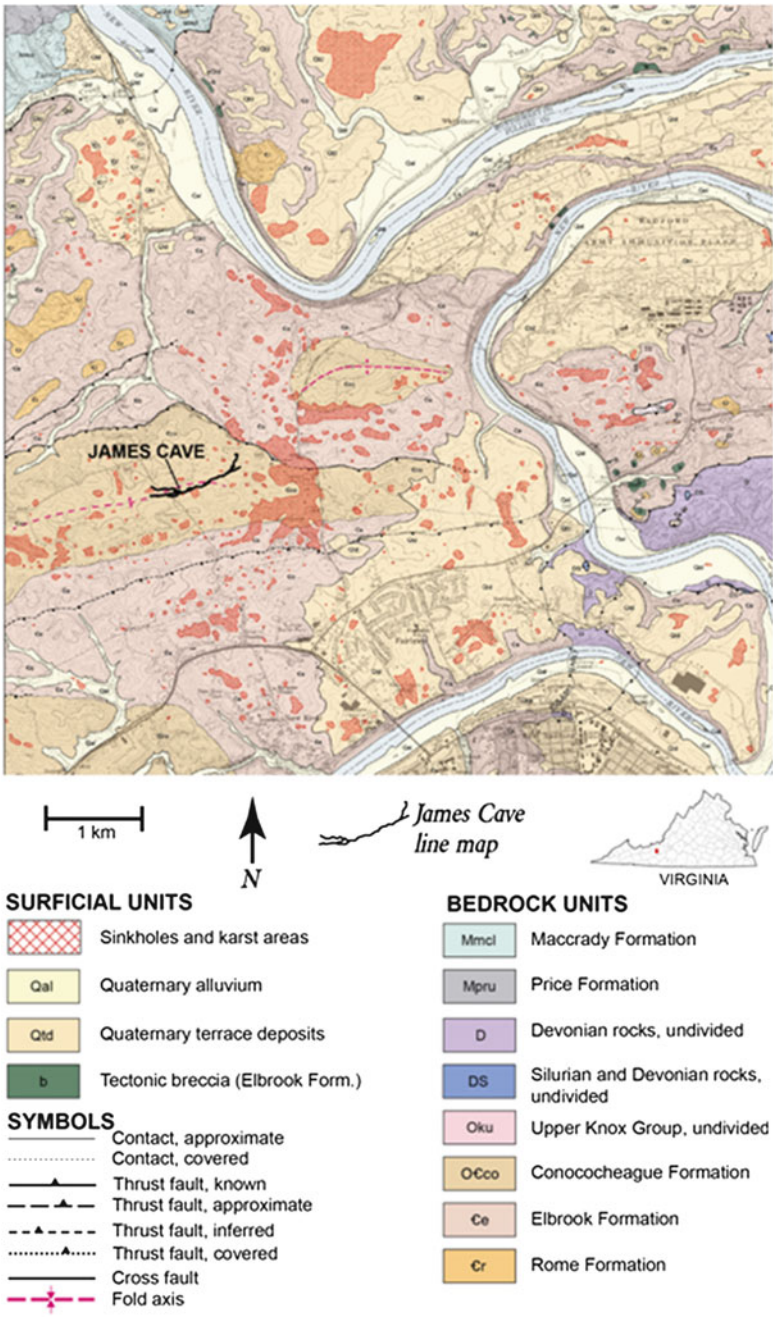

Fig. 1 Location map of James Cave and geologic map. Geologic data from Schultz and Bartholomew [25]

Fig. 2 Outcrop of a portion of the Conococheague Limestone above James Cave. A 30 cm thick dolomite bed caps the limestone, which contains thin dolomitic layers. Two knee pads, each about 20 cm long, are shown for scale (*Source*: Author)

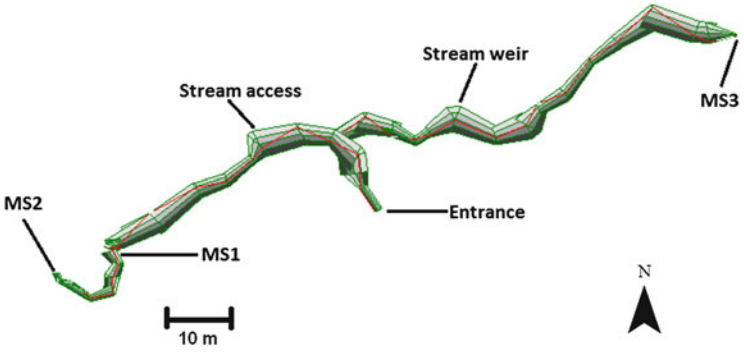

Fig. 3 Survey of James Cave monitoring stations. Data from T. Malabad

3 Instrumentation Methods

3.1 Instrumentation Design

The instrumentation of James Cave was designed to collect data to meet the main research objective, which was to characterize the quantity and quality of recharge, i.e., epikarst dripwater. During early discussions of study design, the research team consulted literature and experts working in similar settings and also used

Fig. 4 Sinkhole entrance of James Cave (*Source*: Author)

professional judgment to guide the choice of equipment. As temporal patterns were a priority, the decision was made to pursue automated monitoring to allow for collection of high-frequency data. Capturing the spatial patterns of dripwater rates in the cave was initially a priority, but the goal was impractical as there are only a few regions in the cave that have actively dripping stalactites.

During the planning stages, there was careful consideration given to the type of equipment to be installed, as both equipment and supplies had to withstand the continuous 100 % humidity and splashy conditions of a cave environment. Preference was given to off-the-shelf equipment, as equipment could then be easily modified, serviced, or replaced as needed. Also during planning, standard operating procedures for maintaining equipment, sampling, sample analysis, and data management were developed. These procedures are periodically revised and updated to reflect current conditions and evolving project objectives.

The final design for monitoring stations included a total of five stations with automated monitoring equipment: one surface station to collect climate data, three in-cave stations to collect dripwater data, and one stream station to collect stream data. Equipment was installed to collect continuous and grab water samples for geochemical analysis. Water samples were collected for precipitation, soil water, dripwater, and the stream. Table 1 shows the location of instrumentation and the parameters measured at James Cave. Table 2 provides details on the instrumentation, including manufacturer and part/model numbers. Table 3 presents the chronology of instrumentation from 2007 to 2012. The instrumentation has not changed since July 2012. Table 4 shows the data types for the data collected using the automated instrumentation. To date (2014), 7 years of hydrologic and geochemical data have been collected at the James Cave site. The discussion below provides details of the instrumentation and of instrument maintenance.

Table 1 Monitoring station location, instrumentation, and parameter being sampled

Station name	Location	Continuous air data	Continuous hydrologic data	Continuous hydrogeochemical data	Geochemical sample collection
Surface	Near cave entrance, ~605 m AMSL	Air temperature, relative humidity (2008–current)	Precipitation rate	–	Composite precipitation (2008–2012)
Soil entrance (lysimeter)	Near cave entrance, ~604 m AMSL	–	–	–	Grab soil water sample (2009–2012)
Soil 2 (lysimeter)	Surface projection of MS2, ~605.8 m AMSL	–	–	–	Grab soil water sample (2009–2012)
Soil 3 (lysimeter)	Surface projection of MS3, ~600 m AMSL	–	–	–	Grab soil water sample (2009–2012)
MS1	Subsurface, 597 m AMSL	Air temperature (2007–current)	Drip discharge (2007–current)	Water temperature, specific conductance (2011–current)	Composite drip sample (2008–2012)
MS2	Subsurface, 595.1 m AMSL	Air temperature (2007–current)	Drip discharge (2007–current)	Water temperature, specific conductance (2011–current)	Composite drip sample (2008–2012)
MS3	Subsurface, 593 m AMSL	Air temperature (2008–current)	Drip discharge (2008–current)	Water temperature, specific conductance (2011–current)	Composite drip sample (2008–2012)
Cave stream	Subsurface, ~592 m AMSL	–	Stream discharge (2009–current)	Water temperature, specific conductance (2011–current)	Grab stream sample (2008–2012)

Table 2 James Cave instrumentation, including manufacturer and part/model number

Item	Manufacturer	Part/model number
Multiparameter sonde	Hanna Instruments	HI9828
Tipping bucket rain gauge	Onset HOBO	RGB-M002
Microstation data logger	Onset HOBO	H21-002
Level logger	Solinst	3001
Air temperature	Onset HOBO	S-TMB-M002
Temperature/relative humidity	Onset HOBO	S-THB-M002
Barometric pressure logger	Solinst	3001
Water level logger	Onset HOBO	U20-001-01
Barometric pressure logger	Onset HOBO	U20-001-01
Specific conductance logger	Onset HOBO	U24-001
Reed switch	Texas Electronics	120-0018
Terminal block	Texas Electronics	009-0059
Pendant logger	Onset HOBO	UA-003-64
Pulse adaptor	Onset HOBO	S-UCD-M001
Tension lysimeter	Soil Moisture	1900L

3.2 Surface Instrumentation

3.2.1 Climate Data

Climate data, including precipitation rate, air temperature, and relative humidity, are collected outside the cave entrance with a tipping bucket rain gauge and an air temperature/relative humidity sensor. Both instruments are connected to a microstation for data logging at 10-min intervals. Precipitation data represent the potential hydrologic input to the epikarst. The air temperature and relative humidity data are combined with other climate data (wind speed, solar radiation) collected at nearby Virginia Tech Kentland Farm, to calculate potential evapotranspiration (using the Penman–Monteith method), a parameter needed to estimate recharge to the karst system. Although this study was designed to collect climate data at the site, other studies may be able to fully rely on data collected from nearby weather stations, thus eliminating the need to install surface equipment.

3.2.2 Precipitation Samples

Precipitation samples were collected near the cave entrance on a monthly basis from summer 2008 to early 2012 to provide information on chemical and isotopic inputs to the epikarst. Samples were collected using a closed system precipitation collector, designed to channel precipitation through a funnel in which a circular float was placed to minimize evaporation (modeled after [27]) (Fig. 5, top). Precipitation samples were collected using two different approaches, described below. From 2008 to 2011, the funnel was attached via plastic tubing to the bottom

Table 3 Chronology of instrumentation changes at James Cave

Date	Site(s)	Description
09/2007	Surface	Rain gauge with temperature, relative humidity sensor installed
09/2007	MS1, MS2	Suspended tarps and rain gauges installed; multiparameter sondes installed
02/2008	MS3	Suspended tarp and rain gauge installed; multiparameter sonde installed
08/2008	Surface	Precipitation collector installed
03/2009	Stream weir	Stream weir installed
03/2009	Stream weir	Solinst pressure transducers (level and barometric loggers) installed
07/2009	Soil2, Soil3, soil entrance	Tension lysimeters installed (1 m depth)
04/2010	Stream	Multiparameter sonde installed
01/2011	Stream	Sonde moved upstream from weir to near entrance
01/2011	MS1, MS2, MS3	Sondes removed; specific conductance loggers installed
01/2011	Stream weir	Stream weir replaced with concrete V-notch weir
06/2011	Stream	Sonde removed; specific conductance logger installed
02/2012	All sites	Cease composite geochemical sampling
05/2012	MS1, MS2, MS3	Replaced microstation and smart sensor rain gauge with reed switch and pendant logger combination
05/2012	Stream weir	Replaced Solinst level and barometric loggers with Onset loggers
06/2012	Surface	Replaced smart sensor rain gauge with reed switch and pendant logger combination
07/2012	MS1, MS2, MS3	Replaced pendant logger with pulse adaptor and microstation combination

Table 4 Data types and units for continuous data collection

Data type	Recording units
Precipitation/drip	mm/in or counts
RH	%
Air temperature	°C or °F
Drip SC	µS/cm
Drip temperature	°C or °F
Stream stage	Water and barometric pressure

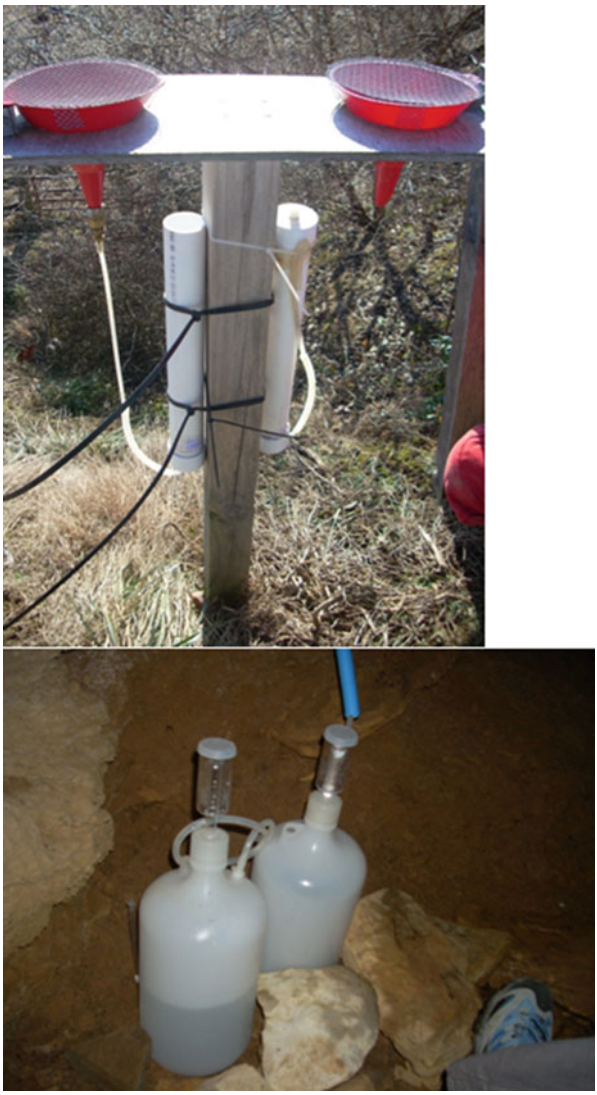

Fig. 5 Precipitation collectors. *Top*: funnel attached to PVC tubes for precipitation (*left*) and isotopic control (*right*), used from 2008 to 2011. *Bottom*: modified design, used from 2011 to 2012. Precipitation from surface routed into the cave entrance with tubing (*right*) fitted with airlock. Isotopic control with airlock shown at *left* (*Source*: Author)

of a sealed PVC collection device with a vent tube at the top. The vent tube was coiled with water in the coils to prevent evaporation while still allowing air to escape as the tube filled during rain events. A second collection device, disconnected from the funnel, was used as a control to determine the influence of evaporation on isotope fractionation. Deionized (DI) water was poured into the control device between sample collection dates. Control samples were collected at the beginning and end of each monthly period to test for evaporitic enrichment in liquid water stable isotopes. Results of this comparison showed fractionation due to evaporation during the summer months, thus necessitating a different collection

system. Another problem with this design was that winter freeze-thaw cycles caused the PVC tubes to crack and leak.

To remedy the dual problems of isotopic fractionation due to evaporation in the tubes and the cracking of the tubes in the winter, the precipitation collector system was retrofitted in 2011. The new system still relied on the funnels at the surface to collect the precipitation, but the funnels were drained into the cave via tubing to a carboy fitted with an airlock. This system also included an isotopic control (Fig. 3, bottom). Because the cave air temperature remains relatively constant (12–13 °C) over the year, the vessels did not experience freeze-thaw cycles. In addition, the narrow range in temperature of the cave reduced sample evaporation.

3.3 Soil Water Monitoring

Soil water data were collected from 2009 to 2012 to examine the chemical characteristics of water entering the epikarst. Samples were collected from porous cup tension lysimeters, installed at 1 m depths in three locations: the bottom of the sinkhole containing the cave entrance, the surface overlying MS2, and the surface overlying MS3. Lysimeters were sampled monthly by applying a vacuum to the lysimeter using a handheld pump, waiting 2 h, then purging the lysimeter sample with positive pressure applied using a handheld bicycle pump.

3.4 Cave Monitoring

Within the cave, instrumentation has been installed to collect nearly continuous (10 min) measurements of dripwater rates, specific conductance, and temperature; cave air temperature and relative humidity; and cave stream discharge, specific conductance, and temperature. Dripwater rates and stream discharge data provide critical information about recharge to the karst system, which is one of the focal points of the James Cave research project. In addition to hydrologic characteristics, the experimental apparatus was designed to allow for collection of dripwater and stream samples for geochemical analysis.

Dripwater monitoring sites were installed where cave ceilings are within 15 m of the cave surface, which is within the known vertical range of the epikarst observed in most karst regions [28]. Data from a survey (see Fig. 3) was used to locate the three dripwater sites (MS1, MS2, and MS3) and to determine the thickness of the epikarst overlying the stations. Results show that MS1 and MS2 are 15 m apart, located ~50 m west of the cave entrance. MS3 is ~60 m east of the cave entrance. The sites are located far enough from the cave entrance that the influence of surface environmental conditions is minimized. Depths of drip monitoring stations below ground surface are 8 m (597 m above mean sea level (AMSL)) at MS1, 10.7 m (595.1 m AMSL) at MS2, and 7 m (593 m AMSL) at MS3.

Fig. 6 Tarp system constructed to capture dripwater from speleothems (*Source*: Author)

3.4.1 Drip Rate

In 2007–2008, suspended tarp systems were built to collect dripwater in three areas with active speleothems (Fig. 6; design modified from [18]). The tarps are built with plastic sheeting suspended from frames constructed of lightweight 1 in. PVC tubing. Frames are supported by a combination of resting on the cave wall and suspension from anchors set in the cave wall and/or ceiling. The three drip tarps drain to a tipping bucket rain gauge to measure and log drip rates (Figs. 7 and 8). Initially, the rain gauges were used as-built, but due to frequent corrosion of exposed circuitry and subsequent failure, the rain gauges were retrofitted in 2012 with a reed switch connected to a pulse input adapter and data logger. The combination of these four items (tipping bucket rain gauge, reed switch, pulse adapter, and data logger) provides for both reliable measurement and storage of dripwater rates in the cave environment.

3.4.2 Drip Chemistry

Methods for continuous measurement of basic geochemical characteristics of dripwater have evolved over the course of the project. In 2007–2008, when the dripwater sites were first instrumented, waters from individual stalactites were drained directly into a sealed flow cell using latex balloons and silicone tubing. A multiparameter sonde was sealed in the flow cell and measured and logged dripwater pH, temperature, DO, and specific conductance. This design created a

Fig. 7 Current dripwater site instrumentation. Sarah Eagle in background (*Source*: Author)

closed, airtight system, which minimized atmospheric interaction. An overflow tube from each sonde was connected to a sampling container fitted with an airlock. Composite samples were collected monthly from this container for geochemical analysis.

The sondes were dismantled in 2011 due to problems with maintaining and calibrating the sensors and the monthly replacement of batteries. The pH and DO sensors required more frequent calibration than was practical for this project and were also subject to fouling. For example, calcite precipitated on the DO membrane, resulting in unreliable measurements. For the purposes of the James Cave project, these parameters were of lower level importance, but if pH and DO are

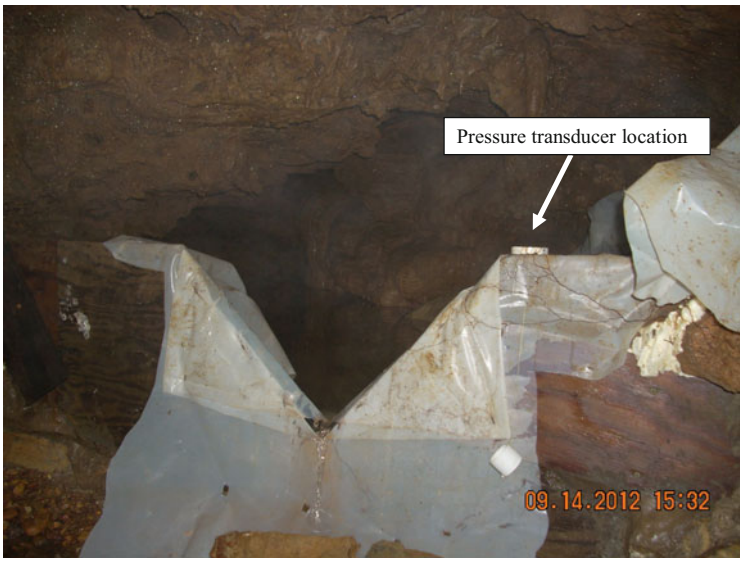

Fig. 8 James Cave stream weir with location of stilling well and pressure transducer noted. Barometric logger is not included in picture but is used to correct the transducer data for changes in barometric pressure (*Source*: Author)

critical parameters to measure, there are newer technologies, such as rapid pulse and optical DO sensors, which may be more practical for long-term deployment. Another challenge with the sonde was the battery power requirements (four 6 V lead acid batteries for each sonde), which required monthly replacement after charging.

In 2011, the sondes were replaced with a specific conductance/temperature (SCT) logger. The SCT logger contains a long-lasting internal battery (3 years with 1 min logging), avoiding the problem of monthly replacement of heavy batteries. In addition, the SCT logger contains a sensor with a titanium oxide coating, which prevents direct contact with water, thus preventing corrosion and fouling.

Also in 2011, at the same time the sondes were replaced with the SCT loggers, the design of the drip collection system was also modified to funnel dripwaters from the tarps into a reservoir containing the SCT logger before overflowing into the rain gauge. The rain gauge drains to a composite sample bottle outfitted with an airlock and overflow (Fig. 7). The time period integrated by the composite sample varies significantly over time, but can range from several days during the dry period to less than 2 min during large recharge events. The purpose of changing the design was to create a singular collection system for dripwater from multiple stalactites for measurement of both dripwater rate and chemistry. This works well for the James Cave project, where the focus is on recharge quantity and quality, but for cave monitoring projects with a focus on geochemical controls on speleothem growth and especially in caves where drip rates are slow, collection of dripwater on a tarp

would not be recommended due to calcite precipitation on the tarp and detention of flow that could cause shifts in certain geochemical parameters.

3.4.3 Stream Discharge

Discharge of the cave stream is measured using a 90° V-notch weir and a pressure transducer to measure the hydraulic head behind the weir (Fig. 8). The V-notch weir was constructed in 2009 and was retrofitted using concrete in 2011 to prevent leakage. Transducer measurements are recorded every 10 min to calculate discharge. In 2012, the transducers were replaced with transducer and barometric loggers from the same manufacturer as other equipment in the cave to allow for use of one data shuttle and software package for all instrumentation in the cave. The benefits of using instrumentation and software from one manufacturer are discussed in more detail below.

3.4.4 Stream Chemistry

A multiparameter sonde was installed in the stream from 2010 to 2011. Similar to the dripwater sites, it was difficult to maintain and calibrate the sensors and, as a result, the sonde was replaced in 2011 with an SCT logger.

3.4.5 Cave Atmosphere

Cave air temperature is monitored at each dripwater site using a temperature sensor connected to a data logger. The barometric logger installed near the stream weir also measures cave air pressure.

3.5 Instrumentation Maintenance

An important consideration of cave monitoring projects is maintenance of equipment and instrumentation. Maintenance is conducted on a monthly or bimonthly basis in conjunction with data download from logging sensors. As instruments can fail, and transportation to the site and within the cave takes time and effort, it is useful to have at least one extra of commonly used equipment (i.e., rain gauge, data logger, SCT logger) readily accessible. Tools, instrument manuals, and replacement batteries are essential to bring for each monitoring event, to allow for routine maintenance and troubleshooting in the cave.

3.5.1 Sensor and Instrument Maintenance

As discussed above, maintenance of sensors in the multiparameter sonde became challenging due to requirements of frequent calibration and fouling. The change to

the sealed SCT loggers ameliorated some of these issues. Because sealed sensors/loggers are generally not built for in-field calibration, raw data are software-corrected to values measured in the field with a calibrated conductivity meter at the time of data download. The software applies a linear drift correction using a two-point calibration with values measured in the field at the beginning and end of each logging period.

Another challenge in karst is precipitation of calcite and other carbonate minerals on sensors, as dripwater is often saturated with respect to these minerals. Calcite acts as an insulator and depresses the electrical conductivity measured by the SCT logger. Maintenance procedures include gentle cleaning of the SCT loggers with a soft brush prior to rinsing with a weak acid (acetic) and rinsed with DI water to remove calcite buildup after download and prior to redeployment. These cleaning procedures are effective at removing mineral buildup and biofilms that may form on the sensor surface. All chemical solutions used in rinsing cave equipment are collected and removed from the cave.

Another complication for in-cave monitoring is the development of biofilms on instrument or collection-material surfaces, such as the collection tarp, and growth of bacterial masses in the sample chamber. During each trip to the cave, sample chambers are visually inspected for biofouling. If biofouling is identified, the material is physically removed and the chamber disinfected with acetic acid.

3.5.2 Site Maintenance

Sediment buildup in the drip collection systems is a constant concern, especially during the recharge season with high dripwater flows through the epikarst. Sediment can clog the systems, causing tarp sagging, which can result in tarp collapse. Sediment buildup can also block flow to the sample collectors at the downstream end of the system. Clearing the system of sediment is accomplished by disconnecting the outfall hoses below the tarp funnel, the sample chamber, and the rain gauge. Each of these is rinsed and back-flushed as appropriate to clear and restore flow pathways and then reconnected and flushed with dripwater. The interval for which such maintenance is required varies between sites and depends on sediment yield from the epikarst over time.

4 Sample Collection and Analysis

In addition to the continuous measurements discussed above, samples of precipitation, soil water, dripwater, and stream water were collected monthly for geochemical analyses (anions, cations, alkalinity, dissolved organic carbon, water isotopes, and carbon isotopes of organic and inorganic carbon) from July 2008 to January 2012. Samples were brought back to the Virginia Tech laboratories for processing and analysis. More details on sampling and analytical procedures, as well as results, can be found in two graduate theses [21, 22].

In the laboratory, water samples were filtered (0.2 μm polysulfone GD/X) and separated into subsamples for analysis of cations, anions, alkalinity, dissolved organic carbon (DOC), and dissolved inorganic carbon (DIC) and water isotopes. Cation samples were preserved with HNO_3 and analyzed for Al, Ca, K, Mg, Na, Si, and Sr via inductively coupled plasma atomic emission spectrometry. Anion samples were analyzed for Cl, NO_3, and SO_4 via ion chromatography. Alkalinity was determined using Gran titration [29]. DOC samples were preserved with HCl and analyzed via catalytic oxidation. Samples for stable carbon isotopic composition ($\delta^{13}C$) of DIC were collected without headspace in vials sealed with low-diffusion butyl rubber septa and were preserved with copper sulfate. Analysis of the $\delta^{13}C$-DIC was conducted at the Reston Stable Isotope Laboratory of the US Geological Survey [30]. Liquid water stable isotopes (δD and $\delta^{18}O$) were analyzed using a liquid water isotope analyzer at Texas State University-San Marcos.

5 Data Collection and Management

5.1 Data Recording and Downloading

Nearly continuous time series data are recorded at 10-min intervals and data are stored either on the equipment or on separate data loggers. Instruments with internal storage include the SCT loggers, the pressure transducers, and the barometric pressure loggers. Instruments with external data storage devices include rain gauges and air temperature and temperature/relative humidity sensors.

Time series data are downloaded on monthly or bimonthly intervals. Because of the range of instrumentation, there is an associated range of software that has been used at the James Cave site both to offload data from loggers and to post-process data. Software that we used at the start of the project included (a) HOBOware for Onset instrumentation,[1] (b) Hanna Instruments software for Hanna instrumentation, and (c) Level Logger software for Solinst pressure transducers. With the aforementioned changes in instrumentation, HOBOware is the only software currently (2014) needed to program and download data from all cave instruments.

5.2 Data Processing

Data collected by a variety of instruments and methods may result in data in a variety of units and formats, requiring consistent naming conventions and clearly outlined data processing procedures. Eagle [21] outlines the data management and processing procedures used for the James Cave project. Initially, for the project,

[1] The use of product or trade names is for descriptive purposes only and does not constitute endorsement by the US government.

spreadsheets were used for data organization, manipulation, and editing. As the collected data became more numerous and unwieldy for use in spreadsheets, we purchased AQUARIUS Workstation [31] in 2011 for time series aggregation, manipulation, and preprocessing. After each monitoring event, data downloaded from the data loggers onto data shuttles are imported into HOBOware and converted to CSV files, which are then imported into Aquarius. Within Aquarius, the data are appended to previous datasets. Aquarius has tools to join datasets, trim outliers (i.e., in the case of instrument failure), convert units and do other calculations, resample the data at different time intervals (e.g., hourly, daily, monthly), and conduct descriptive statistics, in addition to other functions. As the datasets at James Cave currently contain an excess of several million data points, using a software package that can integrate and process the data has eased data management considerably.

5.3 Data Storage

The use of multiple data storage options and sharing data allows for maximum availability and collaborative efforts. For the James Cave project, both raw and processed data are stored on hard drives at Virginia Tech, on a cloud server, and on a project management system at Virginia Tech to allow for exchange between researchers. The stored datasets are public domain and can be accessed by contacting the corresponding author of this chapter.

6 Results and Discussion

This section outlines the datasets that have been collected at James Cave as an example of a comprehensive and integrated cave monitoring program. The section also presents selected results from the James Cave project thus far and includes recommendations for establishing and maintaining a long-term cave monitoring project.

6.1 James Cave Datasets

At James Cave, the following data are collected at 10-min intervals (2007–current (2014)):

- Precipitation at the surface
- Air temperature and relative humidity at the surface
- Drip rate at three drip sites (Fig. 9)

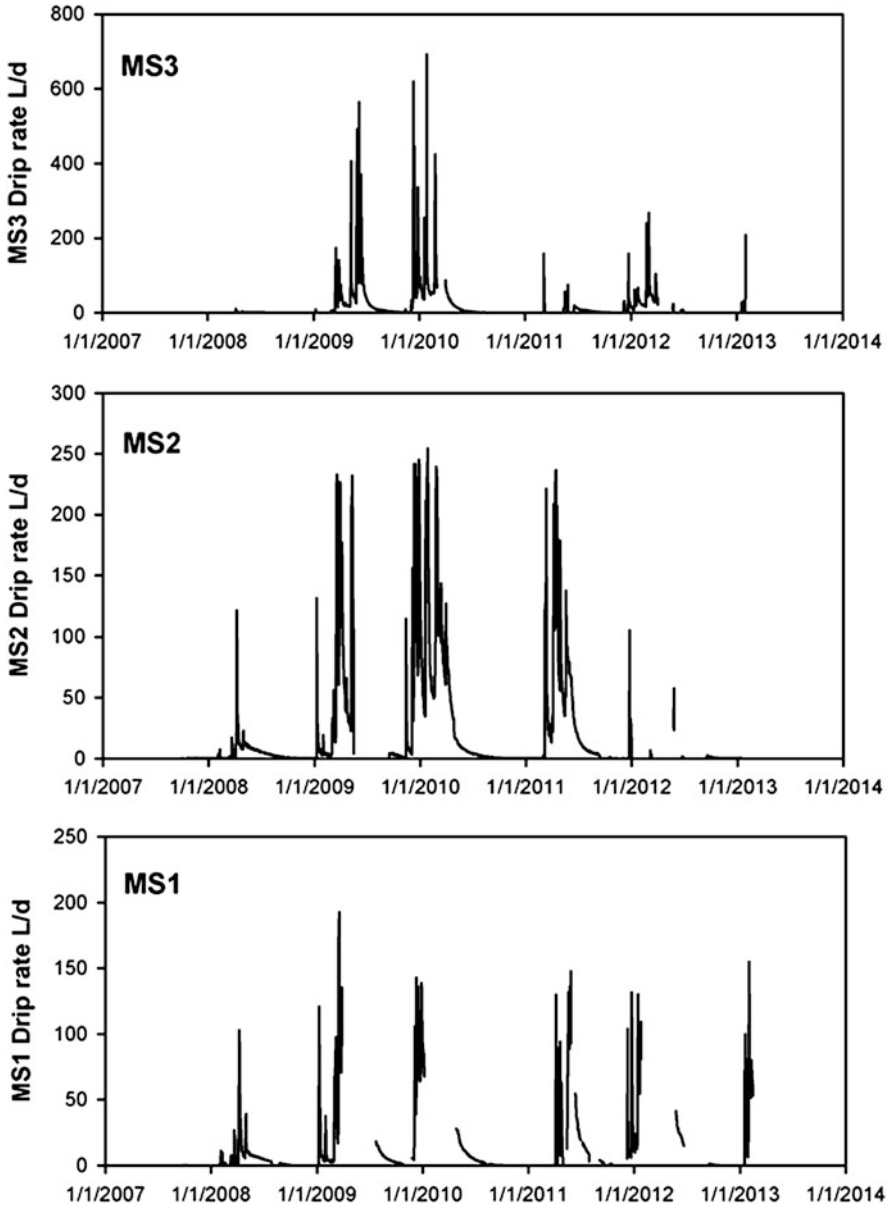

Fig. 9 James Cave drip hydrographs between late 2007 and early 2013. Note the different scales on drip rates for the three sites

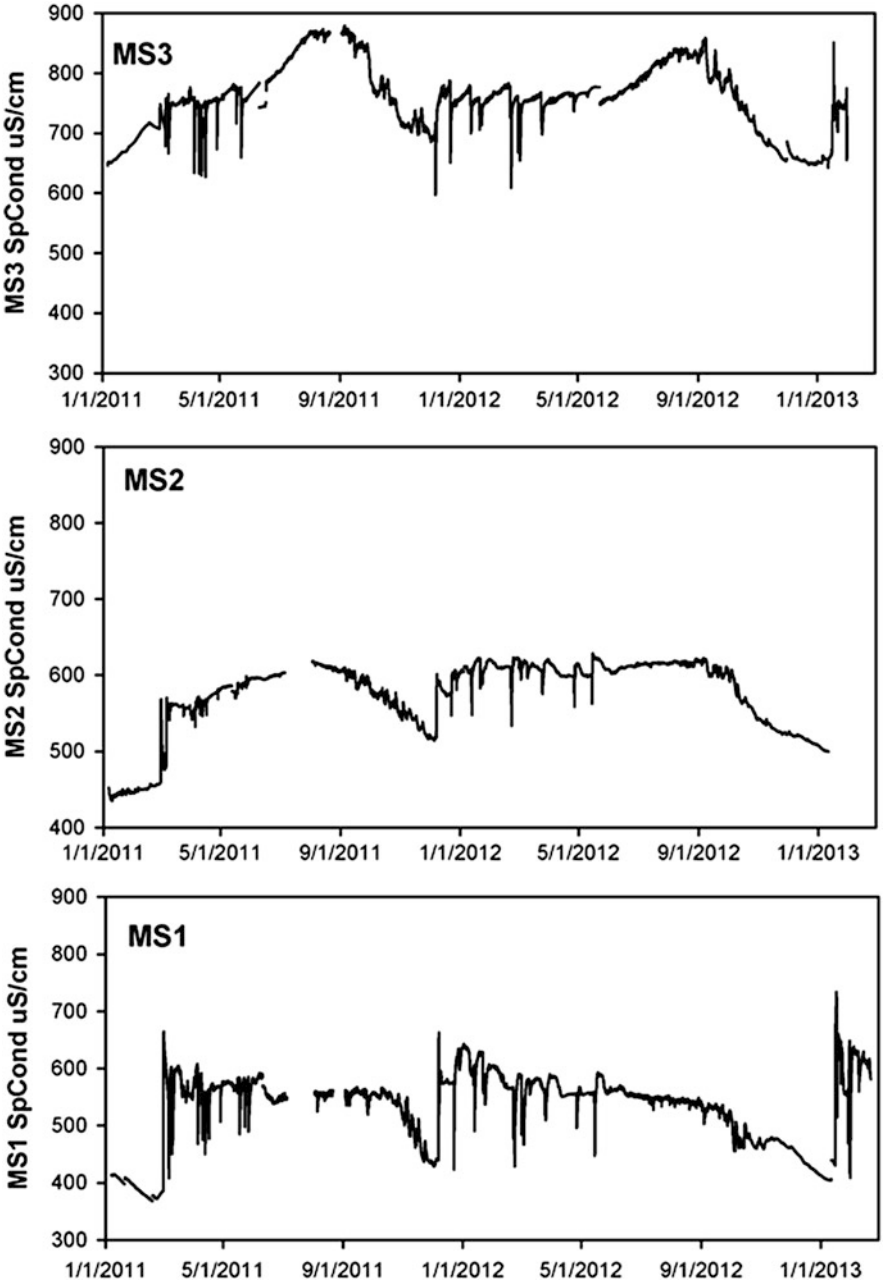

Fig. 10 Specific conductance datasets for the three drip sites (MS1, MS2, MS3) at James Cave from Jan 2011 to Feb 2013. Missing data reflect periods of instrument failure

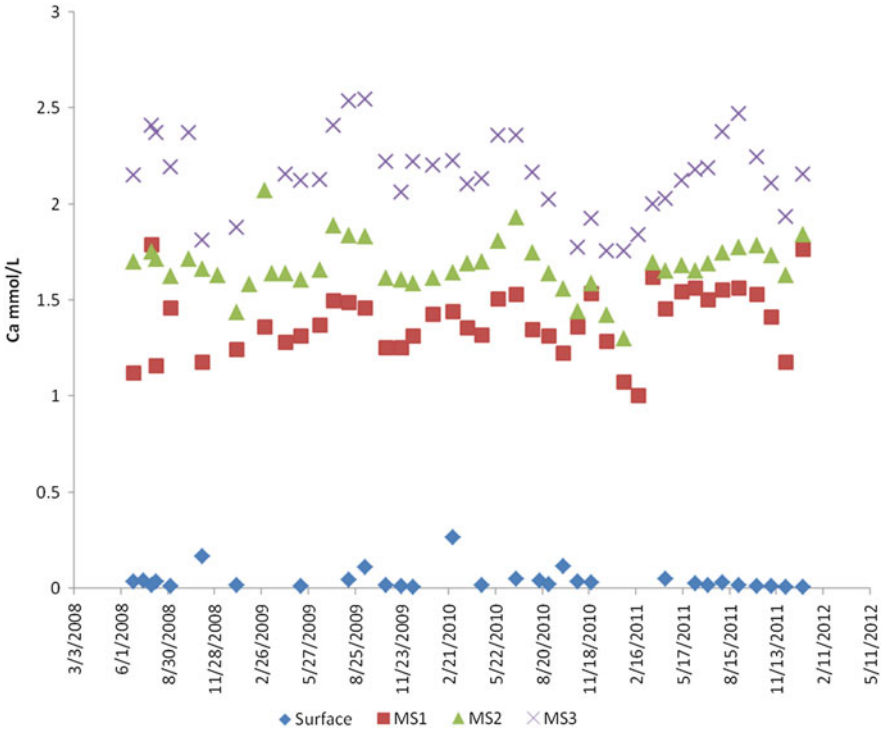

Fig. 11 Calcium concentrations (mmol/L) in precipitation and dripwaters at the three drip sites in James Cave from June 2008 to January 2012. Note both spatial (between the different sites) and temporal variabilities in Ca concentrations

- Cave air temperature at three drip sites
- Dripwater-specific conductance at three drip sites (Fig. 10)
- Dripwater temperature at three drip sites
- Cave stream level at the weir
- Cave air barometric pressure at the weir

Geochemical analyses were conducted for samples collected from 2008 to 2012 for:

- Composite samples of precipitation (calcium shown in Fig. 11)
- Composite samples of cave dripwater (calcium shown in Fig. 11)
- Grab samples of soil water
- Grab samples of cave stream

The above datasets allow for calculation of the following parameters:

- Penman–Monteith potential evapotranspiration, using climate data from James Cave and Kentland Farm
- Excess precipitation (also called water excess), using precipitation data and calculated potential evapotranspiration values
- Cave stream discharge, using cave stream level and cave air barometric pressure data

- Recession coefficients on drip and cave stream hydrographs, using hydrograph recession analysis
- Saturation indices of specific minerals in cave dripwater, using geochemical data

More detailed presentation and interpretation of these datasets are included in two graduate theses [21, 22]. The reader may consult these sources to learn more about current findings at James Cave. Presentation of selected datasets with brief interpretation is presented below.

6.2 Dripwater Hydrology

Based on recurring patterns in the drip dataset (Fig. 9), Eagle [21] divided the drip record into three hydrologic seasons: (1) a dry period during which there is no response to precipitation events and the discharge is at or near zero; (2) a subsequent recharge period characterized by high drip rates and responses to precipitation events; and (3) a recession period during which drip rates decline with no response to precipitation events until reaching base flow, marking the onset of the next dry period. Eagle [21] also examined the changes in the start and duration of the hydrologic seasons, dividing the record into hydrologic years (HY) beginning with the start of dry period, typically early October. For example, HY2010 refers to the period October 2009–September 2010.

Over the period of record at James Cave, the onset of the dry period was the most consistent seasonal marker, occurring in late September to early October and followed by a dry season lasting 1–6 months. The recharge season has started in December (HY2010, 2012), January (HY2009, 2013), February (HY2008), and March (HY2011). The duration of the recharge season ranged from 2 (HY2008) to 6 months (HY2009, 2012). The recession period generally began in late spring to early summer and lasts from 3 to 5 months before onset of the next dry period and start of the next hydrologic year.

6.3 Dripwater Geochemistry

6.3.1 Specific Conductance of Dripwater

The specific conductance dataset is essentially a high-resolution time series record of total solute concentrations in dripwater (Fig. 10). These patterns show significant variation over the period of record with short-term perturbations and longer-term (multiple month) trends. For example, MS3 has consistently higher conductivity, while MS1 and MS2 generally have similar and lower conductivity values. Worth noting are three prominent patterns: (1) the decline in conductivity in the fall of both 2011 and 2012, (2) the increase (more prominent at MS3) from spring to

summer, and (3) the response of specific conductance to initiation of the recharge season. At the initiation of recharge, there is a small but measurable increase in conductivity, followed by a sudden drop, then gradual increase. For subsequent fluxes in drip discharge, only the sudden drop in conductivity and gradual increase are observed. The first increase likely represents a pulse of water with high dissolved solids that was stored in the epikarst and flushed at the onset of recharge. Later events are likely dominated by newer water or direct recharge along hydraulically conductive "wetted" or "primed" flow paths.

6.3.2 Geochemical Characteristics of Dripwater

Examining concentrations of select analytes over time can provide information about seasonal geochemical processes. For example, Fig. 11 shows Ca concentrations in drips from 2008 to early 2012. This time series shows a pattern of seasonal variability, with higher concentrations observed in the late summer (August–September) and lowest concentrations observed in late fall and early winter (November–January) when the deep epikarst is the driest and likely well ventilated, resulting in calcite precipitation in the epikarst. The Ca concentration data, in combination with the continuous specific conductivity datasets, were used by Eagle [21] to infer patterns of calcite dissolution and precipitation in the epikarst.

6.4 Successes and Pitfalls

Instrumentation of the James Cave site has been an iterative process that continues to be refined. For example, at the start of the project, a multiparameter sonde was installed to collect pH and DO, in addition to specific conductance and temperature of the dripwater. After a series of probe failures, the sonde was exchanged for a more robust specific conductivity/temperature logger. As technological advances in this field continue at a rapid pace, affordable, reliable, and robust loggers capable of measuring parameters such as pH and DO, and others, are likely to become available. Improvement in sensor durability and reliability may in the future facilitate collection of parameters such as these and allow calculation of important geochemical parameters such as calcite and dolomite saturation and partial pressures of dissolved gases.

Failure of rain gauges was a source of frustration for the project. Initially, off-the-shelf gauges were deployed, but after circuit boards corroded and failed, despite additional protective shellacking prior to deployment, the rain gauges were retrofitted with simple reed switches in 2012 (see Table 2 for details). Since this retrofit, the gauges have not failed.

Downloading of data and software requirements for different instruments was a project challenge. Initially, instruments from multiple manufacturers were used, each with their own equipment for downloading data (e.g., data shuttles and special

cables) and each with their own software. Over time, all instrumentation has been replaced with equipment from one manufacturer. This approach greatly simplified the process of data download, data processing, and troubleshooting of instrument malfunctions in the field. Standardizing equipment as much as possible within data quality and budgetary considerations is recommended.

Data management is an ongoing challenge for high-resolution time series data such as those associated with cave monitoring projects. Collection of closely spaced data from multiple locations and of different types can quickly yield large amounts of data. At James Cave, collection of precipitation, drip rates, stream stage/discharge, air and drip temperature, and drip-specific conductance has generated several millions of data points. Specific software options (such as Aquarius, used for this project) are available and designed to facilitate integration and processing of large, time series datasets. Other approaches, such as custom software, may be possible if in-house capacity exists for their development, modification, and maintenance. Cave monitoring projects are likely to be data rich, which requires planning for data management, ideally before initiating data collection.

Last, installation and maintenance of equipment for cave monitoring projects often requires substantial labor. For the James Cave project, labor was supplied by researchers, students, and volunteers, some with limited caving experience. The field crew had to navigate cave passages including tight confined spaces and exposed climbs and tote equipment from the surface to sites in the cave and back out again. Because workers have no way to communicate with anyone on the surface, development of a communication (sign-out) protocol as part of the health and safety plan is a critical element of any cave project.

7 Conclusions

Collecting long-term, high-resolution datasets in caves is a challenging endeavor, as it involves not only installation of instrumentation but also long-term maintenance of the equipment. An additional challenge is the storage, processing, and management of the data. However, with careful planning, design, and flexibility to alter instrumentation during the course of the project, these rich datasets can be applied to answer a variety of scientific questions. For example, results derived from the James Cave datasets have provided insight into hydrologic and geochemical processes that influence recharge to the underlying karst aquifer.

Continued research on recharge in karst systems is needed to accurately characterize the important water resources they contain. Improvements in sensor technology, data storage, and data processing are critical for collecting long-term high-quality datasets that can be used to address theoretical and applied questions about water and chemical flow in karst. The resulting information will assist scientists and planners in making the informed decisions that are required for effective management of karst aquifer systems and for water supply planning for domestic, agriculture, municipal, and industrial applications.

Acknowledgments We extend our thanks to the Ferrell family of Pulaski County for graciously allowing us unfettered access to the cave. Funding for the James Cave project was provided by the Virginia Water Resources Research Center, the US Geological Survey/National Institutes for Water Resources, the Cave Conservancy of the Virginias, the Geological Society of America, and the Virginia Tech Department of Geosciences. We thank Bev Shade and David Culver for discussions about study design and data collection, Don Rimstidt for geochemical insight, and Tom Malabad for conducting the cave survey. Helpful reviews were provided by MaryLynn Musgrove (USGS) and the editors of this volume. We are also extremely grateful to Stuart Hyde, Heather Scott, Sally Morgan, Nathan Farrar, Ariel Brown, Anna Hardy, Matthew Blower, and members of the VPI Cave Club for valuable assistance in the cave.

References

1. KWI (2003) What is karst and why is it important? http://www.karstwaters.org/kwitour/whatiskarst.htm. Accessed 16 Oct 2014
2. Ford DC, Williams PW (2007) Karst hydrogeology and geomorphology. Wiley, Chichester, p 562
3. Bakalowicz MJ (2004) The epikarst, the skin of karst. In: Epikarst: Special Publication 9. Karst Waters Institute, Charles Town
4. Pipan T, Christman MC, Culver DC (2006) Dynamics of epikarst communities: micro-geographic pattern and environmental determinants of epikarst copepods in Organ Cave, West Virginia. Am Midl Nat 156(1):75–87
5. Smart PL, Friederich H (1987) Water movement and storage in the unsaturated zone of a maturely karstified carbonate aquifer, Mendip Hills, England. In: Proceedings of the conference on environmental problems in Karst Terranes and their solutions October 1986, pp 59–87
6. Tooth AF, Fairchild IJ (2003) Soil and karst aquifer hydrological controls on the geochemical evolution of speleothem-forming drip waters, Crag Cave, southwest Ireland. J Hydrol 273(1–4):51–68
7. Fairchild IJ, Tuckwell GW, Baker A, Tooth AF (2006) Modelling of dripwater hydrology and hydrogeochemistry in a weakly karstified aquifer (Bath, UK): implications for climate change studies. J Hydrol 321(1–4):213–231
8. Musgrove M, Banner JL (2004) Controls on the spatial and temporal variability of vadose dripwater geochemistry: Edwards Aquifer, central Texas. Geochim Cosmochim Acta 68(5): 1007–1020
9. Baker A, Barnes WL, Smart PL (1997) Variations in the discharge and organic matter content of stalagmite drip waters in Lower Cave, Bristol. Hydrol Process 11(11):1541–1555
10. Baldini JUL, McDermott F, Fairchild IJ (2006) Spatial variability in cave drip water hydrochemistry: implications for stalagmite paleoclimate records. Chem Geol 235(3–4): 390–404
11. Genty D, Baker A, Vokal B (2001) Intra- and inter-annual growth rate of modern stalagmites. Chem Geol 176(1):191–212
12. Genty D, Deflandre G (1998) Drip flow variations under a stalactite of the Pere Noel cave (Belgium). Evidence of seasonal variations and air pressure constraints. J Hydrol 211(1–4): 208–232
13. Pape JR, Banner JL, Mack LE, Musgrove ML, Guilfoyle A (2009) Controls on oxygen isotope variability in precipitation and cave drip waters, central Texas, USA. J Hydrol 385(1–4): 203–215
14. Spötl C, Fairchild IJ, Tooth A (2005) Cave air control on dripwater geochemistry, Obir Caves (Austria): implications for speleothem deposition in dynamically ventilated caves. Geochim Cosmochim Acta 69(10):2451–2468

15. Baker A, Brunsdon C (2003) Non-linearities in drip water hydrology: an example from Stump Cross Caverns, Yorkshire. J Hydrol 277(3–4):151–163
16. Mattey D et al (2006) Seasonal changes in the isotopic composition of cave air, water and speleothem calcite in new St. Michaels Cave, Gibraltar: unwanted noise or a tool for decoding speleothem climate records? KarstIV, The climate record, Baille Herculane, Romania
17. Collister C, Mattey D (2008) Controls on water drop volume at speleothem drip sites: an experimental study. J Hydrol 358(3):259–267
18. Shade B, Veni G (2005) Intensive monitoring of drip waters in two shallow caves. International Congress of Speleology, Athens
19. Baker A, Ito E, Smart PL, McEwan RF (1997) Elevated and variable values of C-13 in speleothems in a British cave system. Chem Geol 136(3–4):263–270
20. Fairchild IJ, Borsato A, Tooth AF, Frisia S, Hawkesworth CJ, Huang Y, McDermott F, Spiro B (2000) Controls on trace element (Sr-Mg) compositions of carbonate cave waters: implications for speleothem climatic records. Chem Geol 166(3–4):255–269
21. Eagle SD (2013) Analysis of hydrologic and geochemical time series data at James Cave, Virginia: implications for Epikarst influence on recharge, M.Sc. Virginia Tech, Blacksburg
22. Gerst JD (2013) Epikarst control on flow and storage at James Cave, VA: an analog for water resource characterization in the Shenandoah Valley karst, M.Sc. Virginia Tech, Blacksburg
23. SRCC (2014) Historical climate summaries for Virginia (cited 2014). http://www.sercc.com/climateinfo/historical/historical_va.html. Accessed 16 Oct 2014
24. Bartholomew MJ (1987) Structural evolution of the Pulaski thrust system, southwestern Virginia. Geol Soc Am Bull 99(4):491
25. Schultz AP, Bartholomew MJ (2009) Geologic map of the Radford North quadrangle, Virginia. In: Cross A, Campbell EVM (eds) Digital Open-File Report OFR-09-01. Virginia Division of Mineral Resources, Charlottesville
26. USDA-NRCS (2006) Web soil survey. http://websoilsurvey.nrcs.usda.gov/app/WebSoilSurvey.aspx. Accessed 16 Oct 2014
27. Kazahaya K, Yasuhara M (1994) A hydrogen isotopic study of spring waters in Mt. Yatsugatake, Japan: application to groundwater recharge and flow processes. J Jpn Assoc Hydrol Sci 24:107–119
28. Klimchouk A (2003) Towards defining, delimiting and classifying epikarst: its origin, processes and variants of geomorphic evolution. In: Epikarst. Karst Waters Institute, Shepherdstown
29. Radtke DB et al (2012) Alkalinity and acid neutralizing capacity (version 4.0). In: Rounds SA (ed) National field manual for the collection of water-quality data: U.S. Geological Survey techniques of water-resources investigations. U.S. Geological Survey, Reston
30. Révész KM, Doctor DH (2014) Automated determination of the stable carbon isotopic composition (δ 13C) of total dissolved inorganic carbon (DIC) and total nonpurgeable dissolved organic carbon (DOC) in aqueous samples: RSIL lab codes 1851 and 1852. In: Techniques and methods, book 10, Chapter: C20, U.S. Geological Survey, Reston
31. Aquatic Informatics (2011) AQUARIUS 3.0 R3. 1032. Vancouver

Principles for the Development of Contemporary Bioassessment Indices for Freshwater Ecosystems

Andrew L. Garey and Leonard A. Smock

Contents

Abstract Bioassessment can be broadly defined as the use of biota to assess the nature and magnitude of anthropogenic impacts to natural systems. We focus on an important and specific type of bioassessment: the use of ecological assemblages, primarily fish, macroinvertebrates, and algae, as indicators of anthropogenic impairment in aquatic systems. Investigators have long known that biota provide spatially and temporally integrative indicators of impairment. This chapter provides an introduction to the process of developing assemblage-level indices that provide

A.L. Garey (✉) • L.A. Smock
VCU Rice Rivers Center, Virginia Commonwealth University, Richmond, VA, USA
e-mail: gareyal@vcu.edu

T. Younos, T.E. Parece (eds.), *Advances in Watershed Science and Assessment*, The Handbook of Environmental Chemistry 33,
DOI 10.1007/978-3-319-14212-8_9

quantitative estimates of the ecological integrity of freshwater ecosystems. We discuss important developments made in the latter half of the twentieth century which are still relevant and useful for bioassessment, as well as more recent developments that have improved the effectiveness of bioassessment strategies. Throughout the chapter, we focus on analytical approaches for improving the effectiveness of bioassessment indices for detecting anthropogenic impairment. In the concluding section of the chapter, we widen our perspective and include excerpts from discussions with three expert practitioners on topics that are more broadly applicable to the assessment of the ecological integrity of aquatic systems. The major challenge for all bioassessment programs is to separate the effects of anthropogenic impairment on biota from the effects of natural environmental variability unrelated to impairment. Analytical developments, such as advanced predictive modeling techniques, coupled with emerging technologies and the development of large-scale bioassessment programs will continue to increase our ability to meet this challenge and to improve our understanding of how aquatic assemblages are affected by anthropogenic impairment.

Keywords Aquatic ecosystems • Bioassessment • Biomonitoring • Biotic assemblages • Predictive modeling

1 Introduction

The US Environmental Protection Agency (USEPA) defines biological assessment as the "...evaluation of the condition of a waterbody using biological surveys and other direct measurements of the resident biota in surface waters" [1]. Investigations that fall under this broad definition may be focused on any level of biological organization, from studies of subcellular effects of toxic compounds [2] to ecosystem-scale assessments using multiple taxonomic assemblages [3]. The terms biological assessment, bioassessment, biological monitoring, and biomonitoring are often used interchangeably. For clarity, we restrict our discussion to the term bioassessment.

The value of aquatic organisms as pollution indicators has been recognized by scientists for over 100 years. The Saprobiensystem of Kolkwitz and Marsson [4], most probably the first bioassessment index, was a system for quantitatively rating the tolerance of aquatic organisms to sewage pollution, much akin to modern pollution tolerance values. This concept has been adapted and modified many times, and both the concept and use of the word "saprobity" persist in contemporary literature [5, 6]. The practice of bioassessment invokes the concept of biological integrity, defined as "the capability of supporting and maintaining a balanced, integrated, adaptive community of organisms having a species composition, diversity, and functional organization comparable to that of natural habitat of the region" [7, 8]. Practitioners conducting bioassessments assume that biotic integrity reflects

overall ecological integrity, which describes the state of an ecosystem with respect to biology as well as physical and chemical factors [8]. Therefore, the purpose of using biota to assess environmental conditions is that they integrate the effects of all environmental factors to which they are exposed over their entire life-spans and habitat ranges [8, 9]. However, because biota are responsive to such a multitude of environmental factors acting over multiple temporal and spatial scales, determining clear and unambiguous relationships between biota and anthropogenic impairment remains a challenging and active area of research.

This chapter addresses the development of numerical indices, based on biological assemblage-level data, to make inferences regarding anthropogenic stress to freshwater ecosystems. We follow the framework of Fauth et al. [10] in defining the terms community and assemblage. Communities refer to all organisms within the spatial boundaries of the system of interest. For bioassessment, the spatial boundaries of communities are generally artificial constructs, rather than distinct, natural boundaries, and are chosen based on some combination of scientific, logistical, and political criteria. The term assemblage refers to a taxonomically defined subset of a given community, for example, the benthic macroinvertebrate assemblage of a stream system.

The general objective of all bioassessments is to separate the signal of anthropogenic impairment effects from the noise of effects related to natural variations in space and time that are not related to anthropogenic impairment. Evaluation of the relative importance of these two effects requires measurement or estimation of variables related to anthropogenic impairment, which we refer to hereafter as stressors, as well as those related to natural variation, which we refer to as natural environmental variables.

The assemblages chosen for bioassessments depend on the expertise and resources available to investigators, public interest, and on those that are most expected to respond to anthropogenic stress. Algae, fish, and macroinvertebrates are the most commonly used assemblages, and numerous examples of useful bioassessment indices exist for each. Investigations comparing these assemblages commonly show that they respond differently to anthropogenic stress, and each represents a unique aspect of ecological integrity [11–13]. Therefore, we focus on describing the analytical methods used for the development of contemporary indices, not on comparing the usefulness of different assemblages. We do not address descriptions of field and laboratory methods, but do note that sampling methodology [14, 15], sampling effort [16, 17], and taxonomic resolution [18, 19] have important and well-documented effects on bioassessments. Our focus is on perennial streams and rivers, as these systems dominate the literature and are the focus of most bioassessment programs. We also provide examples from lakes, impoundments, and wetlands when they enhance our discussion. The analytical methods presented here are also applicable to other aquatic systems and assemblage types.

Biological integrity is defined by one or a series of bioassessment metrics, which are quantitatively defined aspects of assemblages that are expected to vary in response to impairment. Some investigators favor the use of multiple metrics,

Table 1 Selected fish, macroinvertebrate, and algae metrics used as indicators of anthropogenic impairment

Metric category	Assemblage	Metric	Impairment response	Description
Composition and diversity	Fish	Percent of nonnative species [20]	Increase	Percent of species that are nonnative
	Macroinvertebrates	EPT richness [21]	Decrease	Number of taxa (genera or species) in the orders Ephemeroptera, Plecoptera, and Trichoptera
	Algae	Similarity to reference [22]	Decrease	Bray–Curtis similarity index of test site compared to reference sites
Trait based	Fish	Percent lithophilic spawners [17]	Decrease	Percent of individuals that spawn on coarse gravel substrate
	Macroinvertebrates	Percent collector–gatherer taxa [23]	Increase	Percent of taxa in the collector–gatherer functional feeding group
	Algae	N-heterotrophic taxa [24]	Increase	Number of taxa that derive nitrogen from the uptake of amino acids
Pollution tolerance	Fish	Tolerance value [25]	Increase	Weighted average tolerance value based on an impairment gradient derived by principal components analysis (PCA)
	Macroinvertebrates	Percent tolerant taxa [23]	Increase	Percent of individuals with tolerance value >6 (10-point scale, increasing with tolerance). Tolerance values derived based on best professional judgment and literature review
	Algae	Alkaliphilous taxa richness [26]	Increase	Number of taxa (genera or species) primarily occurring at pH > 7
Individual condition	Fish	Percent of individuals with anomalies [27]	Increase	Percent of individuals with deformities, erosion, lesions, or tumors
	Macroinvertebrates	Toxic score index [28]	Increase	Index of effluent toxicity based on mentum deformities of *Chironomus* spp.
	Algae	Percent deformed cells [29]	Increase	Percent of diatom frustules with deformities

which are aggregated within a multimetric index (MMI). MMIs provide a checks-and-balances system to account for variable responses of metrics to multiple stressors. Others prefer single-metric indices, most notably the observed-to-expected (O/E) index, which we introduce in Sect. 3.1. Developers of MMIs commonly group metrics based on the general type of ecological information they express. Metrics from different ecological categories are included in MMIs in order to reduce the redundancy of information and increase the explanatory power of indices. In practice, a vast array of assemblage-level metrics has been used for aquatic bioassessments.

To provide relevant examples, we have assembled a short list of fish, macroinvertebrate, and algae metrics, which we group into four broad categories (Table 1). Diversity and composition metrics are taxonomy-based metrics associated with assemblage characteristics such as richness, evenness, diversity, and dominance. Trait-based metrics incorporate information on ecological habits, habitats, morphology, life history, and life cycle characteristics of populations in the assemblage of interest. Pollution tolerance metrics are numerical ratings of the degree to which individuals in the assemblage are tolerant to stressors. Individual condition metrics are associated with visually apparent morphological anomalies of individual specimens. In addition to these general metric types, the absolute abundance of fish and biomass of algae are also sometimes used, although the absolute abundance of macroinvertebrates is rarely used.

In Sect. 2, we introduce the most widely used method for bioassessment, the Reference Condition Approach (RCA) [30–32]. In Sect. 3, we discuss predictive modeling of aquatic assemblages, which is conducted to control for the effects of natural environmental variation in order to obtain an unambiguous determination of anthropogenic effects. Once selected and properly calibrated for natural environmental variation, metrics are used individually, or are aggregated within an MMI, to provide a scoring system that reflects the assemblage-inferred level of anthropogenic impairment at a given study site. This process, as well as methods for evaluating the performance of metrics and indices, is reviewed in Sect. 4. In Sect. 5, we take a broader perspective and present interviews with three experts who provide valuable insights into some of the most important emerging issues and challenges in the field of bioassessment.

2 The Reference Condition Approach

Reference conditions serve as surrogates for negative controls, representing the assemblage characteristics at test sites that would occur in the absence of impairment. Following the RCA, reference conditions are derived from assemblage data at least-disturbed reference sites (sensu Stoddard et al. [32]). In comparison to experimental studies, where variation among replicates is carefully controlled and expected to be minimal, variation among reference site assemblages is high and difficult to predict. Replicate samples from the same site are generally insufficient

to account for this variation. Therefore, the RCA calls for the use of multiple reference sites in order to adequately account for the effects of natural environmental variation on assemblages [30–32].

We use the term reference to broadly encompass streams considered to be in least-impaired conditions, though as discussed in Sect. 2.2, the actual level of impairment at reference sites is highly variable among studies [32]. We use the term impaired to refer, in general, to sites that are subject to the deleterious effects of stressors and the term test sites to refer to those of unknown impairment status (i.e., those for which bioassessments are needed). This chapter focuses on the RCA, although alternative approaches for estimating reference conditions may be used when system conditions and data availability warrant (Sect. 2.1). Application of the RCA proceeds by first screening multiple potential reference sites to determine if they reflect appropriate least-impaired conditions (Sect. 2.2), then classifying the screened reference sites as to expected or quantified patterns of variability among their biotic assemblages (Sect. 2.3).

2.1 Alternatives to the Reference Condition Approach

Though not often available, data describing past assemblages may provide valuable information for inferring reference conditions. Investigations of sediment records, historical accounts of landscape conditions, and museum records have been used to infer past environmental conditions and assemblage composition in aquatic systems [33–36]. Historical approaches, while important, lack broad applicability for bioassessment. In lotic ecosystems, sediment deposition is generally insufficient to provide a historical record. Moreover, data that describe assemblage composition before anthropogenic development occurred may reflect conditions that are no longer attainable given the effects of factors acting at large spatial and temporal scales such as atmospheric deposition of pollutants and global climate change.

When anthropogenic impacts are spatially discernable, a paired-site approach may be useful. For example, lotic sites impacted by point source pollution such as mine effluent [37, 38] or municipal wastewater [39] may be paired with upstream sites above the source of stressors. Plafkin et al. [40] referred to paired upstream sites as controls, though this implies that confounding natural environmental factors on the upstream–downstream comparison are being actively controlled, which is generally not feasible. For bioassessments conducted over large spatial scales (e.g., ecoregions), the paired-site approach is problematic because much assemblage variation is driven by local-scale differences in natural environmental variables [41, 42]. Assemblage variation among reference sites, that is, variation that is not likely caused by impairment, is typically much larger than variation among replicate samples collected at a single site. Therefore, comparisons of replicate samples from a single reference and test site pair often do not provide a realistic representation of the effects of impairment on assemblage characteristics [43].

2.2 Reference Site Screening

Reference site screening is the process of estimating the degree of anthropogenic impairment at study sites, such that those with acceptably low stress levels may be designated as reference sites. Screening criteria vary among studies based on both data availability and on the opinions of investigators as to which criteria are most appropriate. Some have advocated for the use of professional judgment regarding whether observed assemblages represent reference conditions [44, 45]. Professional judgment may also be applied to the environmental conditions at the sites, providing a more independent, and potentially less biased, means of estimating impairment status [46]. Advocates of professional judgment often favor consensus opinions among groups of experts [45, 47]. Potential criticisms of such approaches include a lack of empirical support for decisions regarding reference designations and circular logic when sites are designated as reference based on the assemblage that is also used for bioassessment. However, Davies and Jackson [45] recently showed that the opinions of trained experts were highly consistent when rating ecological integrity based on assemblage data, leading the authors to assert that well-informed professional opinions provide reliable, ecologically relevant benchmarks for bioassessment.

Independent stressor variables (i.e., those not related to the assemblage used for bioassessment) are often used to estimate impairment status. Screening approaches that employ both professional judgment and independent stressor variables produce reference sites that are of higher ecological integrity than those selected using either approach alone [48]. Variables used to estimate anthropogenic stress include physicochemical water quality parameters, land-cover features derived using a geographic information system (GIS) that indicate development, and physical habitat quality assessments based on site observations. Studies often employ a filtering approach, whereby threshold levels for each measured stressor variable are set to designate sites as reference or impaired [21, 49]. The filtering criteria used to select reference sites are generally evaluated with an all approach for reference sites and any approach for non-reference sites. For example, Blocksom et al. [49] required that sites meet all of the reference criteria listed in Table 2 to be designated as reference, but considered sites impaired if any one of the impaired criteria was met.

The level of anthropogenic impairment considered acceptable varies greatly among studies, and many authors fail to provide clear descriptions of how reference conditions are defined. Recognizing this problem, Stoddard et al. [32] advocated for the use of the terms minimally disturbed condition (MDC) to describe expected conditions in the absence of substantive anthropogenic disturbance, least-disturbed condition (LDC) to describe the best available conditions present under current disturbance regimes, and best attainable conditions (BAC) to describe the expected conditions when all avoidable sources of anthropogenic influence are removed (BAC is generally intermediate between LDC and MDC). MDC sites, within virtually unimpacted, near pristine watersheds, are rarely available, and most

Table 2 Filtering criteria used by Blocksom et al. [49] to differentiate between reference and impaired streams in the Mid-Atlantic Highlands (USA)

Criterion	Reference	Impaired
pH	NA	<5
Sulfate	<400 μeq/l	>1,000 μeq/l
Acid neutralizing capacity	>50 μeq/l	NA
Chloride	<1,000 μeq/l	>1,000 μeq/l
Total phosphorus	<20 μeq/l	>100 μeq/l
Total nitrogen	<750 μeq/l	>5,000 μeq/l
Mean RBP score	>15	<10

RBP refers to the rapid bioassessment habitat protocol of Barbour et al. [1], where scores range from 0 to 20
It is possible for sites to have intermediate characteristics and therefore fall between the two classes
NA no filter specified

often reference sites are chosen based on the best available conditions (LDC sites; e.g., [50, 51]).

The reliability of bioassessments depends largely on the existence of a sufficient number of reference sites to encompass the range of natural variability in the study region. Given the pervasiveness of human impacts on aquatic ecosystems, achieving a sufficient number of reference sites is often difficult, and may be impossible if standards regarding the acceptable level of impairment are unrealistically high [50, 51]. Impairment is highly variable among geographic regions because development pressure is nonuniform. Recognizing this, Yates and Bailey [50] developed a novel strategy for selecting reference sites that allowed for flexibility in the standards used for screening to select LDC sites within study regions exposed to different impairment regimes. This is a pragmatic strategy, as flexibility in the level of impairment allowed is unavoidable in areas where impairment is pervasive; however, clear comparisons of bioassessment results among studies are hindered when the standards used to select reference sites vary.

2.3 Reference Site Classification

Reference sites that successfully pass the screening process are used to predict assemblage conditions under minimal impairment. Classification of reference sites is intended to increase the precision and accuracy of these predictions by grouping sites inhabited by similar ecological assemblages. Broadly, there are two major types of classification systems: (1) typologies, wherein sites are grouped based on spatial proximity and/or similarity in their natural environmental variation, and (2) biotic classifications, which employ statistical analyses on assemblage data to group sites. We begin by discussing the two as distinct approaches, although bioassessment programs often use elements of both to develop the best site classifications. Throughout this section, we discuss analytical techniques that are

specialized for the analysis of assemblage data. McCune and Grace [52] and Legendre and Legendre [53] present additional details on most of the analytical methods presented here. Software for conducting most of the techniques is available free of cost in the R statistical programming language [54].

The objective of classification is to maximize assemblage similarity within classes, while maintaining sufficient replication to allow for statistical comparisons of test sites with the reference classes. Many measures of assemblage similarity exist [52, 53]. The Bray–Curtis coefficient [55] for abundance data and the Sorenson coefficient [56, 57], the equivalent of Bray–Curtis for presence-or-absence data, are most commonly used. Both are well suited to the numerical structures of assemblage datasets. Similarity may also be calculated using bioassessment metric values in place of taxonomic data (a sound but under-used technique, [58]).

Similarity is summarized as the mean within-class similarity (W, the mean of all pairwise similarities of sites within classes) and the mean between-class similarity (B, the mean of all pairwise similarities of sites not in the same class). The precision of a classification is described by the relationship of W to B, referred to as the classification strength [58]. High classification strength is indicated by a large positive difference or large ratio of within- to among-class similarity (i.e., high W–B or W/B). Predictions regarding assemblage conditions are most reliable when classification strength is high. Multivariate techniques such as MEANSIM [58], analysis of similarity [59], multiresponse permutation procedure [60], and nonparametric, multivariate analysis of variance [61] are used to test the hypothesis that classification strength is higher than expected by chance, providing an indication of whether the classification improves the reliability of predictions regarding reference conditions.

2.3.1 Typological Site Classification

Typological site classifications are based on a priori judgments regarding the site conditions that best group reference sites with similar assemblages. Early typological approaches focused on coarse-scale, map-based classifications (e.g., ecoregions) [62, 63]; however, typological classifications that do not account for the effects of local-scale variables typically exhibit much lower classification strength than biotic classifications [43, 64, 65]. Typological classifications are a convenient and useful tool that should be at least considered as an initial step toward site classification [65, 66]. Like all classifications, the effectiveness of a priori-defined typologies should be assessed by a posteriori, quantitative evaluations of the assemblages of interest [66]. For example, investigators in Virginia (USA) observed a striking difference in stream macroinvertebrate assemblage structure between low-gradient coastal plain sites and upland piedmont and mountain sites, requiring the use of separate bioassessment indices for coastal and non-coastal sites (Fig. 1) [67, 68]. Because assemblages are affected by both regional- and local-scale environmental factors, typological classifications that consider smaller spatial-scale variables as well as large-scale zones may provide comparable, or greater, classification strength than biotic classifications [64, 69].

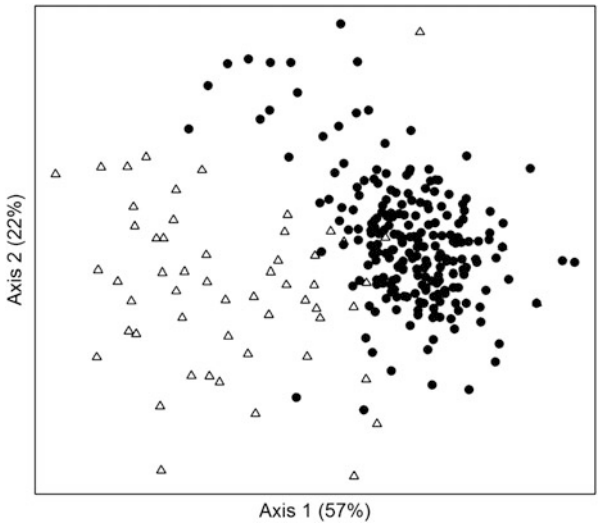

Fig. 1 Nonmetric multidimensional scaling ordination of macroinvertebrate assemblages, identified at the family level, from 269 least-impaired, reference Virginia stream sites. *Symbols*: (*open triangles*) coastal plain sites; (*filled circle*) non-coastal sites. Distances between sites correspond to their proximity in Bray–Curtis distance space. Percentages indicate the percent of variance in the Bray–Curtis coefficients explained by the axis coordinates. Adapted from Dail et al. [67] with permission

2.3.2 Biotic Site Classification

Biotic classification of reference sites came to prominence with the introduction of the River Invertebrate Prediction and Classification System (RIVPACS, [70, 71]). Agglomerative cluster analysis is used in many variations of the RIVPACS approach, including those developed for the USA [72] and the Australian River Assessment Scheme (AUSRIVAS, [73]), both of which employ presence/absence data for clustering, and the Benthic Assessment of Sediment (BEAST) method of Canada [74] which clusters based on abundance data. Agglomerative clustering proceeds from the bottom up, progressively grouping sites of increasingly dissimilar taxonomic composition. Most investigators cluster sites based on Bray–Curtis or Sorenson dissimilarity [72–76], although other measures such as Euclidean distance can be employed [77]. Figure 2 shows a cluster analysis of 46 Kentucky (USA) stream reference sites where genus-level macroinvertebrate data were collected by the USEPA.

The standard RIVPACS approach classifies sites using two-way indicator species analysis (TWINSPAN, [79]). In contrast to agglomerative cluster analysis, TWINSPAN is a divisive technique, whereby sites are progressively divided based on taxa (indicator species) that best differentiate them. Also unlike agglomerative clustering, the user cannot choose a dissimilarity measure [80]. TWINSPAN has

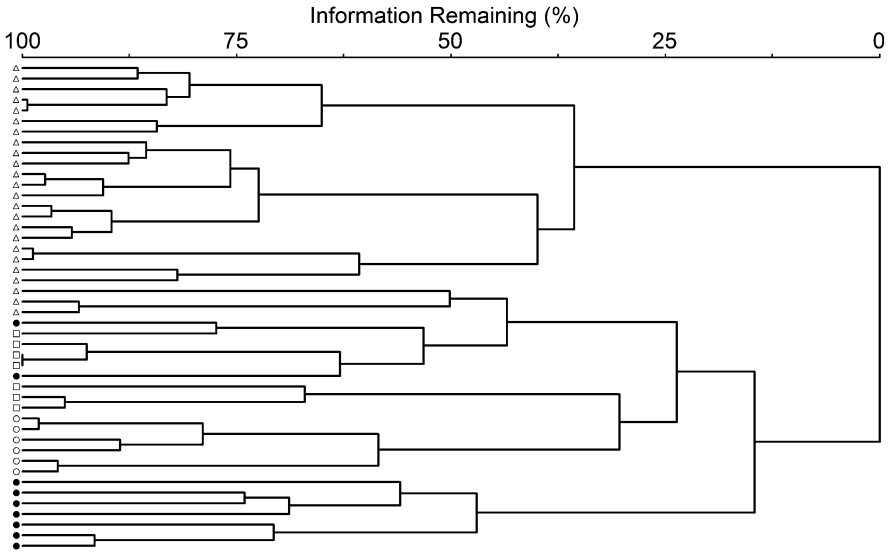

Fig. 2 Agglomerative cluster dendrogram generated using the flexible-beta method ($\beta = -0.30$) on a Bray–Curtis dissimilarity matrix of genus-level macroinvertebrate data at 46 least-impaired Kentucky stream sites. Branch lengths correspond to dissimilarities between sites and clusters. Bioregions are regional classifications as described by Pond et al. [78]: (*open triangle*)—Mountain; (*filled circle*)—Miss. Valley-Interior River; (*open square*)—Pennyroyal; (*open circle*)—Bluegrass. The Mountain and Bluegrass regions separate perfectly. Some overlap occurs for other bioregions because Julian day and latitude (not included in the analysis) were also important variables related to assemblage structure in these bioregions. Data courtesy of Gregory Pond, USEPA

received criticism for poor performance and seemingly arbitrary methodology [52, 81]. However, based on comparisons with other techniques, the developers of RIVPACS concluded that TWINSPAN performed well, and the method is still used within the current RIVPACS framework [80].

Relationships among sites can be visualized using a variety of ordination techniques, which reduce the *n*-dimensional hyperspaces created by ecological distance matrices to fewer (usually 2 or 3) dimensions that best explain the overall pattern of variability (Fig. 1) [52, 53]. When assemblage–environment responses are assumed to be linear, principal components analysis (PCA) is commonly used, whereas when responses are assumed to be unimodal, reciprocal averaging-based techniques such as correspondence analysis (CA) and detrended correspondence analysis (DCA) are often used. We agree with others [52, 82] in preferring nonmetric multidimensional scaling (NMS) to these techniques because NMS includes no assumptions regarding the underlying data distribution and is highly effective at explaining assemblage structure while reducing dimensionality. Ordinations are often used for exploratory purposes, for example, to confirm classifications made using other analyses [76], but also may be used directly for site classification [67, 83].

Multivariate analyses on assemblage data aid in showing the user where distinctions between classes may occur. However, subjectivity in drawing distinctions among classes is unavoidable, as investigators must decide on the appropriate level of similarity at which to consider sites within the same class [84]. The final decision is made as a compromise between including as many reference classes as possible, while still including enough replicate sites within classes to adequately represent within-class assemblage variability among sites. Bowman and Somers [85] recommend "a minimum of 20, but preferably 30–50 reference sites per group," though this may be overly optimistic given the data constraints experienced in many studies.

2.3.3 Conclusions Regarding Site Classification

Hawkins et al. [43] and Melles et al. [86] draw distinctions between geography-based methods in which reference classes can be clearly delineated within discrete spatial units and geography-independent methods driven by patterns in assemblage variation regardless of physical location. Typological classifications which include map-based delineations of classes are geography dependent, whereas biotic classifications, focused on patterns of assemblage variation, are geography-independent. However, the most effective classifications consider both geography-dependent and geography-independent factors, for example, limitations on the spatial scale over which biotic classifications are developed can increase their classification strength [87]. While biotic classifications provide precise descriptions of the patterns of variability with respect to the assemblage of interest, the resulting classifications may not be applicable to other assemblages. Inclusion of geography-dependent variables that implicitly encompass a wide range of environmental factors provides a more comprehensive classification of sites [88]. A priori typological classification based on large-scale variables (e.g., ecoregions) provides useful, convenient, and easily communicated initial classifications of sites, though classifications are often improved when supplemented by smaller-scale variables that are not spatially discrete (e.g., flow regime; [89]) or not associated with geography (e.g., sampling date; [75]). Good scientific practice requires that the effectiveness of a priori approaches be evaluated with a posteriori evaluations of relationships between classes and biota [64–67, 88].

3 Predictive Modeling of Aquatic Assemblages

The objective of predictive modeling for bioassessment is to control for the confounding effects of natural environmental variables so that the effects of stressors on metrics can be clearly evaluated. The methods used to meet this objective are as diverse and varied as the assemblages themselves. As an introduction to the core concepts in predictive modeling, we outline the basic steps of the

Table 3 Example calculation of *O*/*E* based on biotic classes and distances in environmental space shown in Fig. 2

Reference class	Distance from test site in discriminant space	Class probability of test site	Probabilities of capture at reference sites		
			Taxon A	Taxon B	Taxon C
1	4.4	0.47	0.70	0.20	0.10
2	5.2	0.31	0.70	0.25	0.05
3	5.9	0.20	0.20	0.50	0.10
	Probability of capture at test site:		0.59	0.29	0.09
	Expected richness at test site (*E*):		0.97		

Data were simulated for example purposes only
Distances were converted to class probabilities following equations 2 and 3 in Clarke et al. [90] (distances are D^2 values as described in [90])
All classes contain 20 sites
The probability of capturing a taxon at the test site is given by multiplying the class probabilities of the test site for each reference class by the corresponding probabilities of capture of the taxon at sites within each reference class
For example, the probability of capturing Taxon A at the test site is $0.47 \times 0.70 + 0.31 \times 0.70 + 0.20 \times 0.20 = 0.59$
The probabilities of capture for each taxon are summed to give the expected richness (*E*) at the test site

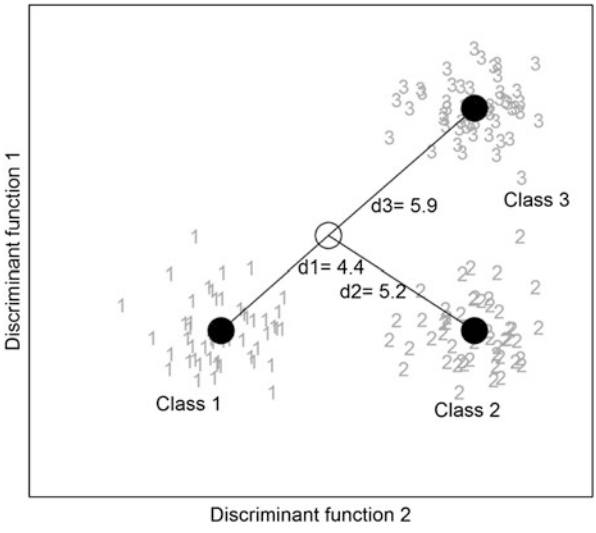

Fig. 3 Reference and test sites displayed in environmental distance space as defined by two discriminant function axes. Discriminant function scores were simulated from normal distributions with variance = 1. *Symbols*: (*filled circle*) reference class centroids, (*open circle*) test site, (1, 2, 3) reference sites, (d1, d2, d3) distances in discriminant function space between test sites and reference class centroids

RIVPACS framework and present an example of its use in Table 3 and Fig. 3. Although now 30 years old, the framework remains relevant and is still used with little modification of the original methodology [70, 75, 80]. The conceptual basis and technical details of RIVPACS have been described thoroughly by others [71, 72, 90]. Following our introduction to RIVPACS, we present several promising recent advancements in predictive modeling.

3.1 The Observed-to-Expected (O/E) Index

The standard metric derived from RIVPACS-type predictive modeling approaches is the observed-to-expected ratio (O/E), a single-metric index that compares the observed taxonomic richness at a study site to the expected richness under minimally impaired conditions. The O/E ratio indicates the degree of "taxonomic completeness" (sensu Hawkins [91]) of the test site. O/E values less than one indicate that taxa expected to be present if the sites were unimpaired are absent.

Following biotic classification of reference sites, RIVPACS employs Multiple Discriminant Analysis (MDA) to develop linear functions that best describe the relationships of natural environmental variables to the biotic classes. The discriminant functions are used to determine the distance, in environmental variable space, of the test site to the biotic reference classes, which in turn are used to estimate the probabilities that the test site belongs in each reference class (referred to here as class probabilities). For all native taxa in the study region, the proportion of reference sites within a given biotic class where a taxon is present represents the probability of observing that taxon at a site in that class (referred to as the probabilities of capture). The probabilities of capture of a given taxon within each reference class, and the class probabilities of the test site for each reference site, are used to estimate the probability of capturing the taxon at the test site assuming unimpaired conditions. The expected richness at the test site (the E in O/E) is given by summing probabilities of capture at the test site for all taxa (see Fig. 3 and Table 3 for additional details).

O/E values greater or less than one indicate departures from what is predicted under unimpaired conditions. Simpson and Norris [92] recommended that O/E values below the tenth percentile of the reference site distribution indicate impairment, with the extent of impairment increasing as the ratio decreases. They also postulated that O/E values greater than one may indicate areas of exceptionally high natural biodiversity or those subject to mild impairment that artificially increases richness.

A common modification to the basic framework is to exclude rare taxa from the analysis, as their inclusion can result in a site receiving an O/E score near one when the assemblage observed deviates considerably from statistical expectations. Several authors have indicated that excluding taxa with probabilities of capture less than 0.5 (producing the $O/E_{0.5}$ index) improves accuracy and precision [72, 93, 94]. As an alternative, Van Sickle [93] adapted the Bray–Curtis dissimilarity measure to compare observed and expected assemblages (referred to as BC) and showed that BC was generally more accurate than O/E for identifying impairment across a wide range of assemblages and study systems. $O/E_{0.5}$ and BC indices developed for Appalachian stream macroinvertebrate assemblages exhibited similar accuracy and precision [75].

3.2 Advances in Predictive Modeling

The widespread application of RIVPACS-type models has inspired many alternative approaches. Recognizing that assemblages occur along continuous environmental gradients, investigators have developed nearest neighbor methods that compare the environmental similarity of test sites to each individual reference site, rather than to the average assemblage of each class as is done using RIVPACS [83, 95]. Modeling approaches often skip the biotic classification step and predict assemblage characteristics at reference sites directly using natural environmental variables [96–98]. Direct prediction approaches may allow for different sets of environmental variables to be used as predictors for each taxon. Though appealing in this respect, the development of separate models for each taxon may be overly complex for taxon-rich systems.

In contrast to the long history of predictive modeling for *O*/*E* indices [70], until recently, developers of MMIs rarely employed predictive modeling to account for natural environmental variability. McCormick et al. [99] used linear regression to control for the effects of watershed size on a fish MMI. Equations derived from the regression of metric values on watershed size at reference sites were applied to test sites, and the residuals from the regression were used to indicate deviations from the expected metric values in the absence of impairment. Oberdorff et al. [100] expanded this approach, modeling metrics based on a suite of natural environmental variables using logistic regression (for presence/absence metrics) and multiple linear regression (for abundance-based metrics). Variations on this residualization technique have been developed for more advanced modeling strategies such as prediction tree approaches (discussed below), improving both the accuracy and precision of MMIs by removing the confounding effects of natural environmental variables [21, 101, 102].

Although conventional techniques such as MDA and linear and logistic regression have provided utility for predictive modeling, several newer methods better account for the variable, often nonlinear and interactive effects of environmental predictors on biota. The generalized additive modeling approach of Yuan [103] shows the flexibility of this nonparametric regression technique for predicting variable responses among different taxa to a suite of environmental factors. Bayesian frameworks provide a comprehensive evaluation of uncertainty in predictive models [104–106] and have been used for this purpose in MMI development. Machine learning techniques, including artificial neural networks (ANNs) and ensemble prediction trees, where models are iteratively trained at prediction to minimize error, have received much recent attention for predictive modeling in ecology [107–110]. Though the method is not yet widely used, support vector machines have performed favorably compared with other machine learning techniques for predicting the occurrence of macroinvertebrate taxa [111, 112].

ANNs structure predictor–response relationships in a manner similar to vertebrate neurological systems. Variables are represented as neurons connected by a multitude of axons representing the possible interrelationships among variables

[113]. ANNs have shown substantial improvement over traditional RIVPACS-type models for predicting the richness of macroinvertebrate and fish assemblages [97, 114].

Prediction tree approaches such as classification and regression trees account for the complex effects of both continuous and categorical predictors by recursively bisecting the dataset into groups that are increasingly similar with respect to the response variable after each division [52, 53, 115]. Ensemble prediction tree approaches such as random forests and boosted regression trees combine the results of hundreds to thousands of trees to reduce prediction error. Random forests have been used to model assemblage metrics directly [21, 101, 116] and to define relationships between environmental variables and predefined biotic classes, effectively replacing MDA as used in RIVPACS [12, 101]. Comparisons of random forests to boosted regression trees, a related ensemble tree method, indicate that the latter may provide superior performance [108, 117].

In the absence of suitable reference sites, investigators have used whole-set approaches that employ all sites in the dataset, rather than only reference sites, to control for the effects of natural environmental variables. Most whole-set approaches involve the use of regression techniques to model the responses of metrics to stressors and then to estimate metric values at the point where the model estimates that no impairment occurs [118, 119]. Because few to no minimally impaired sites are included in these analyses, they are effectively estimates by extrapolation of a stressor–response gradient and therefore may be subject to greater prediction errors than models for which reference sites are available. Such errors, however, may be unavoidable when test sites cannot be matched with comparable reference sites. As an alternative whole-set approach, Chessman and Royal [120] estimated the tolerance limits and preferences of macroinvertebrates to substrate, temperature, and flow conditions across an extensive dataset of Australian rivers. These limits were then used to predict the presence of taxa and derive *O*/*E* values at test sites, which exhibited stronger correlations with stressor gradients than *O*/*E* values derived using the AUSRIVAS method.

A case for using the whole-set approach as a replacement for the RCA was recently presented [121]. Data simulations were conducted to model scenarios in which natural environmental variables and stressors affected biotic metrics independently and also interactively. Metrics that were model-adjusted using the whole-set approach exhibited more accurate and precise relationships with the simulated stressor gradient than metrics adjusted using the RCA. The difference in performance was greatest when stressors and natural environmental variables interacted, as the RCA cannot account for such interactions. While the authors present a compelling case, additional field-based empirical comparisons of the whole-set approach to the RCA are needed.

4 Index Development and Performance Evaluation

We begin this section by discussing methods for evaluating the performance of metrics and indices (Sects. 4.1–4.4). For MMIs, these characteristics should be evaluated in order to include the best-performing metrics in the final index. Final metric selection, scoring, and aggregation are discussed in Sect. 4.5. After scoring and aggregation of metrics within an MMI or alternatively the development of an *O*/*E* index, performance should be re-evaluated using the finished index scores, ideally using independent data not used for index construction (Sect. 4.5). Further information on MMI development has been presented by others [1, 32, 122]. For clarity, these works present index development in a stepwise manner; however, it is important to note that index development is an iterative, rather than a linear process. Metrics that are acceptable based on one criterion (e.g., numerical range, Sect. 4.1) may subsequently be considered unacceptable based on another criterion (e.g., accuracy, Sect. 4.2), requiring the evaluation of new metrics.

4.1 Numerical Range

Assemblage data are often plagued with abundant zeros due to the patchy distribution of biota among habitats, and metrics related to rare taxa typically have narrow numerical ranges. Metrics with limited ranges, and those for which many sites in the dataset exhibit the same value, are unlikely to exhibit clear numerical responses to stressors [123]. Others have presented guidelines for acceptable numerical ranges for metrics, though these vary among studies [123–125]. Simple distribution plots of metric values often provide clear indications of highly limited metrics (e.g., see Fig. 2 in [122]).

4.2 Accuracy and Precision

We broadly define accuracy as the degree to which a given metric or index is quantitatively related to variations in anthropogenic stress. Accurate metrics and indices exhibit low Type II error rates by correctly identifying impairment and low Type I error rates by correctly identifying reference conditions. As others have indicated [126], the precise impairment state of a system, and therefore the absolute accuracy of metrics, can never be truly known. We therefore use the term accuracy to refer to estimated accuracy for identifying impairment, as indicated by relationships of metrics with a priori-selected stressor variables.

Relationships between metrics with continuously varying stressor variables may be expressed using correlation analysis. The objective is often to assess the responsiveness of metrics to overall stressor gradients. PCA is commonly used

to aggregate individual stressor variables into a comprehensive index of impairment. Metrics and indices can then be evaluated as to the strength of their correlation with this aggregate stressor index [124, 127, 128]. Tests of whether metrics differ significantly from reference conditions provide binary results regarding whether a metric classifies sites correctly. Standard approaches such as ANOVA, however, may indicate statistically significant differences that are not biologically meaningful [123, 129]; therefore, specialized techniques have been developed that are more practical for determining whether metrics differ from reference conditions [129–131]. The magnitude of the departure from reference conditions is most important, regardless of statistical significance. To this end, test statistics such as ANOVA F-statistics or t-scores, rather than p-values, are used to determine the degree to which metrics differentiate between reference and stressed sites [116, 123, 125]. Estimates of Type II error rates are given by choosing a threshold value in the reference site distribution that indicates impairment (e.g., 5th or 25th percentile for metrics that decrease with stress and the 95th or 75th percentile for those that increase with stress) and determining the proportion of impaired sites where metric scores exceed this threshold (for metrics that increase with stress), indicating that impairment has not been correctly identified [132]. Barbour et al. [133] developed a similar, graphical approach for evaluating the degree to which metrics and indices discriminate between reference and impaired conditions (Fig. 4). Distribution-based methods such as these are especially susceptible to the confounding effects of outliers, which should be carefully scrutinized to determine whether they are caused by imprecise metrics or site misclassification.

Measures of precision describe the reliability of metrics and indices for consistently indicating site conditions. Those that exhibit high variability that is not attributable to environmental predictors are not useful for bioassessment. Precision is expressed by measures of variability in metric or index values among samples, most commonly as the standard deviation (SD) or coefficient of variation (CV). Variance partitioning is conducted to determine the relative importance of the three primary sources of variation: among-site spatial variation, within-site spatial variation, and temporal variation [29, 134].

Temporal precision is often evaluated using the signal-to-noise ratio (S/N) [135], which is the ratio of metric variance among sites to variance among multiple visits at the same site. When evaluated using both stressed and reference sites, S/N reflects both accuracy and temporal precision. Stevenson et al. [125] set $S/N > 2$ as the acceptable ratio for diatom metrics. Stoddard et al. [123] indicated that acceptable S/N values should vary, based on organisms' generation times, from >1 for algae to >4 for fish (though these preliminary guidelines require further evaluation). Within-site spatial precision is reflected by metric variability in samples collected at the same site and time, which may be affected by sampling error among spatially or temporally replicated samples [134, 136] or by variation among bioassessments employing different protocols [134, 137].

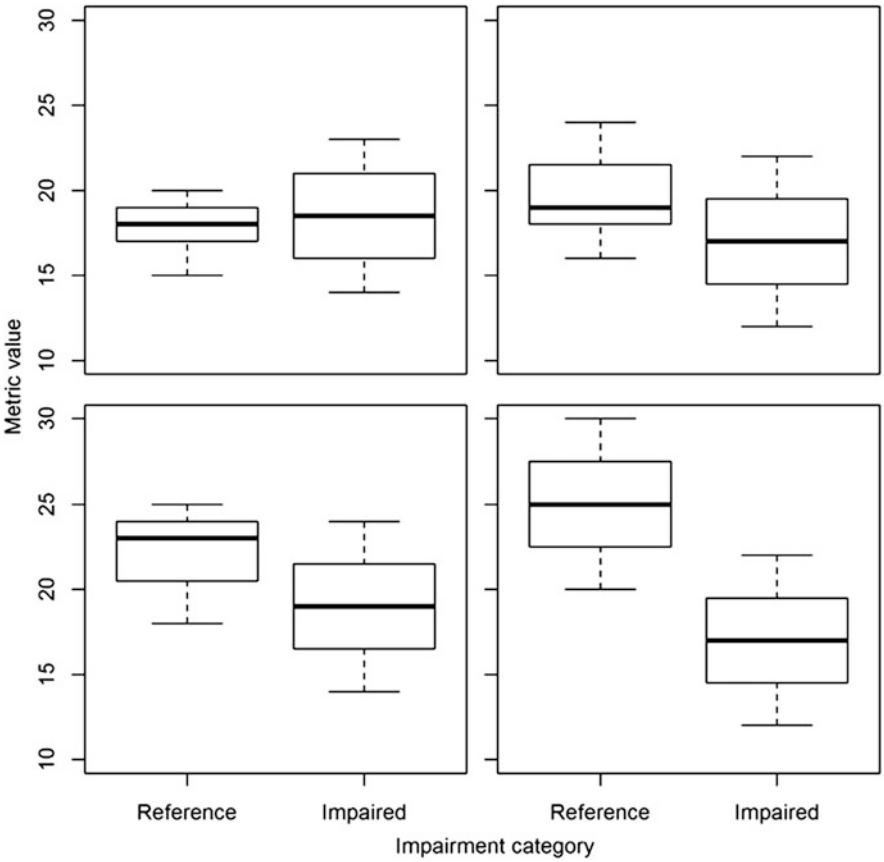

Fig. 4 Box plots of simulated data illustrating the method of Barbour et al. [133] for evaluating the discriminatory power of metrics and indices. Boxes represent 25th and 75th percentiles; whiskers represent non-outlier maximum and minimum values. The metric is expected to decrease with impairment. *Top left*: discriminatory power = 0 (lowest), as the reference and impaired site interquartile ranges (IQRs) overlap and include both medians. *Top right*: discriminatory power = 1 because the IQR overlap includes only one median value. *Bottom left*: discriminatory power = 2 because the overlap does not involve either median. *Bottom right*: discriminatory power = 3 (highest) because the IQRs do not overlap

The among-site precision of metrics and indices may be assessed among sites within the same reference class, thus limiting the confounding effects of environmental variability on the evaluation. For both *O*/*E* indices and MMIs, the ratio of observed-to-expected metric values at reference sites should differ negligibly from one, and thus the standard deviation (SD) for this ratio should be nearly equal to its coefficient of variation (CV). The distribution of observed-to-expected metric or index values provides a graphical illustration of both accuracy and precision (Fig. 5) [72].

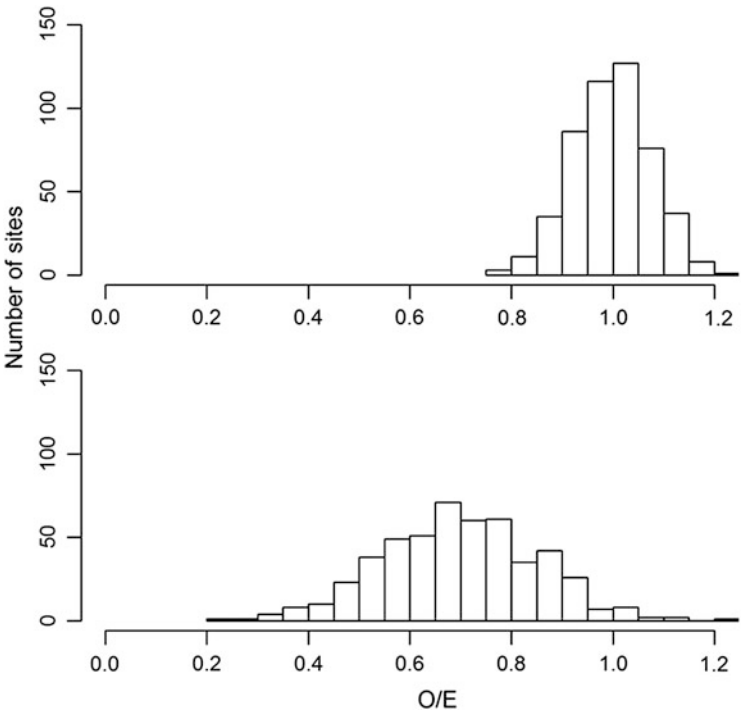

Fig. 5 A graphical comparison of the accuracy and precision of two *O/E* indices (after methods in [72]). Figure *panels* depict frequency distributions of *O/E* values for two indices at reference sites. The data were simulated for example purposes only. The *O/E* index in the *top panel* is relatively accurate (mean = 1.01) and precise (SD = 0.08). In contrast, the index depicted in the *bottom panel* is less accurate (mean = 0.70) and less precise (SD = 0.16, also note the greater spread of the distribution). This approach can be modified to assess the value distribution of any metric or index at reference sites (e.g., [125])

4.3 Metric Redundancy

Redundant metrics may respond in the same manner to stress and if used together result in overly complex indices that include metrics that do little to increase (and may decrease) accuracy. The problem of redundancy has long been recognized, although the best approach for minimizing it remains unclear. Some investigators prefer to focus on ecological redundancy by including metrics from different ecological categories [122, 128], while others focus on reducing statistical redundancy by evaluating pairwise correlations among metrics and choosing only one metric within each pair that is correlated [124]. Combinations of these approaches may be employed, which consider both ecological and statistical redundancy [138].

Correlations among metrics generally reduce MMI precision and accuracy, but these characteristics appear to be most related to the mean pairwise correlation rather than the maximum correlation among metrics in an index [139]. To best

reduce the mean correlation among a group of potential metrics, multivariate analyses such as PCA and cluster analysis can be used to aggregate correlated metrics [21, 101, 102]. The correlation of metric errors (e.g., residuals of stressor–metric regressions) rather than the correlation of metric values may be more appropriate for judging redundancy, a concept whose applicability should be further evaluated [140].

4.4 Metric Aggregation and Scoring

MMI development is completed by aggregating the best-performing metrics to derive an index score. The number of metrics used in the index varies among studies, and the choice is rarely supported by clear empirical justification [139]. Professional judgment is often used to select metrics based on best overall performance, although ordered stepwise processes have been recommended and present more comprehensive and objective options [139, 140]. To express metrics on an equivalent numerical scale, raw values are commonly rescaled to reflect percent or proportional comparability to values in the reference site distribution or to the distribution of all sites producing metric scores on continuous 0–100 or 0–1 point scales that increase with impairment. Blocksom [49] reviewed the details of these and other common scoring methods. After scoring, metrics are nearly always aggregated into an index by simple averaging, although other methods, such as differential weighting based on relative importance [131, 141] or to account for variations in metric precision [131], have been used. Alternative aggregation strategies for MMIs represent yet another area where additional research is needed.

4.5 Index Validation

Validation of the index with independent data provides the most comprehensive evaluation of performance. Validation typically proceeds by randomly selecting subsets of impaired and reference sites, which are excluded from the dataset used for index development and used for *a posteriori* evaluation of the performance characteristics described above. The feasibility of index validation depends on the amount of data available, as statistical power is compromised by dividing datasets for this purpose. Categorical approaches for validating index accuracy are data expensive, as the validation set must be divided according to impairment status. When only a few sites are available, index accuracy may be validated by analyzing for correlations of index scores with stressor gradients, which requires fewer validation sites. This approach is especially useful in highly developed landscapes where there are few reference sites [127, 142]. Index accuracy is often prioritized over other performance characteristics, although more thorough validation strategies also evaluate precision [21, 106, 143]. Evaluation of index bias, as indicated by

relationships between indices and natural environmental variables, provides further information on index performance [21, 101, 106, 116].

The effectiveness of predictive models used for reference site classification is often evaluated using cross-validation by constructing models using only subsets of the available data. Leave-one-out cross-validation is a data-efficient method in which reference sites are excluded from the dataset one at a time. After each exclusion, the classification and modeling process is repeated. Each left-out site is then classified using the model constructed without that site. The proportion of agreements between original and cross-validated classifications, relative to the total number of reference sites, is a measure of the effectiveness of the model. This technique can be used with any site classification approach [114, 134, 144]. Null models, which are constructed by predicting metric values across all reference sites, with no classification, are useful for evaluating all types of classifications. If classification strength does not exceed that of the null model, then the classification provides no advantage [145].

5 Expert Interviews: Challenges and Important Considerations in Bioassessment

To provide a broader and more comprehensive perspective, we conducted interviews with three expert practitioners and developers of bioassessment programs. Their responses to our questions, provided here in a question-and-answer format, have been summarized with a focus on emerging issues relevant to bioassessment in aquatic systems.

Expert 1 Michael Barbour, Ph.D.—Adjunct Senior Scientist, Mote Marine Laboratory, Sarasota, FL, USA, and retired Director, Center for Ecological Sciences, Tetra Tech, Inc., Owings Mills, MD, USA

Q: What factors limit the potential for increased use of genetic information in bioassessment surveys? Is it likely that molecular genetic analysis will replace traditional taxonomic approaches, or will these processes be used in conjunction with each other?

A: A major challenge in the use of genetic data for bioassessment will be in determining how reference conditions are expressed and how to account for the effects of natural environmental variability on reference populations. It is unlikely that genetic analysis will replace traditional taxonomic approaches in the near future. Evolving DNA methods, however, should help to decrease taxonomic uncertainty and improve our evaluations of aquatic assemblages.

Q: What are the most important factors to consider in developing a bioassessment program?

A: Adherence to the Critical Elements Process in the design and implementation of bioassessment protocols should provide an objective means of evaluating the rigor of regulatory assessment programs and a basis for comparing data quality

among programs [146]. This process is used to evaluate programs with respect to 13 critical elements within three general categories: study design, methods implementation, and data interpretation. The process considers logistic feasibility and cost-effectiveness, calling for the highest methodological and data-quality standards that are reasonably attainable given existing technological and monetary constraints. When high-quality methods exist, new bioassessment programs should employ methods consistent to these to maximize efficiency (i.e., use of preexisting datasets) and historical significance.

Q: What are the most important recent developments that have improved comparability among assessment programs?

A: In addition to the critical elements process, the Biological Condition Gradient approach (BCG, [45]) provides a framework for developing consistent, meaningful, and understandable aquatic life use standards and is applicable to a wide variety of monitoring strategies and assemblages. The BCG establishes a baseline by employing best professional judgment within an organized framework whereby experts assign bioassessment samples to ecological condition tiers. Biologists trained to use the BCG produce highly consistent evaluations of site conditions. The use of the BCG should greatly facilitate the comparability of bioassessments conducted by different agencies and using different protocols.

Large-scale monitoring programs, such as the USEPA National Aquatic Resource Survey, are of great importance. This nationwide assessment program includes standardized sampling protocols and a probabilistic study design for the assessment of US streams, rivers, lakes, wetlands, and coastal waters. The ongoing intercalibration exercise, a key component of the European Union (EU) Water Framework Directive (EC 2000/60/EC; [147]), and resulting multi-country aquatic ecosystem surveys are other important examples. The major advantage of these programs is the development of consistent and rigorous protocols that allow for large-scale biological assessments of aquatic ecosystems.

Expert 2 Simone D. Langhans, Ph.D.—Humboldt Research Fellow, Leibniz Institute of Freshwater Ecology and Inland Fisheries, Berlin, Germany

Q: What factors are most important in limiting comparability among bioassessment schemes?

A: Variability in the definition of reference conditions (i.e., the allowable amount of impairment within the reference dataset) can hinder the comparison of index scores from different assessment programs. Index scores are typically an expression of how similar a site is from the reference state; therefore, the use of similar reference criteria facilitates comparability among assessment indices.

The expression of index scores in a continuous manner, rather than as categorical ratings, is helpful when aggregating scores derived from different assessment schemes. Due to their discrete nature, categorical ratings may differ for scores that are actually quite similar; therefore, the most reliable aggregated indices are based on continuous scoring systems. For management purposes, categorical ratings can be applied after aggregation. Langhans et al. [141] present a method for standardizing metric scores or attribute measures among indices to a continuous

0–1 scale. The method can be applied to both categorical and continuous scales and preserves the best professional judgment of developers regarding the interpretation of score or measurement values.

Q: What aspects of the relationships of anthropogenic activities and ecological integrity are most misunderstood by nonscientists?

A: The watershed (or catchment) concept is of great importance, though often not understood by the layperson. Following from the simple concept that water flows downhill, water bodies integrate the effects of human activities everywhere within their watersheds. Responsible management of aquatic ecosystems must consider not only in-stream and local effects but also effects at much larger spatial scales. The range of relevant spatial scales that should be considered increases with the size of the water body, with the largest river systems integrating the effects of anthropogenic activities over thousands of square kilometers.

Q: In considering streams in different natural settings and at different positions along the general gradient of impairment, which are the most important candidates for preservation or restoration?

A: How best to prioritize conservation and restoration efforts for aquatic ecosystems is currently a popular and important topic in the EU. A strategy that considers the conservation of existing ecological integrity and the restoration of impaired systems simultaneously is best. When biological assemblage objectives are given high priority, the most effective areas for restoration are those in close proximity to high-quality conservation areas because the conservation areas provide sources for recolonization. For example, Tonkin et al. [148] evaluated the likelihood of recolonization by invertebrates at 21 river restoration sites in Germany. They determined that the density of occurrence of a taxon at surrounding sites (proportion of sites with the taxon present) and the distance to the nearest potential source site were important factors for predicting recolonization.

Expert 3 Gregory J. Pond, M.S.—Aquatic Biologist, USA Environmental Protection Agency, Region III, Wheeling, WV, USA

Q: Given the myriad protocols currently employed to conduct assemblage-level assessments, what considerations should be made by investigators and managers to select the most accurate, precise, and cost-effective strategies?

A: Protocols should be flexible, thoroughly documented in standard operating procedures, and based on the varying assessment goals, characteristics of the system being studied and available funding. For example, species-level macroinvertebrate data may in some cases produce the most effective assessment results. In other situations, temporal variation among samples may produce confusion at high levels of taxonomic resolution, for example, if errors in identification increase at times of the year when early instars predominate in the samples. In such cases, coarser taxonomic resolution at the genus or family level may be necessary to avoid inconsistency among samples.

If assessment on a large spatial scale is a priority, investigators may use less time-intensive methods to assess a greater number of sites within the time and monetary constraints of the project. In an attempt to provide a spatially

comprehensive assessment of Pennsylvania (USA) waters, the state's Department of Environmental Protection (DEP) conducted rapid surveys focused on macroinvertebrate assemblage characteristics that could be evaluated in the field by trained biologists without the need of extensive sampling and laboratory processing. This protocol allowed DEP to conduct an initial screening of several thousand stream sites over a 2-year period within budgetary constraints. However, the accuracy and precision of field-based rapid surveys such as this are likely far lower than would be expected from more intensive sampling and processing protocols that produce quantitative, genus- or species-level datasets.

Data consistency and comparability are also of great concern. When USEPA conducts bioassessments, the protocols developed by the state are typically followed. This insures that the data collected are comparable with those produced by state biologists and that the methods have been calibrated for the region of interest. Natural variability of system-specific characteristics should also be considered. For example, Virginia (USA) is currently developing a new protocol for swamp streams, which have not been previously assessed for regulatory purposes.

Q: What are your thoughts regarding the use of continuous environmental variables within a predictive modeling framework versus typological approaches for reference site classification?

A: Large-scale typological approaches have generally been insufficient in accounting for the variation in natural environmental factors that affect biota among aquatic systems. Typological approaches, however, are convenient, easy to use and understand, and can be effective within relatively small and homogenous geographic regions. Natural environmental gradients often persist within typological categories, and care should be taken to ensure that typological approaches do not oversimplify these gradients. Predictive modeling is more analytically intensive and requires more precise data, but generally provides more reliable results in highly heterogeneous regions. In the development of an *O*/*E* model for Central Appalachian streams, Pond and North [75] determined that subecoregion [149], Julian day and latitude were the most important natural predictors of reference macroinvertebrate assemblages. For that study region, a predictive modeling approach was chosen as the best strategy, given the importance of the continuous variables Julian day and latitude. A typological approach, where reference conditions are developed at the subecoregion level, could also be effective; however, the effects of latitude and seasonality should be carefully observed and potentially controlled.

6 Conclusions

In this chapter, we provided an introduction to the major components of assemblage-level bioassessments of aquatic systems. Macroinvertebrates, fish, and algae are the most commonly used assemblages, although the methods described here are applicable to, and have been successfully used with, other biotic

assemblages [150–152]. One emerging strategy is in the use of prokaryote assemblages, which has historically been limited because many prokaryotes are not readily cultured in the laboratory. However, emerging technologies that allow for quantification of assemblage composition through DNA sequencing have largely removed this limitation, making prokaryote assemblage assessments an emerging new option for bioassessment of aquatic systems [152, 153]. Rapidly evolving DNA sequencing methods have the potential to greatly enhance not only bioassessments using prokaryotes but also those using assemblages that have traditionally been evaluated by identification of specimens based on morphological characteristics [154–157].

Regardless of the assemblage type chosen or the methods used for identifying taxa in the assemblage, the most challenging aspect of bioassessments has been, and remains, the difficulty in separating environmental effects on assemblages that are the result of naturally varying factors such as climate and geology from those caused by anthropogenic factors. The use of the RCA, coupled with advanced predictive modeling methods such as machine learning techniques, has enhanced our ability to predict how assemblages should vary based on natural environmental factors. Such enhanced predictive power should ultimately allow for more accurate determination of assemblage variation patterns that indicate impairment. Despite these advancements, predictive modeling and the use of the RCA are greatly confounded by the lack of suitable reference sites in many regions. To this end, alternative strategies that employ both impaired and reference sites to derive expected reference conditions have been proposed [118–121] and warrant further evaluation to determine their widespread applicability. Because of the scarcity of reference sites in many regions and the high potential for complex interactions between natural environmental factors and stressors, the development of additional data-efficient methods for predicting expected assemblages under unimpaired conditions and for quantifying deviations from these expectations is much needed.

An additional challenge for contemporary bioassessment programs is the shifting baseline syndrome (sensu Hawkins et al. [43]) wherein future climate change is likely to alter temperature and precipitation regimes globally, thus changing the assemblage compositions that might reasonably be expected under minimally impaired conditions. To meet this challenge, spatially and temporally extensive monitoring is essential to derive realistic reference conditions. Several large-scale assessment programs have been recently developed, such as the EU Water Framework Directive, the US Geological Survey's National Water Quality Assessment program, the US EPA's National Aquatic Resources Survey, the US National Science Foundation's National Ecological Observatory Network, and the Canadian Biological Monitoring network. These programs include rigorous and thoroughly documented bioassessment protocols focused on monitoring aquatic assemblages over large spatial and long temporal scales. Data produced by these important programs will enhance our ability to overcome the inherent challenges in evaluating ecological integrity when least-impaired reference conditions are rare, highly variable among regions, and changing in response to global climate change.

Acknowledgments We wish to thank Michael Barbour, Simone Langhans, and Gregory Pond for providing the material that resulted in our "interviews with the experts" section. Their insights have provided an invaluable contribution to this work. This is VCU Rice Rivers Center Contribution Number 49.

References

1. Barbour MT, Gerritsen J, Snyder B et al (1999) Rapid bioassessment protocols for use in streams and wadeable rivers: periphyton, benthic macroinvertebrates and fish, 2nd edn. EPA 841-B-99-002. U.S. Environmental Protection Agency, Office of Water, Washington, DC
2. Ahrens L, Bundschuh M (2014) Fate and effects of poly- and perfluoroalkyl substances in the aquatic environment: a review. Environ Toxicol Chem 33:1921–1929
3. Mueller M, Pander J, Geist J (2014) A new tool for assessment and monitoring of community and ecosystem change based on multivariate abundance data integration from different taxonomic groups. Environ Syst Res 3(1):12. doi:10.1186/2193-2697-3-12
4. Kolkwitz R, Marsson M (1902) Grundsätze für die biologische beurtheilung des wassers, nach seiner flora und fauna. Mitteilungen der Prufungsansalt fur Wasserversorgung und Abwasserreining 1:1–64
5. Junqueira MV, Friedrich G, de Araujo PR (2010) A saprobic index for biological assessment of river water quality in Brazil (Minas Gerais and Rio de Janeiro states). Environ Monit Assess 163:545–554
6. Usseglio-Polatera P, Bournaud M, Richoux P et al (2000) Biological and ecological traits of benthic freshwater macroinvertebrates: relationships and definition of groups with similar traits. Freshw Biol 43:175–205
7. Frey DG (1977) Biological integrity of water-an historical approach. In: The integrity of water: proceedings of a symposium, US Environmental Protection Agency, Washington, DC, 10–12 Mar 1975
8. Karr JR, Dudley DR (1981) Ecological perspective on water quality goals. Environ Manage 5:55–68
9. Barbour MT, Paul MJ (2010) Adding value to water resource management through biological assessment of rivers. Hydrobiologia 651:17–24
10. Fauth J, Bernardo J, Camara M et al (1996) Simplifying the jargon of community ecology: a conceptual approach. Am Nat 147:282–286
11. Carlisle DM, Hawkins CP, Meador MR et al (2008) Biological assessments of Appalachian streams based on predictive models for fish, macroinvertebrate, and diatom assemblages. J North Am Benthol Soc 27:16–37
12. Bae M, Kwon Y, Hwang S et al (2011) Relationships between three major stream assemblages and their environmental factors in multiple spatial scales. Ann Limnol—Int J Lim 47: S91–S105
13. Pilière A, Schipper AM, Breure AM et al (2014) Comparing responses of freshwater fish and invertebrate community integrity along multiple environmental gradients. Ecol Indic 43:215–226
14. Carter JL, Resh VH (2001) After site selection and before data analysis: sampling, sorting, and laboratory procedures used in stream benthic macroinvertebrate monitoring programs by USA state agencies. J North Am Benthol Soc 20:658–682
15. Potapova M, Charles DF (2005) Choice of substrate in algae-based water-quality assessment. J North Am Benthol Soc 24:415–427
16. Li J, Herlihy A, Gerth W et al (2001) Variability in stream macroinvertebrates at multiple spatial scales. Freshw Biol 46:87–97

17. Pritt JJ, Frimpong EA (2014) The effect of sampling intensity on patterns of rarity and community assessment metrics in stream fish samples. Ecol Indic 39:169–178
18. Lenat DR, Resh VH (2001) Taxonomy and stream ecology—the benefits of genus-and species-level identification. J North Am Benthol Soc 20:287–298
19. Jiang X, Xiong J, Song Z et al (2013) Is coarse taxonomy sufficient for detecting macroinvertebrate patterns in floodplain lakes? Ecol Indic 27:48–55
20. Uzarski DG, Burton TM, Cooper MJ et al (2005) Fish habitat use within and across wetland classes in coastal wetlands of the five Great Lakes: development of a fish-based index of biotic integrity. J Great Lakes Res 31:171–187
21. Chen K, Hughes RM, Xu S et al (2014) Evaluating performance of macroinvertebrate-based adjusted and unadjusted multi-metric indices (MMI) using multi-season and multi-year samples. Ecol Indic 36:142–151
22. Smucker NJ, Vis ML (2009) Use of diatoms to assess agricultural and coal mining impacts on streams and a multiassemblage case study. J North Am Benthol Soc 28:659–675
23. Blocksom KA, Kurtenbach JP, Klemm DJ et al (2002) Development and evaluation of the lake macroinvertebrate integrity index (LMII) for New Jersey lakes and reservoirs. Environ Monit Assess 77:311–333
24. Pan Y, Hughes RM, Herlihy AT et al (2012) Non-wadeable river bioassessment: spatial variation of benthic diatom assemblages in Pacific Northwest rivers, USA. Hydrobiologia 684:241–260
25. Whittier TR, Hughes RM, Lomnicky GA et al (2007) Fish and amphibian tolerance values and an assemblage tolerance index for streams and rivers in the western USA. Trans Am Fish Soc 136:254–271
26. Black RW, Moran PW, Frankforter JD (2011) Response of algal metrics to nutrients and physical factors and identification of nutrient thresholds in agricultural streams. Environ Monit Assess 175:397–417
27. Zhu D, Chang J (2008) Annual variations of biotic integrity in the upper Yangtze River using an adapted index of biotic integrity (IBI). Ecol Indic 8:564–572
28. Lenat DR (1993) Using mentum deformities of Chironomus larvae to evaluate the effects of toxicity and organic loading in streams. J North Am Benthol Soc 12(3):265–269
29. Fore LS, Grafe C (2002) Using diatoms to assess the biological condition of large rivers in Idaho (USA). Freshw Biol 47:2015–2037
30. Reynoldson T, Norris R, Resh V et al (1997) The reference condition: a comparison of multimetric and multivariate approaches to assess water-quality impairment using benthic macroinvertebrates. J North Am Benthol Soc 16:833–852
31. Bailey RC, Kennedy MG, Dervish MZ (1998) Biological assessment of freshwater ecosystems using a reference condition approach: comparing predicted and actual benthic invertebrate communities in Yukon streams. Freshw Biol 39:765–774
32. Stoddard JL, Larsen DP, Hawkins CP et al (2006) Setting expectations for the ecological condition of streams: the concept of reference condition. Ecol Appl 16:1267–1276
33. Birks H, Line J, Juggins S et al (1990) Diatoms and pH reconstruction. Philos Trans R Soc Lond B Biol Sci 327:263–278
34. Hughes RM, Kaufmann PR, Herlihy AT et al (1998) A process for developing and evaluating indices of fish assemblage integrity. Can J Fish Aquat Sci 55:1618–1631
35. Thoms M, Ogden R, Reid M (1999) Establishing the condition of lowland floodplain rivers: a palaeo-ecological approach. Freshw Biol 41:407–423
36. Shirey PD, Cowley DE, Sallenave R (2008) Diatoms from gut contents of museum specimens of an endangered minnow suggest long-term ecological changes in the Rio Grande (USA). J Paleolimnol 40:263–272
37. Nelson SM, Roline RA (1996) Recovery of a stream macroinvertebrate community from mine drainage disturbance. Hydrobiologia 339:73–84

38. Clark JL, Clements WH (2006) The use of in situ and stream microcosm experiments to assess population- and community-level responses to metals. Environ Toxicol Chem 25:2306–2312
39. Applegate JM, Baumann PC, Emery EB et al (2007) First steps in developing a multimetric macroinvertebrate index for the Ohio River. River Res Appl 23:683–697
40. Plafkin JL, Barbour MT, Porter KD, et al (1989) Rapid bioassessment protocols for use in streams and rivers: benthic macroinvertebrates and fish. EPA 444-4-89-001. U.S. Environmental Protection Agency, Office of Water, Washington, DC
41. Mykrä H, Heino J, Muotka T (2007) Scale-related patterns in the spatial and environmental components of stream macroinvertebrate assemblage variation. Global Ecol Biogeogr 16:149–159
42. Hoeinghaus DJ, Winemiller KO, Birnbaum JS (2007) Local and regional determinants of stream fish assemblage structure: inferences based on taxonomic vs. functional groups. J Biogeogr 34:324–338
43. Hawkins CP, Olson JR, Hill RA (2010) The reference condition: predicting benchmarks for ecological and water-quality assessments. J North Am Benthol Soc 29:312–343
44. Ganasan V, Hughes RM (1998) Application of an index of biological integrity (IBI) to fish assemblages of the rivers Khan and Kshipra (Madhya Pradesh), India. Freshw Biol 40:367–383
45. Davies SP, Jackson SK (2006) The biological condition gradient: a descriptive model for interpreting change in aquatic ecosystems. Ecol Appl 16:1251–1266
46. Mazor RD, Reynoldson TB, Rosenberg DM et al (2006) Effects of biotic assemblage, classification, and assessment method on bioassessment performance. Can J Fish Aquat Sci 63:394–411
47. Hawkes H (1998) Origin and development of the biological monitoring working party score system. Water Res 32:964–968
48. Whittier TR, Stoddard JL, Larsen DP et al (2007) Selecting reference sites for stream biological assessments: best professional judgment or objective criteria. J North Am Benthol Soc 26:349–360
49. Blocksom KA (2003) A performance comparison of metric scoring methods for a multimetric index for Mid-Atlantic Highlands streams. Environ Manage 31:670–682
50. Yates AG, Bailey RC (2010) Selecting objectively defined reference sites for stream bioassessment programs. Environ Monit Assess 170:129–140
51. Blocksom KA, Flotemersch JE (2005) Comparison of macroinvertebrate sampling methods for nonwadeable streams. Environ Monit Assess 102:243–262
52. McCune B, Grace JB (2002) Analysis of ecological communities. MjM Software Design, Glendale Beach
53. Legendre P, Legendre LF (2012) Numerical ecology. Elsevier, Amsterdam
54. R Core Team (2014) R: a language and environment for statistical computing. http://www.r-project.org/
55. Bray JR, Curtis JT (1957) An ordination of the upland forest communities of southern Wisconsin. Ecol Monogr 27:325–349
56. Dice LR (1945) Measures of the amount of ecologic association between species. Ecology 26:297–302
57. Sorenson T (1948) A method of establishing groups of equal amplitude in plant sociology based on similarity of species content. Kongelige Danske Videnskabernes Selskab 5:4–7
58. Van Sickle J, Hughes RM (2000) Classification strengths of ecoregions, catchments, and geographic clusters for aquatic vertebrates in Oregon. J North Am Benthol Soc 19:370–384
59. Clarke K, Green R (1988) Statistical design and analysis for a "biological effects" study. Mar Ecol Prog Ser 46:213–226
60. Mielke PW Jr, Berry KJ, Johnson ES (1976) Multi-response permutation procedures for a priori classifications. Commun Stat Theory Methods 5:1409–1424
61. Anderson MJ (2001) A new method for non-parametric multivariate analysis of variance. Austral Ecol 26:32–46

62. Omernik JM (1987) Ecoregions of the conterminous United States. Ann Assoc Am Geogr 77:118–125
63. Hughes RM, Larsen DP, Omernik JM (1986) Regional reference sites: a method for assessing stream potentials. Environ Manage 10:629–635
64. Aroviita J, Mykra H, Muotka T et al (2009) Influence of geographical extent on typology- and model-based assessments of taxonomic completeness of river macroinvertebrates. Freshw Biol 54:1774–1787
65. Hawkins CP, Norris RH, Gerritsen J et al (2000) Evaluation of the use of landscape classifications for the prediction of freshwater biota: synthesis and recommendations. J North Am Benthol Soc 19:541–556
66. Dallas HF (2004) Spatial variability in macroinvertebrate assemblages: comparing regional and multivariate approaches for classifying reference sites in South Africa. Afr J Aquat Sci 29:161–171
67. Dail MR, Hill JR, Miller RD (2013) The Virginia coastal plain macroinvertebrate index. Technical bulletin WQA/2013-002. Virginia Department of Environmental Quality, Richmond
68. Burton J, Gerritsen J (2003) A stream condition index for Virginia non-coastal streams. Tetra-Tech, Owings Mills
69. Hawkins CP, Vinson MR (2000) Weak correspondence between landscape classifications and stream invertebrate assemblages: implications for bioassessment. J North Am Benthol Soc 19:501–517
70. Wright J, Moss D, Armitage P et al (1984) A preliminary classification of running-water sites in Great Britain based on macro-invertebrate species and the prediction of community type using environmental data. Freshw Biol 14:221–256
71. Wright JF, Sutcliffe DW, Furse MT (2000) Assessing the biological quality of freshwaters. RIVPACS and other techniques. Freshwater Biological Association, Ambleside
72. Hawkins CP, Norris RH, Hogue JN et al (2000) Development and evaluation of predictive models for measuring the biological integrity of streams. Ecol Appl 10:1456–1477
73. Smith M, Kay W, Edward D et al (1999) AusRivAS: using macroinvertebrates to assess ecological condition of rivers in Western Australia. Freshw Biol 41:269–282
74. Reynoldson TB, Bailey R, Day K et al (1995) Biological guidelines for freshwater sediment based on BEnthic Assessment of SedimenT (the BEAST) using a multivariate approach for predicting biological state. Aust J Ecol 20:198–219
75. Pond GJ, North SH (2013) Application of a benthic observed/expected-type model for assessing Central Appalachian streams influenced by regional stressors in West Virginia and Kentucky. Environ Monit Assess 185:9299–9320
76. Pardo I, Gómez-Rodríguez C, Abraín R et al (2014) An invertebrate predictive model (NORTI) for streams and rivers: sensitivity of the model in detecting stress gradients. Ecol Indic 45:51–62
77. Linke S, Bailey RC, Schwindt J (1999) Temporal variability of stream bioassessments using benthic macroinvertebrates. Freshw Biol 42:575–584
78. Pond G, Call S, Brumley J et al (2003) The Kentucky macroinvertebrate bioassessment index: derivation of regional narrative criteria for headwater and wadeable streams. Kentucky Department for Environmental Protection, Division of Water, Frankfort. http://water.ky.gov/Documents/QA/MBI/Statewide_MBI.pdf
79. Hill MO (1979) TWINSPAN: a FORTRAN program for arranging multivariate data in an ordered two-way table by classification of the individuals and attributes. Cornell University, Ithaca
80. Davy-Bowker J, Clarke R, Corbin T (2008) River invertebrate classification tool—final report. Scotland and Northern Ireland Forum for Environmental Research, Edinburgh
81. Oksanen J, Minchin PR (1997) Instability of ordination results under changes in input data order: explanations and remedies. J Veg Sci 8:447–454

82. Austin M (2013) Inconsistencies between theory and methodology: a recurrent problem in ordination studies. J Veg Sci 24:251–268
83. Linke S, Norris RH, Faith DP et al (2005) ANNA: a new prediction method for bioassessment programs. Freshw Biol 50:147–158
84. Olden JD (2003) A species-specific approach to modeling biological communities and its potential for conservation. Conserv Biol 17:854–863
85. Bowman MF, Somers KM (2005) Considerations when using the reference condition approach for bioassessment of freshwater ecosystems. Water Qual Res J Can 40:347–360
86. Melles S, Jones N, Schmidt B (2014) Evaluation of current approaches to stream classification and a heuristic guide to developing classifications of integrated aquatic networks. Environ Manage 53:549–566
87. Ode PR, Hawkins CP, Mazor RD (2008) Comparability of biological assessments derived from predictive models and multimetric indices of increasing geographic scope. J North Am Benthol Soc 27:967–985
88. Aroviita J, Koskenniemi E, Kotanen J et al (2008) A priori typology-based prediction of benthic macroinvertebrate fauna for ecological classification of rivers. Environ Manage 42:894–906
89. Joy M, Death R (2002) Predictive modelling of freshwater fish as a biomonitoring tool in New Zealand. Freshw Biol 47:2261–2275
90. Clarke RT, Wright JF, Furse MT (2003) RIVPACS models for predicting the expected macroinvertebrate fauna and assessing the ecological quality of rivers. Ecol Model 160:219–233
91. Hawkins CP (2006) Quantifying biological integrity by taxonomic completeness: its utility in regional and global assessments. Ecol Appl 16:1277–1294
92. Simpson J, Norris R, Wright J et al (2000) Biological assessment of river quality: development of AUSRIVAS models and outputs. In: Wright J, Sutcliffe D, Furse M (eds) Assessing the biological quality of fresh waters: RIVPACS and other techniques. Freshwater Biological Association, Ambleside
93. Van Sickle J (2008) An index of compositional dissimilarity between observed and expected assemblages. J North Am Benthol Soc 27:227–235
94. Van Sickle J, Larsen DP, Hawkins CP (2007) Exclusion of rare taxa affects performance of the O/E index in bioassessments. J North Am Benthol Soc 26:319–331
95. Bates Prins SC, Smith EP (2007) Using biological metrics to score and evaluate sites: a nearest-neighbour reference condition approach. Freshw Biol 52:98–111
96. Moss D, Wright J, Sutcliffe D et al (2000) Evolution of statistical methods in RIVPACS. In: Wright J, Sutcliffe D, Furse M (eds) Assessing the biological quality of fresh waters: RIVPACS and other techniques. Freshwater Biological Association, Ambleside
97. Hoang H, Recknagel F, Marshall J et al (2001) Predictive modelling of macroinvertebrate assemblages for stream habitat assessments in Queensland (Australia). Ecol Model 146:195–206
98. Waite IR, Brown LR, Kennen JG et al (2010) Comparison of watershed disturbance predictive models for stream benthic macroinvertebrates for three distinct ecoregions in western US. Ecol Indic 10:1125–1136
99. McCormick FH, Hughes RM, Kaufmann PR et al (2001) Development of an index of biotic integrity for the Mid-Atlantic Highlands region. Trans Am Fish Soc 130:857–877
100. Oberdorff T, Pont D, Hugueny B et al (2002) Development and validation of a fish-based index for the assessment of river health in France. Freshw Biol 47:1720–1734
101. Vander Laan JJ, Hawkins CP (2014) Enhancing the performance and interpretation of freshwater biological indices: an application in arid zone streams. Ecol Indic 36:470–482
102. Cao Y, Hawkins CP, Olson J et al (2007) Modeling natural environmental gradients improves the accuracy and precision of diatom-based indicators. J North Am Benthol Soc 26:566–585
103. Yuan LL (2004) Assigning macroinvertebrate tolerance classifications using generalised additive models. Freshw Biol 49:662–677
104. Wintle BA, McCarthy MA, Volinsky CT et al (2003) The use of Bayesian model averaging to better represent uncertainty in ecological models. Conserv Biol 17:1579–1590

105. Clark JS (2005) Why environmental scientists are becoming Bayesians. Ecol Lett 8:2–14
106. Marzin A, Delaigue O, Logez M et al (2014) Uncertainty associated with river health assessment in a varying environment: the case of a predictive fish-based index in France. Ecol Indic 43:195–204
107. Cutler DR, Edwards TC Jr, Beard KH et al (2007) Random forests for classification in ecology. Ecology 88:2783–2792
108. De'ath G (2007) Boosted trees for ecological modeling and prediction. Ecology 88:243–251
109. Olden JD, Lawler JJ, Poff NL (2008) Machine learning methods without tears: a primer for ecologists. Q Rev Biol 83:171–193
110. Goethals PL, Dedecker AP, Gabriels W et al (2007) Applications of artificial neural networks predicting macroinvertebrates in freshwaters. Aquat Ecol 41:491–508
111. Hoang TH, Lock K, Mouton A et al (2010) Application of classification trees and support vector machines to model the presence of macroinvertebrates in rivers in Vietnam. Ecol Inform 5:140–146
112. Feio M, Viana-Ferreira C, Costa C (2014) Combining multiple machine learning algorithms to predict taxa under reference conditions for streams bioassessment. River Res Appl 30 (9):1157–1165. doi:10.1002/rra.2707
113. Bishop CM (1995) Neural networks for pattern recognition. Clarendon, Oxford
114. Olden JD, Joy MK, Death RG (2006) Rediscovering the species in community-wide predictive modeling. Ecol Appl 16:1449–1460
115. Breiman L, Friedman J, Olshen R et al (1984) Classification and regression trees (CART). Wadsworth International Group, Belmont
116. Hawkins CP, Cao Y, Roper B (2010) Method of predicting reference condition biota affects the performance and interpretation of ecological indices. Freshw Biol 55:1066–1085
117. Waite IR, Kennen JG, May JT et al (2012) Comparison of stream invertebrate response models for bioassessment metrics. J Am Water Resour Assoc 48:570–583
118. Baker EA, Wehrly KE, Seelbach PW et al (2005) A multimetric assessment of stream condition in the Northern Lakes and Forests Ecoregion using spatially explicit statistical modeling and regional normalization. Trans Am Fish Soc 134:697–710
119. Angradi TR, Pearson MS, Bolgrien DW et al (2009) Multimetric macroinvertebrate indices for mid-continent US great rivers. J North Am Benthol Soc 28:785–804
120. Chessman BC, Royal MJ (2004) Bioassessment without reference sites: use of environmental filters to predict natural assemblages of river macroinvertebrates. J North Am Benthol Soc 23:599–615
121. Schoolmaster DR Jr, Grace JB, Schweiger EW et al (2013) A causal examination of the effects of confounding factors on multimetric indices. Ecol Indic 29:411–419
122. Hering D, Feld CK, Moog O et al (2006) Cook book for the development of a multimetric index for biological condition of aquatic ecosystems: experiences from the European AQEM and STAR projects and related initiatives. Hydrobiologia 566:311–324
123. Stoddard JL, Herlihy AT, Peck DV et al (2008) A process for creating multimetric indices for large-scale aquatic surveys. J North Am Benthol Soc 27:878–891
124. Blocksom K, Johnson B (2009) Development of a regional macroinvertebrate index for large river bioassessment. Ecol Indic 9:313–328
125. Stevenson RJ, Zalack JT, Wolin J (2013) A multimetric index of lake diatom condition based on surface-sediment assemblages. Freshw Sci 32:1005–1025
126. Cao Y, Hawkins CP (2011) The comparability of bioassessments: a review of conceptual and methodological issues1. J North Am Benthol Soc 30:680–701
127. Baptista DF, Henriques-Oliveira AL, Oliveira RBS et al (2013) Development of a benthic multimetric index for the Serra da Bocaina bioregion in Southeast Brazil. Braz J Biol 73:573–583
128. Fetscher AE, Stancheva R, Kociolek JP et al (2014) Development and comparison of stream indices of biotic integrity using diatoms vs. non-diatom algae vs. a combination. J Appl Phychol 26:433–450

129. McBride GB, Loftis JC, Adkins NC (1993) What do significance tests really tell us about the environment? Environ Manage 17:423–432
130. Smith J, Beauchamp J, Stewart A (2005) Alternative approach for establishing acceptable thresholds on macroinvertebrate community metrics. J North Am Benthol Soc 24:428–440
131. Bowman MF, Somers KM (2006) Evaluating a novel Test Site Analysis (TSA) bioassessment approach. J North Am Benthol Soc 25:712–727
132. Stribling J, Jessup B, Gerritsen J (2000) Development of biological and physical habitat criteria for Wyoming streams and their use in the TMDL process. Tetra-Tech, Owings Mills
133. Barbour M, Gerritsen J, Griffith G et al (1996) A framework for biological criteria for Florida streams using benthic macroinvertebrates. J North Am Benthol Soc 15(2):185–211
134. Clarke R, Furse M, Gunn R et al (2002) Sampling variation in macroinvertebrate data and implications for river quality indices. Freshw Biol 47:1735–1751
135. Kaufmann PR, Levine P, Peck DV et al (1999) Quantifying physical habitat in wadeable streams. EPA/620/R-99-003, US Environmental Protection Agency, Washington, DC
136. Hose G, Turak E, Waddell N (2004) Reproducibility of AUSRIVAS rapid bioassessments using macroinvertebrates. J North Am Benthol Soc 23:126–139
137. Houston L, Barbour M, Lenat D et al (2002) A multi-agency comparison of aquatic macroinvertebrate-based stream bioassessment methodologies. Ecol Indic 1:279–292
138. Lyons J (2012) Development and validation of two fish-based indices of biotic integrity for assessing perennial coolwater streams in Wisconsin, USA. Ecol Indic 23:402–412
139. Van Sickle J (2010) Correlated metrics yield multimetric indices with inferior performance. Trans Am Fish Soc 139:1802–1817
140. Schoolmaster DR, Grace JB, Schweiger EW (2012) A general theory of multimetric indices and their properties. Methods Ecol Evol 3:773–781
141. Langhans SD, Lienert J, Schuwirth N et al (2013) How to make river assessments comparable: a demonstration for hydromorphology. Ecol Indic 32:264–275
142. Wu W, Xu Z, Yin X et al (2014) Assessment of ecosystem health based on fish assemblages in the Wei River basin, China. Environ Monit Assess 186:3701–3716
143. Lunde KB, Resh VH (2012) Development and validation of a macroinvertebrate index of biotic integrity (IBI) for assessing urban impacts to Northern California freshwater wetlands. Environ Monit Assess 184:3653–3674
144. Breiman L (2001) Random forests. Mach Learn 45:5–32
145. Van Sickle J, Hawkins CP, Larsen DP et al (2005) A null model for the expected macroinvertebrate assemblage in streams. J North Am Benthol Soc 24:178–191
146. Yoder CO, Barbour MT (2009) Critical technical elements of state bioassessment programs: a process to evaluate program rigor and comparability. Environ Monit Assess 150:31–42
147. Commission E (2000) Water Framework Directive 2000/60/EC of the European Parliament and of the Council of 23 October 2000 establishing a framework for Community action in the field of water policy. Off J Eur Community L327:1–73
148. Tonkin JD, Stoll S, Sundermann A et al (2014) Dispersal distance and the pool of taxa, but not barriers, determine the colonisation of restored river reaches by benthic invertebrates. Freshw Biol 59(9):1843–1855
149. Woods A, Omernik J, Brown D et al (1996) Level III and IV ecoregions of Pennsylvania and the Blue Ridge mountains, the Ridge and Valley, and the central Appalachians of Virginia, West Virginia, and Maryland. EPA/600/R-96/077, US Environmental Protection Agency, Washington, DC
150. Bryce S, Hughes R, Kaufmann P (2002) Development of a bird integrity index: using bird assemblages as indicators of riparian condition. Environ Manage 30:294–310
151. Kanninen A, Vallinkoski V, Leka J et al (2013) A comparison of two methods for surveying aquatic macrophyte communities in boreal lakes: implications for bioassessment. Aquat Bot 104:88–100

152. Washington VJ, Lear G, Neale MW et al (2013) Environmental effects on biofilm bacterial communities: a comparison of natural and anthropogenic factors in New Zealand streams. Freshw Biol 58:2277–2286
153. Burgos-Caraballo S, Cantrell SA, Ramírez A (2014) Diversity of benthic biofilms along a land use gradient in tropical headwater streams, Puerto Rico. Microb Ecol 68(1):47–59
154. Baird DJ, Hajibabaei M (2012) Biomonitoring 2.0: a new paradigm in ecosystem assessment made possible by next-generation DNA sequencing. Mol Ecol 21:2039–2044
155. Pfrender M, Hawkins C, Bagley M et al (2010) Assessing macroinvertebrate biodiversity in freshwater ecosystems: advances and challenges in DNA-based approaches. Q Rev Biol 85:319–340
156. Manoylov KM (2014) Taxonomic identification of algae (morphological and molecular): species concepts, methodologies, and their implications for ecological bioassessment. J Phycol 50:409–424
157. Stein ED, White BP, Mazor RD et al (2014) Does DNA barcoding improve performance of traditional stream bioassessment metrics? Freshw Sci 33:302–311

Microbial Source Tracking: Advances in Research and a Guide to Application

Brian Badgley and Charles Hagedorn

Contents

Abstract Microbial source tracking (MST) is a still-new and developing discipline that allows users to discriminate among the many potential sources of fecal pollution in environmental waters. As MST continues to transition from the realm of research to that of application, it is being widely used in beach monitoring, total maximum daily load (TMDL) assessment of pollution sources, and any other

B. Badgley (✉) • C. Hagedorn
Department of Crop and Soil Environmental Sciences, Virginia Tech, Blacksburg, VA, USA
e-mail: badgley@vt.edu

T. Younos, T.E. Parece (eds.), *Advances in Watershed Science and Assessment*, The Handbook of Environmental Chemistry 33,
DOI 10.1007/978-3-319-14212-8_10

waters that do not meet designated use criteria as determined by high densities of fecal indicator bacteria (FIB). The main area of research activity in MST focuses on the identification of source-specific genetic markers that can be used to detect contributions from different hosts such as humans, livestock, and wildlife. However, a variety of other accessible approaches can also be used including detailed investigations of the watershed and infrastructure, chemical tracers and leak tests, and increased FIB sampling. This chapter can serve as a guide for decision-making on where, when, and how to deploy MST. Included are discussions of the main drivers of MST and how these have shaped the development of past and present methodological approaches, plus current research initiatives such as community analysis that could usher in yet another new and improved methodological basis for the entire field of MST. Finally, a tiered system is presented as a recommended means to navigate the multiple options for MST analyses that will assist the reader in how best to use MST within the context of more traditional approaches.

Keywords DNA-based source markers • Fecal indicator bacteria • Fecal pollution • Microbial community analysis • Microbial source tracking • Recreational water quality

1 Introduction

The new and expanding field of microbial source tracking (MST) typically involves sensitive and specific DNA-based methods that use either presence–absence polymerase chain reaction (PCR) or quantitative PCR (qPCR) to detect and quantify particular gene fragments that have been found to be relatively source specific (e.g., humans, cattle, birds, dogs). These gene fragments are often referred to in the MST literature as source-specific "markers" [1–3] and frequently exist in the bacterial genus *Bacteroides*. Two recent endeavors by the MST community are available that cover the entire field in detail. The first was a comprehensive book on MST that included 26 chapters written by 74 authors and coauthors representing 17 countries and demonstrated the development and application of MST at the international level [4]. The second was the Source Identification Protocol Project (SIPP), undertaken to identify the best DNA-based methods from 41 that have been developed within approximately the past decade. This large undertaking involved 27 labs and resulted in a series of 12 articles published in a special edition of *Water Research* [5]. In addition, the SIPP study generated a fecal source identification guidance manual that framed MST within the context of more conventional and less expensive methodologies and presented a tiered approach for using different methods in a step-wise and cost-effective manner [6]. This chapter will summarize the lessons learned within these three key documents, supplemented by recent publications, to provide practitioners and water quality managers with advice on when, where, and how to best use MST.

1.1 Fecal Indicator Bacteria Monitoring in the USA

Recent monitoring data compiled annually across the USA shows that many interior and coastal waters are chronically polluted with fecal indicator bacteria (FIB) [7]. The situation has actually worsened in recent years along heavily urbanized coastlines [8]. As an example, in 2006 FIB levels in US waters were the highest in 17 years, with over 25,000 advisories and recreational closures nationwide, 30 % higher than in 2004 [9]. The dry summer of 2007 was also a problem, with 22,571 days of closings and advisories for US oceans, bays, and Great Lakes beaches [10]. These examples are alarming, as high FIB concentrations indicate unhealthy waters and cause economic losses to local communities [11, 12]. Advisories posted by state agencies for recreational waters are typically covered by the news media and have a negative impact on the public perceptions of water safety and the agencies responsible for protecting public health [13].

Many beach studies have demonstrated that direct contact with water and sand contaminated with fecal pollution can result in gastrointestinal illnesses that can be severe, especially for immunocompromised individuals [14–16]. Swimming, especially total immersion in recreational waters, is an activity that allows transmission of waterborne pathogens by the fecal–oral route [17]. Although there are pathogens from non-human sources that can be harmful to humans (e.g., livestock and wildlife), the greatest risk of illness is fecal contamination from human sources, which may contain enteric viruses and parasites not normally found outside of human hosts [14]. Direct monitoring for waterborne human pathogens is impractical due to the wide variety of pathogens that might be present, low concentrations that make detection difficult, and the high cost of laboratory analysis [18]. Instead, water monitoring strategies target FIB, which were chosen based on their presence in the feces of warm-blooded animals, low rates of survival and/or low natural occurrence in extra-intestinal habitats, and their association with human pathogens of concern [19]. Because these indicators of fecal contamination are found in the intestines of all warm-blooded animals, they can be helpful in locating general sources of pollution, but they are not useful in differentiating between environmental, agricultural, and human sources of pollution [20].

Water quality criteria based on FIB were originally adopted because epidemiological research linked increased swimmer illness to raw sewage discharges [21]. Today most wastewater in the USA is treated to secondary standards, but FIB, including DNA-based *Enterococcus* measurements, still indicates that many waters are unhealthy as per epidemiological relationships [15]. While FIB are legitimately the "gold standard" in food and potable water safety, they are imperfect tracers for threats to public health from pathogen-containing fecal material in environmental waters [22]. One reason for this is because culture-based assays require 18–24 h incubation, during which contamination and field conditions can change. To address this problem, newer culture-independent methods for quantitative PCR (qPCR) of *Enterococcus* spp. are now available that allow FIB measurements in 4–6 h [23]. However, a second challenge, related to using FIB as tracers, is

that they can arise from many non-human sources and subsequently persist in the environment [3]. More broadly, FIB in coastal urban regions could arise from a variety of different sources [7] including leaking sewer lines [24], decaying wrack [25], beach sands [16], algae [26] and aquatic vegetation [27], or coastal wetlands with birds and waterfowl [28]. Septic systems in non-sewered areas are sometimes a source as well [29], as are livestock in agricultural areas [30] and pets in suburbia [31]. Urban development generally correlates with high FIB in surface waters arriving via runoff or dry-weather drains, but individual sources are mostly unknown [32, 33]. Evaluating recreational waters by FIB assays is further complicated because FIB survive differently than most pathogens [34], leading to unnecessary beach closures, and they can become non-culturable but still viable, giving an erroneous illusion of safe water [35].

Clearly, with the many different potential FIB sources in recreational waters, effective water quality management requires more information than FIB monitoring data alone can provide. Fortunately, new MST methodologies and approaches developed and tested over the past decade are now available that provide reasonably accurate differentiation of specific sources of fecal pollution [3, 5, 36].

2 The Drivers for Microbial Source Tracking

2.1 Total Maximum Daily Load Program

In the USA much of the MST research and application has occurred in the development of TMDLs to meet the requirements of the US Clean Water Act [37–39]. A TMDL is a regulatory term that describes the maximum amount of a pollutant that a body of water can receive and still meet established water quality standards. Waters that do not meet regulatory standards for designated uses are listed as impaired waters. Designated uses of waters include fishing, swimming, aquatic life support, and drinking water. A TMDL assessment report is required for impaired waters. A TMDL assessment report is followed by developing a TMDL implementation plan with the goal of improving the quality of a water body listed as impaired.

High FIB concentrations in the USA are typically the major cause of surface water impairments and are subject to the TMDL regulatory program. For example, in Virginia (USA) concentrations of FIB cause the largest number of impairments; 50 % of assessed rivers/streams, 1.3 % of assessed lake areas, and 3.4 % of assessed estuarine waters are listed as impaired for recreational use [40]. Across a watershed, a variety of potential FIB sources can exist, including livestock and poultry operations, urban runoff, leaking sanitary and storm sewers, large wildlife and migratory bird populations, and pets such as dogs and cats. Identifying the different sources of fecal contamination in a watershed is needed for developing and implementing TMDLs and to evaluate the effectiveness of best management

practices (BMPs) for improving water quality [41]. In a watershed where fecal contamination sources are not clearly known, MST can often identify the source of fecal bacteria. Options for bacterial source identification include determining whether the source is human or non-human, or identifying the non-human species (e.g., cow, dog, deer), and then eliminating insignificant sources of fecal bacteria. Developing accurate and implementable TMDLs relies on identifying and appropriately characterizing the pollutant sources causing the impairment [42].

Regular monitoring for FIB and using MST can often assist in determining trends and sources of impairments related to nutrients and aquatic life use [41]. In Virginia, 30 % of assessed rivers/streams, 43 % of assessed lake areas, and 92 % of assessed estuarine waters are listed as impaired for aquatic life use due to nutrient enrichment and low dissolved oxygen [40]. Nutrient enrichment or eutrophication contributes to the formation of oxygen-depleting algae blooms and hypoxia. Low dissolved oxygen is a common impairment cause in Virginia, impacting lakes and estuarine waters, especially the Chesapeake Bay.

In addition to the assessment process, MST can also support pollutant source allocation analysis and the development of a TMDL implementation plan [41]. More specifically, MST can help identify the sources that contribute to the observed impairment, determine which sources are likely dominant in the watershed of interest, and focus management actions through targeting implementation and identifying controls that are appropriate and relevant to the identified sources. MST can also be useful for obtaining stakeholder buy-in for supporting watershed management activities during TMDL implementation in locales with contentious issues. MST can provide more acceptable or concrete evidence to stakeholders regarding their role in bacterial inputs and resulting impairments, often facilitating acceptance of responsibility and subsequent implementation of BMPs.

Many of the TMDLs in Virginia and the US mid-Atlantic region have been developed as part of the initiative to improve water quality of the Chesapeake Bay, the largest estuary in the USA. The Chesapeake Bay TMDL program is the most prominent in the USA to date, and about 90 % of the estuarine water category in Virginia represents waters of the Chesapeake Bay [43]. These estuarine waters have additional uses underneath the umbrella of "aquatic life use." These "sub-uses" are specific to the diverse assemblages of aquatic organisms that live in the Bay. One special sub-use is the shallow-water submerged aquatic vegetation (SAV) use. As the name suggests, this use supports conditions favorable to the growth and survival of submerged vegetation. SAV provides critical nursery habitat for blue crabs and fishes. Reduced water clarity due to shoreline erosion and suspended sediments is the major cause of impairment for the shallow-water SAV use. Currently, 53 % of SAV use in the entire Bay system is impaired. MST has been useful in identifying sources of pollution that impact SAV use [44].

2.2 Beach Water Pollution

Beaches across the USA are regularly monitored for FIB to protect the public from waterborne diseases associated with fecal contamination, as required by the Beaches Environmental Assessment and Coastal Health (BEACH) Act [45, 46]. When FIB concentrations exceed regulatory standards, swimming advisories are issued and beaches may be closed to recreational use. Closed beaches lead to frustration for beachgoers and substantial economic losses for associated communities. To protect public health, regulatory officials and beach managers need fast and reliable tests for analyzing the bacteriological quality of beach waters. To meet this need, a qPCR method for enterococci is now available as a rapid analytical USEPA-approved tool for testing beach water quality. Test results can be obtained in 2–4 h as compared to 18–24 h for conventional culture-based methods [23, 47, 48]. A second benefit is that deployment of a qPCR-based protocol for *Enterococcus* enumeration makes it relatively easy to use a qPCR-based MST marker for human-source contamination. This second source-specific assay could be run either in tandem or as a same-day follow-up to enterococci counts that were determined to exceed the regulatory standard earlier in the day [6]. Similar to watersheds, a variety of sources of fecal pollution potentially exist at recreational beaches. It is therefore important to place the highest priority on evaluating whether human fecal pollution contributes significantly to the FIB load, as human fecal material contains a greater number of human pathogens and represents the greatest potential health threat.

3 Microbial Source Tracking Methods

3.1 Library-Dependent Approach

Throughout the history of MST development, two basic strategies for host identification have been employed. Many early studies used a library-dependent approach that involves constructing a database of FIB isolate types from known fecal sources [19, 49]. Typing of indicator bacteria can be done in a variety of ways, including antibiotic resistance [50, 51], carbon source utilization [52], or genetic diversity [53, 54]. Isolates of FIB from water samples can then be similarly typed and classified to a particular source by referencing the library. While this approach showed some early success and is abundant in the literature, it is not currently recommended for general application. Initial construction of the reference library is costly, and geographic and temporal variability in FIB subtypes can result in incorrect source classification as well as the need for constant library maintenance and validation [55].

3.2 Library-Independent Approaches

Library-independent analyses target the presence or concentration of genetic markers associated with specific fecal sources in a water sample, typically using qPCR and thereby requiring no reference database [56, 57]. Currently, this approach is generally considered to be simpler to employ and validate and is widely recommended as the best approach to begin any project that might include MST.

For obtaining the equipment and setting up a lab to perform qPCR, an initial capital investment (approximately $100K) is required; the subsequent cost for supplies totals roughly $50 per sample; and a competent technician can process more than 40 samples in one day (following DNA extraction). The USEPA is currently developing standard methods for two human-associated qPCR markers (HF183 and HumM2), based largely on the protocols developed during the SIPP method evaluation study [5, 6]. The combined use of the two qPCR-based approaches to measure FIBs and make a rapid determination for the presence of human-source pollution should further reduce the analytical time needed and increase affordability and accuracy of monitoring recreational waters. Because of the many methodological nuances of qPCR, those desiring to adopt this technology would be best served by partnering with a university research program for guidance and training until the needed level of expertise has been reached.

3.3 DNA-Based Markers

At present, many DNA-based marker assays have been developed for MST, and application results have been published in the scientific literature [57–60]. New assays that target human and other waste sources are continuously being developed and reported [61]. Around a dozen DNA-based markers for detecting human sources have been developed over the last decade. Additional assays are applicable for tracing fecal wastes of other sources such as different types of livestock, wildlife, domestic pets, and birds [57, 59]. Also, advances in PCR technology have stimulated reevaluation of earlier markers for their sensitivity (detecting the correct host fecal material when it is present) and specificity (no detection of any other fecal sources; 62, 63). Thus, it is important to keep up to date with emerging scientific literature that publicizes new assays and their performance or new developments on older assays. All the markers recommended in this chapter use PCR directed towards bacterial targets. In general, this process includes sample collection, filtering, DNA extraction, amplification, and data analysis. The majority of markers use qPCR for the amplification step, meaning they provide information about the relative amount of target material in a particular water sample. Those assays termed “end-point” or conventional PCR provide only qualitative (presence or absence) data. When both quantitative and end-point PCR assays exist for a given assay, the quantitative is always preferred.

Table 1 Source-specific DNA-based markers covered in this chapter and recommended based on performance in the SIPP validation study [5]

Marker name	Source	Quantitative?	Original reference
HF183	Human	Yes	[65]
HumM2	Human	Yes	[66]
Adenovirus	Human	Yes	[67, 68]
Polyomavirus	Human	Yes	[69]
Gull2SYBR	Gull/birds	Yes	[70]
LeeSeaGull	Gull/birds	Yes	[71]
Dog-Bact	Dog	Yes	[72]
BacCan-UCD	Dog	Yes	[59]
HoF597	Horse	No	[1]
CowM2	Cow	Yes	[73]
Rum2Bac	General ruminant	Yes	[74]
Pig2Bac	Pig	Yes	[74]

Updated protocols for some are available in the SIPP guidance manual [6]

The human and non-human markers included in this chapter are summarized in Table 1 and restricted to those that performed the best in the California SIPP study, the most comprehensive method comparison and evaluation project conducted to date. The SIPP guidance manual includes the detailed protocols for all of the recommended DNA-based markers [6] and is available on the Southern California Coastal Water Research Project website (www.sccwrp.org). This does not mean that only the SIPP-validated markers can be used, but they should be the first ones considered. For example, the human viruses lack sensitivity but are almost completely host specific, so there may be situations such as highly urban coastal environments where it would be appropriate to include a human viral assay (see following section). The European source tracking project has also done method comparison studies and continues to use and recommend host-specific bacteriophage assays [64]. Also, a research lab might have had success with an assay that either did not perform well in the SIPP study or was not included. There is no problem in partnering with such a lab as long as use of the assay can be supported by meeting certain performance criteria either as described in the SIPP study [5] or by other equally rigorous measures [36, 55].

3.4 Human-Source Markers

The California SIPP study evaluated 41 MST assays and identified several that met or exceeded the design performance criteria [5, 75]. The human marker HF183-Taqman® [65] performed best overall of the 23 human methods tested, and a slightly less sensitive but highly specific human marker, HumM2 [66], also performed well, making it a good choice for an alternative or backup marker to

HF183. The HF183 marker is the recommended starting point for detecting human fecal material because it provides the best combination of sensitivity and specificity. Although it was ranked as the best on sensitivity among the human markers tested, it has been shown to occasionally detect ("cross-react") both chicken and dog feces. If those sources pose a concern in the watershed under investigation, or if managers simply desire to add certainty about the results, HF183 can be paired with HumM2.

A different approach that is worth considering is adding human virus measurements to validate bacterial marker results [76]. If cross-reactivity has occurred with the human bacterial markers or if the cost of mitigation is high, as is typical in urban coastal cities, the costs might justify additional verification for the presence of human fecal material, especially municipal sewage. Human viruses have a very high specificity to human waste and almost no cross-reactivity with other fecal sources. Of the many fecal viruses that exist, markers for DNA viruses such as human adenovirus [67, 68] and human polyomavirus [68] are among the more sensitive and robust. These viruses are fairly widespread among humans and a sizable portion of the population sheds polyomaviruses passively. However, the low-density occurrence of viruses in water and the difficulty of concentrating them efficiently with the current technology provide barriers to routinely use viral markers. Detection may be enhanced by collecting and concentrating large volumes of water samples, up to 1,000 times more water than the typical 100 mL sample needed for bacterial source markers. Such large sample volumes add logistical challenges and expense as the sample must be processed on-site or transported to the laboratory in large volumes. Due to the specialized steps required in virus concentration and recovery, partnering with an experienced research laboratory is mandatory if virus detection is used as part of an ongoing MST effort [6, 76, 77].

3.5 Non-human-Source Markers

The SIPP study identified markers that sufficiently meet the design performance criteria and are recommended for source identification from birds, dogs, horses, cattle/ruminants, and pigs.

At present, four bird markers (Gull2SYBR, LeeSeaGull, Gull2Taqman, Gull2Endp) from several sea bird-associated assays have been evaluated and published [78, 79]. Of these four markers, the Gull2SYBR [70] and the LeeSeaGull [71] markers were considered best for routine use because these markers consistently displayed sensitivity and specificity across participating laboratories. All four bird markers detected gull and sometimes goose and pigeon feces. Also, the distribution of the bird marker bacterium (*Catellicoccus marimammalium*) among all the various species of shorebirds is not known. Therefore, the Gull2SYBR and LeeSeaGull markers should be considered general "bird" assays and not necessarily specific to gulls. Several new bird-associated MST assays for gulls, Canada geese, ducks, and chickens were reported too late for inclusion in the SIPP study, but may

prove superior to Gull2SYBR and LeeSeaGull, and will require a comparable evaluation before adoption for widespread use [80].

At present, several dog-associated qPCR and end-point PCR marker assays have been published. Two assays were included and evaluated in the SIPP study, DogBact [72] and BacCan-UCD [59]; both performed equally well when dogs were a potential fecal source [81]. Though highly sensitive and specific, both markers occasionally cross-react with other species such as humans and cattle, and such potential cross-reactions should be evaluated with local fecal material in whatever region these two recommended dog markers are desired to be used.

Horse-associated markers are relatively uncommon to date, and only two have been published. Only one PCR-based horse marker, conventional HoF597 (1), was included in the SIPP study, and it was adequately sensitive and specific. Its use is recommended when horses are present in the watershed and all other potential sources have been already ruled out. The horse marker does not show as much sensitivity as most other host-associated assays. Since another quantitative horse assay has not yet been thoroughly evaluated for inclusion in the SIPP study, the conventional HoF597 assay remains the recommended horse marker for now.

Multiple cow- and ruminant-associated DNA marker assays have been developed in the past decade, and several evaluation studies have been conducted to validate their performance. Three qPCR assays have consistently performed well in locales around the world and were included in the SIPP validation: BacR, CowM2, and Rum2Bac. Although the performances of all three markers were good [82], CowM2 [73] is the recommended cattle marker, and it is expected to become the USEPA-approved method in the near future. When a non-bovine ruminant fecal source such as deer or goat is suspected, Rum2Bac [74] should be used instead of CowM2. When both cattle and other ruminants live in the watershed, both CowM2 and Rum2Bac markers are recommended. Rum2Bac occasionally demonstrates false-positive results with septage, so in watersheds containing both septage and ruminant sources, septage presence should be conclusively ruled out before employing Rum2Bac.

Relatively few pig-specific markers have been developed to date and two pig markers, one based on conventional PCR (PF163) (1) and one quantitative (Pig2Bac) [74], were included in the SIPP study. Due to its demonstrated high sensitivity, Pig2Bac performs better than PF163 and is the recommended method for detection of pig feces. However, Pig2Bac sometimes cross-reacts with human/septage and dogs so these would either need to be ruled out first or accounted for when employing Pig2Bac.

4 Microbial Community Analysis Approach

In spite of the considerable progress that has been achieved employing DNA-based MST markers described in Sect. 3, they share one disadvantage with traditional FIB measurements in that they are still based on a single marker. This is limiting

because (a) a single marker can only be used to identify one particular type of fecal source and (b) it is unlikely that any one marker will ever be found to be 100 % sensitive and specific for a particular source in all environments. As a result, a multivariate "toolbox" approach to MST has been advocated where multiple markers are measured to obtain a stronger weight of evidence for a particular source [83]. More recently, an emerging extension of this concept has been to simply characterize the entire microbial community in a water sample and determine any potential similarities with fecal microbial communities from suspected sources [84, 85].

Microbial communities are complex assemblages of populations representing hundreds to thousands of microbial taxa, which is the primary attraction of using community analysis in MST. These taxa can not only be considered as numerous potential individual markers, but whole assemblages of taxa may also be identified that provide higher resolution in discerning sources of fecal pollution than any single indicator or marker alone. The underlying rationale is based on the evidence that different host species typically contain measurably and consistently different microbial communities in the gut and feces, which differ from environmental communities [86, 87]. Therefore, when fecal contamination occurs, the shift in the presence and abundance of microbial taxa can be detected and used to help discern the source. The use of community analysis in MST is a very recent development and remains an active research area; its use should not be considered established or routine. This is largely because methods to characterize whole microbial communities without dependence on laboratory culture (which typically fails to detect >90 % of microbial taxa) are a new and novel development. As a result, the methods by which microbial communities can be characterized are rapidly evolving, and at least three different approaches have been used recently for MST. Cao et al. [88] employed terminal restriction fragment length polymorphism (TRFLP), a community-scale genetic "fingerprinting" approach, to identify human sources of contamination. Dubinsky et al. [89] used the PhyloChip microarray, which can simultaneously assay a sample against numerous genetic probes for known microbial taxa, to discern animal and human sources of fecal contamination in marine waters. Finally, Unno et al. [84] and McLellan et al. [86] both identified sources of fecal contamination in river and lake systems, respectively, using next-generation pyrosequencing, which is quickly becoming the gold standard for microbial community analysis [90, 91].

Most recently, Cao et al. [92] simultaneously employed all three of these methods to identify fecal sources present in the SIPP challenge samples to evaluate the performance of evolving community analysis methods. All three approaches correctly identified dominant fecal sources in >90 % of the samples and rarely detected a source that was not present, illustrating the potential power of community analysis method. This study also identified two other benefits of this approach to conventional MST methods. Firstly, community analysis has the potential to discern different sources of the same host-associated marker. For example, all three methods were able to distinguish septage from human feces and sewage. Secondly, community analysis can be used to identify sources for which no suitable marker

has been developed, such as deer or chicken. Finally, other studies have highlighted the potential for community analysis to partition assemblages within microbial communities to known sources and quantify the contribution of those sources to the total sample [93]. Refinement of this approach for fecal sources would be a powerful MST tool.

It is important to note that the use of community analysis for MST is in its infancy so it is necessary to be aware of method limitations. For example, the typical approach is to characterize microbial community structure in known sources and then compare these to unknown samples. This approach is very similar to earlier library-dependent MST methods and therefore has similar limitations such as the need to collect, analyze, and maintain data on known sources, as well as dealing with temporal and geographical variability. In addition, the methods are expensive (although costs are dropping rapidly) and require considerable expertise to analyze and interpret. Often, this expertise will not be locally accessible and will require collaboration with a research laboratory. Community analysis simultaneously characterizes hundreds to thousands of markers; thus, it is not particularly sensitive for detecting individual markers and is not suitable for detecting very low levels of a particular source [94].

Newer methods (e.g., next-generation sequencing) may potentially overcome this limitation and improve sensitivity, but they also require the highest level of expertise for managing and analyzing large, complex data sets. As a result of these limitations, community analysis should be considered a method of last resort, only to be employed when it is suspected that information that can be gained could not be gathered from simpler and more cost-effective approaches. It is likely best suited to large TMDL projects or waters of high economic value where potential benefits justify the required resources. In these situations, community analysis can be a potentially powerful tool for discerning sources of fecal contamination. As DNA sequencing and other culture-independent methods continue to evolve, community analysis will likely continue to become a more universally accessible tool for MST.

5 The Tiered Approach for Microbial Source Tracking

When deciding to use MST, it is important to recognize that there are still deficiencies with every type of MST approach [63]. First, no single DNA-based marker accounts for FIB, human waste, and pathogens; if such exists, it has not yet been discovered. Second, most assays are insufficiently tested to know their absolute specificity to host fecal material, especially in geographical areas different from coastal California, the region included in the SIPP study [95]; third, the environmental fate, mainly degradation over time, of most DNA-based fecal markers is unknown, so linking quantities (e.g., via fate and transport modeling) to far-upstream sources or predicting the health consequences is not feasible at this point [96, 97]. These deficiencies indicate that DNA-based assays for determining

the presence of human and other fecal sources are increasingly powerful tools for source tracking, but considerable guidance is needed for when and how to best use them.

The SIPP manual identifies and describes six tiered steps to implement a program that will identify the sources of fecal pollution, while conserving resources through progressive deployment [6]. It is not until step 4 that the DNA-based assays are brought into play, and steps 1–3 should be performed or accounted for prior to using the assays.

Step 1: Fully characterize the watershed by obtaining infrastructure and topographical maps, interviewing relevant local experts, and conducting visual inspections to develop a list of potential fecal pollution sources in the watershed. This step should include developing hypotheses about the most likely fecal sources and conditions under which they contribute pollution to the watershed.

Step 2: Examine all available historical and current FIB monitoring data for spatial, temporal, and seasonal trends to help identify conditions that result in elevated FIB levels (e.g., tides, precipitation) and look for any potential linkages in elevated FIB levels to what appears to be the largest likely sources of fecal contamination in the watershed. Examples of likely sources include: the presence of seasonal migratory birds, hot summer days when livestock and wildlife are attracted to water; large number of seasonal bathers at recreational waters; and combined sewer overflow (CSO) events associated with precipitation (if a CSO system is present). At this point, localized intensive sampling for FIB may be appropriate. Such additional sampling can provide considerable clarification about potential sources of FIBs and should support or disprove hypotheses developed in step 1. Some reevaluation will be needed for any initial hypotheses that are not supported. Even though numerous case studies have demonstrated the utility of progressing through the tiered approach in the step-wise sequence, if intensive sampling is necessary at this point, then it may be appropriate to jump to step 4 and employ one or more DNA markers to confirm or disprove the presence of pollution from a highly suspected source.

Step 3: When leakage or cross-connections from a sanitary system is a potential source, it should best be investigated at this point using traditional tools such as smoke testing, tracer dyes, or camera inspection. Smoke and dye testing are also useful in rural watersheds where leaking or failing septic tank and drainfield systems may be a problem. This testing may also involve additional sampling for FIB and might include the human markers, sewage-specific chemicals, or even the new approach of canine scent tracking. Sewage-specific chemicals include optical brighteners in laundry detergents, caffeine, fecal sterols that are metabolic by-products of human digestion processes, and a metabolite of nicotine (cotinine) excreted by tobacco users. However, these methods are rarely used because they tend to be quickly diluted to levels below detection limits once the waste stream enters the ambient environment. Also, the cost to measure the organic chemicals is high and requires both specialized equipment and trained personnel. However, for those with the necessary instruments for detailed chemical analysis, chemical methods might be useful for independently confirming human fecal sources in a

cost-effective manner. More detailed recommendations on chemical source tracking are found in the SIPP manual [6] and Hagedorn and Weisberg [98]. Canine scent tracking is a new and novel field approach that involves dogs trained to respond to the scent of municipal wastewater [99]. Only a few reports of fecal scent tracking with dogs are available, but the reports indicate reasonable success. A major advantage of canine scent tracking is that it provides instant, on-the-ground results. At this point, canine scent tracking appears to be a promising tool for screening and prioritizing sampling locations before DNA-based and other similarly expensive assays are used to confirm human fecal contamination.

Step 4: Where steps 1–3 have indicated that human sources are a likely contributor, waters should be tested for the human-source-specific genetic markers described in Sect. 3.4 (even if traditional or novel tools have not identified a leaking sanitary or CSO system). The highest priority at this point is placed on either detecting or confirming a human fecal source as human fecal pollution poses the greatest relative health risk to people. Sampling for this purpose might consist of routine sampling schemes in ambient waters or involve more intensive sampling around precipitation or tidal events.

Step 5: Where human sources have been documented (or dismissed if conclusively proven not present) and the relative human loadings are better understood and/or animal fecal pollution sources are likely (e.g., birds or dogs at beaches, agricultural runoff in rural watershed areas), then waters should be tested using the non-human (animal) source-specific markers described in Sect. 3.5. Like the human markers, such sampling might be in ambient waters or more intensive sampling around precipitation or tidal events.

Step 6: If fecal sources are suspected where markers have yet to be developed (sources not included in Sect. 3.5), then testing waters with community analysis methods as described in Sect. 4 should be considered. Another potential use of community analysis methods may be to differentiate human fecal sources between municipal sewage and rural septage. Community methods may be complemented with chemical methods (as appropriate) to provide additional independent information, particularly when sewage or other human waste is a suspected source or when multiple major sources are suspected.

6 Ongoing Research

Substantial efforts have been undertaken over the past decade to identify and remove human sources of fecal contamination in recreational waters, especially in urban coastal environments in California and the Great Lakes [100]. However, numerous beaches and other recreational waters still have persistent advisories due to high FIB counts [101]. Further improvement in water quality at such locations requires two necessary developments [102]. First, establishing with a high degree of certainty whether or not the remaining fecal signature is human or non-human in origin (as described in Sects. 3, 4, and 5). Second, identifying what is needed to

deploy site-specific options such as quantitative microbial risk assessment (QMRA) or natural source exclusion (NSE) that are becoming part of the regulatory framework [103–105].

6.1 Quantitative Microbial Risk Assessment

The goal of quantitative microbial risk assessment (QMRA) is to quantify the relative risks to humans from exposure to recreational water impacted by different sources of fecal contamination and to clarify which pathogens cause illnesses to swimmers in water bodies that are impacted by specific sources of fecal contamination. To accomplish this, it will be necessary to determine the degree to which risks of illness depends on or varies with the source(s) of contamination. The context for regulators and the regulated community is to assess if the relative risk differences are sufficient to warrant consideration for alternative (yet equivalent) water quality standards. While QMRA has proven useful for increasing the understanding of apparent and relative human health risks from exposure to various sources of fecal pollution, regulators currently do not have the information necessary to develop nationally applicable water quality criteria based on different sources of fecal contamination. However, it may be possible to develop site-specific criteria protective of recreational use that take into account the relative risk of sources, provided the sources affecting a specific water body are well understood both spatially and temporally.

6.2 Natural Source Exclusion

The goal of NSE is to implement alternative site-specific FIB objectives for water quality, assuming that dischargers (1) control all anthropogenic sources of indicator bacteria to a water body, (2) demonstrate that all anthropogenic sources of indicator bacteria to a water body are controlled, and (3) demonstrate that the remaining indicator bacteria densities do not indicate a health risk. When the sources can be proven less risky to recreational users, a different (larger) criterion value for FIB might be appropriate. Like QMRA, regulators do not yet have sufficient information to develop such new water quality criteria as each case will be geographically specific. Any case-by-case consideration for NSE must be scientifically defensible, well documented, and supported with data and information and provide for public comment and access to information.

7 Conclusions

The MST field is still evolving rapidly and the associated evaluation tools described in Sects. 3, 4, and 6 are in various stages of development, and it is unknown at present what direction future methodological approaches might take. The SIPP study was a success as it identified a select group of DNA-based markers (Sect. 3) that are suitable for deployment, especially in California coastal waters. How well these same markers might perform in other regions is not clear, so the SIPP study makers (as well as any new ones that are developed) should be used with caution until sensitivity and specificity have been evaluated outside of California. Also, interpretation of results and subsequent management decisions are very difficult without knowing how various DNA-based markers age and degrade over time in different environmental matrices. Such SIPP-level aging studies are badly needed as the results could have a major impact on just how useful DNA-based markers really are. Many researchers are now investigating community analysis (Sect. 4) as the next big improvement in MST approaches, but community analysis is very new and it may or may not turn out to have much application in source tracking. Lastly, before other new approaches like NSE and QMRA can be implemented with confidence (Sect. 6), there are additional research questions that need to be addressed including (a) the overall accuracy of present techniques for determining whether the fecal signature at a given site is human or non-human in origin, (b) the relative health risks associated with human and non-human fecal sources, and (c) the level of scientific uncertainty in using this information in a management context [105]. Such new approaches will likely be controversial wherever they are considered for implementation. However, such consideration is only possible when the science is able to fully support their feasibility in problematic recreational waters [106]. The best overall approach at present is to follow the tiered system (Sect. 5) that places MST within the proper context of a larger suite of methods that are all useful in their appropriate context for accurately identifying the sources of fecal pollution in water [6].

References

1. Dick LK, Bernhard AE, Brodeur TJ, Domingo JWS, Simpson JM, Walters SP, Field KG (2005) Host distributions of uncultivated fecal *Bacteroidales* bacteria reveal genetic markers for fecal source identification. Appl Environ Microbiol 71:3184–3191
2. Santo Domingo JW, Bambic DG, Edge TA, Wuertz SD (2007) Quo vadis source tracking? Towards a strategic framework for environmental monitoring of fecal pollution. Water Res 41(16):3539–3552
3. Litton RM, Ahn JH, Sercu B, Holden PA, Sedlak DL, Grant SB (2010) Evaluation of chemical, molecular, and traditional markers of fecal contamination in an effluent dominated urban stream. Environ Sci Technol 44(19):7369–7375
4. Hagedorn C, Blanch A, Harwood J (2011) Microbial source tracking: methods, applications, and case studies. Springer, New York, p 642

5. Boehm AB, Van De Werfhorst LC, Griffith JF, Holden PA, Jay JA, Shanks OC, Wang D, Weisberg SB (2013) Performance of forty-one microbial source tracking methods: a twenty-seven lab evaluation study. Water Res 47:6812–6828
6. Griffith JF, Layton BA, Boehm AB, Holden PA, Jay JA, Hagedorn C, McGee CD, Weisberg SB (2013) The California microbial source identification manual: a tiered approach to identifying fecal pollution sources to beaches. Southern California Coastal Water Research Project technical report 0804, p 88. http://ftp.sccwrp.org/pub/download/DOCUMENTS/TechnicalReports/804_SIPP_MST_ManualPag.pdf. Accessed 15 July 2014
7. Dorfman M, Rpsselot KS (2010) Testing the waters: a guide to water quality at vacation beaches. Natural Resources Defense Council, Washington DC, p 44
8. Beach D (2002) Coastal sprawl: the effects of urban design on aquatic ecosystems in the United States. Pew Oceans Commission, Arlington, p 40
9. Dorfman M, Stoner N (2007) Testing the waters: a guide to water quality at vacation beaches. Natural Resources Defense Council, Washington DC, p 377
10. Dorfman M, Rosselot KS (2008) Testing the waters: a guide to water quality at vacation beaches. Natural Resources Defense Council, New York, p 447
11. NOAA (National Oceanic and Atmospheric Administration) (2005) Welfare estimates for five scenarios of water quality change in Southern California: a report from the Southern California Beach Valuation Project, Washington DC, p 32
12. Given S, Pendleton LH, Boehm AB (2006) Regional public health cost estimates of contaminated coastal waters: a case study of gastroenteritis at southern California beaches. Environ Sci Technol 40(16):4851–4858
13. Allender-Hagedorn S (2011) Community analysis-based methods. In: Hagedorn C, Blanch A, Harwood VJ (eds) Microbial source tracking: methods, applications, and case studies. Springer, New York, pp 283–300
14. Fleisher J, Kay D, Wyer MD, Godfree AF (1998) Estimates of the severity of illnesses associated with bathing in marine recreational waters contaminated with domestic sewage. Int J Epidemiol 27:722–726
15. Turbow DJ, Osgood ND, Jiang SC (2003) Evaluation of recreational health risk in coastal waters based on enterococcus densities and bathing patterns. Environ Health Perspect 111 (4):598–603
16. Yamahara KM, Sassoubre LM, Goodwin KD, Boehm AB (2012) Occurrence and persistence of human pathogens and indicator organisms in beach sands along the California coast. Appl Environ Microbiol 78:1733–1745
17. Haile RW, Witte JS, Gold M, Cressey R, McGee C, Millikan RC, Glasser A, Harawa N, Ervin C, Harmon P, Harper J, Dermand J, Alamillo J, Barrett K, Nides M, Wang G (1999) The health effects of swimming in ocean water contaminated by storm drain runoff. Epidemiology 10(4):355–363
18. Savichtcheva O, Okabe S (2006) Alternative indicators of fecal pollution: relations with pathogens and conventional indicators, current methodologies for direct pathogen monitoring and future application perspectives. Water Res 40:2463–2476
19. U.S. Environmental Protection Agency (2005) Microbial source tracking guide document. EPA/600-R-05-064. Office of Research and Development, Cincinnati
20. Van De Werfhorst LS, Sercu B, Holden PA (2011) Comparison of the host specificities of two *Bacteroidales* quantitative PCR assays used for tracking human fecal contamination. Appl Environ Microbiol 77(17):6258–6260
21. Cabelli VJ, Dufour AP, McCabe LJ, Levin MA (1982) Swimming-associated gastroenteritis and water quality. Am J Epidemiol 115(4):606–616
22. U.S. Environmental Protection Agency (2009) Review of published studies to characterize relative risks from different sources of fecal contamination in recreational water. EPA 822-R-09-001. Office of Water, Washington DC

23. Haugland RA, Siefring SC, Wymer LJ, Brenner KP, Dufour AP (2005) Comparison of *Enterococcus* measurements in freshwater at two recreational beaches by quantitative polymerase chain reaction and membrane filter culture analysis. Water Res 39:559–568
24. Boehm AB, Fuhrman JA, Mrše RD, Grant SB (2003) Tiered approach for identification of a human fecal pollution source at a recreational beach: Case study at Avalon Cay, Catalina Island, California. Environ Sci Technol 37(4):673–680
25. Weiskel PK, Howes BL, Heufelder GR (1996) Coliform contamination of a coastal embayment: sources and transport pathways. Environ Sci Technol 30:1872–1881
26. Whitman RL, Shivley DA, Pawlik H, Nevers MB, Byappanahalli MN (2003) Occurrence of Escherichia coli and enterococci in *Cladophora* (*Chlorophyta*) in nearshore water and beach sand of Lake Michigan. Appl Environ Microbiol 69(8):4714–4719
27. Badgley BD, Thomas FIM, Harwood VJ (2010) The effects of submerged aquatic vegetation on the persistence of environmental populations of *Enterococcus* spp. Environ Microbiol 12:1271–1281
28. Grant SB, Sanders BF, Boehm AB, Redman JA, Kim JH, Mrše RD, Chu AK, Gouldin M, McGee CD, Gardiner NA, Jones BH, Svejkovsky J, Leipzig GV, Brown A (2001) Generation of enterococci bacteria in a coastal saltwater marsh and its impact on surf zone water quality. Environ Sci Technol 35(12):2407–2416
29. Whitlock JE, Jones DT, Harwood VJ (2002) Identification of the sources of fecal coliforms in an urban watershed using antibiotic resistance analysis. Water Res 36(17):4273–4282
30. Fisher DS, Steiner JL, Endale DM, Stuedemann JA, Schomberg HH, Franzluebbers AJ, Wilkinson SR (2000) The relationship of land use practices to surface water quality in the Upper Oconee watershed of Georgia. For Ecol Manage 128(1–2):39–48
31. Burnes BS (2003) Antibiotic resistance analysis of fecal coliforms to determine fecal pollution sources in a mixed-use watershed. Environ Monit Assess 85(1):87–98
32. Jiang S, Noble R, Chui WP (2001) Human adenoviruses and coliphages in urban runoff—impacted coastal waters of Southern California. Appl Environ Microbiol 67(1):179–184
33. Petersen TM, Rifai HS, Suarez MP, Stein AR (2005) Bacteria loads from point and nonpoint sources in an urban watershed. J Environ Eng ASCE 131(10):1414–1425
34. Wyer MD, Fleisher JM, Gough J, Kay D, Merrett H (1995) An investigation into parametric relationships between enterovirus and faecal indicator organisms in the coastal waters of England and Wales. Water Res 29(8):1863–1868
35. Leadbetter ER (1997) Prokaryotic diversity: form, ecophysiology, and habitat. In: Hurst CJ, Crawford RL, Garland JL, Lipson DA (eds) Manual of environmental microbiology. American Society for Microbiology, Washington DC, pp 14–24
36. Harwood VJ, Stoeckel D (2011) Performance criteria. In: Hagedorn C, Blanch A, Harwood VJ (eds) Microbial source tracking: methods, applications, and case studies. Springer, New York, pp 7–30
37. U.S. Environmental Protection Agency (2001) Protocol for developing pathogen TMDLs. EPA 841-R-00-002. Office of Water (4503F). Washington DC, p 132
38. Painter W (2005) Origins and status of TMDL regulation. In: Younos T (ed) Total maximum load—approaches and challenges. PenWell Books, Tulsa, pp 1–45
39. U.S. Environmental Protection Agency (2011) National summary of impaired waters and TMDL information. http://www.epa.gov/waters/ir/index.html. Accessed 1 July 2014
40. Virginia Department of Environmental Quality (2012) TMDLs in Virginia. http://www.deq.state.va.us/programs/water/waterqualityinformationtmdls/tmdl.aspx
41. Benhem B, Krometis LA, Yagow G, Kline K, Dillaha T (2011) Applications of microbial source tracking in the TMDL process. In: Hagedorn C, Blanch A, Harwood VJ (eds) Microbial source tracking: methods, applications, and case studies. Springer, New York, pp 313–336
42. U.S. Environmental Protection Agency (2008) Handbook for developing watershed plans to restore and protect our waters. EPA 841-B-08-002. Washington DC, p 400

43. U.S. Environmental Protection Agency (2013) Chesapeake Bay TMDL. http://water.epa.gov/lawsregs/lawsguidance/beachrules/act.cfm. Accessed 1 July 2014
44. Virginia Department of Environmental Quality (2012) Final 2012 305(b)/303(d) water quality assessment integrated report. http://www.deq.virginia.gov/Programs/Water/WaterQualityInformationTMDLs/WaterQualityAssessments/2012305%28b%29303%28d%29IntegratedReport.aspx. Accessed 1 July 2014
45. Wade TJ, Pai N, Eisenberg JNS, Colfor JMJ (2003) Do U.S. Environmental Protection Agency water quality guidelines for recreational waters prevent gastrointestinal illness? A systematic review and meta-analysis. Environ Health Perspect 111(8):1102–1109
46. U.S. Environmental Protection Agency (2011) Beach act. http://water.epa.gov/lawsregs/lawsguidance/beachrules/act.cfm. Accessed 1 July 2014
47. Wade TJ, Calderon RL, Sams E, Beach M, Brenner KP, Dufour AP (2006) Rapidly measured indicators of recreational water quality are predictive of swimming associated gastrointestinal illness. Environ Health Perspect 114(1):24–28
48. Wade TJ, Sams E, Brenner KP, Haugland R, Chern E, Beach M, Wymer L, Rankin CC, Love D, Li Q, Noble R, Dufour AP (2010) Rapidly measured indicators of recreational water quality and swimming-associated illness at marine beaches: a prospective cohort study. Environ Health 9:66
49. Mott J, Smith A (2011) Library-dependent source tracking methods. In: Hagedorn C, Blanch A, Harwood VJ (eds) Microbial source tracking: methods, applications, and case studies. Springer, New York, pp 31–60
50. Parveen S, Murphree RL, Edmiston L, Kaspar CW, Tamplin ML (1997) Association of multiple-antibiotic-resistance profiles with point and nonpoint sources of *Escherichia coli* in Apalachicola Bay. Appl Environ Microbiol 63:2607–2612
51. Harwood VJ, Whitlock J, Worthington V (2000) Classification of antibiotic resistance patterns of indicator bacteria by discriminant analysis: use in predicting the source of fecal contamination in subtropical waters. Appl Environ Microbiol 69:3698–3704
52. Hagedorn C, Robinson SL, Filtz JR, Grubbs SM, Angier TA, Reneau RB Jr (1999) Determining sources of fecal pollution in a rural Virginia watershed with antibiotic resistance patterns in fecal streptococci. Appl Environ Microbiol 65:5522–5531
53. Parveen S, Portier KM, Robinson K, Edmiston L, Tamplin ML (1999) Discriminant analysis of ribotype profiles of *Escherichia coli* for differentiating human and nonhuman sources of fecal pollution. Appl Environ Microbiol 65:3142–3147
54. Moore DF, Harwood VJ, Ferguson DM, Lukasik J, Hannah P, Getrich M, Brownell M (2005) Evaluation of antibiotic resistance analysis and ribotyping for identification of faecal pollution sources in an urban watershed. J Appl Microbiol 99:618–628
55. Stoeckel DM, Harwood VJ (2007) Performance, design, and analysis in microbial source tracking studies. Appl Environ Microbiol 73:2405–2415
56. Seurinck S, Defoirdt T, Verstraete W, Siciliano SD (2005) Detection and quantification of the human-specific HF183 *Bacteroides* 16S rRNA genetic marker with real-time PCR for assessment of human faecal pollution in freshwater. Environ Microbiol 2:249–259
57. Wuertz S, Wang D, Reischer GH, Farnleitner AH (2011) Library-independent bacterial source tracking methods. In: Hagedorn C, Blanch A, Harwood VJ (eds) Microbial source tracking: methods, applications, and case studies. Springer, New York, pp 61–112
58. Layton A, McKay L, Williams D, Garrett V, Gentry R, Sayler G (2006) Development of *Bacteroides* 16S rRNA gene TaqMan-based real-time PCR assays for estimation of total, human, and bovine fecal pollution in water. Appl Environ Microbiol 72(6):4214–4224
59. Kildare BJ, Leutenegger CM, McSwain BS, Bambic DG, Rajal VB, Wuertz S (2007) 16S rRNA-based assays for quantitative detection of universal, human-, cow-, and dog-specific fecal *Bacteroidales*: a Bayesian approach. Water Res 41(16):3701–3715
60. Harwood VJ, Staley C, Badgley BD, Borges K, Korajkic A (2014) Microbial source tracking markers for detection of human sewage and fecal contamination in environmental waters: relationships to pathogens and human health outcomes. FEMS Microbiol Rev 38:1–40

61. Dorai-Raj S, O'Grady J, Cormican M, Colleran E (2012) Identification of host-specific *Bacteroidales* 16S rDNA sequences from human sewage and ruminant feces. J Basic Microbiol 52(3):277–284
62. Layton BA, Walters SP, Boehm AB (2009) Distribution and diversity of enterococcal surface protein (*esp*) gene in animal hosts and the Pacific coast environment. J Appl Microbiol 106:1521–1531
63. Stewart JR, Boehm AB, Dubinsky EA, Fong T, Goodwin KD, Griffith JF, Noble RT, Shanks OC, Vijayavel K, Weisberg SB (2013) Recommendations following a multi-laboratory comparison of microbial source tracking methods. Water Res 47(18):6829–6838
64. Haugland RA, Varma M, Sivaganesan M, Kelty C, Peed L, Shanks OC (2010) Evaluation of genetic markers from the 16S rRNA gene V2 region for use in quantitative detection of selected Bacteroidales species and human fecal waste by qPCR. Syst Appl Microbiol 33 (6):348–357
65. Shanks OC, Kelty CA, Sivaganesan M, Varma M, Haugland RA (2009) Quantitative PCR for genetic markers of human fecal pollution. Appl Environ Microbiol 75(17):5507–5513
66. Xu W, McDonough MC, Erdman DD (2000) Species-specific identification of human adenoviruses by a multiplex PCR assay. J Clin Microbiol 38:4114–4129
67. Jothikumar N, Cromeans TL, Hill VR, Lu X, Sobsey MD, Erdman DD (2005) Quantitative real-time PCR assays for detection of human adenoviruses and identification of serotypes 40 and 41. Appl Environ Microbiol 71(6):3131–3136
68. McQuaig SM, Scott TM, Lukasik JO, Paul JH, Harwood VJ (2009) Quantification of human polyomaviruses JC Virus and BK Virus by TaqMan quantitative PCR and comparison to other water quality indicators in water and fecal samples. Appl Environ Microbiol 75:3379–3388
69. Sinigalliano CD, Fleisher JM, Gidley ML, Solo-Gabriele HM, Shibata T, Plano LRW, Elmir SM, Wanless D, Bartkowiak J, Boiteau R, Withum K, Abdelzaher AM, He G, Ortega C, Zhu X, Wright ME, Kish J, Hollenbeck J, Scott T, Backer LC, Fleming LE (2010) Traditional and molecular analyses for fecal indicator bacteria in non-point source subtropical recreational marine waters. Water Res 44:3763–3772
70. Lee C, Marion JW, Lee J (2013) Development and application of a quantitative PCR assay targeting Catellicoccus marimammalium for assessing gull-associated fecal contamination at Lake Erie beaches. Sci Total Environ 454–455:1–8
71. Shibata T, Solo-Gabriele HM, Sinigalliano CD, Gidley ML, Plano LRW, Fleisher JM, Wang JD, Elmir SM, He G, Wright ME, Abdelzaher AM, Ortega C, Wanless D, Garza AC, Kish J, Scott T, Hollenbeck J, Backer LC, Fleming LE (2010) Evaluation of conventional and alternative monitoring methods for a recreational marine beach with nonpoint source of fecal contamination. Environ Sci Technol 44(21):8175–8181
72. Shanks OC, Atikovic E, Blackwood AD, Lu J, Noble RT, Santo Domingo J, Siefring S, Sivaganesan M, Haugland RP (2008) Quantitative PCR for detection and enumeration of genetic markers of bovine fecal pollution. Appl Environ Microbiol 74(3):745–752
73. Mieszkin S, Yala JF, Joubrel R, Gourmelon M (2010) Phylogenetic analysis of Bacteroidales 16S rRNA gene sequences from human and animal effluents and assessment of ruminant faecal pollution by real-time PCR. J Appl Microbiol 108(3):974–984
74. Reischer GH, Ebdon JE, Bauer JM, Schuster N, Ahmed W, Astrom J, Blanch AR, Bloschl G, Byamukama D, Coakley T, Ferguson C, Goshu G, Ko G, Husman AMD, Mushi D, Poma R, Pradhan B, Rajal V, Schade MA, Sommer R, Taylor H, Toth EM, Vrajmasu V, Wuertz S, Mach RL, Farnleitner AH (2013) Performance characteristics of qPCR assays targeting human and ruminant-associated *Bacteroidetes* for microbial source tracking across sixteen countries on six continents. Environ Sci Technol 47(15):8548–8556
75. Layton B, Cao Y, Ebentier DL, Hanley KT, Van De Werfhorst L, Wang D, Madi T, Whitman RL, Byappanahalli MN, Balleste E, Meijier W, Schriewer A, Wuertz S, Converse RR, Noble RT, Srinivasan S, Rose JB, Lee CS, Lee J, Shields J, Stewart JR, Reischer G, Farnleitner A, Sinagalliano CD, Rodrigues R, Lozach S, Gourmelon M, Peed L, Shanks OC, Jay J,

Holden P, Boehm AB, Griffith JF (2013) Performance of human fecal-associated PCR-based assays: an international source identification method evaluation. Water Res 47 (18):6897–6908
76. Harwood VJ, Boehm AB, Sassoubre LM, Vijayavel K, Stewart JR, Fong TT, Caprais MP, Converse RR, Diston D, Ebdon J, Fuhrman JA, Gourmelon M, Gentry-Shields J, Griffith JF, Kashian DR, Noble RT, Taylor H, Wicki M (2013) Performance of viruses and bacteriophages for fecal source determination in a multi-laboratory, comparative study. Water Res 47 (18):6929–6943
77. McQuaig SM, Noble RT (2011) Viruses as tracers of fecal contamination. In: Hagedorn C, Blanch A, Harwood VJ (eds) Microbial source tracking: methods, applications, and case studies. Springer, New York, pp 113–136
78. Lee DY, Weir SC, Lee H, Trevors JT (2010) Quantitative identification of fecal water pollution sources by TaqMan real-time PCR assays using Bacteroidales 16S rRNA genetic markers. Appl Microbiol Biotechnol 88:1373–1383
79. Sinigalliano CD, Ervin JS, Van De Werfhorst LC, Badgley BD, Ballesté E, Bartkowiak J, Boehm AB, Byappanahalli M, Goodwin KD, Gourmelon M, Griffith JF, Holden PA, Jay J, Layton BA, Lee C, Lee J, Meijer WG, Noble R, Raith M, Ryu H, Sadowsky MJ, Schriewer A, Wang D, Wanless D, Whitman RL, Wuertz S, Santo Domingo JW (2013) Multi-laboratory evaluations of the performance of *Catellicoccus marimammalium* PCR assays developed to target gull fecal sources. Water Res 47:6883–6896
80. Green HC, Dick LK, Gilpin B, Samadpour M, Field KG (2012) Genetic markers for rapid PCR-based identification of gull, Canada goose, duck, and chicken fecal contamination in water. Appl Environ Microbiol 78(2):503–510
81. Schriewer A, Goodwin KD, Sinigalliano CD, Cox AM, Wanless D, Bartkowiak J, Ebentier DL, Hanley KT, Ervin J, Deering LA, Shanks OC, Peed LA, Meijer WG, Griffith JF, SantoDomingo J, Jay JA, Holden PA, Wuertz S (2013) Performance evaluation of canine-associated Bacteroidales assays in a multi-laboratory comparison study. Water Res 47:6909–6920
82. Raith MR, Kelty CA, Griffith JF, Schriewer A, Wuertz S, Mieszkin S, Gourmelon M, Reischer GH, Farnleitner AH, Ervin JS, Holden PA, Ebentier DL, Jay JA, Wang D, Boehm AB, Aw TG, Rose JB, Ballesté E, Meijer WG, Sivaganesan M, Shanks OC (2013) Comparison of PCR and quantitative real-time PCR methods for the characterization of ruminant and cattle fecal pollution sources. Water Res 47:6921–6928
83. Harwood VJ, Levine AD, Scott TM, Chivukula V, Lukasik J, Farrah SR, Rose JB (2005) Validity of the indicator organism paradigm for pathogen reduction in reclaimed water and public health protection. Appl Environ Microbiol 71:3163–3170
84. Unno T, Jang J, Han D, Kim JH, Sadowsky MJ, Kim OS, Chun J, Hur HG (2010) Use of barcoded pyrosequencing and shared OTUs to determine sources of fecal bacteria in watersheds. Environ Sci Technol 44:7777–7782
85. Cao Y, Wu CH, Andersen GL, Holden PA (2011) Community-analysis based methods. In: Hagedorn C, Blanch A, Harwood VJ (eds) Microbial source tracking: methods, applications, and case studies. Springer, New York, pp 251–282
86. McLellan SL, Huse SM, Mueller-Spitz SR, Andreishcheva EN, Sogin ML (2010) Diversity and population structure of sewage-derived microorganisms in wastewater treatment plant influent. Environ Microbiol 12:378–392
87. Shanks OC, Kelty CA, Archibeque S, Jenkins M, Newton RJ, McLellan SL, Huse SM, Sogin ML (2011) Community structures of fecal bacteria in cattle from different animal feeding operations. Appl Environ Microbiol 77:2992–3001
88. Cao Y, Van De Werfhorst LC, Sercu B, Murray JLS, Holden PA (2011) Application of an integrated community analysis approach for microbial source tracking in a coastal creek. Environ Sci Technol 45(17):7195–7201

89. Dubinsky EA, Esmaili L, Hulls JR, Cao Y, Griffith JF, Andersen GL (2012) Application of phylogenetic microarray analysis to discriminate sources of fecal pollution. Environ Sci Technol 46(8):4340–4347
90. Sogin ML, Morrison HG, Huber JA, Welch DM, Huse SM, Neal PR, Arrieta JM, Herndi GJ (2006) Microbial diversity in the deep sea and the underexplored "rare biosphere". Proc Natl Acad Sci 103(32):12115–12120
91. Caporaso JG, Lauber CL, Walters WA, Berg-Lyons D, Huntley J, Fierer N, Owens SM, Betley J, Fraser L, Bauer M, Gormley N, Gilbert JA, Smith G, Knight R (2012) Ultra-high-throughput microbial community analysis on the Illumina HiSeq and MiSeq platforms. ISME J 6:1621–1624
92. Cao Y, Van der Werfhorst LC, Dubinsky EA, Badgley BD, Sadowsky MJ, Andersen GL, Griffith JF, Holden PA (2013) Evaluation of molecular community analysis methods for discerning fecal sources and human waste. Water Res 47(18):6862–6872
93. Knights D, Kuczynski J, Charlson ES, Zaneveld J, Mozer C, Collman RG, Bushman FD, Knight R, Kelley ST (2011) Bayesian community-wide culture-independent microbial source tracking. Nat Methods 8:761–763
94. Unno T, Di DYW, Jang J, Suh YS, Sadowsky MJ, Hur HG (2012) Integrated online system for a pyrosequencing-based microbial source tracking method that targets bacteroidetes 16S rDNA. Environ Sci Technol 46(1):93–98
95. Keity CA, Varma M, Sivaganesan M, Haugland RA, Shanks OC (2012) Distribution of genetic marker concentrations for fecal indicator bacteria in sewage and animal feces. Appl Environ Microbiol 78(12):4225–4232
96. Girones R, Ferrús MA, Alonso JL, Rodriguez-Manzano J, Calgua B, Corrêa Ade A, Hundesa A, Carratala A, Bofill-Mas S (2010) Molecular detection of pathogens in water—the pros and cons of molecular techniques. Water Res 44(15):4325–4339
97. Green HC, Shanks OC, Sivaganesan M, Haugland RA, Field KG (2011) Differential decay of human faecal *Bacteroides* in marine and freshwater. Environ Microbiol 13(12):3235–3249
98. Hagedorn C, Weisberg SB (2011) Chemical source tracking methods. In: Hagedorn C, Blanch A, Harwood AJ (eds) Microbial source tracking: methods, applications, and case studies. Springer, New York, pp 189–206
99. Van De Werfhorst LC, Murray JLS, Reynolds S, Reynolds K, Holden PA (2014) Canine scent detection and microbial source tracking of human waste contamination in storm drains. Water Environ Res 86(6):550–559
100. Dorsey JH (2010) Improving water quality through California's Clean Beach Initiative: an assessment of 17 projects. Environ Monit Assess 166:95–111
101. Stewart JR, Gast RJ, Fujioka RS, Solo-Gabriele HM, Meschke JS, Amaral-Zettler LA, del Castillo E, Polz MF, Collier TK, Strom MS, Sinigalliano CD, Moeller PD, Holland AF (2008) The coastal environment and human health: microbial indicators, pathogens, sentinels and reservoirs. Environ Health 7(Suppl 2):S3
102. Schoen ME, Soller JA, Ashbolt NJ (2011) Evaluating the importance of fecal sources in human-impacted waters. Water Res 45(8):2670–2680
103. Ashbolt NJ, Schoen ME, Soller JA, Roser DJ (2010) Predicting pathogen risks to aid beach management: the real value of quantitative microbial risk assessment. Water Res 44 (6):4692–4703
104. Schoen ME, Ashbolt NJ (2010) Assessing pathogen risk to swimmers at non-sewage impacted recreational beaches. Environ Sci Technol 44(7):2286–2291
105. U.S. Environmental Protection Agency (2010) Quantitative microbial risk assessment to estimate illness in freshwater impacted by agricultural animal sources of fecal contamination. EPA 822-R-10-005. Office of Water, Washington DC
106. Soller JA, Schoen ME, Bartrand T, Ravenscroft JE, Ashbolt NJ (2010) Estimated human health risks from exposure to recreational waters impacted by human and non-human sources of faecal contamination. Water Res 44:4674–4691

Index

T. Younos, T.E. Parece (eds.), *Advances in Watershed Science and Assessment*, The Handbook of Environmental Chemistry 33,
DOI 10.1007/978-3-319-14212-8